# Molecular functions of CdGAP in prostate cancer and embryonic development

Ji-Hyun Chung

Department of Anatomy & Cell Biology
McGill University, Montréal, Québec, Canada

Submitted April 2024

A thesis submitted to McGill University in partial fulfillment
of the requirements of the degree of

Doctor of Philosophy

## Abstract

Understanding the molecular mechanisms underpinning human diseases is critical for the development of targeted therapeutic strategies. In cancer research, we have seen significant advances in deciphering the roles of various proteins in tumorigenesis. In contrast, studies in developmental biology have revealed how protein misregulation can lead to severe congenital anomalies and neonatal mortality. However, an understanding gap exists between these fields. Our work aims to bridge this gap by examining the dual roles of a specific protein, CdGAP, in both cancer progression and embryonic development.

Initially, we investigated CdGAP's role in prostate cancer progression. Our analysis of *ARHGAP31*, the gene encoding CdGAP, across multiple prostate cancer cell lines indicated a positive correlation with cancer aggressiveness. High mutated CdGAP levels were linked with an increased likelihood of biochemical recurrence. These findings led us to hypothesize CdGAP as an oncogene in prostate cancer. Testing this hypothesis, we manipulated CdGAP levels in various cell lines and assessed their effects on cell migration and invasion. Our *in vivo* studies suggest that CdGAP loss impairs prostate cancer progression, marking it as a promising therapeutic target.

In the second part of our study, we explored CdGAP’s role in embryonic development, particularly in Adams-Oliver syndrome (AOS). Although largely deficient, literature shows placental dysfunction in AOS patients and a marked CdGAP expression increase in late-onset severe preeclampsia. Thus, we postulated that alterations in CdGAP expression or function could contribute to AOS pathogenesis. Using a CdGAP-AOS knock-in mouse model, we studied the ensuing embryonic and placental abnormalities. We found a link between placental dysfunction onset, impaired growth of the labyrinth, and embryonic lethality during late gestation. Also, we observed defective syncytial fusion in severe cases, concurrent with heart anomalies.

In conclusion, our study offers valuable insights into the dual roles of CdGAP in prostate cancer progression and embryonic development. These findings enrich our understanding of both cancer biology and developmental biology, and offer new avenues for therapeutic interventions in the fight against cancer and rare diseases.

## Résumé

Comprendre les mécanismes moléculaires sous-jacents aux maladies humaines est essentiel pour le développement de stratégies thérapeutiques ciblées. Dans la recherche sur le cancer, nous avons assisté à des avancées significatives dans le déchiffrement des rôles de diverses protéines dans la tumorigenèse. En revanche, les études en biologie du développement ont révélé comment la dérégulation des protéines peut entraîner de graves anomalies congénitales et une mortalité néonatale. Cependant, un écart de compréhension existe entre ces domaines. Notre travail vise à combler cet écart en examinant les différents rôles d'une protéine spécifique, CdGAP, à la fois dans la progression du cancer et le développement embryonnaire.

Au départ, nous avons étudié le rôle de CdGAP dans la progression du cancer de la prostate. Notre analyse du gene *ARHGAP31* codant pour la protéine CdGAP, dans plusieurs lignées cellulaires de cancer de la prostate a indiqué une corrélation positive avec l'agressivité du cancer. Des niveaux élevés de CdGAP mutée ont été liés à une probabilité accrue de récidive biochimique. Ces résultats nous ont amenés à émettre l'hypothèse que CdGAP agit comme un oncogène dans le cancer de la prostate. Pour tester cette hypothèse, nous avons manipulé les niveaux d'expression de CdGAP dans diverses lignées cellulaires et évalué leurs effets sur la migration et l'invasion des cellules. Nos études *in vivo* suggèrent que la perte de CdGAP entrave la progression du cancer de la prostate, suggérant que celle-ci pourrait representer une cible thérapeutique prometteuse.

Dans la seconde partie de notre étude, nous avons exploré le rôle de CdGAP dans le développement embryonnaire, en particulier dans le syndrome d'Adams-Oliver (SAO). Bien que peu documentée, la littérature montre une dysfonction placentaire chez certains patients atteints du SAO et une augmentation marquée de l'expression de CdGAP dans la prééclampsie sévère à début tardif. Ainsi, nous avons postulé que des altérations de l'expression ou de la fonction de CdGAP pourraient contribuer à la pathogenèse du SAO. En utilisant un modèle de souris knock-in CdGAP-SAO, nous avons étudié les anomalies embryonnaires et placentaires qui en résultent. Nous avons trouvé un lien entre le début de la dysfonction placentaire, la croissance altérée du labyrinthe et la létalité embryonnaire pendant la gestation tardive. De plus, nous avons observé une fusion syncytiale défectueuse dans les cas graves, simultanément à des anomalies cardiaques.

En conclusion, notre étude offre des informations précieuses sur les différentes fonctions de CdGAP dans la progression du cancer de la prostate et le développement embryonnaire. Ces résultats enrichissent notre compréhension de la biologie du cancer et de la biologie du développement, et offrent de nouvelles perspectives thérapeutiques dans la lutte contre le cancer et les maladies rares.

## Contribution to original knowledge

Original contributions (presented as Chapters 2 and 3, respectively):

1. Chahat Mehra*, Ji-Hyun Chung*, Yi He, Monica Lara-Márquez, Marie-Anne Goyette, Nadia Boufaied, Véronique Barrès, Véronique Ouellet, Karl-Phillippe Guérard, Carine Delliaux, Fred Saad, Jacques Lapointe, Jean-François Côté, David P. Labbé, and Nathalie Lamarche-Vane. "CdGAP promotes prostate cancer metastasis by regulating epithelial-to-mesenchymal transition, cell cycle progression, and apoptosis". Manuscript published in *Communications biology.*

   ** co-first authors*

This study represents the first report on CdGAP's role as an oncogene in prostate cancer tumorigenesis. It demonstrates that CdGAP is essential not only for regulating cell cycle and conferring the ability to evade apoptosis but also for promoting aggressive prostate cancer metastasis through the upregulation of several mesenchymal markers, such as N-cadherin and Slug. Moreover, using castration-resistant prostate cancer (CRPC) cell lines and xenograft mouse models, we provide initial insights into potential mechanisms through which CdGAP may exert its oncogenic function in prostate cancer.

2. Ji-Hyun Chung, Yi He, Shiva Shafei, Brian Meehan, Nadia Boufaied, Janusz Rak, David P Labbé, Daniel Dufort, and Nathalie Lamarche-Vane. "Loss-of-function Adams-Oliver syndrome mutation of mouse *CdGAP* results in defective syncytial fusion and placental dysfunctions". Manuscript in preparation.

This study offers molecular insights into the molecular consequences of the human Q683X mutation in CDGAP, observed in Adams-Oliver syndrome (AOS) patients, using the P670X CdGAP-AOS knock-in (KI) mouse model. This model represents the first mouse model created specifically to mimic AOS, a unique tool for studying this condition. Importantly, the study bridges the gap between placental development and AOS, an association previously overlooked despite several case reports. It provides new insights into the pathogenic origin of AOS due to placental dysfunction and is the first to identify defective syncytial fusion as the major pathological event underlying labyrinth defects in the CdGAP-AOS KI mouse model. Syncytial

fusion defects were correlated with significant congenital heart development abnormalities in affected embryos and led to embryonic lethality.

## Acknowledgments

I would like to begin by thanking Dr. Nathalie Lamarche-Vane for opening her door to me in 2018. More importantly, her support and guidance have allowed me to cultivate an ever-growing passion for science. I would also like to thank my mentor, Dr. Dieter Reinhardt, and other members of my advisory committee, Drs. David Labbé and Christian Rocheleau, for your scientific input and encouragement.

For funding support, I extend my gratitude to the Canadian Institutes for Health Research (CIHR) and the Heart and Stroke Foundation. Special thanks go to all my colleagues in the neighboring labs at Glen, especially Audrey and Dianne, from the laboratory of Dr. Peter Metrakos, for their training, troubleshooting with the rotary microtome, and permission to use their equipment for countless hours, which is vital for my project. Without your generosity, I wouldn't have reached this point; thank you. Most importantly, I wouldn't be here without the help and support of all our lab members. Yi, Jimmy, Moni, and Leif, I appreciate all your constructive feedback during my lab meetings. A special gratitude to Jimmy for countless hangout nights and for introducing me to my girlfriend, Yunxi. Leif, although I wasn't able to get to know you more, I greatly value your kind words and countless encouragements, which helped me through many tough times!

My appreciation continues to Brian from Dr. Janusz Rak's lab, for his continuous technical assistance, shared reagents, and positive encouragement. Brian, it was an honor to know you, and I can never thank you enough. I won't forget your heart-warming encouragement, which always helped me stand up again after facing difficulties. You helped me believe in the attainable, even when it seemed so far-fetched! I must also recognize Dr. Hong Choi, another lifetime mentor whom I met as an undergraduate. Without him, I wouldn't have been able to push beyond my limits.

My family's support has been indispensable. Having spent 17 years studying abroad, I've come to value the opportunity my parents afforded me. I send my love to my maternal grandmother, who always loved me unconditionally. Though Alzheimer's disease has taken away her ability to recognize me, I carry her wishes in my heart, continuing to be generous, caring, and hardworking.

My thanks continue to my lovely girlfriend, Yunxi. Your positive energy helped me reach the finish line, especially during those difficult times in June. Thank you for your endless support, and for sharing the beautiful memories and adventures in Montreal.

Finally, I thank one of my favorite motivational speakers, Mr. Les Brown, whose speech resonated deeply with me. To my future self, I want you to remember the lessons learned on this journey. No matter the obstacles, always have faith and never stop running toward your dream!

# Table of Contents

# List of Figures and Tables

**Chapter 1: Literature Review**



**Chapter 2: Manuscript I**



**Chapter 3: Manuscript II**

## Publications and Contribution of Authors

Chapter 2:

Chahat Mehra*, Ji-Hyun Chung*, Yi He, Monica Lara-Márquez, Marie-Anne Goyette, Nadia Boufaied, Véronique Barrès, Véronique Ouellet, Karl-Phillippe Guérard, Carine Delliaux, Fred Saad, Jacques Lapointe, Jean-François Côté, David P. Labbé, and Nathalie Lamarche-Vane. "CdGAP promotes prostate cancer metastasis by regulating epithelial-to-mesenchymal transition, cell cycle progression, and apoptosis". Manuscript published in *Communications biology.*

** co-first authors*

My contribution involves the generation of CdGAP-depleted 22Rv1 cells and performing *in vitro* experiments in Figure 2f, Figure 3, Figure 4a, Figure 5e, f, and orthotopic xenografts experiments of control or CdGAP-depleted PC-3 cells, in Figure 8. I contributed to the writing of the manuscript and to the organization of the figures and final presentation of the manuscript.

Chapter 3:

Ji-Hyun Chung, Yi He, Shiva Shafei, Brian Meehan, Nadia Boufaied, Janusz Rak, David P Labbé, Daniel Dufort, and Nathalie Lamarche-Vane. "Loss-of-function Adams-Oliver syndrome mutation of mouse *CdGAP* results in defective syncytial fusion and placental dysfunctions". Manuscript in preparation.

I performed all the experiments presented in this manuscript. I also performed the data analysis and figure preparation for all experiments, except for Figure 8a, which was prepared by Nadia Boufaied. I wrote the first draft of the manuscript with Dr. N. Lamarche-Vane.

## Abbreviations

ACC Aplasia Cutis Congenita

ADT Androgen-Deprivation Therapy

AF-1 Activation Function-1

AGM Aorta-Gonad Mesonephros

AITL Angioimmunoblastic T-cell lymphoma

AKAP-Lbc A-Kinase Anchoring Protein-Lbc

AMP Adeonsine Monophosphate

AOS Adams-Oliver Syndrome

AR Androgen Receptor

ARE Androgen Response Element

ATLL Adult T-cell leukemia/lymphoma

AVE Anterior Visceral Endoderm

BAR Bin/Amphiphysin/Rvs

BCA Bicinchoninic Acid Assay

BCR Biochemical Recurrence

BLI Bioluminescence Imaging

BMI1 B-cell specific Moloney murine leukemia virus integration site 1

BORG3 Binds to Rho GTPases 3

β-PIX β-P21-activated kinase-interacting exchange factor

BR Basic Region

BSA Bovine Serum Albumin

cAMP Cyclic AMP

CdGAP Cdc42 GTPase-Activating Protein

CDK Cyclin-Dependent Kinase

cDNA Complementary DNA

CMTC Cutis Marmorata Telangiectatica

CRC Colorectal cancer

CRIB Cdc42/Rac-interactive binding

CRIK Citron kinase

CRPC Castration-Resistant Prostate Cancer

CTB Cytotrophoblast

DAPI 4’6’-diamidino-2-phenylindole

DBL Diffuse B-cell lymphoma

DEF Dok/Erv/FPS/FER

DH DBL-homology

DHR DOCK homology region

DIA Diaphanous 1

DLC1 Deleted in liver cancer 1

DLL Delta-Like Ligand

DOCK Dedicator of cytokinesis

DSL Delta/Serrate/Lag-2

E1A Early region 1A

ECL Enhanced chemiluminescence

ECM Extracellular matrix

ECT2 Epithelial cell transforming 2

EGF Epidermal Growth Factor

EGFR Epidermal Growth Factor Receptor

EH Eps-Homology

EMT Epithelial-to-mesenchymal transition

EOGT EGF-domain specific O-linked N-acetylglucosamine

ER Endoplasmic reticulum

ERK Extracellular signal-regulated kinase

EV Empty Vector

EVT Extravillous Trophoblast

FBS Fetal Bovine Serum

FOXO1 Forkhead Box O1

FMNL2 Formin-like protein 2

GAP GTPase-activating protein

GBD GTPase-binding domain

GCM1 Glial Cells Missing Homolog 1

GEF Guanine-nucleotide exchange factor

GSK Glycogen Synthase Kinase

GST Glutathione S-transferase

GTP Guanosine triphosphate

GDP Guanosine diphosphate

GEO Gene Expression Omnibus

GSEA Gene Set Enrichment Analysis

hCG Human Chronic Gonadotrophin

H&E Hematoxylin and Eosin

hnSCC Head and neck squamous cell carcinoma

HR Hazard Ratio

ICMT Isoprenylcysteine carboxyl methyltransferase

IHC Immunohistochemistry

ILK Integrin-Linked Kinase

ISUP International Society of Urologic Pathology

IUGR Intrauterine Growth Restriction

JNK c-Jun N-terminal kinase

KI Knock-In

LIMK LIM Domain Kinase

MAML Mastermind-like

MAPK Mitogen-Activated Protein Kinase

MEF Mouse Embryonic Fibroblast

MEK Mitogen-Activated Protein Kinase Kinase

MHC Major Histocompatibility Complex

MLK3 Mixed-Lineage Kinase 3

mTOR Mammalian Target of Rapamycin

MTT 3-(4,5-Dimethylthiazol-2-yl)-2,5-diphenyltetrazolium bromide

NE Neuroendocrine

NICD NOTCH Intracellular Domain

NMuMG Nontumorigenic Murine Mammary Gland

NO Nitric Oxide

NOX4 NADPH Oxidase 4

NRTK non-receptor tyrosine kinase

NSCLC Non-small cell lung cancer

O-GlcNAc O-linked N-acetylglucosamine

PAH Polycyclic Aromatic Hydrocarbon

PAK p21-activated kinase

Par Partitioning defective

PBR Poly-Basic Region

PBS Phosphate-buffered saline

PCa Prostate Cancer

PCDH12 Protocadherin 12

PDGF Platelet-Derived Growth Factor

PH pleckstrin homology

PI Propdium Iodide

PI3K Phosphoinositide 3-Kinase

PIN Prostatic Intraepithelial Neoplasia

PKC Protein Kinase C

PKN protein kinase novel

PRD Proline-Rich Domain

P-REX1 Phosphatidylinositol-3,4,5-triphosphate-dependent Rac exchange factor 1

PSA Prostate-Specific Antigen

PTEN Protein Phosphatase and Tensin Homolog

PTCL-NOS peripheral T-cell lymphoma not otherwise specified

qPCR Quantitative PCR

RAF Rapidly Accelerated Fibrosarcoma

RBPJ Recombination signal Binding Protein for immunoglobulin kappa J region

RCE1 Ras converting CAAX endopeptidase 1

Rho Ras homolog

RhoBTB Rho-Related BTB Domain-containing protein

RhoGAP Rho GTPase-activating protein

RhoGEF Rho guanine-nucleotide exchange factor

RhoGDI Rho guanine nucleotide dissociation inhibitor

RIPA Radioimmunoprecipitation Assay

ROCK Rho-Associated Coiled-Coil Kinase

ROS Reactive Oxygen Species

rPlf proliferin-related protein

RSK1 Receptor Serine Kinase 1

RTK Receptor tyrosine kinase

RTKN Rhotekin

SDS-PAGE Sodium Dodecyl Sulfate-Polyacrylamide Gel Electrophoresis

SEPT9 Septin 9

sFlt-1 Soluble Fms-like tyrosine kinae-1

SH Src Homology domain

shRNA Short Hairpin RNA

siRNA Silencing RNA

SMURF1 SMAD ubiquitin regulatory factor 1

Sos1 Son of sevenless homolog 1

SpT Spongiotrophoblast

SrGAP1 Slit-Robo GTPase-activating protein 1

sTGC Sinusoidal Trophoblast Giant Cell

STOX1 Storkhead Box 1

SynT Syncytiotrophoblast

TCGA The Cancer Genome Atlas

TGF-β Transforming Growth Factor-Beta

TIAM1 T-cell lymphoma Invasion and Metastasis-inducing protein 1

TMA Tissue Microarray

TNF-α Tumor Necrosis Factor alpha

TPR Tetratricopeptide repeat

TTLD Transverse Terminal Limb Defect

uNK Uterine Natural Killer

Vcam1 Vascular Cell Adhesion Molecule-1 (fix from protein)

VEGF Vascular Endothelial Growth Factor

VEGFR Vascular Endothelial Growth Factor Receptor

VSMC Vascular Smooth Muscle Cell

WASP Wiskott-Aldrich syndrome protein

WAVE WASP-family verprolin-homologous protein

WHO World Health Organization

YAP Yes-Associated Protein

Zeb2 Zinc Finger E-Box Binding Homeobox 2

ZO-1 Zonula Occludens-1

# Chapter 1: Literature Review

## *1.0 General introduction*

Several parallels can be drawn between the progression and development of various cancers in humans and the process of embryonic development. This is particularly evident as cancer cells co-opt the molecular mechanisms responsible for migratory and invasive potential in cells, typically utilized for wound healing and immune responses[1]. Despite decades-long efforts by researchers to bridge the gap between molecular mechanisms, which are either compromised or selectively exploited by cancer cells, and their potential role in underpinning developmental defects that often result in neonatal mortality[2], this area remains incompletely understood. Presently, more than 7,000 known rare diseases in humans can cause early death before the age of five[3]. Importantly, these conditions, often linked with anomalies in embryonic development, would impact an estimated 473 million individuals worldwide, out of a global population of 7.6 billion. This implies that despite the "rare" designation, the collective prevalence of these diseases is indeed significant. However, the therapeutic landscape is disproportionately sparse, with less than 5% of FDA-approved drugs catering to these conditions, often at exorbitant costs due to the rarity of the disease[3]. Therefore, it becomes crucial to explore the potential roles of proteins, especially those previously linked with cancer, in embryonic development. Such concerted efforts can greatly augment therapeutic strategies and ultimately aid in reducing neonatal mortality rates. This broader investigation into the dual roles of these proteins not only contributes to our understanding of developmental biology but also provides potential avenues for the development of effective treatments for rare diseases and potentially cancer.

## *1.1 Rho GTPases: general overview*

The RAS homolog (RHO) family of GTPases, part of the larger RAS superfamily of guanine nucleotide-binding proteins, plays a fundamental role in various aspects of human life[4]. Dysfunctions in Rho GTPases can contribute to a range of human diseases[5], given their diverse functions in regulating cell polarity, movement, cell division, and cytoskeleton reorganization[6]. The crucial nature of these GTPases is underscored by the fact that nearly 1% of the human genome encodes proteins that either regulate or are regulated by direct interaction with Rho GTPases[6].

Rho GTPases are regulated through a well-characterized mechanism that enables them to function as “molecular switches”. This allows them to cycle between inactive, GDP-bound states and active, GTP-bound states (Figure 1.1)[7]. Biochemical and structural studies have provided crucial insights into this regulatory cycle. Four classes of protein families participate in this process: Rho GTPase-activating protein (RhoGAP), Rho guanine-nucleotide exchange factor (RhoGEF), Rho Guanine nucleotide dissociation inhibitor (RhoGDI), and downstream effector molecules[7]. The RhoGAPs and RhoGEFs have opposing roles in this process, with RhoGAPs enhancing the intrinsic GTP hydrolysis reaction of Rho GTPases and RhoGEFs facilitating nucleotide exchanges from GDP to GTP[8]. Upon activation, the typically GTP-bound Rho GTPases[9] interact with downstream effectors to orchestrate a variety of biological functions[10]. Among their many roles, Rho GTPases are known to influence actin cytoskeleton reorganization. For instance, RhoA mediates the formation of stress fiber and focal adhesions, enabling actomyosin contractility[11], while Cdc42 and Rac1 are responsible for the formation of filopodia and lamellipodia at the cell periphery, respectively[12-14].

In humans, 20 members of the Rho family have been identified, falling into eight distinct subfamilies (Figure 1.2)[9, 15]. These members can be further divided into two categories: “typical” and “atypical” Rho GTPases (Figure 1.2)[9]. Atypical Rho GTPases differ from typical ones in the absence of the classical switch mechanisms[16, 17].

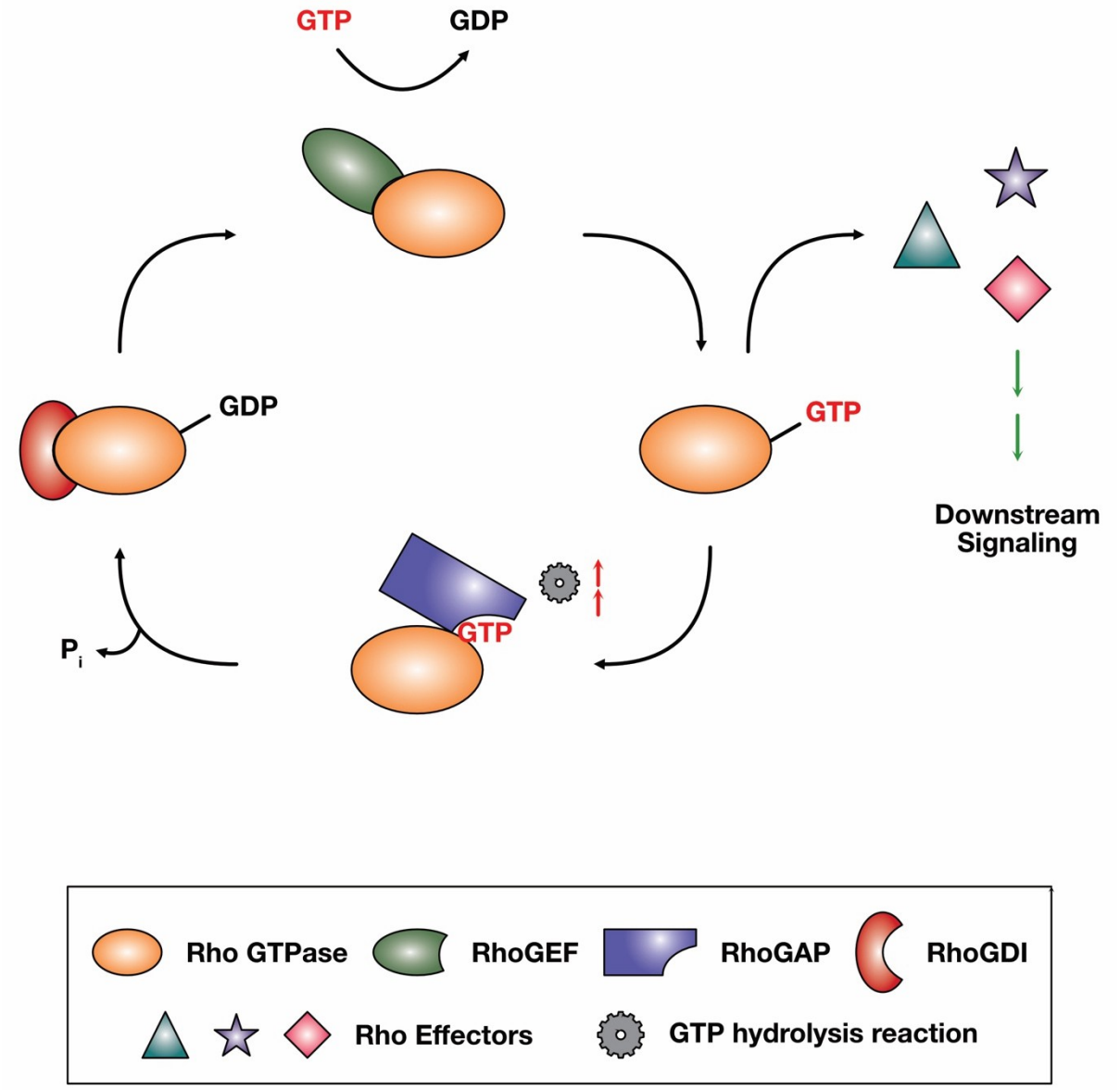


**Figure 1.1: Rho GTPase cycle.**

Rho GTPases act as "molecular switches"[7]. This cycle commences with inactive, GDP-bound Rho GTPases being activated by RhoGEFs, which enable the exchange of GDP for GTP[8]. Upon activation, these GTP-bound Rho GTPases interact with effector proteins, initiating a range of biological functions via downstream signaling pathways[9, 10]. RhoGAPs then regulate the cycle by accelerating the intrinsic GTP hydrolysis of Rho GTPases, effectively deactivating them and returning them to their GDP-bound states[8]. Further regulation is accomplished by RhoGDIs, which bind to GDP-bound Rho GTPases, preserving their inactive states[7].

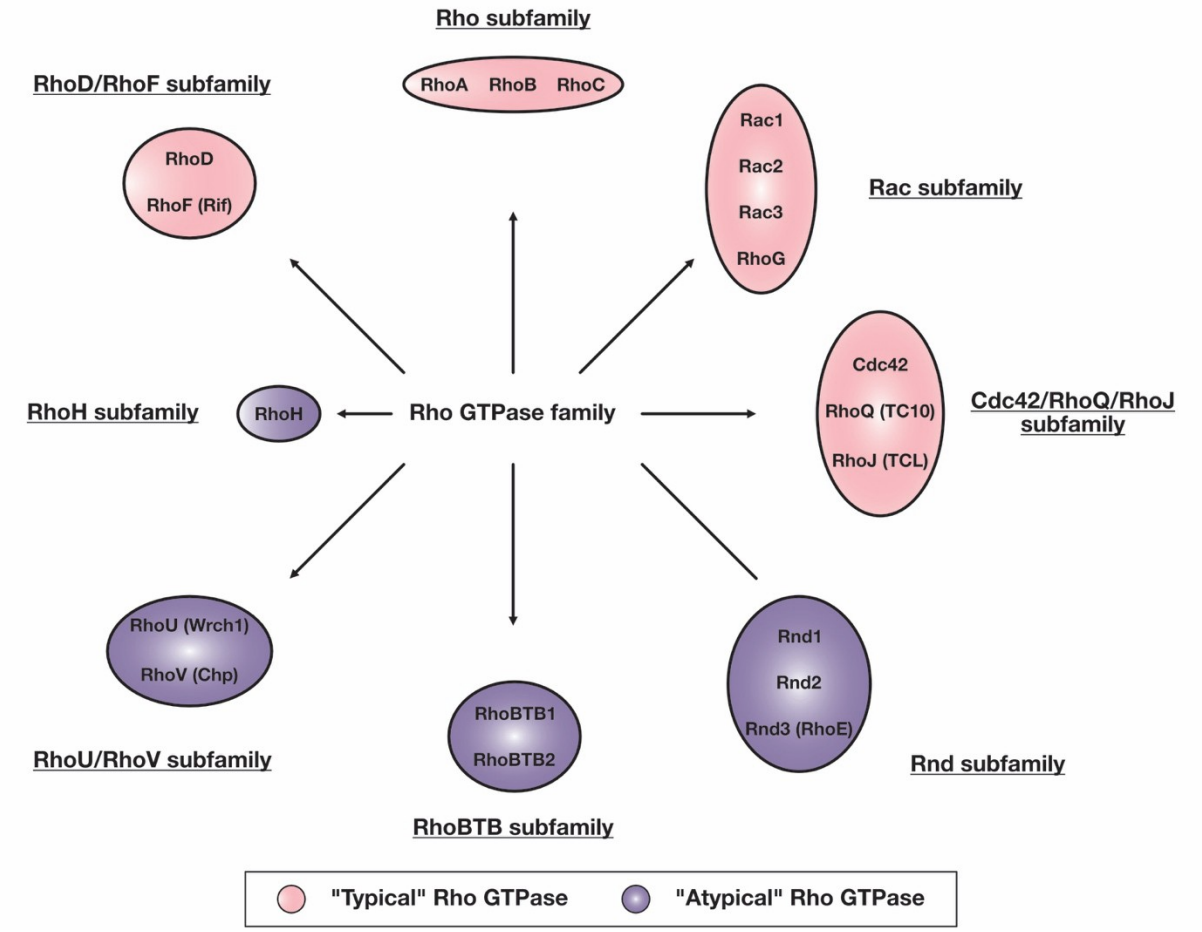


**Figure 1.2: Subfamilies within Rho GTPases.**

The Rho GTPase family comprises 20 distinct members, which can be further subdivided into eight different subfamilies[9, 15]. These members can be broadly segregated into "typical" and "atypical" Rho GTPases. This classification largely depends on the existence or non-existence of classic molecular switch mechanisms and their preferred intracellular nucleotide-binding status[9, 16, 17].

### *1.1.1 Regulation of Rho GTPase activity*

Rho GTPases, with a molecular weight ranging between 21-25 kDa[18], often contain two essential domains: the conserved GDP-/GTP-binding domain (G domain) and a C-terminal hypervariable region with a CAAX motif[7, 19-21]. Five conserved motifs within the G domain (G1 -G5) mediate nucleotide binding and hydrolysis[21]. G2 and G3, also referred to as the switch I and switch II regions of Rho GTPases, undergo structural rearrangements, thus regulating the

activity of Rho GTPases[7, 21]. Atypical Rho GTPases, such as those from the RND subfamily and RhoH, do not follow the classical switch mechanism. This could be due to missing several crucial amino acids in the G1 and G3 motifs (switch II region) within their G domains[16, 17], which are vital for nucleotide binding and hydrolysis[7, 21]. The regulation of the subcellular localization of activated Rho GTPases, often to the plasma membrane, adds an additional regulatory layer to Rho GTPase signaling. Notably, the CAAX motif within the C-terminal hypervariable region of Rho GTPases is susceptible to various posttranslational modifications on the cysteine residue, including prenylation[19, 20]. Furthermore, following prenylation on the CAAX motif, Rho GTPases may undergo carboxymethylation by isoprenylcysteine carboxyl methyltransferase (ICMT). This happens after the AAX tripeptide tail is cleaved by Ras converting CAAX endopeptidase 1 (RCE1) in the endoplasmic reticulum (ER)[22]. Finally, Rho GTPases undergo phosphorylation, which has been shown to affect not only their activation or downstream signaling but also their stability on the membrane[23-25].

### *1.1.2 RhoGDI*

Rho guanine nucleotide dissociation inhibitor (RhoGDI) plays a pivotal role in keeping Rho GTPases in their inactive state and protects them against degradation or non-specific activations[26, 27]. The N-terminal region of GDI carries out key functions. Firstly, its interaction with the switch region of Rho GTPases through the N-terminal regulatory arm prevents the dissociation of GDP[28]. Secondly, the N-terminal region of GDI attracts the positively charged Rho hypervariable region, promoting the insertion of the CAAX motif. This motif undergoes post-translational modifications, including isoprenylation—a lipid modification that adds either a geranylgeranyl or farnesyl moiety. Such modifications allow the CAAX motif to fit into the hydrophobic pocket within the GDI, thereby facilitating the detachment of Rho GTPases from the membrane[28]. It is also suggested that RhoGDIs can shuttle Rho GTPases to different subcellular compartments[29, 30]. This occurs through the formation of inhibitory cytosolic GDI-Rho GTPase complexes following the release of Rho GTPases from donor membranes[29, 31]. The human genome houses only three identified GDIs, making up the RhoGDI family: GDI1 (GDIα)[32], GDI2 (GDIβ, LY-GDI, D4-GDI)[33], and GDI3 (GDIγ)[34]. While GDI1 is ubiquitously expressed[32], the expression of GDI2 and GDI3 is confined to specific tissues;

hematopoietic tissue for GDI2, and brain, lung, and pancreas, for GDI3[34]. Uniquely, GDI3 possesses an N-terminal extension that enables it to anchor into the Golgi membrane[35].

### *1.1.3 RhoGEF*

Rho guanine nucleotide exchange factors (RhoGEFs) play a critical role in the selective exchange of GDP for GTP in Rho GTPases[19]. Interestingly, the nucleotide exchange process involves an intermediate stage where the nucleotide-free Rho protein forms a complex with the GEF. Considering the nucleotide-free Rho protein's higher affinity for intracellular GTP than for GEFs, the complex quickly dissociates, leading to the formation of an active Rho-GTP complex[36-38]. At present, the human RhoGEF family includes 74 Diffuse B-cell lymphoma (DBL) proteins and 11 dedicator of cytokinesis (DOCK) proteins[9, 39, 40].

DBL proteins, initially isolated from diffuse B-cell lymphoma cells[41], influence Rho GTPases through the DBL-homology (DH) domain[39, 42]. A genomic search for DH domain-containing proteins resulted in the discovery of 74 DBL-related GEF proteins. Of these, 46 are monospecific for Rho, Rac, and Cdc42, five are bispecific for Rho and Cdc42, and six are oligospecific for all three Rho protein subgroups[9]. Notably, despite the presence of the DH domain, usually followed by the pleckstrin homology (PH) domain, there is a low degree of homology among GEFs within the DBL family[43]. The DH domain serves a dual role: not only does it accelerate the nucleotide exchange of GDP-bound Rho GTPases by up to $10^7$-fold[39], but it also determines substrate specificity[9, 44]. Within the DH domain, three characteristic and conserved regions, each composed of 10-30 amino acid residues, form α-helices[45, 46]. The PH domain, part of the DH-PH tandem and a signature motif of the DBL family, adds additional functionality to DBL proteins by promoting membrane targeting through its ability to bind phosphoinositides[47]. This binding aids in directing DBL proteins to their appropriate partners[39]. However, some exceptions exist: nine members of the DBL family lack the C-terminal tandem PH domain, and seven of the 20 DBL proteins studied do not mediate nucleotide exchanges[9]. Moreover, the DBL family presents a wide range of functional domains that facilitate interactions with other proteins or membrane lipids[48].

On the other hand, the DOCK family of GEFs, consisting of 11 members[40], can be further classified into four subfamilies: DOCK-A, DOCK-B, DOCK-C, and DOCK-D[40, 49]. The DOCK family features two characteristic and highly conserved domains. The DOCK homology region (DHR)-1 domain guides membrane localization via lipid binding, while the DHR-2 domain provides catalytic activity, resulting in the formation of an active Rho GTPase-GTP complex[40, 49, 50]. It is important to note that while DOCK GEFs play a crucial role in regulating a broad range of biological functions, abnormal activities can contribute to diseases such as breast cancer, by promoting actin polymerization[51], and Alzheimer's disease, through the accelerated formation of amyloid β plaques[52, 53]. DOCK GEFs are known to activate Rac1 and Cdc42, but not RhoA[54, 55].

### *1.1.4 RhoGAP*

The Rho GTPase-activating protein (RhoGAP) plays an essential role in the control of the Rho GTPase cycle. It terminates Rho GTPase signaling by accelerating the intrinsic GTP hydrolysis activity of Rho GTPases, converting them back to their inactive, GDP-bound form[43, 56-58]. RhoGAPs have similarities with RhoGEFs due to their highly conserved catalytic domains[40, 45, 46, 49, 50]. The hallmark of the RhoGAP family is the highly conserved catalytic GAP domain, made up of seven α-helices [59-61]. To date, almost 70 RhoGAPs have been discovered, including p50RhoGAP, the first family member identified through biochemical analysis[59, 62-64]. The significance of RhoGAP was highlighted by observing faster GTP hydrolysis in living cells compared to under cell-free conditions, following the microinjection of GTP-bound RAS into cells[65]. The "arginine finger", a highly conserved arginine residue in the GAP domain, stabilizes the GTP-hydrolysis transition state when inserted into the GTP-binding site of the respective Rho GTPases[36, 37, 66, 67]. Structural analyses reveal that RhoGAPs interact with residues within the switch regions (I and II) of Rho GTPase[7, 57, 68], helping manage the negative charges formed during the transition state and coordinating Rho GTPases with nucleophilic water molecules[69, 70]. Comparative structural analysis has revealed similarities in tertiary structures between the GAP domains in RAS and Rho family proteins, despite differences in amino acid sequences[69, 71, 72]. Inhibitory mutations replacing the conserved arginine residue with alanine in the arginine finger can lead to persistent Rho GTPase signaling[57, 59, 73].

RhoGAP family members share functional domains with the DBL family of RhoGEFs, including PH, coiled-coil, P, SH3, and BAR/F-BAR domains. These domains provide additional capabilities such as lipid and membrane binding, peptide and protein interaction, or enzymatic activities[41, 48, 58, 66]. Around 20% of RhoGAPs lack additional domains except for highly variable N or C-termini[59]. The activity of RhoGAPs may require the cooperative function of multiple domains and/or motifs, as the GAP domain alone may be non-selective and inefficient in cell-free conditions[59]. Intramolecular autoinhibition (e.g., GRAF and OPHN1)[74] and susceptibility to posttranslational modifications (e.g., p190GAP, CdGAP, and Mgc-RacGAP)[75] have been observed. The SH3 domain in p120RasGAP can competitively and selectively inhibit the well-known tumor suppressor deleted in liver cancer 1 (DLC1), a RhoGAP, by masking the catalytic arginine finger through protein-protein interactions[76, 77]. Given the vast number and wide expression of the RhoGAP family in humans, their tightly controlled activity is essential[59]. RhoGAPs also exhibit non-conventional, GAP-independent functions that broaden our understanding of their roles. For instance, *ARHGAP36, CNTD1, DEP1, DEP2, FAM13B, INPP5P*, and *OCRL1* lack the highly conserved arginine finger within the catalytic GAP domain, rendering them catalytically inactive[59, 78]. Nevertheless, they can activate transcription factors (e.g., GLI), function as GAPs for other GTPase families (e.g., ARFGAP), and interfere with Rho GTPase signaling (e.g., regulation of cell cycle progression)[78].

### *1.1.5 Rho effectors*

Rho GTPases, upon activation, orchestrate a broad range of biological functions through their association with Rho effector proteins[79-83]. More than 70 effectors have been identified for RhoA, Rac1, and Cdc42[25], and these are broadly categorized into two types: kinases[79-81] and scaffolding proteins[82, 83]. These types participate in downstream Rho GTPase signaling once they interact with the active, GTP-bound Rho GTPases[84]. Notably, kinases such as p21-activated kinase (PAK), Rho-associated coiled-coil kinase (ROCK), citron kinase (CRIK), and protein kinase novel (PKN) mediate phosphorylation cascades[79-81]. In contrast, scaffolding proteins like the mammalian homolog of Drosophila diaphanous 1 (DIA1), Wiskott-Aldrich syndrome protein (WASP), and Rhotekin (RTKN) aid in signaling complex formation[82, 83]. Advancements in protein structure examination techniques have significantly enhanced our

understanding of the interactions between Rho effectors and Rho GTPases. The interaction between RhoA and ROCK, for instance, heavily depends on the GTPase-binding domain (GBD) within ROCK. This domain, composed of 13 residues of left-handed coiled-coil α-helices, binds to the switch and α2 regions of RhoA[85]. Similarly, the interaction and activation of Cdc42/Rac-interactive binding (CRIB) motif-containing effector proteins, such as PAK1 and WASP, by Cdc42 and Rac1, are dependent on tight structural associations with their respective Rho GTPases. The GBDs within CRIB motif-containing effectors make extensive contact α1, switch regions, as well as α5 and β2 regions of Rho GTPases[86-88]. Various mechanisms have been proposed to explain Rho effector activation by Rho GTPases. The basic region just upstream of the CRIB motif within WASP is suggested to form electrostatic interactions with glutamate residues within Cdc42 (Glu49, Glu171, and Glu178), enhancing their interaction[89, 90]. Also, two invariant leucine residues at positions 69 and 72 within Cdc42 and Rac1 have been identified to form hydrophobic contacts with CRIB motif-containing effectors, contributing to their activation[91]. Further research is needed to fully understand these activation mechanisms. For example, in the case of p67PHOX, which interacts with various Rac1 regions using an α-helical domain composed of four tetratricopeptide repeat (TPR) motifs, it does not seem to interact with the switch II region[92, 93]. This interaction appears to be common and vital for the activation of other Rho effectors[85-88].

## *1.2 Rho GTPase signaling and oncogenic transformation of cells*

Cells that have undergone transformation frequently display altered cytoskeleton organization, resulting in a fibroblast-like morphology with prominent stress fibers [94]. This characteristic is intimately associated with Rho GTPase signaling[95]. Overexpression of constitutively active mutant forms of RhoA, Rac1, and Cdc42 in rodent fibroblasts has been observed to induce anchorage-independent growth and tumor formation in nude mice[96, 97]. Similarly, overexpression of atypical Rho GTPases, like RhoU/Wrch1 and RhoV/Wrch2, in mouse fibroblasts can also exhibit oncogenic transformation capabilities, particularly when the negative regulatory $NH_2$ terminus is removed[98-100]. Elevated expression levels of Cdc42 and RhoC have been connected with increased metastasis risks in patients with hepatocellular carcinoma, which negatively impacts patient survival[101, 102]]. However, the precise mechanisms

of Rho GTPase signaling in cancer need further investigation due to its complex interactions with other potent oncogenes like *RAS* or *DBL*[96, 103]. The reliance on Rho GTPase signaling seen in malignant transformations induced by various receptor tyrosine kinases (RTKs) and non-receptor tyrosine kinases (NRTKs) may be related to the control of their subcellular localization by Rho GTPase signaling[104]. Additionally, Rho GTPase signaling contributes to the formation and maintenance of cancer stem cells. For example, RhoA and Rac1, when activated by VAV2, signal through c-Myc and Yes-associated protein (YAP) pathways. This leads to transcriptional changes that trigger a stem cell-like state with higher proliferative potential, signifying high tumorigenicity in head and neck squamous cell carcinoma (hnSCC) cells[105].

### *1.2.1 Mutations in RHOA, RAC1, and CDC42 genes in human cancers*

"Hotspot" mutations are frequently observed in various oncogenes linked to RAS-signaling, such as *RAS* and *RAF*[106]. However, aberrations in expression levels are more commonly reported than mutations for Rho GTPases[15, 107-109]. This implies a potential cooperative relationship between Rho GTPases and their effectors, as well as RAS signaling effectors such as BRAF, CRAF (RAF-1), and mitogen-activated protein kinase kinase (MEK). This relationship highlights a diminished transformative capability of Rho GTPases[96-98, 110, 111]. Crosas-Molist and colleagues proposed that Rho GTPases could play a pivotal role in tumor progression following an initial driver mutation instigated by potent oncogenes like *RAS*[95]. This hypothesis is corroborated by two observations: 1) The oncogenic transformations induced by RAS are lost when dominant-negative mutant forms of Rho GTPases are expressed, and 2) the localization and activity of the tumor suppressor protein phosphatase and tensin homolog (PTEN) are regulated by Cdc42 and RhoA[112, 113]. Numerous mutations have been identified in *RHOA*, *RAC1*, and *CDC42*, with *RHOA* mutations being the most prevalent[114-117].

Advancements in next-generation sequencing have identified three primary mutation hotspots on the *RHOA* gene, leading to alterations in the RhoA protein at sites R5, G17, and Y42. These mutations affect 15-25% of patients with diffuse gastric cancer[114]. Notably, the Y42 mutation, specifically Y42C and located within the RhoA's switch I domain[118], is the most common among patients with diffuse gastric cancer[114]. These mutations have also been detected in stomach adenocarcinoma and Burkitt lymphoma[119]. From a mechanistic perspective, the

RhoA-Y42C mutation is often associated with the loss of E-cadherin or the tumor suppressor p53 in diffuse gastric carcinoma[120-122]. This mutation enhances binding to the effector protein ROCK and impedes GTP hydrolysis, leading to a gain-of-function phenotype. However, the interaction of RhoA-Y42C with GEFs and GDIs remains unchanged[122]. Besides diffuse gastric cancers[114], mutations in *RHOA* have been associated with bladder cancer, hnSCC, and breast cancer in humans, involving E40Q, G17A, and R5W point mutations[116, 117]. Furthermore, fast-cycling mutations, specifically C16R and A161P, have been observed in adult T-cell leukemia/lymphoma (ATLL), leading to an accelerated exchange between GDP and GTP-bound states[115]. In contrast to Y42 mutation, the G17V mutation in RhoA is predominantly found (> 90%) in certain subtypes of peripheral T-cell lymphomas including angioimmunoblastic T-cell lymphoma (AITL) and peripheral T-cell lymphoma not otherwise specified (PTCL-NOS). The G17V mutation impacts nucleotide binding as well as interactions with RhoGEFs, functioning as a dominant negative mutant[123-126]. Considering these mutations can significantly alter the three-dimensional structure of RhoA[122-126], the signaling pathways activated by mutant RhoA may greatly vary[95].

Similar to RhoA, fast-cycling mutations have been identified in the *RAC1* gene, leading to alterations in the Rac1 protein. These changes include Rac1-N92I in melanoma, myeloma, and sarcoma; Rac1-C157Y in prostate cancer; and most notably, Rac1-P29S[127-129]. At the molecular level, these mutations enhance interactions with downstream effectors such as PAK1, mixed lineage kinase 3 (MLK3), and the WASP-family verprolin-homologous protein (WAVE) complex[130, 131]. These interactions are implicated in oncogenic transformation, characterized by the cells' growth factor and anchorage-independent survival. Upon systemic overexpression, these interactions can further precipitate mesenteric lymphomas, thymic lymphomas, and squamous cell skin tumors in mice[132]. Furthermore, evidence exists indicating crosstalk between Rho GTPase signaling and RAS-MAPK signaling pathways. Increased tumorigenesis has been observed in melanoma mouse models expressing both the Braf-V600E and Rac1-P29S mutations[132]. The Rac1-P29S mutation has also been found to promote melanoma in mice deficient in *Nf1* and *Trp53*[132]. Mechanistically, the combined effect of these mutations grants resistance against apoptosis and reduces the effectiveness of RAF and MEK inhibition[133]. This resistance is mediated by escalated expression of PD-L1, an immune system suppressor, in melanoma patients carrying Rac1-P29S mutations[134].

Compared to *RHOA* and *RAC1*, where numerous point mutations are found, *CDC42* has only one known mutational hotspot, K166[114-117]. At present, mutations are largely limited to *RHOA*[116]. This could be due to their frequent involvement in cancer metastasis[135, 136], where typical pathogenic events involve transcriptional reprogramming and altered gene expressions, rather than specific mutations[137].

### *1.2.2 Role of Rho GTPases in cancer metastasis*

Influenced by Rho GTPases, cancer cells can dynamically switch their mode of migration to invade and colonize distant organs. A critical event in this process is the epithelial-to-mesenchymal transition (EMT), a mechanism exploited by cancer cells to dismantle cell-cell adhesions and establish front-rear polarity[1]. Three key Rho GTPases, RhoA, Rac1, and Cdc42, orchestrate migration by balancing protrusive and retractile movements. Rac1 and Cdc42 guide the formation of lamellipodia and filopodia, respectively—actin-rich protrusions at the leading edge—while actomyosin contractility, driven by the RhoA-ROCK-Myosin II pathway, controls the retraction at the rear[138]. Cancer cells can migrate either individually or as a collective, maintaining cell-to-cell adhesions (collective migration). Individual migration can be subdivided into elongated-mesenchymal migration and amoeboid migration[139-142]. Interestingly, amoeboid migration, characterized by lower matrix adhesion, high cortical actomyosin contractility[139, 140], and protease-independence[140, 143] or diffuse protease-mediated extracellular matrix (ECM) degradation[144], offers faster migration speeds. The plasticity of cancer cells is demonstrated by hypoxia-induced switches from collective to amoeboid migration in both breast cancer and squamous cell carcinoma[145]. Intravasation, the process by which cancer cells penetrate circulation by breaching blood vessel walls, is another critical aspect of metastasis[146, 147]. Tumors with greater vascularization show increased intravasation rates[147]. Once in the bloodstream, cancer cells must withstand various stressors, including immune system attacks, shear stress, and a lack of matrix adhesion, illustrating the complex, multi-step nature of metastasis[146]. Importantly, Rho GTPases, particularly RhoA, appear to play a crucial role in survival of cancer cells in the bloodstream[146, 148]. Depletion of ROCK1/2 in amoeboid melanoma cells has been shown to reduce tumor cell retention in the lung, and when ROCK activity is inhibited, cancer cells display decreased viability, matrix attachment, and proliferation

upon exposure to mechanical shear stress[146]. Therefore, a deeper understanding of Rho GTPase function could lead to innovative strategies to limit cancer cell survival and metastasis.

#### *1.2.2.1 RhoA*

RhoA plays an essential role in the migration of cancer cells, regulating both the protrusive and retractile movements of the cell[138, 149]. The strong interaction between RhoA and ROCK governs the retraction of the cell body in breast cancer cells[138]. An important aspect of this retractile movement may be the formation of caveolae, small invaginations in the cell membrane, in response to low membrane tension. In this scenario, the RhoGEF, epithelial cell transforming 2 (ECT2), is recruited by caveolin-1 to promote RhoA activation, which may be critical for retraction[150]. The retractile movement, regulated by RhoA, is particularly significant in collective migration[141, 142], where high actomyosin contractility at the rear of migrating groups is crucial[151]. Numerous studies have emphasized that cancer cells and leukocytes rely on actomyosin contractility, controlled by RhoA-ROCK interaction, to facilitate a switch towards amoeboid migration when confined[152-154]. Another mechanism for switching migration involves the ubiquitin ligase, SMAD ubiquitin regulatory factor 1 (SMURF1). This enzyme targets RhoA for degradation at the leading edge of cells displaying mesenchymal migration. When SMURF1 is inhibited, it promotes amoeboid migration and simultaneously enhances the invasion and intravasation abilities of melanoma and colorectal cancer (CRC) cells[155]. The significance of the Rho family in modulating cell migration, especially the amoeboid style of movement, is further signified by studies involving RhoB[156] and RhoC[157]. For instance, the loss of RhoC in a mouse mammary adenocarcinoma model led to a significant decrease in cell motility and metastasis development[136]. In contrast, overexpression of RhoC promoted metastatic dissemination in melanoma cells, establishing its relevance to the metastatic process[135]. The role of Rho GTPases extends beyond cell migration to intravasation, a critical step in metastasis. For example, in a zebrafish model, overexpression of *RHOC* in breast adenocarcinoma cells resulted in a rounded amoeboid behavior, aiding cancer cell intravasation[158]. Additionally, amoeboid cancer cells with high RhoA-ROCK activity, further sustained by the direct physical interaction and induction of RhoA activity by macrophages[159], showed an increase in invasion and intravasation[155].

#### *1.2.2.2 Rac1*

Overexpression of Rac1 often associates with an increase in EMT, linked with poor prognosis in multiple human cancers, such as non-small cell lung cancer (NSCLC)[160] and ovarian cancer[161]. Within ovarian cancer cells, extracellular signal-regulated kinase 2 (ERK2) stimulates Rac1/c-Jun N-terminal kinase (JNK) signaling via the activation of the Rac1 GEF, DOCK10. This activation leads to increased expression of the transcription factor, Forkhead Box O1 (FOXO1), conferring migratory phenotypes to the cells[162]. The activity of Rac1 is related to various modes of individual cell migration, including elongated-mesenchymal movement and amoeboid migration[163, 164], as well as collective migration, where Rac1-driven protrusions are seen in leader cells[165, 166]. For instance, breast cancer cells showcased Rac-facilitated, mesenchymal migration in wider channels, whereas, in confined narrow microchannels, they displayed blebbing, an amoeboid phenotype hallmark, and faster migration[167]. Most notably, the elongated-mesenchymal migration of melanoma cells can be attributed to Twist1, which collaborates with B-cell specific Moloney murine leukemia virus integration site 1 (BMI1) to suppress the microRNA *let-7i*, resulting in elevated expression of the Rac1 GEF, DOCK3[139, 168, 169]. These findings underscore the significance of active Rac1 levels as a critical determinant of migration mode. This is influenced by the interaction between Rac1 and p67PHOX, which culminates in the production of reactive oxygen species (ROS)[170-172]. Specifically, the activation of the ROS-sensitive RhoGAP, ARHGAP5, inhibits Rho signaling in melanoma cells engaging in elongated-mesenchymal movements. Conversely, ROS inhibition by antioxidants triggered a surge in three-dimensional amoeboid invasion and metastasis[163, 164]. This observation is corroborated by the fact that blocking Rac1 signaling steers metastatic melanoma colonization through the preferential use of amoeboid migration[139]. However, maintaining the ability to switch between different modes of migration, hence bestowing plasticity upon cancer cell migration, might be crucial for cancer metastasis. Supporting this idea, melanoma cells bearing the Rac1-P29S mutation, which likely curtails ROS production[172], failed to construct functional invadopodia[173] and could not synergize with v-Raf murine sarcoma viral oncogene homolog B (BRAF) mutant mouse models to promote lung metastasis further[132].

#### *1.2.2.3 Cdc42*

Cdc42 is a major player in cell migration, regulating the protein Formin-like protein 2 (FMNL2), which, in partnership with profilin, enables this essential cellular function[174]. Notably, the activation of Cdc42 is dictated by its environment, particularly collagen at the leading edge of the cell, via the GEF β-P21-activated kinase-interacting exchange factor (β-PIX) and Slit-Robo GTPase-activating protein 1 (SrGAP1), fostering migration in fibrillar collagen[175]. The ECM surrounding the cell profoundly influences this activation process. For instance, the fibronectin matrix fails to activate β-PIX via α2β1 integrin signaling[175], highlighting the intricate interplay between cellular migration and the adjacent microenvironment. A study involving melanoma cells unveiled the variety of ways Cdc42 can impact cancer cell migration. In this research, Cdc42, through its effector protein Binds to Rho GTPases 3 (BORG3) and in conjunction with septin 9 (SEPT9), mediated actomyosin contractility and three-dimensional amoeboid migration[176]. Importantly, inhibition of Cdc42 in melanoma cells stifled both amoeboid and mesenchymal migration[176], implying that Cdc42 facilitates migration via diverse activator/effector pathways. Beyond cell motility, Cdc42 significantly contributes to the generation of mechanical forces at cell-cell junctions. Through P-cadherin mediated Cdc42 activation, it governs cell polarization and induces collective migration[177]. In terms of the role of Cdc42 in intravasation, a downstream effector of Cdc42 named N-WASP, is crucial for the formation of invadopodium and intravasation of mammary tumor cells[178]. Consequently, Cdc42 appears as a multifaceted participant in various stages of cell migration and intravasation.

### *1.2.3 Role of Rho GTPase signaling as tumor suppressors*

While it is less common, both *in vitro* and *in vivo* studies have provided evidence suggesting that Rho GTPases and their regulators can also function as tumor suppressors[179-184]. For instance, RhoB was shown to impair tumor growth by inducing apoptosis, in response to stress stimuli such as DNA damage and hypoxia[179-181]. In mouse fibroblasts, HRAS was found to repress RhoB expression via AKT, while HRAS-induced transformation was countered by the ectopic expression of RhoB[182]. Further evidence of the tumor-suppressive role of RhoB was demonstrated by increased skin tumor formations in mice subjected to a global *RhoB* knockout[181]. Rac1 has been identified to play tumor-suppressive roles, influencing cellular

senescence[130, 131, 185, 186], cell cycle[187, 188], and apoptosis[189-191]. For instance, Rac1 was found to hinder the assembly and constriction of the contractile ring, mediated by RhoA, ROCK, and Myosin II[192, 193], rendering its inactivation crucial for successful cytokinesis in mammalian cells[187]. Moreover, the induction of senescence during HRAS-driven transformation of normal human fibroblasts was mediated by Rac1 and NADPH oxidase 4 (NOX4), which increased ROS levels, elevated genomic instability, and subsequently led to p53 activation[130, 131, 194, 195]. In *Rac1*-knockout mouse embryonic fibroblasts (MEFs), the compensatory upregulation of *Rac3* triggered cellular senescence through ROS-mediated activation of p53[196]. In addition to Rac1, Cdc42 has also been identified as having a tumor-suppressive role through the induction of cellular senescence[197, 198]. For example, elevated Cdc42 activity was observed in several tissues of aged mice. Furthermore, a reduced function of Cdc42 GAP was inversely associated with increased genomic instability and premature induction of p53-dependent senescence in MEFs[198].

Aside from typical Rho GTPases, there are indications of the tumor-suppressive roles of atypical GTPases, which may be regulated by different mechanisms[15]. For example, Rnd3/RhoE was found to inhibit the transformation of mouse fibroblasts induced by RAS or RAF[183]. The role of atypical Rho GTPases as tumor suppressors was further supported by RhoBTB3, whose activity significantly reduced the tumorigenic potential of RAS or Early region 1A (E1A)-transformed MEFs[184], and by RhoBTB2 in *Drosophila* epithelial models. In the latter case, the deletion of *RhoBTB* (*Drosophila* ortholog of human *RHOBTB2*) not only increased anchorage-independent growth but also tumorigenesis through cooperation with Yki (YAP/TAZ orthologs)[199].

#### *1.2.3.1 Mechanisms underlying tumor suppressive roles of Rho GTPases*

Rho GTPases are potentially capable of preventing tumor formation through several proposed mechanisms: 1) by controlling progenitor differentiation[200-202], 2) by maintaining and regulating cell polarity[202, 203], and 3) by promoting apical extrusion[204-206]. For example, the deletion of a chromosomal region, leading to the loss of one copy of the *CDC42* allele, is frequently observed in neuroblastomas with *N-MYC* amplification[200]. A reverse correlation between *N-MYC* and *CDC42* gene expression was further evidenced by a reduction in *CDC42* gene expression in neuroblastoma cells following *N-MYC* overexpression[200]. Crucially,

increased differentiation of neuroblastoma cells into neurons was associated with the ectopic expression that elevated Cdc42 activity[200]. Similarly, deletion of the *CDC42* gene from mouse bone marrow resulted in the suppression of erythroid differentiation and the hyperproliferation of blood progenitors[201]. Finally, epithelial cells transformed by HRAS-G12V were eliminated into the lumen via a process known as "apical extrusion". This process, resembling the expulsion of apoptotic cells from an epithelium[207], involves the cooperative functions of Cdc42, ROCK, and Myosin-II[205, 206].

## *1.3 Prostate cancer: general overview*

The prostate plays an essential role in preserving sperm health post-ejaculation and enhancing fertility by adding nutrient-rich alkaline fluid to the semen[208]. Relative to other structures in the urogenital tract, the prostate possesses a heightened predisposition towards malignant transformations[209]. Prostate cancer (PCa) typically arises from the epithelium, comprised of luminal, basal, and rare neuroendocrine (NE) cell types[210]. Luminal epithelial cells, expressing androgen receptors (AR), line the internal surfaces of the prostate ducts and secrete fluids and glycoproteins, known as prostate-specific antigens (PSA). The basal and NE cell types, in contrast, do not express ARs and remain ligand-independent (i.e., testosterone), allowing for their survival and proliferation in the absence of androgen[211]. From a socioeconomic standpoint, PCa is a major concern, affecting roughly one in six men[212]. The World Health Organization (WHO) records nearly 1.5 million new diagnoses worldwide, making PCa the second most frequently diagnosed disease and the fifth leading cause of cancer-associated deaths among males[213]. Clinically, PCa affects regional lymph nodes in the pelvis below the bifurcation of the common iliac arteries and can metastasize to the lung, liver, and most commonly, the bone[214]. Over 90% of newly diagnosed PCa patients are reported to present with organ-confined or locally advanced cases[215], suggesting a favorable prognosis for the majority of cases[212]. However, despite these early-stage diagnoses, the 5-year survival rate plummets from approximately > 99% to 32% if cancer has spread to other body parts[216]. Additionally, despite the use of diagnostic techniques such as blood tests to assess PSA levels and digital rectal examinations[212], nearly 20% of patients are found to have widespread metastasis at the time of diagnosis[217]. This discrepancy in reported percentages may stem from

variations in study populations, diagnostic criteria, or other factors[212, 217], but it underscores the challenge in accurately predicting disease progression and highlights the urgent need for molecular biomarkers to better understand PCa pathogenesis. Histopathological changes such as disruption of normal cellular architecture and nuclear atypia of luminal cells[218], may be graded using the "Gleason Score" system, established by the International Society of Urologic Pathology (ISUP), to depict the aggressiveness of adenocarcinoma[219]. Higher Gleason Scores are associated with increased PCa aggressiveness and a higher risk of 5-year biochemical recurrence, defined as the rise in PSA levels above nadir—the lowest point in PSA levels following radical prostatectomy[220].

### *1.3.1 Pathogenesis of PCa*

More than 90% of PCa cases are acinar adenocarcinomas, frequently entailing prostatic intraepithelial neoplasia (PIN), which originates from the benign epithelium of the acini or ducts within the prostatic gland[221-223]. PIN can be classified into low-grade and high-grade PIN, with high-grade PIN associated with a greater likelihood of progression toward adenocarcinoma. However, high-grade PIN does not raise PSA levels in the serum and cannot be detected through digital rectal examinations, only by needle biopsy[224, 225]. In the initial stages of pathogenesis, PCa growth is heavily dependent on AR, activated by ligand binding (i.e., testosterone and dihydrotestosterone). Upon ligand-bound receptor translocation to the nucleus[215, 226], interactions of motifs within the DNA-binding domain and ligand-binding domain promote AR homodimerization. This homodimer then binds androgen response elements (AREs) within transcriptional target genes, regulating cellular differentiation, proliferation, and apoptosis[227-229]. Moreover, several post-translational modifications, including phosphorylation, acetylation, and ubiquitination, further fine-tune AR signaling[230, 231]. Due to the diverse roles of AR, androgen-deprivation therapy (ADT), whether via surgical methods or chemical castration aimed at lowering testosterone levels, is commonly employed to thwart PCa spread to other organs[215, 226]. However, resistance to ADT is prevalent, with patients inevitably advancing to castration-resistant prostate cancer (CRPC) within 18 to 36 months[215, 232, 233]. Mechanisms underlying this progression involve modifications in AR signaling, which may transpire through *AR* gene amplification and altered levels of AR cofactors[215, 232-234]. Furthermore, mutations in *AR* or the

use of splice variants, enhancing the functionality of the Activation Function-1 (AF-1) domain (one of the two functional domains of AR, whose activation is androgen-independent), may also contribute to this pathogenic progression[215, 232-235].

### *1.3.2 General Risk factors associated with PCa*

As outlined by Perdana *et al.*, risk factors for PCa can be categorized into non-modifiable and modifiable risk factors[236]. Non-modifiable factors encompass age, race, and family history[236]. Race and ethnicity have a substantial correlation with PCa incidence[237], with elevated rates reported in Europe and Asia (33.5% and 26.5%, respectively), compared to continents such as Africa (6.6%) and Oceania (1.6%)[213]. Based on data from the National Cancer Institute, African American men experience the highest incidence rate within the United States, affecting one in six men compared to other ethnic groups, such as non-Hispanic white men[213]. Transcriptomic analyses have revealed differences in the expression of inflammatory and DNA repair genes between African American men and non-Hispanic white men, with upregulated or downregulated expression among African American men, respectively[238]. Additionally, alterations in metabolic pathways and cell cycle progression have been noted[239]. Moreover, a specific genetic variant, rs72725854, prevalent in populations of African and Caribbean descent and West Africans, which is more susceptible to mutation, has been associated with high PCa frequencies[240]. Analogous to race and ethnicity, a family history of any cancer or PCa in first-degree relatives significantly escalates PCa risks[241, 242]. This risk is attributed to mutations in DNA repair genes (*MLH1, MSH2, MSH6,* and *PMS6*) and homologous recombination genes (*BRCA1/2, ATM, PALB2,* and *CHEK2*)[213]. Age is another prominent non-modifiable risk factor; the risk of PCa rapidly ascends after age 50[243-245], and over two-thirds of newly diagnosed PCa patients are over 65[246].

Modifiable risk factors for PCa include obesity, smoking, and diet[236]. Numerous meta-analyses have confirmed the positive correlation between obesity and PCa incidence[247, 248]. Smoking is recognized to be carcinogenic due to genotoxic and nongenotoxic effects, largely attributable to polycyclic aromatic hydrocarbons (PAH)[249]. This fosters PCa progression by aiding cancer cell proliferation and conferring resistance to apoptosis[250]. Meta-analyses emphasize the risks of smoking, with current smokers having nearly a 30% increased risk of

developing fatal PCa[249] and significantly higher recurrence rates among both current and former smokers compared to lifelong non-smokers[251]. Diet is intricately linked with obesity and significantly impacts PCa risk. A high-fat diet amplifies the risk of developing prostate, breast, and colon cancers[252, 253]. High dairy intake of milk and calcium (> 2,000 mg/day) is strongly associated with heightened PCa aggressiveness[254]. Although the exact mechanisms remain elusive, calcium might stimulate malignant transformations within the prostate by promoting cancer cell growth and providing resistance to apoptosis[255].

### *1.3.3 Molecular risk factors associated with PCa*

At the molecular level, ARs play a significant role in the progression of PCa[209]. An inverse relationship has been discovered between androgen levels and PCa aggressiveness, with low serum androgen levels associated with an increased risk of PCa recurrence and advanced pathology[256]. Under conditions of low androgen, selective pressure on luminal cells may result in androgen-independent growth[209]. The prognostic importance of AR is demonstrated by studies revealing elevated levels of *AR* gene amplification in androgen-independent PCa cells[257]. Mutations in *AR* are rare among primary PCa but prevalent in CRPC[258, 259]. Over 1,000 mutations in *AR* have been reported thus far, with more than 15% (159 mutations) predisposing men to PCa[260]. Mechanistic studies have demonstrated these *AR* mutations can lead to increased AR sensitivity in response to ligand scarcity[257, 261], non-androgen ligand binding, ligand-independent activation of AR signaling, and activation of other growth factor signaling pathways[262]. In addition to *AR* mutations, upregulation of *ERBB2/HER2*, a member of the epidermal growth factor receptor (EGFR) family, has been observed in CRPC and may be accountable for androgen-independent transcriptional activation of ARs[263, 264]. In CRPC, the phosphoinositide 3-kinase (PI3K)-AKT-mammalian target of rapamycin (mTOR) pathway is often excessively activated[265, 266]. The importance of this pathway in CRPC is underscored by the frequent mutations (20%) seen in the tumor suppressor gene *PTEN*, which negatively regulates the PI3K-AKT-mTOR pathway[267]. Loss of *PTEN* can lead to abnormal PI3K-AKT-mTOR signaling and impaired AR regulation[263], contributing to PCa aggressiveness. Up to 20% of high-grade tumors lack PTEN expression[268]. Moreover, the dysregulation of Rho GTPase

signaling, which plays diverse roles in cells, may enhance tumorigenesis as well as metastasis in PCa[269-271].

### *1.3.4 Role of Rho GTPases in PCa*

Rho GTPases, serving as both tumor suppressors and oncogenes, play critical roles in PCa. The tumor suppressive RhoE/Rnd3 negatively regulates cyclin B1 and Cdc42, inducing cell cycle arrest and apoptosis in PCa cells, and is downregulated in prostate tumors[272]. In contrast, RhoA, Rac1, and Cdc42 function as oncogenes in PCa. RhoA, working with ROCK and Myosin II, increases resistance to membrane disruption in PCa cells, as evidenced in a fluid shear stress assay[269]. Furthermore, ROCK, through its association with LIM domain kinase (LIMK) and cofilin, stimulates YAP activity to promote migration in PCa cells, suggesting a mechanism by which Rho GTPase signaling may enhance lymph node invasion[273]. Notably, the gain-of-function mutant, Rac1-Q61R, analogous to Q61 mutants in KRAS, has been identified in PCa[274]. Cdc42 regulates β1-integrin expression, which is essential for the interaction between cancer and endothelial cells. Depletion of Cdc42 hampers metastasis in PCa[270]. Rho GTPase regulators and downstream effectors also play significant roles in PCa. The expression of T-cell lymphoma invasion and metastasis-inducing protein 1 (TIAM1), a Rac1 GEF, is increased in prostate carcinoma[275]. Phosphatidylinositol-3,4,5-triphosphate-dependent Rac exchange factor 1 (P-REX1), a RacGEF, is crucial for resistance to VEGF/VEGFR-targeted therapy. Silencing *P-REX1* diminishes Rac1 hyperactivation in therapy-resistant cancer stem cells and augments responsiveness to bevacizumab (anti-VEGF) and sunitinib (anti-VEGFR)[271].

### *1.3.5 Targeting Rho GTPases in PCa*

A variety of *in vitro* and *in vivo* studies have uncovered promising results in the treatment of PCa by impeding Rho GTPases. For example, NSC23766, a compound engineered to interrupt the interaction between Rac1 and TIAM1 effectively ceases the proliferation, anchorage-independent growth, and invasiveness of PCa cells[276]. Similarly, AZA1, a dual inhibitor of Rac1 and Cdc42, attenuates the proliferation and migration of PCa cells *in vitro* and improves survival rates in xenograft mouse models[277]. Utilizing a targeted approach to inhibit Cdc42, a small molecular inhibitor known as ZCL278 obstructs the interaction between Cdc42 and its GEF,

intersectin, resulting in a substantial reduction in the migration of metastatic PCa cells by inhibiting actin-based motility[278]. Additionally, the downstream signaling of RhoA can be modulated by targeting ROCK[279]. For instance, the ROCK inhibitor, Y-27632, has demonstrated a significant reduction in PCa metastasis in mice[280].

## *1.4 Rho GTPase signaling in development*

*in vivo* studies of Rho GTPases have significantly enriched our understanding of their roles within a physiological setting. Their importance can be underscored by their vital functions during embryonic development[281]. For example, germline deletions of *Rac1* and *Cdc42*, two of the most extensively researched Rho GTPases[9, 15], result in early embryonic lethality around embryonic day (E) 5.5 (E5.5). These embryos exhibit reduced size, suggesting that Rac1 and Cdc42 play pivotal roles prior to the commencement of gastrulation[282, 283]. The role of another Rho GTPase, RhoA, in embryonic development has not been as thoroughly examined, although its removal also culminates in embryonic lethality[284]. The critical role of Rho GTPases in embryonic development is further emphasized by the rare familial disease known as "Adams-Oliver syndrome" (AOS). In this disorder, a nonsense, truncating mutation has been identified in CdGAP, a GAP for Rac1 and Cdc42, encoded by *ARHGAP31*[285]. Moreover, affected individuals frequently display transverse terminal limb defects (TTLD)[286, 287], which bear a striking resemblance to the phenotypes of limb bud-specific deletions of *Rac1* and *Cdc42*, leading to shorter limbs and a plethora of skeletal abnormalities[288, 289].

### *1.4.1 Rac1*

During embryogenesis, Rac1 proves critical in the gastrulation stage, particularly for the establishment of the anterior-posterior body axis[290, 291]. A germline deletion of Rac1 disrupts the anterior-posterior body axis due to defective collective migration of anterior visceral endoderm (AVE) cells[291]. These AVE cells set the presumptive anterior end and create the anterior-posterior axis in E6.0 mouse embryos[292]. Rac1 manages the shape and movement of AVE cells in a cell-autonomous manner, primarily by controlling the actin cytoskeleton[291]. Intriguingly, only the conditional deletion of Rac1 in the visceral endoderm, mediated by a transthyretin-Cre

recombinase, resulted in abnormal AVE cell migration or a disrupted anterior-posterior body axis. In contrast, Rac1 deletion in the epiblast did not trigger these effects[291]. Rac1 is indispensable for both cell-cell and cell-matrix adhesion during collective migration[290, 291]. For instance, upon Rac1 depletion in the epiblast, the resultant embryos display disorganized somites and an enlarged primitive streak. These changes correlate with failures in EMT, exemplified by impaired migration of mesodermal cells away from the primitive streak and pronounced alterations in actin cytoskeleton structures, including lamellipodia and filopodia[290].

### *1.4.2 Cdc42*

Cdc42, acting as a cell polarity regulator, was first implicated as important when Cdc42-null embryoid bodies exhibited unusual apoptosis of cells attached to the basement membrane[293]. Changes were observed in epiblast cells, demonstrating a diffuse expression pattern of α-catenin, β-catenin, and E-cadherin, and in ectodermal cells, where the expression level of the tight junction protein, Zonula Occludens 1 (ZO-1), was diminished[293]. Significantly, the expression level of atypical Protein kinase C (PKC), a pivotal factor in establishing polarity in epithelial cells[294, 295], was also reduced[293]. The key role of Cdc42 in maintaining epithelial cell polarity is due to its ability to assemble a complex with Partitioning-defective 6 (Par6) and αPKC at the apical plasma membrane[294, 295]. PTEN-mediated segregation of phosphoinositides may assist Cdc42 recruitment to the apical membrane[296]. This process is of paramount importance, considering that many organs comprise tubules lined by polarized epithelium, which serve as both a transport and diffusion barrier, selectively enabling nutrient absorption[297]. Therefore, a dysfunctional Cdc42 during embryogenesis could lead to severe outcomes. Evidence of the critical role of Cdc42 during organogenesis comes from targeted ablations of Cdc42 during the development of the pancreas[298], lung[299], and kidney[300]. For instance, when Cdc42 was deleted at the onset of pancreatic development, the localization of the apical membrane protein, mucin, was disrupted[298]. Moreover, Cdc42 proved essential for branching morphogenesis during lung development. The lungs of Cdc42-deficient embryos at E14.5 appeared enlarged and dilated, with disorganized tubules, manifesting neonatal deaths due to respiratory failure[299]. At the molecular level, the expression levels of the apical membrane proteins ZO-1 and Par3 were dramatically reduced, and E-cadherin was mislocated at the apical

surface of the epithelium[299]. Similarly, catastrophic effects were noted following the podocyte-specific deletion of Cdc42, resulting in postnatal death due to renal failure[300].

## *1.5 CdGAP: general overview*

The discovery of CdGAP can be attributed to the utilization of the Y40C mutant of Cdc42 as bait, identifying a novel serine- and proline-rich GAP in a yeast two-hybrid screen[301]. The gene encoded a protein of about 820 amino acids, with a predicted molecular weight of ~90 kDa. Interestingly, when overexpressed in fibroblasts, CdGAP was capable of down-regulating Cdc42-dependent filopodia and Rac-dependent lamellipodia, but not Rho-dependent stress fiber formation[301]. The protein was found to have five proline-rich sequences in the carboxyl terminus, with a potential SH3 binding motif, pXPpXP (where p indicates a preference for proline residues)[301]. Following the discovery of the mouse CdGAP, a search for homologous genes led to the identification of a human cDNA (KIAA1204) that encoded an orthologous protein, exhibiting high sequence similarity within the entire amino acid sequence (76%) and within the RhoGAP domain (97%)[302]. The mRNA of both mouse and human CdGAP showed ubiquitous expression, with higher levels in the heart[302]. Moreover, both forms exhibited a dramatic shift in migration (detection at 250kDa) when resolved by SDS-PAGE, suggesting susceptibility to post-translational modifications[302, 303]. Overexpression of CdGAP in various cell types reduced cell spreading and lamellipodia formation[285, 304, 305], pointing towards its biological functions. The protein's activity has been found to be regulated through phosphorylation[303, 306, 307], protein-protein-interaction with scaffolding proteins[304, 308, 309], as well as autoregulation[285]. Current understanding defines CdGAP as a protein comprising several domains, including an N-terminal GAP domain, a stretch of poly-basic residues[310], a basic-rich (BR) central region, a proline-rich domain (PRD), and a largely unstructured C-terminal region. Each of these domains carries out unique functions[307] (Figure 1.3).

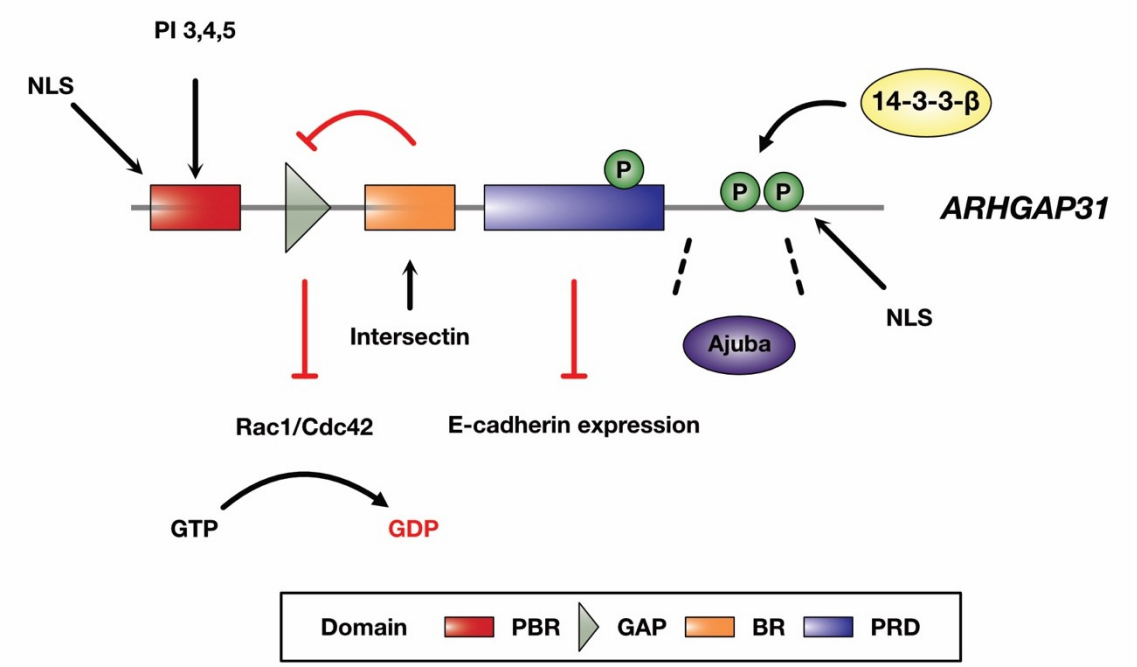


**Figure 1.3: Regulatory domains of CdGAP.**

CdGAP, as it is currently understood, is composed of several regulatory domains, each linked with unique biological functions: PBR, GAP, BR, PRD, and the C-terminus[307, 310]. The subcellular localization of CdGAP can be directed by several mechanisms. For instance, its membrane localization is regulated by the PBR[310], while the scaffolding protein Ajuba preserves CdGAP in its inactive state at cell-cell contacts by interacting with CdGAP's C-terminal region[309]. Furthermore, cytoplasmic retention of CdGAP is assisted by the binding of two phosphorylated serine residues (Ser1093 and Ser1163) by 14-3-3β[307]. In addition, the GAP activity of CdGAP can be impeded via the interaction between its BR and the scaffolding protein intersectin[304, 308]. Of major significance, CdGAP is capable of translocating to the nucleus to modulate the transcription of genes (such as E-cadherin) using its PRD, a function independent of GAP[311]. This action is facilitated by nuclear localization signals found at both the N and C-terminus of CdGAP[312].

### *1.5.1 Functions associated with the poly-basic region (PBR)*

Dysfunctional RhoGAPs, including CdGAP, are intimately associated with the pathogenesis of human diseases[5, 285]. Their activity, therefore, requires stringent spatial and temporal regulation[59]. Multiple mechanisms for this regulation have been identified, one of which involves a small polybasic region (PBR) near the N-terminus of CdGAP. Preceding the GAP domain, this region is essential for dictating the membrane localization of CdGAP[310]. A lipid overlay assay has shown that CdGAP's PBR strongly associates with several lipids, such as PI(4)P, PI(4,5)$P_2$, PI(3,4,5)$P_3$, and cardiolipins. However, only PI(3,4,5)$P_3$ could bind to CdGAP when lipids were inserted into vesicular membranes[310]. This interaction between the PBR and PI(3,4,5)$P_3$ is vital for the translocation of CdGAP to the plasma membrane, a process reliant on phosphatidyl inositol-3 kinase (PI3K). This process further modulates Rac1 activity[310]. The significance of PBR in CdGAP's translocation was further elucidated through site-directed mutagenesis. In this approach, the substitution of lysine residues within the PBR with glutamine residues led to a significant reduction in cell rounding—an outcome ascribed to altered GAP activity of CdGAP. Also, a truncation lacking the PBR (17-1425), or a dysfunctional PBR (KQ mutant), increased the spreading of COS-7 cells on fibronectin, an effect mirroring the phenotype of a GAP-dead CdGAP mutant[310]. Like CdGAP, other RhoGAPs, such as p190RhoGAP and DLC1, also harbor PBRs that mediate their interactions with lipids, crucial for their GAP activity and cellular functions[313-315]. However, the electrostatic interactions between the PBR and lipid heads do not directly determine lipid binding specificity. Instead, affinities against several lipids have been observed to correlate directly with an increase in positively charged CdGAP and DLC1[310].

### *1.5.2 Functions associated with basic-rich (BR) central region*

Researchers embarked on a mission to identify binding partners for the C-terminal PRD of CdGAP. This pursuit led to the uncovering of an endocytic scaffolding protein, intersectin[304]. Intersectin comprises two N-terminal Eps-homology (EH) domains, a putative coiled-coil domain, and five C-terminal SH3 domains (SH3 A-E)[316]. Though the EH domain of intersectin is recognized for its interaction with epsin - enabling its localization to clathrin-coated pits[317] - intersectin also interacts with a host of proteins outside the realm of endocytosis, such as Son of

sevenless homolog 1 (Sos1), Numb, WASP, and CdGAP, using its SH3 domains[317-322]. Upon observing the co-localization of CdGAP with intersectin in fibroblasts stimulated by platelet-derived growth factor (PDGF), researchers proposed a regulatory mechanism involving protein-protein interaction. This mechanism was found to be associated with concurrent inhibition of GAP activity[304]. Intriguingly, while the absence of the C-terminal PRD did not compromise intersectin's capability to bind and interact with CdGAP, the inhibition of GAP activity - an effect observed in tandem with interaction with intersectin - was dependent on PRD[304]. In addition, pull-down assays pinpointed the SH3D domain of intersectin as an essential component for mediating the inhibition of CdGAP activity[304]. Further investigation led to the identification of an unconventional SH3 binding motif, xKx(K/R)K, within the BR region of CdGAP (SKSKK) as a critical element orchestrating the interaction between CdGAP and the SH3D domain of intersectin[308]. Only one other protein, Numb, an adaptor protein featuring a similar SKSKQ motif, has been documented to interact with the SH3D domain of intersectin[321]. This finding underscores the pivotal role of the evolutionarily conserved lysine residues within the BR region of CdGAP[308]. The replacement of these lysine residues with alanine diminished the GAP activity[308]. However, in alignment with earlier observations[304], the inhibition of GAP activity was contingent on PRD. This was evidenced by the fact that substitution in the SKSKK motif that hinders the interaction between the SH3D domain and CdGAP only mildly affected GAP activity in a CdGAP mutant devoid of PRD[308].

### *1.5.3 Functions associated with the proline-rich domain (PRD)*

The proline-rich domain (PRD) within CdGAP has been recognized as a requirement for an array of diverse functions, from its susceptibility to phosphorylation[302, 303] to its involvement in transcriptional regulation[311]. Previous research has revealed that glycogen synthase kinase 3 (GSK-3) and ERK1/2 prominently phosphorylate the serine and threonine residues present in the PRD of CdGAP[303]. The PRD is also characterized by the presence of numerous S/T-P motifs, constituting the minimum consensus motif for ERK phosphorylation[323]. When Swiss 3T3 fibroblasts underwent treatment with the MEK1 inhibitor, PD98059, a marked decrease was noticed in CdGAP phosphorylation in response to growth factors such as PDGF[303], suggesting possible crosstalk between CdGAP and the mitogen-activated protein kinase (MAPK) signaling

pathway. ERK1 targets Thr776 specifically for phosphorylation, thereby suppressing the GAP function of CdGAP. The substitution of the threonine residue with an alanine residue resulted in a notable increase in the GAP activity of CdGAP towards Rac1[303]. Though a similar phosphorylation pattern of serine and threonine residues can be observed in human CdGAP, only Thr776 - the phosphorylation target of ERK1 - is conserved in the human ortholog[302]. Even in the absence of the Dok/Erv/FPS/FER (DEF) domain, an ERK-docking site, in the human ortholog, ERK1/2 proteins persistently coimmunoprecipitate with human CdGAP, suggesting the potential existence of a novel ERK-docking sequence[302]. Further research pinpointed both isoforms (α/β) of GSK-3 as binding partners of CdGAP and mediators of CdGAP phosphorylation under serum-starved conditions[306]. GSK-3 phosphorylates Thr776, a site also targeted by ERK1/2. The inhibition of this activity precipitated a significant reduction in endogenous CdGAP phosphorylation in fibroblasts[306]. Post serum starvation, upon serum reintroduction, both protein and mRNA levels of CdGAP increase; however, GSK-3 mediates only the protein-level increase, not the mRNA levels of CdGAP, indicating its role in the post-transcriptional regulation of CdGAP[306].

Within ErbB2-transformed breast cancer cells, CdGAP employs its PRD to transcriptionally repress E-cadherin gene expression[311]. CdGAP forms a regulatory complex with ZEB2, which subsequently binds to the E-BOX elements of E-cadherin (Figure 1.4). Following CdGAP knockdown, expression levels of transcription repressors Snail1 and ZEB2 diminished in ErbB2 breast cancer cells. This phenomenon correlated with hindered tumor growth and a substantial reduction in lung metastasis *in vivo*[311].

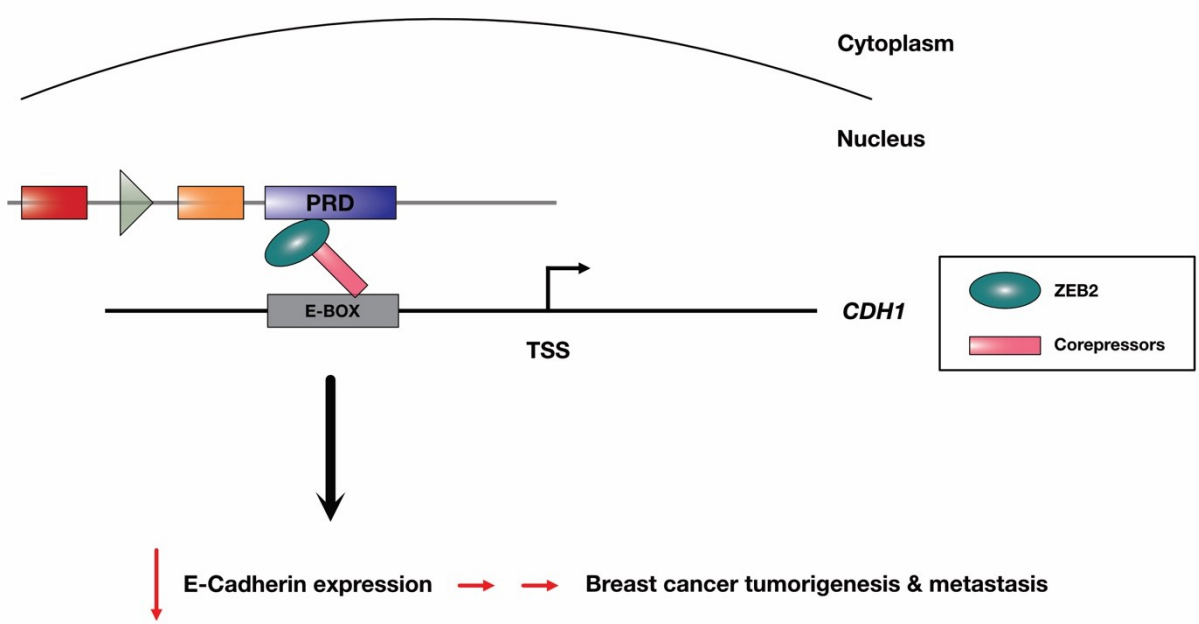


**Figure 1.4: CdGAP is involved in transcriptional regulation of E-cadherin in breast cancer cells.**

In breast cancer cells, CdGAP orchestrates the transcriptional repression of E-cadherin expression. This process involves the localization of CdGAP to the E-BOX elements, situated upstream of the transcriptional start site, within the E-cadherin gene. Crucially, this interaction necessitates the involvement of CdGAP's PRD in partnership with ZEB2 and other corepressors[311].

### *1.5.4 Functions associated with the C-terminus of CdGAP*

The largely unstructured C-terminus of CdGAP is crucial for its spatial and temporal regulation[307, 309]. The C-terminal region of CdGAP, besides the central region that interacts with intersectin, resulting in subsequent inhibition of CdGAP activity[304, 308], is known to interact with the LIM-domain-containing scaffolding protein, Ajuba[309]. The significance of this interaction was underscored by two AOS-associated mutations in CdGAP. These mutations disrupt the interaction, leading to amplified perturbations in cell junctions in a GAP-dependent manner[309]. A subsequent study aimed at pinpointing the amino acid residues phosphorylated by RSK found two serine residues within the C-terminus – Ser1093 and Ser1163 – to be pivotal. These residues enable the binding of the 14-3-3β adaptor protein, leading to the sequestration of CdGAP in the

cytoplasm[307]. The phosphorylation, which creates docking sites for 14-3-3β, had profound functional implications. These included alterations in cell morphologies and migration, which could be attributed to GAP activity towards Rac1. Additionally, there was a loss of E-cadherin transcriptional repression, an effect linked to the impairment of CdGAP's nucleocytoplasmic shuttling[307]. Similar regulatory mechanisms involving 14-3-3β have been documented in several other RhoGAPs, such as DLC1, ARHGAP22, and RhoGEFs, such as A-kinase anchoring protein-Lbc (AKAP-Lbc)[307]. Furthermore, evidence has shown that Ser1093 of CdGAP undergoes phosphorylation through VEGF and angiopoietin-1 signaling in endothelial cells[324]. This suggests that the regulation of CdGAP's C-terminal region may be influenced by various agonists in different cell types[307]. Intriguingly, even upon the replacement of the two serine residues with alanine, a residual interaction was detected, implying the existence of additional domains in CdGAP capable of binding 14-3-3β, including the BR[307].

### *1.5.5 CdGAP is controlling a vast array of biological functions*

The role of CdGAP, a pivotal regulator of cellular migration[325, 326] and durotaxis[327], extends across complex physiological processes. Through its interaction with essential cellular structures and signaling pathways, CdGAP orchestrates a variety of cellular functions[325].

Within the cellular ecosystem, CdGAP, localized to adhesion contacts through its interaction with the scaffolding protein α-parvin (also known as actopaxin), fundamentally controls cell spreading and chemotaxis, especially evident in U2OS osteosarcoma cells[305]. Studies using nontumorigenic murine mammary gland (NMuMG)-immortalized mouse mammary cells, expressing the activated Neu (rat ortholog of ErbB2) receptor, revealed elevated endogenous CdGAP levels in mammary tumor explant cells compared to control cells[328]. Transforming growth factor-β (TGF-β) stimulation led to increased cell motility and invasion in these explants cells, effects substantially curtailed by CdGAP expression downregulation through silencing RNA (siRNA) in a GAP-independent manner[328]. Notably, CdGAP suppression also hampered the proliferation of NMuMG-activated Neu cells, regardless of TGF-β presence[325]. These findings illustrate the extensive influence of CdGAP, extending beyond migration, and suggest a synergy between TGF-β and ErbB2 signaling pathways, reinforcing CdGAP's role in this dynamic interaction[325]. Supporting evidence arises from the regulation of CdGAP

expression and phosphorylation by TGF-β, demonstrated by the rise in CdGAP protein and mRNA levels in TGF-β-treated NMuMG cells[325]. Additionally, TGF-β stimulation of NMuMG cells transiently increased CdGAP phosphorylation, following the kinetic pattern of TGF-β-induced Smad2/3 phosphorylation[325]. Recently, talin has been identified as a novel interacting partner of CdGAP. This new finding not only underscores CdGAP's role in governing focal adhesion dynamics but also expands our understanding of its capabilities by highlighting its involvement in the activation of integrins. This revelation opens up potential therapeutic avenues, suggesting that targeting both the TGF-β and integrin pathways in $HER2^+$ breast cancer may be beneficial for patients[329].

CdGAP's importance is further emphasized by studies showing that mutations in CdGAP enhance Cdc42 activity, resulting in abnormally high migration in patient-derived fibroblasts[285]. In a 2D environment, CdGAP modulates the type and dynamics of adhesion contacts, thereby governing cell migration[326]. When CdGAP function is disrupted by siRNA treatment, cells form small leading edge adhesion contacts, similar to those observed in U2OS cells overexpressing dominant active (V12) forms of either Rac1 or Cdc42 or in cells with inhibited myosin II activity[12, 330]. The role of CdGAP in focal adhesion maturation is apparent when large focal adhesions in CdGAP-overexpressing cells are extraordinarily stable, while those in CdGAP-depleted cells are highly dynamic[326]. This suggests that CdGAP-overexpressing cells have static, hyper-mature adhesion contacts that slow cell migration by anchoring the cell body to the ECM, while CdGAP-depleted cells may migrate more rapidly due to an increased small, rapidly turning over adhesions that provide optimal traction forces for swift cell migration[326]. This behavior in CdGAP-depleted cells mimics that of cells overexpressing Rac1 GEF, Asef2, or cells overexpressing the constitutively active Pak1 (T423E), a Rac1 effector[331, 332].

Lastly, the vital role of CdGAP in "durotaxis", a process steered by the rigidity of the ECM, should not be overlooked. CdGAP not only responds to integrin engagement with the ECM but also senses the matrix rigidity of ECM substrates[327]. CdGAP might form a mechanically sensitive signaling axis with the integrin-linked kinase (ILK)-actopaxin complex, affecting U2OS osteosarcoma cell morphology and motility in response to ECM compliance[327]. Importantly, CdGAP regulates Rac1 activity at the leading edge, resulting in small focal adhesions when CdGAP is depleted, regardless of matrix rigidity[327]. In conjunction with other

studies reporting diminished traction force generation in CdGAP-deficient cells[333, 334], CdGAP is implicated not only in generating but also in mediating traction force oscillation, a crucial aspect for cells in durotaxis[327, 333, 334].

## *1.6 Adams-Oliver Syndrome (AOS): general overview*

AOS is a rare congenital disorder first described in 1945 by Adams and Oliver. It illustrates how disturbances in embryonic development can lead to a diverse range of human malformations[335] (Figure 1.5A). The principal diagnostic criteria for AOS encompass transverse terminal limb defects (TTLD)—often asymmetric, manifesting in various ways such as syndactyly, brachydactyly, oligodactyly, polydactyly, and hypoplastic nails[286]—together with aplasia cutis congenita (ACC) (Figure 1.5B), and a family history of AOS[287]. Initially, the diagnosis of AOS required the presence of two major criteria or a combination of one major and one minor criterion, the latter encompassing cutis marmorata, congenital heart defects, and vascular anomalies[287]. However, the diagnostic guidelines have recently been revised to include the detection of a pathogenic mutation in an established gene, thereby enabling reclassification of isolated cases where patients displayed only ACC or TTLD[336, 337]. Beyond ACC and TTLD, AOS is associated with a wide array of abnormalities, such as congenital cardiac and vascular defects, neurological abnormalities, ophthalmologic, and reproductive system developmental defects[338]. As of now, due to advancements in genetic screening and relentless pursuit of AOS-causing genes, six genes have been identified, underscoring two defective signaling pathways at the core of AOS pathogenesis: 1) the Rac1/Cdc42 pathway (implicated by *ARHGAP31* and *DOCK6* mutations) and 2) the Notch pathway (implicated by mutations in *RBPJ, EOGT, NOTCH1,* and *DLL4*)[337].

A

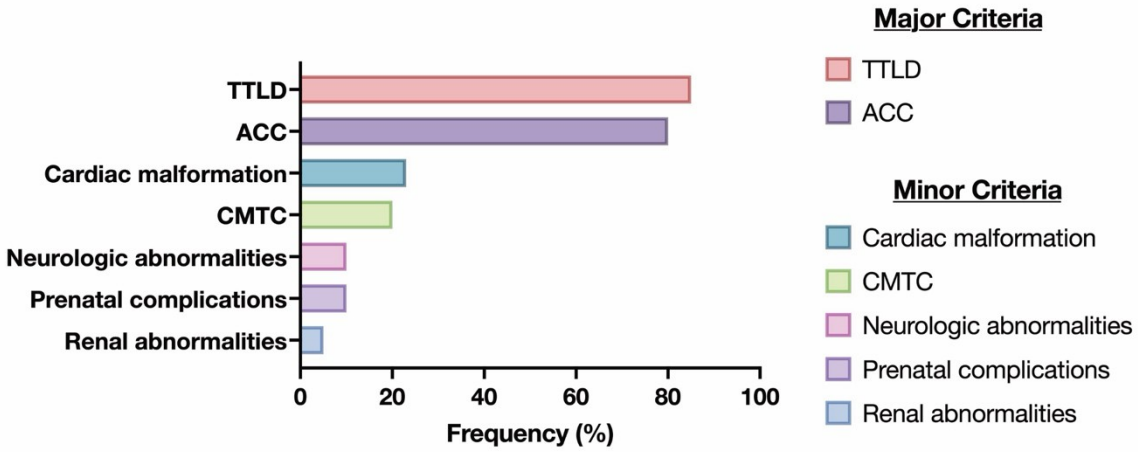
TTLD
ACC
Cardiac malformation
CMTC
Neurologic abnormalities
Prenatal complications
Renal abnormalities
0
20
40
60
80
100
Frequency (%)
Major Criteria
TTLD
ACC
Minor Criteria
Cardiac malformation
CMTC
Neurologic abnormalities
Prenatal complications
Renal abnormalities

B


A
B
C
D
E
F
G
H
I

**Figure 1.5: Phenotypic abnormalities reported among families affected by AOS.**
(A) The array of abnormalities observed in AOS patients can be categorized into major or minor diagnostic criteria. Major diagnostic features such as TTLD and ACC, are commonly seen in over 80% of patients. In contrast, minor diagnostic features are considerably less prevalent, with congenital heart defects and cutis marmorata telangiectatica congenita (CMTC) being the most frequently reported (20%)[336]. (B) The two characteristic phenotypes—ACC and TTLD—that form the major diagnostic criteria for AOS are often seen in patients and can significantly impact their health outcomes. In severe instances of ACC, incomplete scalp formation leaves the brain exposed, thereby elevating the risk of infection. TTLD, on the other hand, demonstrates a broad spectrum of severity among individuals, spanning from complete loss of fingers and/or toes to the simple shortening of distal phalanxes of fingers and toes.

(B): Meester, Josephina A. N., et al. (2015). "Heterozygous Loss-of-Function Mutations in DLL4 Cause Adams-Oliver Syndrome." The American Journal of Human Genetics **97**(3): 475-482, Copyright (2015), with permission from Elsevier.

### *1.6.1 Abnormalities associated with major diagnostic criteria*

TTLD, a condition witnessed in over 80% of AOS patients[338], typically presents as bilateral, asymmetric terminal transverse reduction of digits[335]. This type of limb abnormality, initially described in 1945, can impact both the upper and lower extremities, though defects, particularly foot malformations, are more prevalent in the latter[339]. Nevertheless, establishing a diagnosis of AOS can be intricate due to considerable variation in severity—ranging from the total absence of a hand or foot to mild or subtle clinical manifestations, occasionally seen in carriers[286]. As such, for a comprehensive evaluation, a radiological examination of all four distal limbs is suggested during the clinical assessment of family members[340]. ACC, a condition observed in approximately 75% of AOS patients[338], usually occurs at the vertex and may involve varying levels of damage to the periosteum, bone, and dura[335]. The lack of epidermis on the scalp leaves parts of the brain unprotected, escalating the risk of infection, superior sinus thrombosis, hemorrhage, or herniation[341]. While ACC may be linked with other congenital disorders such as Johanson-Blizzard syndrome, focal dermal hypoplasia (Goltz syndrome), and

trisomy 13, the combination of ACC with scalp defects and limb abnormalities designates a distinct entity[338].

### *1.6.2 Abnormalities associated with minor diagnostic criteria*

Cardiac abnormalities that are present in approximately 20% of AOS patients, span a broad range of concerns, including valvular defects, left heart stenotic lesions, cardiomyopathy, heart block, malformation of pulmonary vessels, and progressive pulmonary hypertension[342-344]. These findings have bolstered the hypothesis that AOS has a vascular origin[340, 345]. Additional vascular anomalies associated with AOS include under-branching of vascular trees, inconsistent vascular smooth muscle cell coverage, tortuous dilated vessels, and a general scarcity of small to medium-sized blood vessels[346, 347]. NOTCH signaling, which plays a key role in vascular development[348], frequently underpins cardiovascular abnormalities in AOS[336]. Remarkably, these cardiac issues often coexist with structural and/or functional vascular irregularities, with around 20% of patients also exhibiting CMTC[338]. While neurological abnormalities are more common in AOS patients with an autosomal-recessive inheritance pattern, they have been reported and span a wide range—from intracranial abnormalities, microcephaly, epilepsy, and intellectual disability to developmental delays[338]. Diagnosis is further complicated by the presence of dysmorphic facial characteristics, abdominal wall defects, genital birth defects, and Poland's anomaly reported in some AOS patients[340, 349, 350]. Finally, a case of a female patient diagnosed with AOS displayed an ocular phenotype resembling familial exudative vitreoretinopathy. This patient also presented clinical manifestations of ACC, a moderate degree of TTLD, and congenital heart defects within the arterial septum[351].

### *1.6.3 AOS-causing genes*

AOS is associated with mutations in genes that are distributed across two distinct pathways: *NOTCH1, DLL4, EOGT, RBPJ,* which are integral to the NOTCH signaling, and *ARHGAP31* and *DOCK6* which operate within the Rac1/Cdc42 pathways[337]. *NOTCH1* (10%) and *DLL4* (6%) account for the majority of familial AOS cases. Large European cohort studies have demonstrated a 36% diagnostic yield for these mutations[337]. Upon its discovery, AOS was

initially thought to exhibit an autosomal-dominant inheritance pattern[335]. However, subsequent genetic counseling uncovered an autosomal-recessive inheritance mode for two of the six AOS-causing genes: *DOCK6*[352] and *EOGT*[353]. It is important to note that the risk of AOS escalates with consanguineous marriages[344, 353], as opposed to a 25-50% probability of disorder when one or both parents have AOS[336]. Yet, sporadic instances of AOS, devoid of mutations in recognized genes, are common[337, 352, 354]. AOS patients frequently display abnormalities in internal organs, leading to increased embryonic lethality and a diminished lifespan[355]. For example, AOS patients with retinopathy often face a severe prognosis, encountering early death, developmental delays, and blindness[355]. This observation is corroborated by the presence of congenital heart defects such as coarctation of the aorta, atrial and ventricular septal defects, valve abnormalities, and double-outlet and hypoplastic left and right ventricles, found in newborns and prematurely terminated pregnancies diagnosed with AOS[338].

### *1.6.4 Disease-causing genes with an autosomal-dominant mode of inheritance*

#### *1.6.4.1 ARHGAP31*

In 2011, the first gene associated with AOS was unearthed through a genome-wide linkage analysis, leading to the discovery of two CdGAP variants: p.Gln683X and p.Lys1087Serfs*4[285]. Intriguingly, these variants, along with the newly identified p.Ser689X and p.Gln728X, result in truncated forms of CdGAP. This process circumvents the nonsense-mediated decay surveillance mechanism[337, 356] (Figure 1.6). Significantly, *in vitro* assays revealed that both p.Gln683X and p.Lys1087Serfs*4 mutations precipitate a gain-of-function in CdGAP. This gain was ascribed to the loss of an auto-inhibitory mechanism caused by the binding of the GAP domain by the C-terminal region of CdGAP, which subsequently resulted in reduced activities of Cdc42 and Rac1[285]. Due to the diverse clinical manifestations of AOS, diagnosing the condition can be challenging. A family showcasing isolated TTLD, which harbored the p.Ser689X mutation in CdGAP, was identified. The severity of abnormalities within this family exhibited a broad spectrum, ranging from terminal reduction defects of the hands and/or feet to merely shortened digits and small nails[357]. Nevertheless, while congenital heart anomalies are evident in 20% of AOS patients, clinical manifestations of cardiac anomalies have yet to be reported in AOS patients bearing mutations in either *ARHGAP31* or *RBPJ*[285, 350, 357].

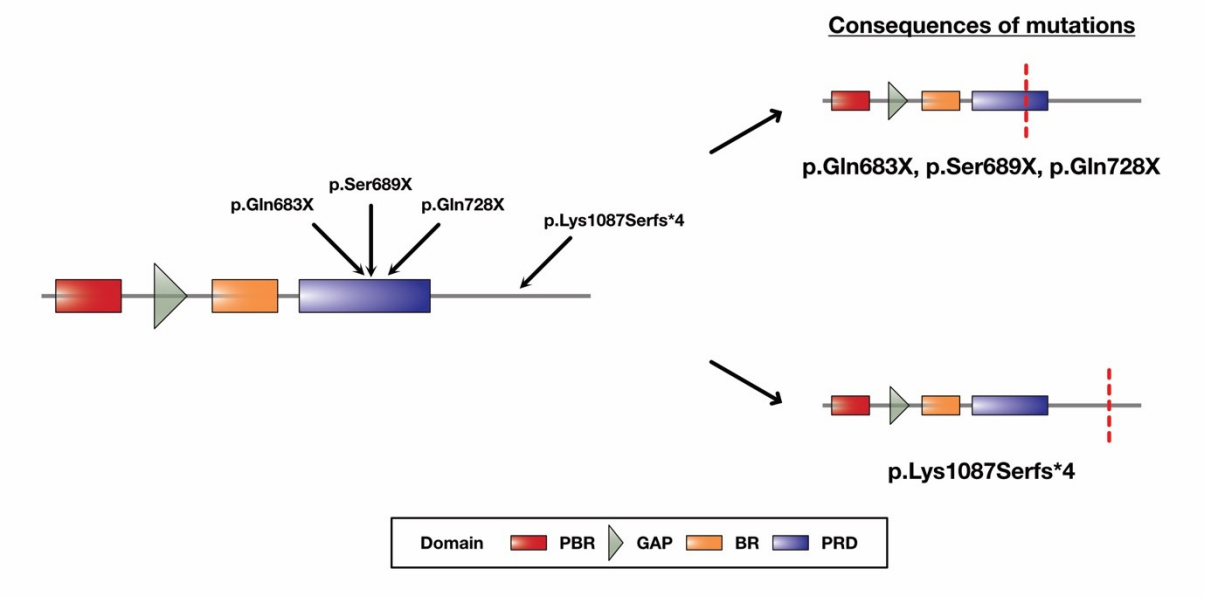


**Figure 1.6: Consequences of AOS-associated mutations in *ARHGAP31.***

Four causative mutations in *ARHGAP31* give rise to truncated variants of CdGAP. However, solely the p.Lys1087Serfs*4 mutation precipitates a partial C-terminal truncation[285, 356]. Conversely, the remaining mutations induce disruption of the PRD and culminate in the complete obliteration of the C-terminus[285, 337, 356].

### *1.6.4.2 RBPJ*

The recombination signal binding protein for immunoglobulin kappa J Region (RBPJ) occupies a central role in NOTCH signaling, forming a transcription complex alongside the NOTCH intracellular domain (NICD) and the co-activator, Mastermind-Like (MAML). In the absence of NICD, the binding of RBPJ to NOTCH targets culminates in transcriptional repression due to the recruitment of corepressors[358]. The identification of an autosomal dominant mutation within the DNA-binding domain of *RBPJ*[350, 358] fueled conjecture surrounding the potential participation of NOTCH signaling in AOS pathogenesis. This groundbreaking discovery greatly accelerated the discovery of additional genes associated with AOS, including *NOTCH1, DLL4,* and *EOGT* [338, 358, 359].

### *1.6.4.3 NOTCH1*

The central role of NOTCH signaling in human development is underscored by its conservation across metazoan species and its governance of myriad tissue-specific cellular processes[360, 361]. For instance, the concurrent activation of NOTCH and β-catenin via cAMP signaling orchestrates the assembly of a complex involving NICD, RBPJ, and β-catenin in arterial endothelial cells, thereby suppressing the differentiation of neural precursor cells[362]. NOTCH1, a member of the NOTCH receptors family (NOTCH 1-4), possesses an extracellular domain featuring 36 EGF-like repeats, 21 of which bear potential calcium-binding properties[348, 363]. Furthermore, the NICD, which is paramount for transcriptional regulation, comprises an RBPJ-associated module, seven ankyrin repeats, and a C-terminal domain rich in proline, glutamic acid, serine, and threonine[364, 365]. AOS patients who carry *NOTCH1* mutations often present with vascular abnormalities[337, 354, 366, 367]. Initial genome-linkage analyses unveiled five distinct mutations in *NOTCH1* affecting both genders. Interestingly, while the loss of highly conserved cysteine residues was anticipated to destabilize the protein through the disruption of disulfide bonds, a missense mutation that introduces an asparagine residue was hypothesized to impede the assembly of the transcription complex consisting of NICD, RBPJ, and MAML[366]. Subsequent studies identified both nonsense and frameshift mutations, leading to haploinsufficiency[359], and missense mutations, which cause protein destabilization through disulfide bond disruption and altered calcium ion binding affinity[354].

### *1.6.4.4 DLL4*

Activation of NOTCH signaling is driven by ligand binding, which encompasses two families: Jagged and Delta. Notably, DLL4 from the Delta family has been instrumental in vascular development and angiogenesis in both mice and humans[348, 368, 369]. In a study of 91 families, nine mutations in the *DLL4* gene were initially identified, including both nonsense and missense mutations[359]. Nonsense mutations in *DLL4* (resulting in p.Gln554X and p.Arg558X protein changes) are believed to prompt a loss of mutant mRNA transcripts via nonsense-mediated decay[356]. Missense mutations in *DLL4* have been predicted to either: 1) destabilize the protein by disrupting or creating disulfide bonds through the replacement (p.Cys455Trp, p.Cys390Tyr, p.Cys390Arg) or the introduction of new cysteine residues (p.Arg186Cys), or 2)

interfere with the ligand-receptor interaction (p.Pro267Thr, p.Ala121Pro, p.Phe195Leu) between DLL4 and NOTCH1[359]. Additionally, a *de novo* missense mutation in *DLL4* (yielding a p.Arg191His protein change) was identified in a male Japanese newborn[370]. This mutation was also anticipated to impede the ligand-receptor interaction by interrupting the interaction between DLL4 and the glycosylated EGF-like domain 11 of NOTCH1[361].

### *1.6.5 Disease-causing genes with an autosomal-recessive mode of inheritance*

#### *1.6.5.1 DOCK6*

DOCK6 belongs to the DOCK family of GEFs, a group composed of four structural classifications (DOCK-A to D) encoded by 11 distinct genes[338]. Contrasting with the DH domain frequently encountered in RhoGEFs, DOCK6 features two DHRs, with the larger C-terminal DHR-2 domain playing a central role in catalytic activity by enabling guanine nucleotide exchange[338]. DOCK6, a constituent of the DOCK-C subfamily, shows specificity towards both Rac1 and Cdc42. This stands in contrast to the DOCK-A and B subfamilies, which primarily target Rac1, and the DOCK-D subfamily, which is specific to Cdc42[371]. Interestingly, while DOCK6 operates as a GEF—activating Rac1 and Cdc42 by facilitating the exchange of GDP for GTP—it acts in direct counterpoint to ARHGAP31, which expedites the hydrolysis of GTP into GDP. Collectively, the AOS-associated mutations in *ARHGAP31* and *DOCK6* lead to decreased activities of Rac1 and Cdc42, attributable to a gain-of-function mechanism in CdGAP and potential loss-of-function in DOCK6, respectively[285, 338].

#### *1.6.5.2 EOGT*

EGF-domain specific O-linked N-acetylglucosamine (O-GlcNAc) transferase (EOGT) has been recognized for its role in glycosylating NOTCH1 in mammalian cells[372]. Although EOGT is known to target EGF domains of Notch receptors, as well as Delta and Serrate ligands in *Drosophila* studies[373], its crucial contribution to human NOTCH signaling, which orchestrates vascular development, was extrapolated from the necessity of Notch receptor glycosylation by Eogt, for Dll4 binding, but not Jag1, in *Eogt*-knockout mice[374]. The initial evidence implying that mutations in *EOGT* could contribute to the pathogenesis of AOS was uncovered during the

study of 11 consanguineous families, where a missense mutation (resulting in a protein change) and a single-bp deletion (a nucleotide change) in *EOGT* were documented[353, 375]. Heightened levels of *Eogt* expression observed in the limb buds and apical ectodermal ridges of developing mouse embryos reinforced a genotype-phenotype correlation[353]. Subsequently, two additional novel mutations in *EOGT* were discovered[376]. Firstly, a male infant from a Turkish family, carrying a missense mutation resulting in a p.Cys135Tyr protein change, manifested clinical symptoms of ACC along with a mild degree of TTLD, complemented by central nervous system defects that resulted in hearing loss[376]. Secondly, a c.311+1G>T nucleotide mutation, anticipated to lead to abnormal splicing of exon 5, was identified in a German family. The affected male infant in this family presented with a large ACC with CMTC but did not show any clear defects in limbs, brain, or heart[376].

### *1.6.6 Current limitations in the understanding of AOS pathogenesis*

The molecular diagnosis of AOS poses significant challenges due to the disorder's rarity and the ever-growing array of related abnormalities[338]. Intriguingly, a substantial fraction of AOS patients (> 60%) — frequently carrying sporadic mutations[337, 338] — do not display pathogenic mutations in the six established AOS-causing genes, despite the recent discovery of 63 probable pathogenic mutations[337]. Moreover, the genetic underpinnings of 22 families demonstrating autosomal-recessive inheritance remain unresolved[337]. Current understanding of the prevalence of large insertions or deletions, which could potentially underlie AOS pathogenesis, is notably limited[338]. However, copy number variations, resultant from partial or complete deletion or duplication of disease-causing genes, might account for roughly 20% of cases[377]. A large deletion in chromosome 15, resulting in the loss of several exons of *DLL4*, has been detected. Yet, due to concurrent deletions in other genes, such as *KIF21B, DNAJC17, ZFYVE19, SPINT1,* and *VPS18*, it remains uncertain whether the loss of DLL4 functionality solely precipitated AOS in the affected individual[338, 354, 378]. Further constraining the progression of molecular diagnosis, genetic screening via DNA sequencing should be actively pursued in AOS patients without a family history and in sporadic cases[338]. Regrettably, limited assess and resources often result in an absence of genetic testing, even amid the presence of unprecedented clinical manifestations[351]. Diagnostic complexities often emanate from incomplete penetrance

and reduced phenotypic expressivity, traits commonly seen amongst AOS patients and carriers[285]. For instance, individuals with milder clinical manifestations might not be diagnosed with AOS until more emblematic feature of the disorder surface[349]. Moreover, family members may exhibit isolated CMTC or nonsyndromic congenital cardiac anomalies in the absence of ACC and TTLD within AOS families[340]. Lastly, while prenatal testing is advocated to allow for early-stage supportive intervention[379], prenatal diagnosis of AOS has been infrequently reported. This is despite the successful application of fetoscopy, which validated the severity of limb abnormalities and a skin defect of the scalp, lasting 15 minutes without affecting fetal heart rate or eliciting maternal complications[367].

### *1.6.7 Evidence supporting the vascular origin of AOS*

The initial proposition of vascular abnormalities accompanying ACC or TTLD was put forth by Kahn and Olmedo in 1950. They encountered a patient with severe ACC and congenital absence of the distal phalanges, who also presented with universal CMTC, a rare condition typified by disordered blood vessel formation, which amalgamates livedo reticularis and telangiectasia[380]. This experience seeded the hypothesis that AOS might stem from vasculogenic defects—a notion buttressed by several instances of vascular anomalies, including hypoplasia of middle cerebral arteries, aortic arch vessels, and pulmonary arteries, alongside pulmonary vasculature disorders like pulmonary arteriovenous malformations and pulmonary hypertension[340, 345, 381]. In tandem, it was postulated that genetic defects could destabilize embryonic vessels due to aberrant pericyte recruitment[381, 382]. At the molecular level, the β-catenin and NOTCH signaling pathways have been unveiled as critical players in arteriovenous specification during vascular development[338]. This concept was corroborated using mouse models—knocking out *Rbpj* induced severe vascular defects coupled with down-regulation of pericyte and smooth muscle cell recruitment to the dorsal aorta[383]. The indispensable nature of NOTCH signaling in cardiovascular development has been accentuated by the emergence of congenital heart defects in mice and humans consequent to dysregulated signaling[358, 384]. A genotype-phenotype correlation was suggested following large pedigree analyses of AOS patients harboring *NOTCH1* mutations. Clinically, these patients manifested right- and left-sided

congenital heart defects, pulmonary hypertension, portal hypertension, cutis marmorata, venous ectasia, and thrombophilia[366].

### *1.6.8 Signs of placental dysfunction among AOS patients*

Since the initial identification of AOS in 1945, abnormalities in the placentas of patients afflicted with AOS have been consistently observed. This prompted speculation that vascular thrombotic incidents occurring *in-utero* might interfere with the embryonic blood supply[385, 386]. The presence of varied cardiac anomalies in AOS patients further substantiated this hypothesis, suggesting a multi-faceted pathogenic mechanism[387]. However, despite these observations, comprehensive examinations of placental morphology, coupled with molecular diagnoses for placental dysfunction, have largely been overlooked in newly diagnosed AOS patients. For instance, an infant male, despite a normal pregnancy, displayed signs of intrauterine growth restriction (IUGR) evidenced by cutaneous lesions, poor feeding habits, and inadequate weight gain, which hinted at potential placental inefficiency[388-390]. Yet, neither a gross morphological characterization of the placenta nor genetic testing was carried out[391]. Similarly, another male infant exhibited signs of IUGR along with a constellation of clinical manifestations. These included ACC, limb defects, and vascular anomalies such as cutis marmorata, all of which were associated with a detected missense mutation in *DLL4*. Yet, even in this instance, a comprehensive placental investigation was not undertaken[370]. Nevertheless, placental irregularities were seen in a female infant diagnosed with AOS and a concurrent congenital heart defect (patent ductus arteriosus). The placenta was markedly hypertrophic with an attached fibrous band bordering it. Interestingly, the mother of this child had previously experienced a stillbirth featuring acrania[392]. The theory proposing that mutations in established genes underlie the pathogenesis of AOS received further support from a familial study conducted in Germany, where a mutation in *EOGT* was associated with AOS. Specifically, a prior pregnancy within this family ended in a stillbirth characterized by low fetal weight, a large ACC, limb defects, hypoplasia of the right umbilical artery, and aberrant development of the chorionic villi in the placenta[376].

## *1.7 Preeclampsia: general overview*

Preeclampsia, the most prevalent pregnancy-associated complication, impacts approximately 5% of pregnancies. It is characterized by maternal systemic vascular endothelial inflammation, activation, and dysfunction—hallmark features of preeclampsia. Preeclampsia places both the mother and the developing fetus at risk, potentially leading to complications such as maternal hypertension, thrombocytopenia, compromised liver function, pulmonary edema, new-onset renal insufficiency, and cerebral complications[393, 394]. Preeclampsia can be further subdivided into early-onset and late-onset types, based on the gestational week of onset. Neonates are linked to poorer outcomes and increased morbidity in cases of early-onset preeclampsia[394-396]. This disorder is considered a two-stage disease, where the first stage involves reduced placental perfusion due to failure of spiral artery remodeling. Subsequently, this triggers the onset of the maternal syndrome, typified by the release of placental factors and syncytial particles into the maternal circulation[394]. Despite the transient nature of the placenta, there is growing concern about long-term socioeconomic consequences. Neonates from preeclamptic pregnancies, who frequently experience preterm birth, face a higher risk for conditions such as diabetes, cardiovascular, and renal disease[397-399]. The current consensus posits that the pathogenesis of preeclampsia involves a series of pathological events throughout gestation, including impaired implantation, endothelial dysfunction, and placental damage due to repeated ischemia-reperfusion[400]. This process is accompanied by systemic inflammation[400, 401]. Moreover, preeclampsia is increasingly viewed as a vasculopathy[395]. Women with pregnancies complicated by preeclampsia have shown significant defects in their capacity to produce vasodilators, such as nitric oxide (NO) and prostacyclin I2. Concurrently, they display increased production of vasoconstrictors, such as endothelin, and a heightened sensitivity of vascular smooth muscle cells (VSMC) to vasoconstrictors[395, 402, 403].

### *1.7.1 Gross morphological/histological changes associated with preeclampsia*

Investigating the molecular mechanisms of preeclampsia is crucial, yet observing the gross morphological and histological alterations in the preeclamptic placenta can also provide significant insights into the cell types or molecular pathways implicated in the development of

preeclampsia. For instance, more than half of severe preeclamptic placentas display morphological changes such as a pale placenta accompanied by infarcts, hematomas, and calcifications[404]. Furthermore, preeclamptic placentas frequently weigh less and have a smaller diameter compared to healthy ones[405]. Histological evaluations of preeclamptic placentas reveal several distinctive changes: 1) defective remodeling of spiral arteries, 2) excessive degradation of the defective syncytium, 3) increased deposition of fibrin plaques, and 4) premature aging of the placenta[388, 406, 407]. A more in-depth examination has unveiled a reduction in the number of syncytial microvilli, an increase in instances of syncytial necrosis, and constriction of fetal capillaries in preeclamptic placentas. These findings all support the theory that placental dysfunction is prevalent in preeclamptic conditions[408].

### *1.7.2 Trophoblast invasion plays a crucial role in spiral artery remodeling*

A predominant histological observation in placentas affected by preeclampsia is the inability to aptly remodel maternal spiral arteries from a high-resistance/low-capacity state to a relaxed condition marked by a low-resistance, high-capacity during pregnancy (Figure 1.7). This remodeling process is essential for enhancing nutrient and oxygen delivery to the developing fetus[394, 406]. Inadequate spiral artery remodeling is tied to the onset of multiple obstetric and neonatal complications, such as preeclampsia, IUGR, early miscarriage, premature birth, and even maternal or fetal mortality[389, 409, 410]. In the early stages of human pregnancy, extravillous trophoblasts (EVT) invade the maternal endometrium, supplanting the vascular smooth muscle cells, endothelial cells, and elastic lamina, hence forming a subtype of EVT, referred to as endovascular trophoblasts (ENVT)[411-414]. However, in preeclamptic placentas, the infiltration of EVTs into the maternal endometrium is considerably hindered, resulting in shallow and diminished invasion[406]. The fundamental roles of trophoblastic invasion in the restructuring of uterine spiral arteries have been further underscored in recent studies. These investigations divulge that both endo-venous and endo-lymphatic trophoblast cells invade uterine veins and lymph vessels[415, 416]. Furthermore, invasive trophoblasts interact with maternal immune cells within the decidua, precipitating hormone secretion that highlights the multifaceted central roles of invasive trophoblasts[417, 418]. Lastly, due to their unique ability to invade the maternal decidua

and remodel spiral arteries, defects in the initiation of EMT are closely linked to failures in spiral artery remodeling[419, 420].

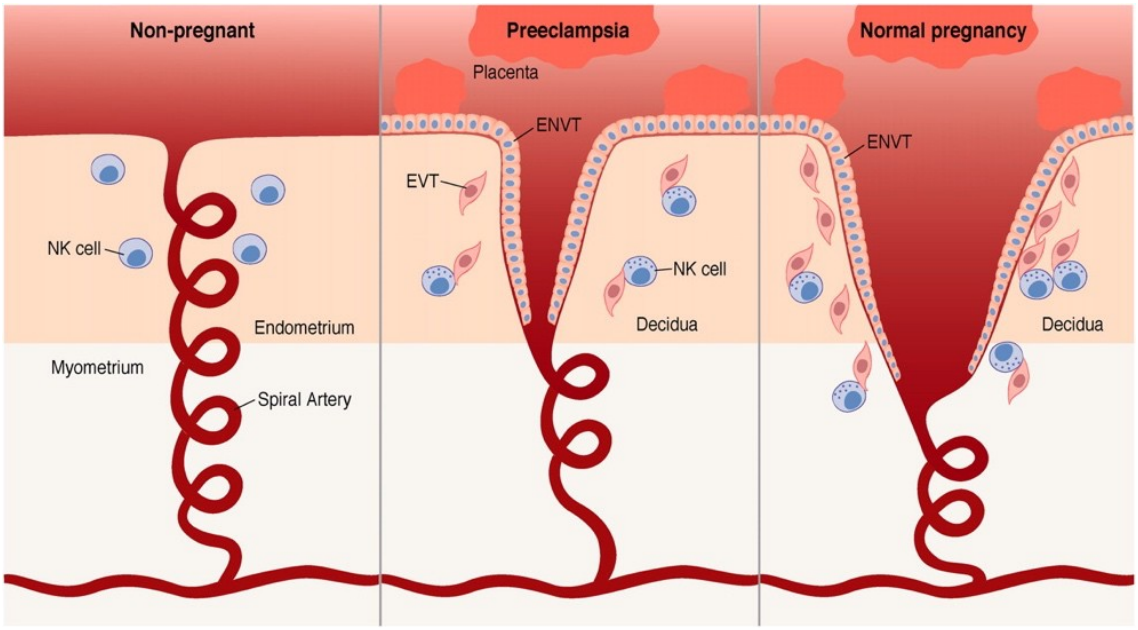


**Figure 1.7: Spiral artery remodeling during pregnancy in mice and humans.**

During the early phases of human and rodent embryogenesis, the remodeling of maternal uterine spiral arteries is imperative. These vessels undergo a transition from a high-resistance, low-capacity state to a dilated, low-resistance, high-capacity state, which ensures efficient delivery of nutrients and oxygen delivery to the developing embryos[393, 394]. In women afflicted with preeclampsia, this pivotal process frequently goes awry, resulting in reduced vessel diameter and the emergence of symptoms such as hypertension[393-395]. Specifically, trophoblasts—cells that typically infiltrate the myometrium, line the vascular wall, and adopt endothelium-like characteristics—often show only shallow invasion[406].

### *1.7.3 Syncytia is formed through cell-cell fusion of villous cytotrophoblasts*

The syncytia, a key component of the fetal-maternal interface, continuously undergoes damage from ROS, immune attacks, and blood flow shear forces, necessitating its constant replenishment[396]. This rejuvenation occurs through a process known as "syncytial deportation", which ensures the elimination of aged and damaged syncytium to maintain syncytial homeostasis[421]. This expulsion releases various cellular or subcellular placental materials into the maternal circulation, including large fragments of multinucleate syncytiotrophoblasts (SynTs), cytotrophoblasts (CTBs), small uninucleate elements, anucleate cytoplasmic fragments, and nanovesicles[421, 422]. Intriguingly, numerous studies have reported an increased rate of syncytial deportation in preeclamptic placentas[423]. However, to preserve the integrity and normal function of the placental barrier, specifically the syncytia, there is a reliance on the balanced regulation of CTB proliferation and fusion, which primarily occur post-mitotically[424]. This process allows for the transfer of nuclei, organelles, proteins, and RNAs into SynTs, thereby replenishing them[421]. The formation of the syncytia is facilitated by an envelope gene of retroviral origin, referred to as fusogen, which induces the fusion of mononuclear CTBs. This fusion process is governed by two types of syncytin: syncytin-1 and syncytin-2 in humans, and Syncytin-A and Syncytin-B in mice[425]. Notably, there is a dramatic increase—more than nine-fold—in the number of nuclei within SynTs throughout gestation, indicative of a continuous fusion process[426].

#### *1.7.3.1 Differences in origin and function of SynTs between rodents and humans*

Despite significant overlap in embryonic and placental development between humans and mice, several distinctions are discernible between the two species. Notably, while bearing the same nomenclature, SynTs fulfill essential functions during the early stages of human embryonic development[427]. Specifically, "primitive syncytium", which originates from the differentiation of CTBs and is invasive in nature[411], plays a direct role in blastocyst implantation into the maternal endometrium. This is achieved by secreting proteolytic enzymes that facilitate uterine stroma breakdown, and human chorionic gonadotrophin (hCG), which stimulates the corpus luteum to produce progesterone, thereby maintaining the endometrial lining's integrity[428, 429]. Around the 9th day of human embryonic development, additional enzymes released by the primitive syncytium degrade the endothelial lining of uterine blood vessels, subsequently filling

the lacunae with maternal blood and forming maternal blood sinusoids[430]. Importantly, despite both species possessing a “hemochorial” placenta, the maternal and embryonic circulations in mice are separated by “hemotrichorial” arrangements involving sinusoidal trophoblast giant cells (sTGCs) and two layers of SynTs[431, 432]. This differs from the “hemomonochorial” arrangements observed in human and non-human primate placentas[433] (Figure 1.8). Strikingly, similarities can be noted in humans from tertiary villi, where a single layer of SynT enveloping fetal vessels expresses an array of transport channels to facilitate fetal-maternal exchanges[434]. Nonetheless, a major difference between mouse and human placenta lies in the fact that terminal differentiation, culminating in the formation of SynTs, does not transpire prior to chorioallantoic fusion in mice[431, 435, 436].

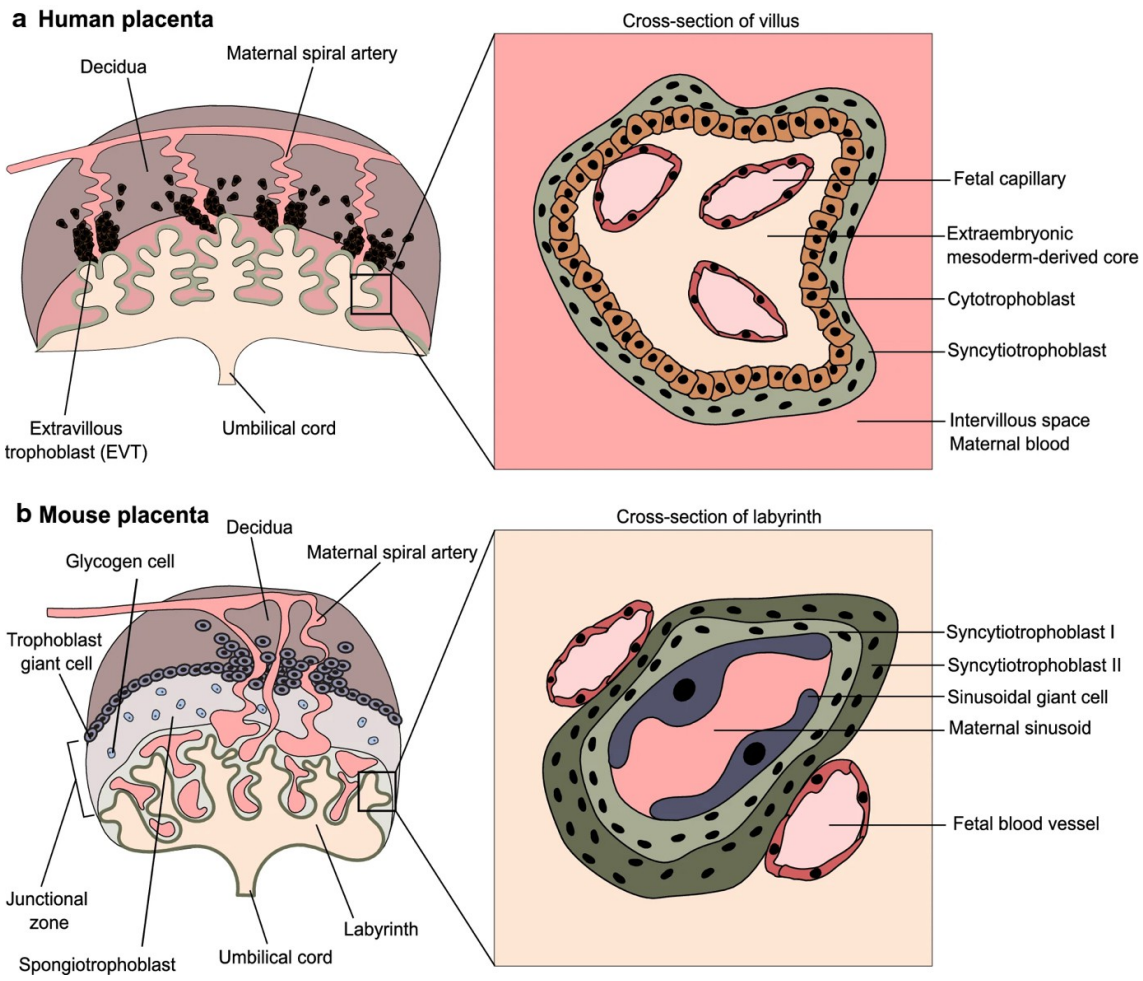


**Figure 1.8: Overview of hemochorial arrangements of human and mouse placenta.**

While the human and mouse placentas both exhibit hemochorial characteristics, the mouse placenta features two SynT layers in its hemotrichorial arrangements. This figure was adapted from: Papuchova, H., Latos, P.A. Transcription factor networks in trophoblast development. Cell. Mol. Life Sci. 79, 337 (2022). https://doi.org/10.1007/s00018-022-04363-6.

## *1.8 Mouse models of placental development: General overview*

Although several limitations exist, mouse models have been instrumental in elucidating the pathogenesis of placental disorders. The advantages of these models, including their large litter size, short gestation period, and significant parallels with human pregnancies, have led to their widespread use (Figure 1.9) [394, 437, 438]. For instance, *in vivo* studies utilizing these models have shed light on the correlation between elevated systemic inflammation, a hallmark of preeclampsia, and the manifestation of preeclampsia-like symptoms. This association is particularly pronounced when there is inhibition of nitric oxide synthase, or upon administration of tumor necrosis factor-alpha (TNF-α) or interleukins[439-441]. Moreover, the indispensable roles of the NOTCH signaling pathway and the Storkhead Box 1 (STOX1) transcription factor in preeclampsia have been emphasized through studies involving *Notch2*-null mice. These mice demonstrated reduced diameters of spiral arteries, subsequently resulting in decreased placental perfusion[442]. In addition, the onset of hypertension in mice has been linked to the overexpression of Stox1[443]. These findings highlight the utility of mouse models in enhancing our understanding of placental pathogenesis.

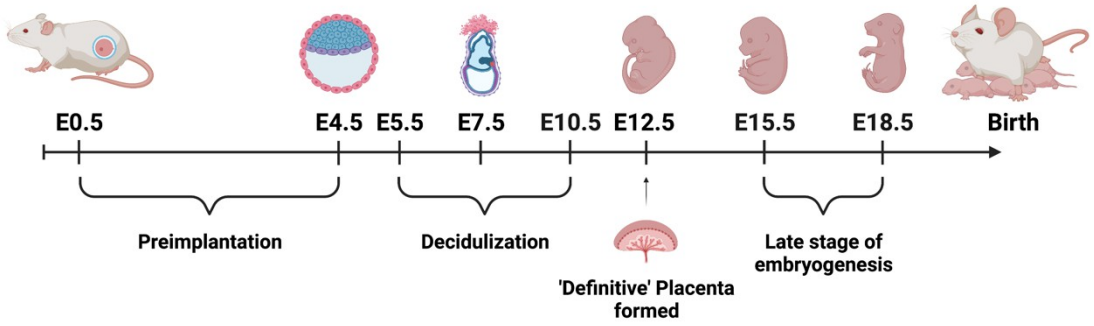


**Figure 1.9: Overview of mouse embryonic development.**

Mouse gestation typically spans between 19 to 20 days and greatly resembles human embryonic development[437]. The period up to E14.5 in mice, corresponding to the first two trimesters in humans, governs the implantation of the blastocyst and the subsequent decidualization, a pregnancy-associated transformation of the maternal endometrium[437, 438]. E12.5 denotes a crucial juncture in mouse embryonic development, marking the completion of the multi-layered, "definitive" placenta. This placenta starts to function to accommodate the increasing demands for rapid fetal growth during the late stages of gestation (starting at E15.0). Notably, the third trimester, or late developmental stage, in mice—unlike in humans—extends to approximately postnatal day 7[437, 444]. Schematics was created with BioRender.

### *1.8.1 Early stages of murine embryogenesis, leading to primitive hematopoiesis*

During the early stages of mouse embryogenesis, the primitive choriovitelline placenta develops as trophoblasts infiltrate the maternal decidua. This placenta orchestrates maternal blood flow and serves as the primary source of nutrition for the embryo[445]. Prestreak gastrulation occurs around E6.0, instigating the formation of the mesoderm germ cell layer and the exocoelomic cavity, which subsequently leads to the genesis of the yolk sac. This phase also witnesses the establishment of various placental constituents such as the amnion, allantois, and chorion[446, 447]. Remarkably, Reichart's membrane, which is unique to rodent placentas, originates from diverse proteins and ECM components secreted by parietal endoderm cells[432, 448]. The Reichart's membrane is homogenous, acellular, and robust, providing protection to the developing embryo by encapsulating the exterior of the yolk sac[432]. The chorionic ectoderm,

which maintains its distinct entity from the amniotic ectoderm, is formed when the proamniotic cavity is partitioned from the chorion by amniochorionic fold[449]. Around E7.5, the proamniotic cavity is completely sealed, forming the amniotic cavity, which isolates the embryo from the ectoplacental cone[432]. Simultaneously, by E7.5, the yolk sac reaches full formation, marking the genesis of "blood islands"—clusters of embryonic red blood cell progenitors[446]. These blood islands, in coordination with the aorta-gonad mesonephros (AGM), facilitate hematopoiesis until definitive hematopoiesis commences in the liver from E10.0 onwards[450-452].

### *1.8.2 Chorioallantioic fusion*

During late-streak gastrulation around E7.0, a key structure termed the "allantoic bud" emerges at the caudal end of the embryo. This bud ultimately develops into the umbilical cord, composed of two arteries and a vein, which establishes a connection between the embryo and the base of the placenta[432, 446, 449, 453]. The allantois affixes itself to the chorionic plate, a specialized region of the chorion that is essential for the development of the labyrinth's intricate vascular networks[454]. A significant event, known as "chorioallantoic fusion", occurs around E8.5 and is marked by the attachment of the allantois to the chorionic plate at the base of the placenta[455]. Remarkably, this fusion event synchronizes with the initiation of the embryo's heartbeat and circulation[456]. Any defects in the chorioallantoic fusion could prove fatal for the embryo since the definitive placenta, which is crucial for nutrient and gas exchanges during late gestation, hinges on its successful completion[432, 446, 457, 458]. Our understanding of this fusion is restricted due to early embryonic lethality observed in mouse models with defective chorioallantoic fusion[459]. Studies have suggested that the chorionic tissue's temporal selectivity in adhesion, regulated by mesothelial cells, assists the attraction and attachment of the distal allantois to the chorionic plate[435, 447, 457, 458, 460]. For example, vascular adhesion cell molecule 1 (Vcam1) in the allantois interacts with α4-integrin (*Itga4*), a Vcam1 ligand expressed by the chorionic mesothelium. Interestingly, not all *Vcam1* or *Itga4*-null mice experience failure in chorioallantoic fusion, implying the existence of additional or compensatory mechanisms[454]. The success of chorioallantoic fusion is paramount, as it triggers the formation of the labyrinth, a major part of the definitive placenta. This labyrinth mediates nutrient, gas, and waste exchanges between the mother and embryo through counter-current blood flows[431, 461].

### *1.8.3 Induction of labyrinth formation*

Upon the successful fusion of the chorioallantoic membranes, which iniates labyrinth formation, the labyrinth continues to grow and differentiate, producing a multitude of branching channels[431, 461, 462]. This expansion of the labyrinth is propelled by chorionic folding, alongside a further invasion into the chorionic plate by the allantoic mesoderm[431]. The significance of the chorioallantoic fusion is highlighted by the induction of differentiated trophoblast lineages by the allantoic vasculature. This lineages include CTBs and SynT types I and II (SynT-I and SynT-II)[431, 435, 436, 461], which are vital for the establishment of the trilaminar structure of the mouse labyrinth[431, 461]. CTBs, also known as sTGC in the mouse placenta, are mononuclear cells. They form the outer, discontinuous layer and secrete hormones by making direct contact with maternal blood[431, 461, 462]. The two SynT layers form the inner strata through cell-cell fusion, contributing to their multinucleated nature[431, 462]. Interestingly, while the SynT layers and the underlying endothelial cell layer maintain a tight connection[431, 461], sTGC has a loose connection with the SynT layers. This loose connection facilitates easier access to maternal blood and enhances placental exchanges through additional protrusions towards embryonic blood spaces[431, 461]. Importantly, the induction of several differentiated trophoblast lineages becomes critical as maternal blood begins to enter from E9.5, following the complete lining of labyrinth sinusoids by the two SynTs[431, 432, 462].

### *1.8.4 Construction of definitive placenta and its role during late gestation*

Following the induction of the labyrinth and the development of a series of distinct trophoblast cell types, the choriovitelline placenta - which facilitates nutrient and gas exchange during early embryogenesis - transitions to the chorioallantoic configuration[463]. This transition notably marks a switch from histiotrophic nutrition, where embryonic cells absorb nutrients from maternal secretions via phagocytosis, to hemotrophic nutrition, a shift essential to meet the growing demand from the fetus during the later stages of embryogenesis[432]. Simultaneously with this transition towards hemotrophic nutrition, around E10.0, primitive hematopoiesis - mediated by blood islands in the yolk sac and AGMs[450-452] – begins to be supplanted by

definitive hematopoiesis. This subsequent process is driven by hematopoietic stem cell colonies localized within the embryonic liver[464]. By E14.5, from a histological perspective, the majority of red blood cells become anucleated, as definitive, anucleated red blood cells take the place of their nucleated counterparts[464]. Throughout the remaining gestation, "branching morphogenesis" occurs within the labyrinth through capillary branching. These capillaries infiltrate the primary villi, consisting of assemblies of trophoblast columns[435], thus supporting embryonic growth[465]. Importantly, by E12.5, the multilayered, definitive placenta - comprising the outermost maternal decidua, the junctional zone, and the innermost labyrinth - completes its construction and commences its function (Figure 1.10)[437, 463].

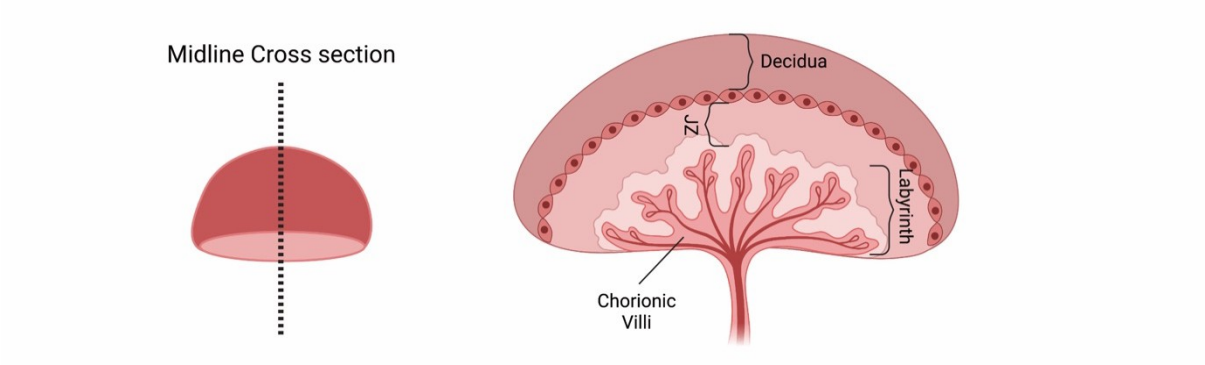


**Figure 1.10: Organization of the multilayered, "definitive" placenta.**
Schematic diagram of E12.5 placenta. This multilayered structure includes the outermost maternal decidua, the junctional zone between the decidua and the innermost labyrinth, and the labyrinth, characterized by extensive "chorionic villi"[437]. Schematics were created with BioRender.

### *1.8.4.1 Maternal decidua*

The decidua, a specialized modification of the maternal endometrium located farthest from the developing embryo, houses the maternal vasculature and spiral arteries[437, 462]. This region is distinctively characterized by the remodeling of spiral arteries, as evidenced by trophoblasts lining the vascular smooth muscle walls[464, 466]. Furthermore, uterine natural killer (uNK) cells play a continuous role in modulating maternal immune responses at the interface between the mother and embryo, during later stages of gestation[432, 467, 468]. In the mouse placenta, a downturn

in the uNK cell population initiates around E16.0, coinciding with a diminution in the decidual area[432]. In tandem with these changes, the decidual tissues experience deterioration, and the surrounding uterine tissue largely reverts to its preimplantation epithelial configuration[460].

#### *1.8.4.2 Junctional zone*

Situated between the outermost maternal decidua and the innermost labyrinth in the mouse placenta lies the junctional zone[437, 463]. This area's establishment follows the induction of sTGCs and SynTs, culminating in the trilaminar trophoblast structure within the mouse labyrinth[436, 461]. The junctional zone houses differentiated trophoblast lineages such as spongiotrophoblasts (SpT) and glycogen cells[462]. Interestingly, SpT, which delineate the maternal venous sinusoids, constitute the majority of the junctional zone by E12.5. However, their population amplifies four-fold by the end of gestation. Concurrently, the glycogen cell population expands by an astonishing 250-fold during the same timeframe[461, 463]. Glycogen cells are postulated to originate from *Tpbp/4311*-expressing SpTs[462], and further distinguish themselves through the expression of *Protocadherin 12* (*Pcdh12*)[469]. Primarily, the junctional zone executes endocrine functions, encompassing the production of hormones, growth factors, and cytokines that direct the progression of placentation[390, 470-472]. SpTs within this zone produce antiangiogenic proteins, such as soluble Fms-like tyrosine kinase-1 (sFlt-1) and proliferin-related protein (rPlf), safeguarding the embryo against intrusive maternal endothelial cells[462, 471, 473]. Contrary to the labyrinth, the junctional zone, despite harboring large venous sinusoids, demonstrates inefficiency in facilitating substrate exchanges between the mother and the embryo. This inefficiency arises because the large vessels predominantly transport maternal blood, already depleted of nutrients and gases through exchanges within the labyrinth, towards the decidua[431, 461, 463]. Analogous to the decidua, the junctional zone's area reduces by E18.5, a transformation ascribed to alterations in cell size, proliferation, and migration[471].

#### *1.8.4.3 Labyrinth*

The escalating demands of fetal growth, alongside the onset of organogenesis, necessitating amplified feto-maternal exchanges, result in a more than nine-fold surge in placental volume throughout gestation. This marked expansion is primarily due to the growth of

the labyrinth[432, 464]. A unique feature of the labyrinth is the counter-current arrangement of fetal and maternal blood flows. This configuration allows the flow of deoxygenated embryonic blood through the umbilical vessels towards the labyrinth. Meanwhile, oxygenated maternal blood enters the placenta via spiral arteries. This blood subsequently descends towards the labyrinth, moves towards the placental base, then reverses direction to flow back toward the draining maternal vessels[463]. It is noteworthy that the sTGCs, while initially loosely tethered to the underlying SynT layers during the early phase of the transition to the chorioallantoic placenta[431, 461], begin to fuse at later stages. This fusion process enables the underlying SynT layers to protrude, releasing hormones and other embryo-derived secretions into the maternal bloodstream[461]. Placental defects from numerous genetically engineered mouse models were most frequently—although not exclusively—observed in the labyrinth, the primary site for nutrient and gas exchange[390, 454, 474]. Placental dysfunction due to labyrinth defects can typically be attributed to two major causes: 1) trophoblast lesions, and 2) vascular defects, leading to a "small labyrinth"[454]. More precisely, trophoblast lesions may arise from impaired generation of SynTs[475] or overproduction of trophoblast lineages[476-478]. Conversely, vascular defects in the labyrinth may stem from hindered production of labyrinth vascular networks due to aberrant vasculogenesis from the chorionic plate[479, 480] or endothelial cell hypoplasia[481].

### *1.8.5 Placental-cardiovascular axis*

Congenital heart defects impose a significant socioeconomic burden, affecting approximately 1% of live births, over 10% of pregnancy-associated complications[482, 483], and nearly 20% of patients with AOS[338]. These defects represent the most prevalent birth abnormalities, yet the etiology of most congenital heart defect cases remains elusive, despite the extensive repertoire of mouse models available[484, 485]. While targeted gene ablation in cardiomyocytes has provided valuable insights, the molecular mechanisms driving congenital heart defect pathogenesis still largely remain enigmatic[484, 485]. This knowledge gap might be attributed to the traditionally focused scope of the investigation, often limited to the affected tissue itself. However, a paradigm shift led by various mouse model studies postulates that placental dysfunction could be the fundamental instigator behind congenital heart defects[474]. This hypothesis is supported by the parallel development of the heart and placenta, both sharing

similar developmental pathways[486]. Empirical findings have further substantiated this theory, revealing that the global deletion of certain genes, such as *Ly6e* and *ATP11a* in placentas and embryos, leads to embryonic lethality due to cardiac anomalies. Intriguingly, the heart-specific deletion of these genes did not precipitate embryonic lethality or congenital heart defects[487-489]. Notably, recent findings have pinpointed placental dysfunction, particularly defects in terminal differentiation and maintenance of the SynT population in the developing mouse placenta, as a common origin of congenital heart defects[490]. These ground-breaking discoveries underscore the urgent need to broaden the scope of congenital heart defect research, emphasizing the potential role of placental dysfunction in its pathogenesis.

## *1.9 Rationale and Objectives*

Understanding the molecular mechanisms driving human diseases is paramount for devising targeted therapeutic strategies. CdGAP, a Cdc42 GTPase-activating protein, is recognized for its role in mediating cellular dynamics and bestowing cells with migratory and invasive potential. This behavior is closely linked to tumorigenesis and progression of breast cancer in humans. The regulation of cellular dynamics, an integral aspect of processes like epithelial-to-mesenchymal transition (EMT), is fundamental to embryonic development. Given CdGAP's crucial role in cellular dynamics, it is reasonable to postulate its potential function in embryogenesis. This is further supported by diverse regulatory domains within CdGAP and its GAP-independent functions, particularly in post-transcriptional regulation, which underscore its involvement in breast cancer progression. Beyond breast cancer, CdGAP expression has been observed to be significantly upregulated in prostate cancer patients, indicating a potential oncogenic role akin to that in breast cancer. However, the precise role of CdGAP in prostate cancer progression is yet to be fully elucidated due to the heterogenic nature of the disease. Of particular interest are findings showing that both Rac1 and Cdc42 knockout mice, which utilize CdGAP as a GAP, suffer significant embryonic lethality at early stages (~ E5.5). This emphasizes the potential of CdGAP's involvement in embryonic development. Intriguingly, CdGAP has been associated with Adams-Oliver syndrome (AOS), a rare developmental disorder marked by limb abnormalities and scalp defects. Considering the reports of placental dysfunction in AOS patients and the identification of *ARHGAP31*, the gene encoding CdGAP, as a causative factor in AOS, further investigation is required to unravel CdGAP's role in AOS pathogenesis.

Given the compelling yet fragmented understanding of CdGAP's functions and roles, the present thesis aims to:

1) Elucidate the role of CdGAP in prostate cancer tumorigenesis, considering its established oncogenic function in breast cancer and its increased expression in prostate cancer. We aim to ascertain whether CdGAP's loss or misregulation impacts prostate cancer progression, thereby providing new insights into potential therapeutic targets.

2) Generate and characterize a CdGAP-AOS knock-in mouse model to gain a better understanding of CdGAP's role in embryonic development and define the molecular

events underlying AOS pathogenesis. This could offer deeper insights into the broad spectrum of AOS abnormalities and potentially identify new disease-causing gene for AOS.

By pursuing these objectives, we aim to shed light on the dual role of CdGAP in the progression of human cancer and its potential involvement in development, thereby enriching our understanding of both cancer and developmental biology.

# Chapter 2: CdGAP promotes prostate cancer metastasis by regulating epithelial-to-mesenchymal transition, cell cycle progression, and apoptosis

Chahat Mehra, Ji-Hyun Chung, Yi He, Monica Lara-Márquez, Marie-Anne Goyette, Nadia Boufaied, Véronique Barrès, Véronique Ouellet, Karl-Phillippe Guérard, Carine Delliaux, Fred Saad, Jacques Lapointe, Jean-François Côté, David P. Labbé, and Nathalie Lamarche-Vane. (2021). ***Communications biology***. 4 (1042).

## Preface to Chapter 2

In previous research from our laboratory, we demonstrated the oncogenic role of CdGAP in human breast cancer. Interestingly, CdGAP was shown to transcriptionally repress E-cadherin expression in a GAP-independent manner. However, given the heterogeneity of cancer and the interplay with the ECM that influences tumor progression and metastasis *in vivo*, the role of CdGAP as an oncogene in prostate cancer remained uncertain. Transcriptomic expression analysis for *ARHGAP31*, the gene encoding CdGAP, across a vast array of prostate cancer cell lines suggested a positive correlation between *ARHGAP31* expression levels and prostate cancer aggressiveness. Moreover, high levels of mutated CdGAP in patients were significantly associated with an increased likelihood of prostate cancer biochemical recurrence. Based on these observations, we hypothesized that CdGAP functions as an oncogene in prostate cancer. To test this hypothesis, we knocked down CdGAP in castration-resistant prostate cancer (CRPC) cell lines, PC-3 and 22Rv1. In contrast, we overexpressed CdGAP in DU-145, 22Rv1, and LNCaP to determine whether elevated levels of CdGAP conferred a significant increase in migratory and invasive potentials in these cells. Our transcriptomic analysis via RNA-sequencing revealed that gene sets associated with epithelial-to-mesenchymal transition (EMT) and apoptosis were enriched in CdGAP-depleted PC-3 cells. Furthermore, we investigated the *in vivo* effects of CdGAP depletion using subcutaneous and orthotopic xenograft models. Our findings suggest that loss of CdGAP significantly impairs prostate cancer progression by hindering tumor growth and metastasis to distant sites such as the intestine and bone.

**CdGAP promotes prostate cancer metastasis by regulating epithelial-to-mesenchymal transition, cell cycle progression, and apoptosis**

**Chahat Mehra[1,2,#], Ji-Hyun Chung[1,2,#], Yi He[1,2], Mónica Lara Márquez[1,2], Marie-Anne Goyette[3], Nadia Boufaied[1], Véronique Barrès[4], Véronique Ouellet[4], Karl-Phillippe Guérard[1], Carine Delliaux[3], Fred Saad[4,5], Jacques Lapointe[1,6], Jean-François Côté[2,3], David P. Labbé[1,2,6,*], Nathalie Lamarche-Vane[1,2,*]**

1. Cancer Research Program, Research Institute of the McGill University Health Centre, Montréal, Québec, Canada.
2. Department of Anatomy and Cell Biology, McGill University, Montréal, Québec, Canada.
3. Institut de recherches cliniques de Montréal, Université de Montréal, Montréal, Québec, Canada.
4. Centre de recherche du Centre hospitalier de l'Université de Montréal et Institut du cancer de Montréal, Montréal, QC, Canada.
5. Department of Surgery, Université de Montréal, Montréal, QC, Canada.
6. Division of Urology, Department of Surgery, McGill University, Montréal, Québec, Canada.
#These authors contributed equally.

***Correspondance**: david.labbe@mcgill.ca (D.P.L.), nathalie.lamarche@mcgill.ca (N.L-V.)
Research Institute of the McGill University Health Centre, 1001 Boul. Décarie, Montréal, Québec, Canada H4A 3J1. Phone: 514-934-1934 ext. 76361 (D.P.L.), 76166 (N.L-V.)

## Abstract

High mortality of prostate cancer patients is primarily due to metastasis. Understanding the mechanisms controlling metastatic processes remains essential to develop novel therapies designed to prevent the progression from localized disease to metastasis. CdGAP plays important roles in the control of cell adhesion, migration, and proliferation, which are central to cancer progression. Here we show that elevated CdGAP expression is associated with early biochemical recurrence and bone metastasis in prostate cancer patients. Knockdown of CdGAP in metastatic castration-resistant prostate cancer (CRPC) PC-3 and 22Rv1 cells reduces cell motility, invasion, and proliferation while inducing apoptosis in CdGAP-depleted PC-3 cells. Conversely, overexpression of CdGAP in DU-145, 22Rv1, and LNCaP cells increases cell migration and invasion. Using global gene expression approaches, we found that CdGAP regulates the expression of genes involved in epithelial-to-mesenchymal transition, apoptosis and cell cycle progression. Subcutaneous injection of CdGAP-depleted PC-3 cells into mice shows a delayed tumor initiation and attenuated tumor growth. Orthotopic injection of CdGAP-depleted PC-3 cells reduces distant metastasic burden. Collectively, these findings support a pro-oncogenic role of CdGAP in prostate tumorigenesis and unveil CdGAP as a potential biomarker and target for prostate cancer treatments.

## Introduction

Prostate cancer is the second most commonly diagnosed cancer in men[1]. While patients bearing a localized tumor display high survival rates, once the tumor advances and metastasizes current therapies are limited and ineffective[2]. Thus, understanding the molecular mechanisms underlying prostate cancer progression is a pressing unmet need and the identification of novel therapeutic targets is necessary for the treatment of this disease.

Rho GTPases are a subfamily of the large Ras superfamily of small GTPases, which have important roles in cytoskeletal remodeling, cytokinesis, cell polarity, cell motility, cell invasion, and apoptosis[3]. Rho proteins act as molecular switches cycling between active GTP-bound and inactive GDP-bound states. This GDP/GTP cycle is regulated by guanine nucleotide exchange factors (GEFs) that promote the exchange of GDP for GTP while GTPase-activating proteins (GAPs) stimulate the intrinsic GTPase activity, leading to protein inactivation[4]. Given their key roles in normal cellular processes, it is not surprising that aberrant Rho signaling is frequently implicated in human tumors[3]. However, as the frequency of activating mutations in *RHO* genes is much less than in *RAS* genes in cancer patients[5], the regulators of Rho GTPases have emerged as targets of subversion in cancer[3, 6]. In particular, GAPs have been assigned tumor suppressor roles in cancer due to their ability to inactivate Rho GTPases, but recent evidence has emerged contradicting the existing dogma and implicating RhoGAPs as oncoproteins in several cancers, including breast and prostate cancers[6-10].

Cdc42 GTPase-activating protein (CdGAP, also known as ARHGAP31) is a RhoGAP specific for Rac1 and Cdc42, but not Rho[11, 12]. CdGAP is highly phosphorylated on serine and threonine residues in response to growth factors and is a substrate of extracellular signal-regulated kinase (ERK), GSK-3, and p90 ribosomal S6 kinase (RSK), mediating cross talk between the Ras/MAP kinase pathway and Rac1 regulation[13]. Previous studies have reported gain-of-function mutations in *ARHGAP31* in patients with the rare developmental Adams-Oliver syndrome (AOS), which is characterized by aplasia cutis congenita and terminal transverse limb defects[14]. In addition, there is compelling evidence to support a pro-oncogenic role for CdGAP in cancer progression. Notably, CdGAP is a serum-inducible gene and modulates cell spreading, lamellipodia formation, focal adhesion turnover, matrix-rigidity sensing and durotaxis —

implicating a role in cytoskeletal remodeling and cellular migration[15-17]. Furthermore, the loss of CdGAP in mice severely compromised embryonic vascular development and resulted in impaired VEGF-mediated angiogenesis, one of the hallmarks of cancer[18]. Moreover, CdGAP has been implicated in the regulation of the expression of E-cadherin — loss of which is a key step of epithelial-to-mesenchymal transition (EMT) — via two different mechanisms. Firstly, the expression of CdGAP has been shown to significantly disrupt mature epithelial cell-cell contacts[19]. Secondly, CdGAP was shown to translocate to the nucleus and form a functional complex with the transcriptional factor ZEB2 to repress E-cadherin expression in breast cancer cells[7]. Importantly, CdGAP mediates transforming growth factor (TGFβ)- and ErbB2-induced breast cancer cell motility and invasion in a GAP-independent manner[8]. *In vivo*, loss of CdGAP in ErbB2-transformed breast cancer cells impaired tumor growth and suppressed metastasis to the lungs[7]. Consistently, high expression of CdGAP correlated with poor disease-free survival in all subtypes of breast cancer patients[7].

In this study, we sought to investigate the role of CdGAP/ARHGAP31 in prostate cancer. We first interrogated publicly available prostate cancer data sets with combined gene expression and clinical data, which demonstrated a positive association between high CdGAP expression and early biochemical recurrence (BCR) in prostate cancer patients. Knockdown of CdGAP in two human castration-resistant prostate cancer cell (CRPC) lines inhibited cell motility, invasion, and proliferation, even though higher levels of Rac1-GTP were detected in CdGAP-depleted PC-3 cells. Using global gene expression approaches, we found that CdGAP regulates the expression of genes involved in EMT but also genes involved in apoptosis and cell cycle progression. We correlated this effect with an increase in the cyclin-dependent kinase (CDK) inhibitor p21 levels, a concomitant arrest in G1 cell-cycle phase and an increased sensitivity of CdGAP-depleted PC-3 cells to doxorubicin-induced apoptosis. Furthermore, loss of CdGAP delayed tumor initiation, decreased tumor volume and tumor size in subcutaneous xenografts and reduced distant metastasic burden in an orthotopic model of prostate cancer. Consistently, an elevated cytoplasmic CdGAP expression in prostate cancer cells was associated with bone metastasis in prostate cancer patients, further supporting an important role for CdGAP in prostate cancer progression. Therefore, our study revealed that CdGAP is an important regulator of prostate tumor progression and metastasis.

## Results

### Elevated levels of CdGAP expression in human prostate cancer is associated with a decreased time to disease recurrence

One of the first indications of prostate cancer recurrence following initial response to therapy is the rise of the prostate-specific antigen (PSA) in the blood of patients defined as time to biochemical recurrence (BCR). Therefore, to assess the clinical relevance of CdGAP in prostate cancer, we first determine whether CdGAP/ARHGAP31expression is associated with BCR by analyzing publicly available datasets. In The Cancer Genome Atlas (TCGA_PRAD) dataset, when stratifying patients according to *ARHGAP31* expression by maximally selected rank statistic (Supplementary Figure 1A), Kaplan-Meier analysis revealed that patients with high *ARHGAP31* expression trends toward a shorter time to BCR (p=0.053; Figure 2.1A). In the Mortensen dataset, Kaplan-Meier analysis showed that patients with high *ARHGAP31* expression had a significantly shorter time to BCR (p=0.0064; Figure 2.1B and Supplementary Figure 1B). Strikingly, no BCR was observed within 5 years in patients with low *ARHGAP31* in contrast to 70% of patients with high *ARHGAP31*. Moreover, Kaplan-Meier analysis of TCGA_PRAD patients stratified based on *ARHGAP31* gain and amplification (cBioPortal, www.cbioportal.org;[20]) demonstrated shorter time to BCR in patients with altered *ARHGAP31* (p=0.0021; Figure 2.1C). Together, these data suggest that CdGAP is a positive modulator of prostate cancer recurrence.

### CdGAP depletion in PC-3 cells increases the levels of active Rac1

We next sought to determine the expression of CdGAP in human prostate cancer cell lines[21]. CdGAP expression was undetectable in the androgen-dependent cell line LNCaP (Figure 2.2A, B, and Supplementary Figure 2A). Low levels of CdGAP were found in the CRPC DU-145 and 22Rv1 cell lines while high CdGAP protein and mRNA levels were detected in CRPC PC-3 cells (Figure 2.2A, B, and Supplementary Figure 2A). Consistently, *ARHGAP31* gene expression level in multiple prostate cancer cell lines obtained from the Prensner dataset[22] revealed the highest *ARHGAP31* expression in PC-3 cell line (Supplementary Figure 2B). Similar to CdGAP expression in human breast cancer cell lines we also found an inverse correlation between CdGAP and E-cadherin expression levels in human prostate cancer cell lines

(Figure 2.2A, B). In addition, we observed a nuclear and cytoplasmic localization of CdGAP in PC-3 cells (Supplementary Figure 2C) as previously reported in breast cancer cells[7, 13].

To examine whether CdGAP is involved in pro-tumorigenic behaviors such as cell motility and invasion, proliferation and tumorigenesis of CRPC cells, we generated stable PC-3 and 22Rv1 cell lines knockdown for CdGAP using short-hairpin RNA (shRNA) lentiviruses (Supplementary Figure 2D, E). Clone 2 of shCdGAP PC-3 cells led to a 90% reduction of CdGAP protein and mRNA levels when compared with control shRNA (Figure 2.2C, D, and Supplementary Figure 2D). Similarly, 90% reduction of CdGAP protein expression was achieved in shCdGAP 22Rv1 cells (Supplementary Figure 2E). We assessed the effect of CdGAP depletion on the levels of active Rac1 in CdGAP-depleted PC-3 cells by performing a GST-CRIB pull down assay. Loss of CdGAP resulted in a 2.7-fold increase in Rac1-GTP levels (Figure 2.2E), leading to significant morphological cell changes (Figure 2.2F). In contrast to the elongated PC-3 control cells, CdGAP-depleted cells showed a rounded cell morphology with a decreased cell area and cell aspect ratio (Figure 2.2F). Therefore, these results demonstrate that CdGAP acts as a major GAP for Rac1 in PC-3 cells.

**CdGAP silencing impairs prostate cancer cell migration, invasion, and proliferation**

To assess the role of CdGAP in prostate cancer cell migration and invasion, we performed transwell migration and invasion assays as well as wound healing assays. Control shRNA or CdGAP-depleted PC-3 and 22Rv1 cells migrated towards the bottom chamber, which contained media with 10% fetal bovine serum over a period of 24 hours. Loss of CdGAP significantly impaired PC-3 and 22Rv1 cell migration and invasion. CdGAP knockdown inhibited PC-3 and 22Rv1 cell migration by 65% and 40%, respectively (Figure 2.3A and Supplementary Figure 3A), and transwell invasion through Matrigel by 74% and 40%, respectively (Figure 2.3B and Supplementary Figure 3B). Furthermore, CdGAP-depleted PC-3 cells were significantly less efficient to migrate in a wound-healing assay over a period of 27 hours (Figure 2.3C and Supplementary Movie 1,2). Even though 22Rv1 cells were less migratory than PC-3 cells, loss of CdGAP in 22Rv1 cells significantly reduced the wound confluence compared to control cells (Figure 2.3D and Supplementary Movie 3,4). We further confirmed the impact of CdGAP on human prostate cancer cell migration and invasion by ectopic expression of CdGAP in DU-145 and 22Rv1 cells and in the androgen-sensitive LNCaP cell line

(Supplementary Figure 3C). Consistently, CdGAP overexpression in all three cell lines significantly increased cell migration and invasion (Figure 2.3E, F and Supplementary Figure 3D, E). Increased migratory capacity of cells depends on their ability to rapidly attach and detach with the extracellular matrix[23]. Thus, we next determine whether CdGAP depletion also affects the ability of PC-3 cells to adhere to fibronectin and type I collagen. We found that loss of CdGAP had no significant impact on the ability of PC-3 cells to adhere to fibronectin or type 1 collagen (Figure 2.3G). Then, we examined the impact of CdGAP on prostate cancer cell proliferation. CdGAP depletion significantly reduced proliferation of PC-3 and 22Rv1 cells over a period of 5 days in culture (Figure 2.4A and Supplementary Figure 3F). We extended this analysis and performed a colony formation assay that revealed a 73% decrease in the number of colonies formed by CdGAP-depleted cells compared to control shRNA PC-3 cells (Figure 2.4B). Collectively, these results indicate that CdGAP is a regulator of prostate cancer cell migration, invasion, and proliferation.

**CdGAP modulates the expression of genes related to EMT, apoptosis, and cell cycle arrest**

To gain mechanistic insights into the pro-migratory and proliferative role of CdGAP in prostate cancer cells, we performed transcriptomic analysis on CdGAP-depleted PC-3 cells compared to control shRNA PC-3 cells. Differential gene expression analysis identified 1384 upregulated and 720 downregulated mRNAs in CdGAP-depleted PC-3 cells compared to control cells (Figure 2.5A and Supplementary Data 1). Gene set enrichment analysis (GSEA; Hallmark) revealed that gene sets associated to EMT and apoptosis were enriched in CdGAP-depleted cells (Figure 2.5B, C). Additionally, gene sets associated to cell proliferation, including G2M checkpoint, E2F and MYC targets were significantly depleted in cells with compromised CdGAP expression (Figure 2.5B, C). Furthermore, gene ontology analysis centered on biological processes revealed that genes related to chemotaxis, cell motility and the urogenital system development were amongst the most significantly affected in CdGAP-depleted cells (Figure 2.5D). In this way, CdGAP has also been shown to modulate EMT and cell motility gene expression profiles in breast cancer cells[7]. Indeed, loss of CdGAP in ErbB2-expressing mouse mammary tumor cells and in human breast cancer MDA-MB-231 cells resulted in a decrease of SNAIL1 and ZEB2 concomitantly with an increase of E-cadherin and reinstatement of cellular adherens junctions[7]. In contrast to the effects observed in breast cancer cells, CdGAP depletion

in PC-3 cells led to a significant increase in SNAIL1 (*SNAI1*) and a decrease in E-cadherin (*CDH1*) mRNA and protein levels (Figure 2.5E, F). On the other hand, the levels of two mesenchymal markers N-cadherin (*CDH2*) and Slug (*SNAI2*) were significantly decreased in CdGAP-depleted PC-3 cells (Figure 2.5E, F). A decrease expression of these genes has been consistently reported as correlated with a decrease in cell motility[24]. Altogether, these results suggest that CdGAP affects cell motility and EMT gene expression in prostate cancer.

In addition, a subset of genes encoding cell cycle checkpoint proteins were significantly increased in CdGAP-depleted cells compared to control shRNA cells (Figure 2.6A). Accordingly, the increased levels of the CDK inhibitor p21 (*CDKN1A*) (Figure 2.6A, B), which is crucial in the regulation of G1 cell cycle progression[25, 26] was validated by qPCR, showing a 3-fold increase in CdGAP-depleted PC-3 cells compared to control shRNA cells (Figure 2.6B). To assess the role of CdGAP on G1 cell cycle progression, flow cytometry analysis was conducted by staining cellular DNA with propidium iodide (PI). It revealed a significant increase of cell population in the G1 phase cell cycle (61%) in CdGAP-depleted PC-3 cells compared to control shRNA cells (53%), therefore limiting the percentage of cells in the S (from 26% to 22%) and G2 (from 21% to 16%) phases (Figure 2.6C). Next, we examined whether CdGAP could affect cell death by inducing apoptosis in PC-3 cells submitted to a 12h-doxorubicin treatment followed by Annexin V/PI flow cytometry analysis. As shown in Figure 2.6D, we observed a significant increase in the apoptotic cell population in CdGAP-depleted PC-3 cells (6%) compared to control cells (0.5 %) when treated with vehicle. Increased concentrations of doxorubicin treatment induced cell apoptosis in a dose-dependent manner in both shRNA control cells and shCdGAP cells. However, CdGAP-depleted cells were significantly more sensitive to doxorubicin-induced cell apoptosis compared to control cells in all doxorubicin conditions tested (doxorubicin 5 μM; 37% in shCdGAP cells compared to 9% in control cells; Figure 2.6D). Therefore, the loss of CdGAP resulted in G1 cell cycle arrest with a concomitant increase in cell apoptosis in PC-3 cells, which correlates with a decrease of cell proliferation observed in CdGAP-depleted cells (Figure 2.4A, B). Taken together, these analyses revealed CdGAP as a key modulator of prostate cancer cell proliferation through the control of apoptosis and cell cycle genes.

**The loss of CdGAP delays subcutaneous tumor formation and attenuates tumorigenesis induced *in vivo***

We next determined the role of CdGAP in tumorigenesis *in vivo* by injecting subcutaneously control shRNA cells or CdGAP-depleted PC-3 cells into athymic mice. The loss of CdGAP significantly delayed tumor formation with a 2.6-fold difference between the control group and the shCdGAP group of mice (Figure 2.7A). Additionally, 73% of the mice injected with CdGAP-depleted cells led to tumor formation compared to 100% of mice injected with control cells (Figure 2.7A). Consistently, the endpoint tumors from the shCdGAP group of mice were smaller compared to the control group (Figure 2.7B), which correlated with a significant 2-fold reduction in tumor volume and tumor weight from the shCdGAP cohort compared to control mice at 34 days post-injection (Figure 2.7C, D). Together, these data demonstrate that CdGAP promotes tumorigenesis.

**CdGAP knockdown attenuates distant metastasis in an orthotopic model**

To further investigate CdGAP function in prostate cancer metastasis, we injected CdGAP-depleted PC-3 cells or control shRNA cells expressing luciferase into athymic mouse prostates. We then measured the resulting orthotopic xenograft formation and evaluated metastasis formation by bioluminescence imaging. In contrast to subcutaneous tumor formation (Figure 2.7), loss of CdGAP did not significantly affect prostate tumor weight and volume at the endpoint (Figure 2.8A-D). Histological analysis of primary tumors showed a typical adenocarcinoma morphology with no major differences between control and CdGAP-depleted injected mice (Figure 2.8E). However, an increase in cell apoptosis as demonstrated by a significant increase in cleaved caspase-3 staining was detected in prostate tumors from mice injected with shCdGAP cells (Figure 2.8F) whereas no difference in the cell proliferation marker Ki-67 or CD-31 staining was detected between control and shCdGAP tumors (Supplementary Figure 4A, B). Local metastasis to the urogenital system, including kidneys and testes, was detected by post-mortem bioluminescence in 100% of control and shCdGAP group of mice (Figure 2.8G, H; Supplementary Figure 5). However, distant metastasis to the intestines was detected by post-mortem bioluminescence in 100% of control mice compared to 50% of CdGAP-depleted injected mice, which showed fewer lesions compared to control mice (Figure 2.8G, H; Supplementary Figure 5). Moreover, post-mortem bioluminescence in the legs and

paws suggested distant metastasis to the bones in control mice, which was reduced in CdGAP-depleted injected mice (80% of control mice vs 33% of shCdGAP mice) (Figure 2.8G, H; Supplementary Figure 5). Histological analysis of kidneys revealed tumorigenic lesions in both control and mice injected with shCdGAP cells (Figure 2.8I), validating the bioluminescence images obtained post-mortem (Figure 2.8G and Supplementary Figure 5). Therefore, these results suggest a role for CdGAP in promoting prostate cancer metastasis.

**Increased levels of cytoplasmic CdGAP expression in human prostate cancer is associated with reduced bone metastasis-free survival**

Next, we examined the expression of CdGAP on a panel of radical prostatectomy specimens from 285 prostate cancer patients using the TF123 tissue microarray (TMA) series[27] (Supplementary Figure 6 and Supplementary Table 1). Since we have previously reported a nuclear and cytoplasmic localization of CdGAP in breast tumor specimens[7], nuclear and cytoplasmic intensity of CdGAP expression was evaluated within each tissue core (Figure 2.8J). Notably, CdGAP cytoplasmic intensity was significantly greater in tumor (T) tissue cores in comparison to matched benign adjacent (BA) tissue cores (Average fold change=4.781; p=1.2e-21; Figure 2.8J). In contrast, comparable CdGAP nuclear intensity was detected between T and matched BA tissue cores (Average fold change=1.123; p=0.013; Figure 2.8J). Kaplan-Meier analyses demonstrated that high CdGAP cytoplasmic intensity in cancer cells was associated with a trend toward increased risk of developing bone metastasis in prostate cancer patients (p=0.057; Figure 2.8K). Strikingly, univariate analyses revealed that patients with greater CdGAP cytoplasmic intensity in their tumor tissues (CdGAP-T) were more likely to develop bone metastatic lesions (p=0.005, Hazard Ratio (HR) = 2.416, 95% CI = 1.310-4.453; Figure 2.8L and Supplementary Table 2). Taken together, these data demonstrate the importance of CdGAP in prostate cancer metastasis and suggest that CdGAP could be used as a biomarker to identify patient at risk of progressing toward a metastatic disease.

## Discussion

Tumorigenesis is a multistep process that involves the modulation of cell proliferation, survival, migration, and invasion. The mechanisms controlling prostate cancer metastasis still remain an unresolved issue and a better understanding of prostate cancer progression will help to identify novel molecular targets for prostate cancer treatment and diagnosis. Our data presented here outline the possibility that CdGAP/ARHGAP31, a negative regulator of Rac1 and Cdc42, acts as an oncoprotein rather than a tumor suppressor in prostate cancer. We demonstrate that CdGAP is required for two CRPC cell lines, PC-3 and 22Rv1 cells, to proliferate, migrate, and invade the extracellular matrix. The mechanisms through which CdGAP promote cell growth and migration involve the regulation of G1 cell cycle progression, apoptosis, and EMT genes (Figure 2.9). Consistently, CdGAP is required for the establishment and growth of subcutaneous primary tumors. However, CdGAP expression did not affect the formation of orthotopic primary prostate tumors, highlighting the influence of the tumor microenvironment in the development of tumorigenesis[28]. Hence, CdGAP supports the development of prostate cancer distant metastasis in an orthotopic model and is associated to bone metastasis in patients. This work has broad implications to further improve our understanding of RhoGAPs as oncogenes and their potential impact as cancer therapeutics.

Several lines of evidence suggest that CdGAP may have a pro-tumorigenic role in cancer. As a GAP for Rac1 and Cdc42, CdGAP is a key regulator of actin-cytoskeletal remodeling conferring pro-migratory roles to CdGAP[11]. Furthermore, CdGAP was shown to have a key role in the regulation of directional membrane protrusions of migrating osteosarcoma cells[16, 17]. Of note, CdGAP appears to be the major RhoGAP expressed in HER2/ErbB2-induced mouse breast tumors[29]. In line with this, downstream of TGFβ and ErbB2 signaling pathways, CdGAP was shown to regulate cell migration and invasion in an ErbB2-induced mouse breast cancer cell model[8]. Furthermore, loss of CdGAP suppressed the ability of breast cancer cells to induce primary tumors and to metastasize to the lungs[7]. Here, we found that elevated levels of CdGAP expression in a cohort of human prostate cancer patients was associated with an increased risk of bone metastasis in patients. These results are in good agreement with the depletion of CdGAP in PC-3 cells resulting in a reduction of distant metastasis to the intestines and potentially to the bones in an orthotopic model. In this way, analysis of gene expression datasets also revealed the positive correlation between elevated CdGAP gene expression and BCR in prostate cancer

patients. Thus, this study presents data regarding *CdGAP/ARHGAP31* as a gene associated with prostate cancer metastasis and a potential target in the treatment of aggressive prostate cancer.

In order to migrate and invade, cells have to undergo a well characterized process known as EMT. Some hallmarks of this process include upregulation of the expression of mesenchymal markers SNAIL1, SLUG, N-cadherin, and downregulation of epithelial markers such as E-cadherin, ZO-1 and claudins. In direct contrast to our previous study of CdGAP in breast cancer[7, 8], downregulation of CdGAP resulted in a further decrease of E-cadherin levels, primarily because of the net increase in the levels of the E-cadherin transcriptional repressor SNAIL1. When we investigated further, we observed a decrease in other mesenchymal markers such as SLUG and N-cadherin. Expression of both SLUG and N-cadherin has been correlated in several reports with increased motility and an aggressive cancer phenotype[30, 31]. Thus, although the marked decrease in E-cadherin levels upon CdGAP downregulation contrasts with the findings in breast cancer, the regulation of other genes hints at a differential mechanism of action of CdGAP in prostate cancer. Whether N-cadherin and SLUG are direct targets of CdGAP during the regulation of EMT in prostate cancer need to be further investigated. Nevertheless, the differential regulation of EMT genes highlights an important role of CdGAP in the migration and invasion of prostate cancer cells.

Further investigation of the proliferative capacities using *in vivo* subcutaneous injections demonstrated that CdGAP-depleted tumors exhibited delayed tumor onset, reduced tumor volume and tumor weight, in comparison to control tumors and this further substantiated the results obtained from the *in vitro* experiments. In contrast, prostate orthotopic injection of CdGAP-depleted cells did not alter the formation of primary tumors. These differences highlight the importance of the tumor microenvironment and stroma-tumor interaction in prostate cancer growth and progression[28]. Cancer cells are sensitive to their surrounding cells and factors that contribute to reprogramming the tumor cells to either grow or arrest proliferation. The global transcriptional reprogramming in CdGAP-depleted PC-3 cells may support a positive niche for the tumors to develop in prostate tissue environment, which may be different in a subcutaneous tumor context. For instance, the upregulation of regulatory factors including TGFβ and FGF1 in CdGAP-depleted cells could differentially influence the role of CdGAP in prostate cancer growth in a specific tumor microenvironment.

In this study, we have also observed a significant reduction in CdGAP-deficient 22Rv1 cell proliferation and a robust attenuation of cell proliferation as well as a decrease in colony-formation ability when CdGAP was depleted in PC-3 cells. The colonies in CdGAP-depleted PC-3 cells were loose and scattered from one another and unable to form compact ones as observed in control PC-3 cells. Furthermore, transcriptomics analysis of CdGAP-depleted cells revealed alterations in a subset of genes encoding cell cycle checkpoint proteins including increased levels of the CDK inhibitor p21. Consistently, we observed that the loss of CdGAP in PC-3 cells led to an arrest in the G0/G1 phase with an increase in cell apoptosis. Previous reports have implicated RhoGAPs in the regulation of CDK inhibitors[6]. Notably, depletion of ARHGAP11A in basal-like breast cancer cells was shown to lead to cell-cycle arrest mediated by p27 while depletion of RacGAP1 led to an increase in p21 protein associated with an increase in senescence[10]. This study identified both these RhoGAPs as oncogenic GAP essential for the regulation of cell proliferation[6, 10]. By contrast, ARHGAP24 (FilGAP) emerged as a tumor-suppressor in renal cell carcinoma by inhibiting G1/S phase cell cycle progression, increasing apoptosis and inhibited tumor growth[32]. ARHGAP10 has also been consolidated as a tumor-suppressor in ovarian cancer cells by inhibiting cell cycle progression and inducing apoptosis resulting in suppression of tumorigenesis[33].

Rho proteins organize the cytoskeleton, therefore their regulators and effectors are involved in maintaining normal homeostasis and are prone to alteration due to oncogenic transformations[3]. The pro-oncogenic role of CdGAP in breast[7, 8] and prostate cancer challenges the existing paradigm and adds to the list of the emerging RhoGAPs acting as positive modulators of cancers[6]. Notably, in ovarian and colorectal cancer the expression of RacGAP1 positively correlated with lymph node metastasis and poor survival, respectively[34, 35]. As well, p190A, a RhoGAP for RhoA has been implicated as an oncogenic GAP in osteosarcoma, colorectal, lung and breast cancer[36].

In conclusion, the current study highlights the involvement of CdGAP in prostate cancer development and metastasis by regulating cell proliferation, migration, and death. CdGAP might be a valuable prognostic biomarker for metastasis and a therapeutic target in the treatment of prostate cancer.

# Methods

### Mortensen and TCGA analyses

The Mortensen dataset (GSE46602)[37] is a microarray-based dataset (Affymetrix U133 2.0 Plus), comprising 36 laser micro dissected prostate cancer samples and 14 normal prostate samples. Data files with probes values (.CEL files) and sample data were downloaded from NCBI Gene Expression Omnibus (GEO) database (GEO, http://www.ncbi.nlm.nih.gov/geo/) using getGEO-function of GEOquery package_2.54.1[38]. Read count and samples clinicopathological information from The Cancer Genome Atlas (TCGA) PRAD dataset were downloaded from the TCGA database (http://tcga-data.nci.nih.gov/tcga/)[39] using Bioconductor package TCGAbiolinks_2.14.1[40]. We used TCGA level 3 data that comprise 52 normal, 498 cancer and 1 metastasis samples excluded from the analysis. *ARHGAP31* gene alteration (gain and amplification) information was downloaded from cBioPortal (cBioPortal, www.cbioportal.org).

Data processing: Microarray raw data (.CEL files) were read and preprocessed by Oligo Bioconductor package_1.50.0[41]. Probe intensities were summarized using Robust Multi Array Average (RMA) algorithm. This step includes a background correction, a quantile normalization and a log2 transformation of the data. Probes with low intensity were filtered and batch effect was corrected using the ComBat-function of the sva Bioconductor package_3.34.0[42]. Hugo Gene Symbol were mapped to each probe in the platform using hgu133plus2.db annotation_3.2.3 package[43] and genes with multiple probe sets were collapsed using CollapseRows-function ("MaxMean" argument) from WGCNA package_1.69[44]. TCGA RNA-seq sequencing read count were normalized for sequencing depth using the size factor method implemented in Deseq2_1.26.0 package[45].

Survival analyses: To conduct survival analyses, expression data from Mortensen *et al*. (microarray based) studies were transformed to z-score while expression data from TCGA (RNA-seq based) datasets was transformed using the variance-stabilizing transformation implemented in the Deseq2_1.26.0 package[45]. Patients were divided into high expression and low expression groups by optimal cutpoint calculated by survcutpoint-function of survminer_0.4.6[46] package (Supplementary Figure 1a, b). Differences in patient's recurrence-free survival between groups were estimated by Kaplan-Meier survival analysis and log-rank tests using R package survival_3.1-12[47] and survival curve were generated using

survminer_0.4.6[46] package. All data analysis and statistical tests were performed in R version 3.6.2 (2019-12-12).

**Cell culture, DNA constructs, and transfection**

PC-3, LNCaP, 22Rv1 and DU-145 prostate cancer cells (ATCC) were cultured in RPMI 1640 (Wisent: 350-000-CL) supplemented with 2 mM L-Glutamine, 10% fetal bovine serum (FBS), 1% penicillin/streptomycin, and maintained in a humidified incubator at 37°C with 5% $CO_2$. Cell lines were regularly tested for mycoplasma contamination but they have not been authenticated. Blasticidin-resistant PC-3 cells previously transfected with empty vector pcDNA6/A (Invitrogen, Carlsbad, CA, USA) were transduced for stable bicistronic co-expression of ZsGreen and luciferase (pHIV-Luc-ZsGreen, AddGene, Watertown, MA, USA). Fluorescence-activated cell sorting was used (BD FACSAria Fusion, San Jose, CA, USA) to select the ZsGreen and luciferase positive PC-3 cells for subsequent experiments. To generate stable CdGAP-knockdown cell lines, PC-3 cells or luciferase-expressing PC-3 cells were infected with short hairpin RNA (shRNA) targeting CdGAP lentiviruses (5'-CCTCATTTAGTTCACCTGGAACTCGAGTTCCAGGTGA
ACTAAATGAGG-3'; Sigma: TRCN0000047639), and 22Rv1 cells were infected with shRNA targeting CdGAP lentiviruses (5'-CCGGCGGAGATCAGTAATTCTGGATCTCGAGATCCA
GAATTACTGATCTCCGTTTTTG-3'; Sigma: TRCN0000047641) or control shRNA (Sigma: SHCON 001) purchased commercially. To select CdGAP-depleted PC-3 cells, puromycin (1 μg/ml) (Sigma: P8833) was added to the medium 48 hours after infection. These cells were then plated in a 96-well plate at 1 cell/well and selected until single cell clones were obtained. To select CdGAP-depleted 22Rv1 cells, puromycin (1 μg/ml) was added to the medium 24 hours after infection. For CdGAP overexpression, DU-145, 22Rv1, and LNCaP cells were transfected with full-length pEGFPC1-mCdGAP or empty vector pEGFPC1 constructs using jetPRIME transfection reagent (Polyplus:114-07) following the manufacturer's instructions. All experiments were carried out 24 hours post-transfection[13].

**Immunoblotting**

Cells were lysed in RIPA buffer containing 50 mM HEPES pH 7.5, 0.1% sodium dodecyl sulfate, 1% Triton X-100, 0.5% sodium deoxycholate, 50 mM sodium fluoride, 150 mM sodium

chloride, 10 mM EDTA pH 8.0, 50 mM sodium orthovanadate, 20 mM leupeptin, 20 mM aprotinin and 1 mM phenylmethylsulfonyl fluoride. Protein lysates were subjected to centrifugation at 10,000 x g for 15 min at 4°C to remove insoluble materials and protein concentrations were determined using the Bicinchoninic Acid Assay (BCA) protein kit (Thermo-Scientific). Equal amounts of protein samples were resolved by SDS-PAGE, transferred to nitrocellulose membranes for immunoblotting with the indicated antibodies in Supplementary Table 3, and visualized by enhanced chemiluminescence (ECL) using Clarity™ western ECL substrate (Bio-Rad: 1705061) and the ChemiDoc™ MP imaging system. All quantitative densitometry analysis on the obtained images were carried out using Image Lab software. The optical density ratios were calculated as followed: CdGAP over tubulin; E-cadherin over tubulin; snail1 over tubulin; n-cadherin over tubulin; slug over tubulin; Rac1-GTP over total Rac1. The optical density fold change was calculated by normalizing the ratio of each condition to control ratio.

**Quantitative real time polymerase chain reaction (Q-PCR)**

Total RNA was extracted using Qiagen RNeasy kit (Qiagen: 74104). mRNA was reverse transcribed using the 5X All-In-One RT MasterMix kit (AbCAM: G485). Next, quantitative real time polymerase chain reaction (Q-PCR) was performed with SYBR Green PCR Master Mix (Applied Biosystems), using primers specific to the genes of interest: CdGAP (Qiagen: QT00076671), β-actin (Qiagen: QT00095431); other primers used are listed in Supplementary Table 4. Q-PCR reactions were carried out at 95°C for 3 min, followed by 40 cycles at 95°C for 20 sec, then at 60°C for 30 sec and finally at 72°C for 30 min. Gene expression was normalized to β-actin RNA[7, 8] and the fold change was calculated by normalizing the ratio to control cells (shCon).

**Immunofluorescence**

Cells grown on glass coverslips were fixed for 30 minutes in 3.7% formaldehyde in PBS before permeabilization for 5 minutes with 0.25% Triton-X-100 in PBS. After blocking for 30 minutes in a solution of PBS with 1% bovine serum albumin (BSA), coverslips were incubated overnight at 4°C with anti-CdGAP antibodies, followed by a 45-minute incubation with Alexa Fluor 488-conjugated anti-rabbit and rhodamine-conjugated phalloidin to stain for F-actin filaments. 4′,6′-

diamidino-2-phenylindole (DAPI) was used to stain the nuclei. Between each step, coverslips were washed three times with PBS. Coverslips were mounted on glass slides using Prolong Gold antifade reagent (Invitrogen: P3696). Cells were examined with a motorized inverted Olympus IX81 microscope using a 40x Plan-S-APO oil objective lens and images were recorded with a CoolSnap 4K camera (Photometrics) and analyzed with Image J software[7, 8]. For actin staining and quantification analyses, cells were examined with a Zeiss LSM780 confocal microscope with a 63X/1.40 oil DIC Plan-Apochromat objective and analyzed with Zen2009 and Image J softwares. A minimum of 30 to 40 cells for control or shCdGAP cells per experiment were analyzed for quantification of the cell area and aspect ratio. Aspect ratio represents the ratio of the length over the width of the cell.

**Cell migration and invasion**

For migration assays, 100 000 PC-3 (shControl; shCdGAP) or DU-145 (EV; GFP-CdGAP) cells, 50 000 22Rv1 (shControl; shCdGAP) cells, 150 000 22Rv1 (EV; GFP-CdGAP) cells, 100 000 LNCaP (EV; GFP-CdGAP) cells were resuspended in serum-free medium and seeded in the top chamber of transwell inserts (Falcon: 353097). For invasion assays, 150 000 PC-3 or DU-145 cells, 250 000 22Rv1 or LNCaP cells were plated onto a 5% Matrigel (ThermoFisher: 356234) layered over the top chamber. Cells were incubated at 37°C overnight (PC-3, DU-145, 22Rv1 cells) or 48h and 60h for migration and invasion of LNCaP cells, respectively, which allowed migration towards the bottom chamber containing complete medium with 10% FBS. Cells on the bottom surface of the insert were fixed in 10% formalin (BioShop: 8G56294) and stained with a crystal violet solution. Five images were taken for each transwell insert using a Nikon inverted microscope camera with a 10X objective lens (Nikon Eclipse TE300 Inverted microscope). Quantitative analysis was assessed using Image J software. Data represent the fold change relative to that of shRNA control cells or empty vector control cells obtained from at least three independent experiments[8].

**Wound-healing assays**

96-well IncuCyte® ImageLock microplate (Sartorius: ImageLock 4379) was coated with 1mg/ml poly-D-Lysine (Sigma: P6407-5MG) for 1h at 37 °C. Then, wells were rinsed once with calcium and magnesium-free PBS. 15 000 PC-3 (shCon;shCdGAP) cells or 60 000 22Rv1

(shCon;shCdGAP) cells per well were seeded in triplicates, and incubated overnight. The following day, confluency of each well was monitored. Then, IncuCyte® 96-well WoundMaker Tool (Essen Bioscience) was used to generate scratch cell monolayers, following manufacturer's instructions. IncuCyte® S3 Live-Cell Analysis System was used for image acquisitions with a 3h-interval during a period of 27 hours.

**Cell adhesion**

An *in vitro* adhesion assay was performed by resuspending 40 000 cells in complete media and seeding them on 96-well plates coated with 10 µg/ml type 1 collagen (BD Bioscience: 354246) or 10 µg/ml fibronectin (Sigma: F1141) for 30 min at 37 °C. Cells were fixed using 3.7% formaldehyde in PBS for 15 minutes, washed twice with washing buffer (0.1% BSA in RPMI) and stained with a crystal violet solution. After washing the excess dye out, the plates were allowed to dry for 1 hour. Then the crystal violet stain absorbed by the cell nuclei was solubilized with 10% acetic acid and the optical density was measured at 570 nm[8].

**Cell proliferation**

To assess cell proliferation, the cell growth determination MTT (3-(4,5-Dimethylthiazol-2-yl)-2,5-diphenyltetrazolium bromide) kit (AbCAM: 211091) was used. Briefly, 250 PC-3 cells (shControl; shCdGAP) or 500 22Rv1 cells (shControl; shCdGAP) were seeded in triplicates in 96-well plates and grown over a period of five days. MTT solution was added to each well for the last 4h of treatment on each day as per manufacturer's protocol. Absorbance was measured at 590 nm[8]. Data represent the fold change in cell proliferation relative to that of Day 1 obtained from three independent experiments.

**Colony formation**

Two hundred and fifty cells per well in 6-well plates were resuspended in complete media for 10 days at 37 °C in a humidified incubator. On day 10, the 6-well plates were washed with PBS, fixed in 10% formalin (BioShop: 8G56294) and stained with a crystal violet solution. The excess dye was washed out with water twice and the plates were then left to dry overnight. Images were obtained with a 10X objective lens using a Nikon Eclipse TE300 Inverted

microscope. Fifty cells were counted as one colony. The data represent the average of all the images per condition obtained from three independent experiments[48].

**Rac1 activation**

The CRIB domain of mouse PAK3 (amino acids 73–146) fused to glutathione S-transferase (GST-CRIB) was used to isolate GTP-bound Rac1 and was purified as follows[13]. Briefly, bacterial pellets were resuspended in the lysis buffer (buffer A) containing 20 mM HEPES pH 7.5, 120 mM sodium chloride, 2 mM EDTA pH 8, 10% glycerol, and 1% Triton-X100, sonicated and centrifuged at 3000 RPM at 4°C. Then, 30 µg of purified GST-CRIB was coupled to glutathione–agarose beads (50%) (Sigma) for 3 hours at 4°C and centrifuged at 1000 RPM for 1 minute, and the pellet was washed in buffer A twice. Cell lysates (1 mg of control or shCdGAP PC-3 total cell protein) were incubated with the GST-CRIB proteins coupled to the glutathione–agarose beads for 45 minutes at 4°C on a rotator. The samples were centrifuged at 1000 RPM at 4°C for 1 minute to collect the beads. After discarding the supernatant, beads were washed three times in cold RIPA buffer and resuspension in SDS sample buffer, heated at 95°C and then examined by immunoblotting. The levels of Rac1-GTP were assessed by densitometry and normalized to the total amount of Rac1 detected in the total cell lysates.

**Cell cycle**

Control or shCdGAP PC-3 cells were serum starved overnight followed by a 24-hour incubation in RPMI containing 10% FBS. 1 x $10^6$ cells were harvested, counted, and washed twice in ice-cold PBS and fixed in 70% ethanol for 1 hour at 4°C. Cells were then washed with PBS and incubated with RNase A for 1 hour at 37°C in a humidified incubator. Finally, cells were stained with 10 µg/ml propidium iodide (PI; Sigma: P4170). Cells were subjected to flow cytometry analysis with BD FACSCanto II system. The cell cycle distribution was analyzed using the FlowJo analysis software v10.7.1 (TreeStar, Inc.)[13].

**Apoptosis**

Apoptosis was assessed in control or shCdGAP PC-3 cells using the Alexa Fluor 488 annexin V/Dead cell apoptosis kit (Invitrogen: V13241). Briefly, cells we serum starved overnight in RPMI media supplemented with 0.25% FBS followed by a 12h treatment with doxorubicin (1, 2

and 5 μM) (Sigma: #D1515) or DMSO 0.05% as vehicle. Cells were subjected to flow cytometry analysis using the BD FACScanto II system. To determine the percentage of cell population distribution, we quantified the population of apoptotic cells with fluorescence in the green emission spectrum (520nm), necrotic cells with red fluorescence (620 nm), and late apoptotic cells with both green and red fluorescence. Data were analyzed using the FlowJo analysis software v10.7.1 (TreeStar, Inc.).

**RNA-sequencing**

RNA-sequencing was performed and analyzed as described below[7]. Briefly, total RNA from three independent samples of control shRNA PC-3 or CdGAP-depleted PC-3 (shCdGAP) cells was extracted using Qiagen RNeasy kit (Qiagen: 74104). Deep sequencing was performed using Illumina TruSeq RNA Sample Preparation Kit, Illumina TruSeq SR Cluster Kit v2, and Illumina TruSeq SBS Kit v2 (50 cycles) according to the manufacturer's procedures. Sequencing was performed at the Génome Québec Innovation Centre (McGill University) using the Illumina HiSeq 2000 platform. Quality of the raw reads was assessed with FastQC_0.11.5 and reads were aligned to the GRCh38 genome with Star 2.5.1b. Raw alignment counts were calculated with featureCounts_1.4.6 and differential expression measurements were performed with DESeq2_1.12.3. Gene ontology analyses and Gene Set Enrichment Analyses (GSEA) were conducted using ClusterProfiler_3.14.3 R package[49]. Input genes for GSEA analysis were ranked in descending order according to moderated *t*-statistic and applied to Hallmark gene sets downloaded from the Molecular Signature Database (MSigDB) using msigdbr_7.1.1 R package.

**Xenograft and orthotopic injections**

To assess primary tumor growth of control or shCdGAP PC-3 cells, 1 x $10^6$ cells were resuspended in 100 μl of serum-free RPMI containing 50% Matrigel (ThermoFisher: 356234) and injected subcutaneously using BD disposable syringe with Leur-Lok Tips (ThermoFisher: 14-823-30) into the right flanks of 7-week-old male athymic mice. Tumors were measured every two days with a digital caliper and the tumor volume was calculated using the following formula: $V = \pi$ (length × width$^2$)/6. After 34 days, mice were sacrificed, and the tumors were harvested, fixed in 10% formalin (Cochiembec: F-5010Z) and subjected to analysis. Orthotopic injections of 7-week-old male athymic mice were performed as follows[50]. Briefly, male athymic mice

were anesthetized and an abdominal small incision was made to expose the prostate. 2.5 x $10^5$ control or shCdGAP PC-3-expressing luciferase cells were resuspended in 10 µl PBS with an equal volume of Matrigel and injected into the right dorsal prostate lobe. Mice were monitored daily for one week and wound clips were removed one-week post-surgery. Tumor growth was monitored weekly thereafter via *in vivo* bioluminescence imaging. On the day of imaging, a 15 mg/ml luciferin solution (Perkin Elmer: #122799) was freshly prepared in PBS. Luciferin was injected intraperitoneally at a concentration of 150 mg luciferin/kg body weight. Bioluminescent imaging was performed using Bruker's *in vivo* Xtreme system following the manufacturer's instruction. Bioluminescence signals were normalized and presented in photons/sec/$mm^2$. After 4 weeks, mice were sacrificed, and the tumors and organs potentially containing metastatic foci were dissected for formalin fixation, paraffin embedding, and tissue analysis. *Ex vivo* bioluminescent imaging at the experimental end point was performed on each mouse exposed for 4 minutes to identify the number of mice with local and distant metastasis. All animal protocols were approved by McGill University Animal Use and Care Committee, in accordance with guidelines established by the Canadian Council on Animal Care.

**Tissue microarray (TMA)**

Construction of TMA: The TMA TF123 series is composed of 300 radical prostatectomy specimens from patients participating in the Centre de recherche du Centre hospitalier de l'Université de Montréal (CRCHUM) prostate cancer biobank. These patients have undergone surgery at the CHUM between 1993 and 2006. For each patient, two cores (0.6 mm) of tumor (T, cancer) and two cores of benign adjacent (BA) glands were extracted from formalin-fixed paraffin-embedded (FFPE) radical prostatectomy specimens and arrayed on receiver blocks. A total of 285 prostate cancer treatment naïve specimens were used for this study (Supplementary Table 2), 15 cases were excluded due to pre-operative treatments[27].

Scoring of CdGAP in TMA: Using digitalized images, two different observers evaluated the nuclear frequency categorized in 0 (none), 1 (1-25%), 2 (26-75%) and 3 (76-100%), and both the nuclear and the cytoplasmic intensity (0 to 3 for negative, weak, moderate, high, respectively) of CdGAP within each tissue core. The average scores obtained from cores with the same histology (T or BA) were used for the statistical analyses.

Survival analyses: Patients were divided in two groups according to the median intensity of CdGAP in the cytoplasm. Bone metastasis-free survival was evaluated by Kaplan-Meier survival analysis and the log-rank test as described previously. Univariate Cox regression analyses were used to estimate the hazard ratios (HRs) for CdGAP using SPSS software 24.0 (SPSS Inc. Chicago, IL, USA). For univariate analyses, the serum PSA level prior to the radical prostatectomy, pathologic staging of the primary tumor (pT 2, 3, 4), Gleason Score category (6, 7 (3+4), 7 (4+3), 8+), and margin status (negative/positive) were included in the model.

**Immunohistochemistry (IHC)**

IHC was performed as described below[7]. Briefly, primary tumors were fixed in 10% formalin and paraffin embedded. IHC was performed with Ki67 (Abcam: #ab15580; 1:300 dilution), CD31 (Abcam: # ab124432; 1:1200 dilution), and cleaved caspase-3 (Cell Signaling: #9661s; 1:300 dilution) antibodies. All slides were counterstained using hematoxylin and eosin (H&E). Slides were scanned using a Scanscope XT digital slide scanner (Aperio, Leica Biosystems Inc., Concord, ON, Canada) and analyzed with Imagecope software (Aperio, Leica Biosystems Inc.). In human TMA staining, IHCs were performed on 4 μm-thick sections of each TMA blocks (n=6) using the Benchmark XT autostainer (Ventana Medical Systems). Antigen retrieval was performed for 60 minutes with Cell Conditioning 1 (#950-124, Ventana Medical System, Tucson, AZ) and sections were stained using a pre-diluted (1:50) anti-CdGAP polyclonal antibody (Sigma: HPA036380) manually added to the slides and incubated at 37˚C for 60 minutes. UltraView universal DAB detection kit (#760-500, Ventana Medical System) revealed CdGAP expression and counterstaining was achieved using hematoxylin and bluing reagents (#760-2021 and #760-2037, Ventana Medical System). Tissues were dehydrated and mounted using SubX mounting media (Leica microsystems, Concord, ON, Canada). All sections were scanned using a VS-110 microscope with a 20x 0.75 NA objective and a resolution of 0.3225 μm (Olympus Canada Inc., Richmond Hill, ON, Canada).

**Statistics and reproducibility**

Statistical analyses in Figs. 2.2, 2.3, 2.4, 2.5E, F, 2.6, 2.7, 2.8A-C, 2.8F, supplementary Figs. 2.2-2.4 were performed using GraphPad Prism **9** (GraphPad software, San Diego, CA, USA). A two-sample unpaired Student's t-test was used for comparisons between two groups. Data are

presented as the mean +/- SEM and a p-value of less than 0.05 was statistically significant. Data are representative of at least three independent experiments.

**Data availability**

Data are available from the corresponding authors upon request. The sequencing data reported in this paper (RNA-seq) were deposited on NCBI Gene Expression Omnibus (GEO; accession number GSE160399). The source data underlying the figures can be accessed in Supplementary Data 1.

## Acknowledgements

We thank Dr. Aurélie Le Page for technical assistance in performing the orthotopic injections. We thank Mr. Mathieu Simard and Dr. Aurore Dodelet-Devillers at the Small Animal Imaging Labs (SAIL) of the Research Institute of the McGill University Health Centre (RI-MUHC) for their assistance and help with the bioluminescence analyses. We thank the Immunophenotyping platform of the RI-MUHC and the Institut de recherches cliniques de Montréal Molecular Biology and Functional Genomics core facility for assistance with the RNA-seq analyses. We thank Dr Noriko Uetani for the drawing of the working model in Figure 9. We are grateful to all patients who agreed to participate into the Centre de Recherche du Centre Hospitalier de l'Université de Montréal (CRCHUM) Prostate cancer tumor bank. Biobanking was done in collaboration with the Réseau de Recherche sur le cancer of the Fonds de Recherche Québec – Santé (FRQS) that is affiliated with the Canadian Tumor Repository Network (CTRNet). TMA construction was supported by the Terry Fox Research Institute. C.M. and J.-H.C. were supported by studentships from the RI-MUHC and M.L.M. from CONACyT. M.A.G. holds a CIHR doctoral studentship. F.S. holds the Raymond Garneau Chair in Prostate Cancer Research – Université de Montréal. V.B., V.O., and F.S. are researchers of the CRCHUM which receives support from the FRQS. J-.F.C. holds the TRANSAT Chair in breast cancer research. D.P.L is a Lewis Katz – Young Investigator of the Prostate Cancer Foundation and is also a Research Scholar – Junior 1 from FRQS. This research was supported by a Cancer Research Society grant to J.-F.C. and Canadian Institutes of Health Research (CIHR) project grants (PJT-162246) to D.P.L and (PJT-153151) to N.L.V.

**Author contributions**

**Conception and design:** C. Mehra, J.-H Chung, DP. Labbé, N. Lamarche-Vane. **Acquisition of data:** C. Mehra, J.-H. Chung, Y. He, M. L. Marquez, MA Goyette, N. Boufaied, V. Barres, V. Ouellet, C. Delliaux, F. Saad. **Analysis and interpretation of data :** C. Mehra, J.-H. Chung, Y. He, M. L. Marquez, MA Goyette, N. Boufaied, V. Ouellet, KP. Guérard, JF. Côté, DP. Labbé, N. Lamarche-Vane. **Writing, review, and/or revision of the manuscript:** C. Mehra, J.-H. Chung, N. Boufaied, V. Ouellet, KP. Guérard, J. Lapointe, JF. Côté, DP. Labbé, N. Lamarche-Vane.

## Competing interests

The authors declare no competing interests.

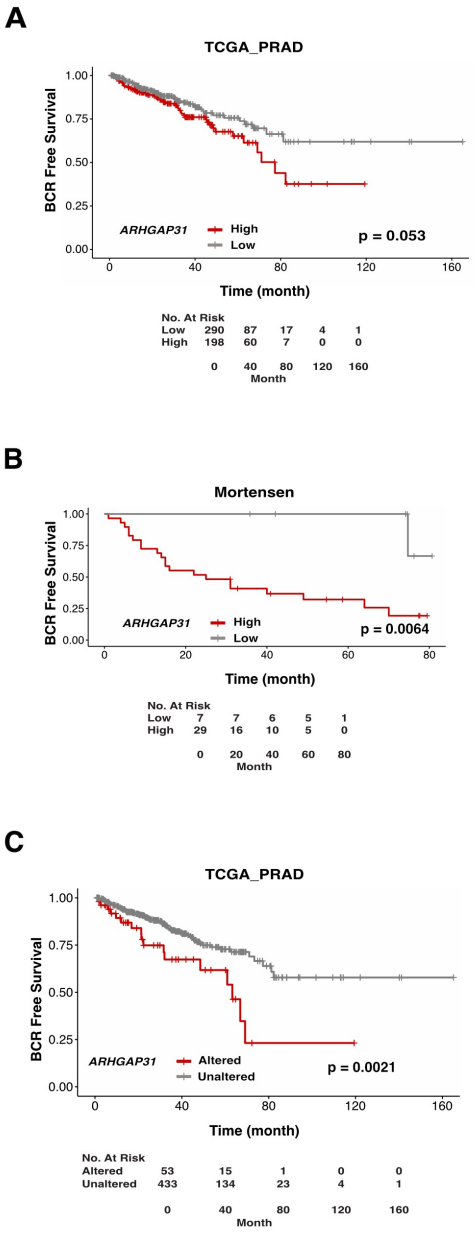


**Figure 2.1: High CdGAP expression is positively correlated with cancer recurrence.**

(A, B) Kaplan-Meier curves of biochemical recurrence (BCR) free survival for TCGA_PRAD (A; n=488 patients; p=0.053) and for Mortensen et al. dataset (B; n=36 patients; p=0.0064) based on ARHGAP31 transcript levels by using maximally selected rank statistics.

(C) Kaplan-Meier curves of BCR-free survival based ARHGAP31 gene alterations (gain and amplification) in TCGA provisional data set (n=486 patients; analyzed through cBioPortal; p=0.0021).

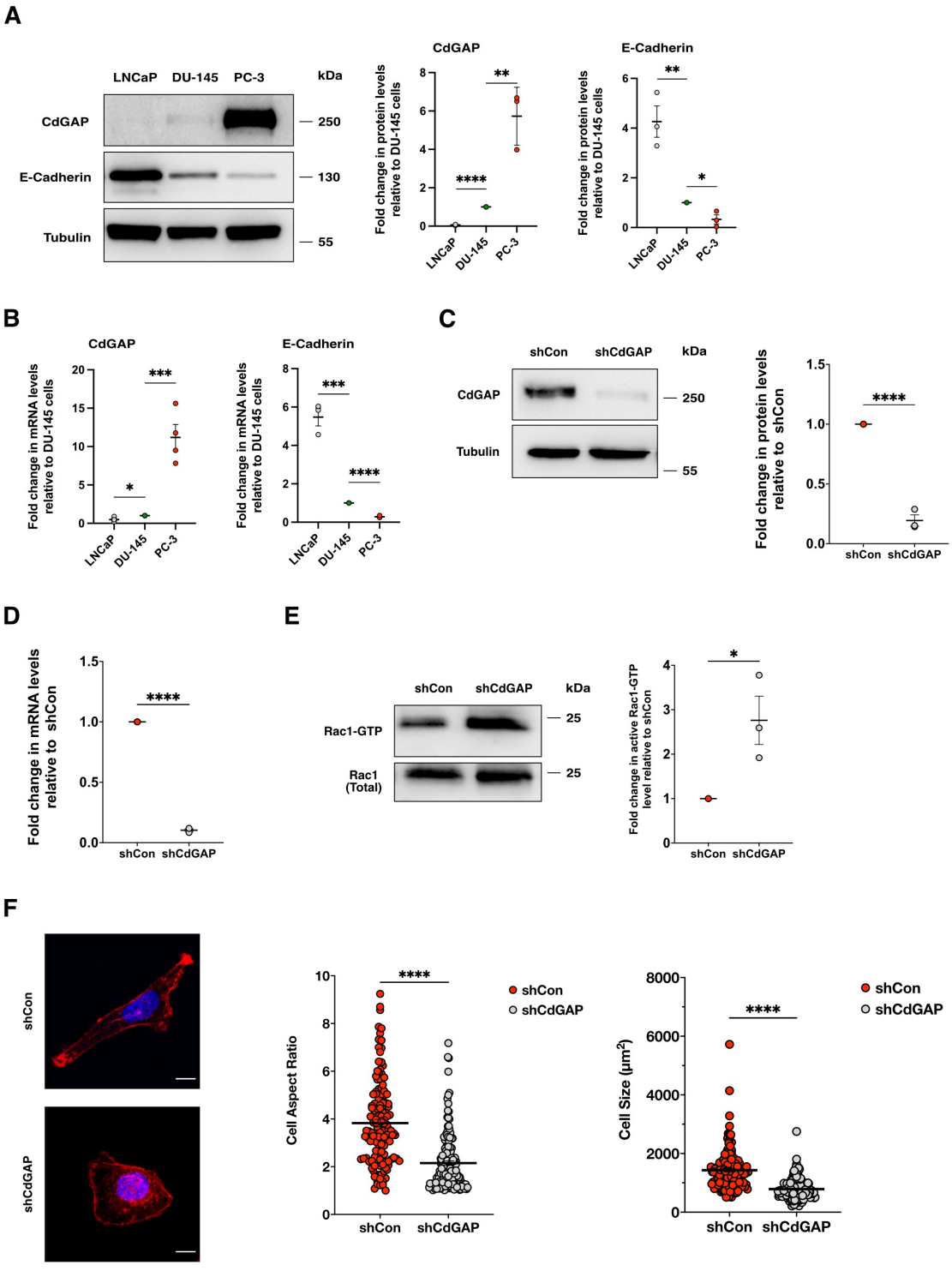
A
LNCaP
DU-145
PC-3
kDa
CdGAP
E-Cadherin
Tubulin
250
130
55
CdGAP
E-Cadherin
Fold change in protein levels relative to DU-145 cells
B
Fold change in mRNA levels relative to DU-145 cells
C
shCon
shCdGAP
Fold change in protein levels relative to shCon
D
Fold change in mRNA levels relative to shCon
E
Rac1-GTP
Rac1 (Total)
Fold change in active Rac1-GTP level relative to shCon
F
Cell Aspect Ratio
Cell Size (μm²)

**Figure 2.2: Loss of CdGAP results in elevated Rac1-GTP levels in PC-3 cells.**

(A) Immunoblot analysis of CdGAP and E-cadherin in human prostate cancer cell lines DU-145, LNCaP and PC-3. Tubulin was used as a loading control. Graphs provide a densitometry analysis of CdGAP and E-cadherin protein levels represented as the fold change relative to DU-145 cells (n=3).

(B) mRNA levels of CdGAP (n=4) and E-cadherin (n=3) represented as the fold change relative to DU-145 cells.

(C) Immunoblot analysis of CdGAP levels in PC-3 cells infected with scrambled control (shCon) or shRNA targeting CdGAP (shCdGAP). Tubulin was used as loading control. Graph provides a densitometry analysis of CdGAP protein levels represented as the fold change relative to control (n=3).

(D) mRNA levels of CdGAP represented as the fold change relative to control (n=3).

(E) GTP-bound Rac1 was pulled down using GST-CRIB from control (shCon) or CdGAP-depleted PC-3 (shCdGAP) cell lysates. TCL: total cell lysates. Graphs provide a densitometry analysis of GTP-bound Rac1/total Rac1 represented as the fold change relative relative to control (n=3).

(F) Control and shCdGAP PC-3 cells were plated on coverslips coated with fibronectin. Actin filaments and nuclei were stained using phalloidin-TRITC and DAPI. Scale bar represents 10 μm. Cell aspect ratio and cell size were quantified (n=3). shCon: total number of cells=130; shCdGAP: total number of cells=166. Two-sample unpaired Student's t-test for comparison between two groups with Welch's correction in f. Error bars indicate SEM. ****, $p < 0.0001$ ***, $p < 0.001$; **, $p < 0.01$; *, $p < 0.05$.

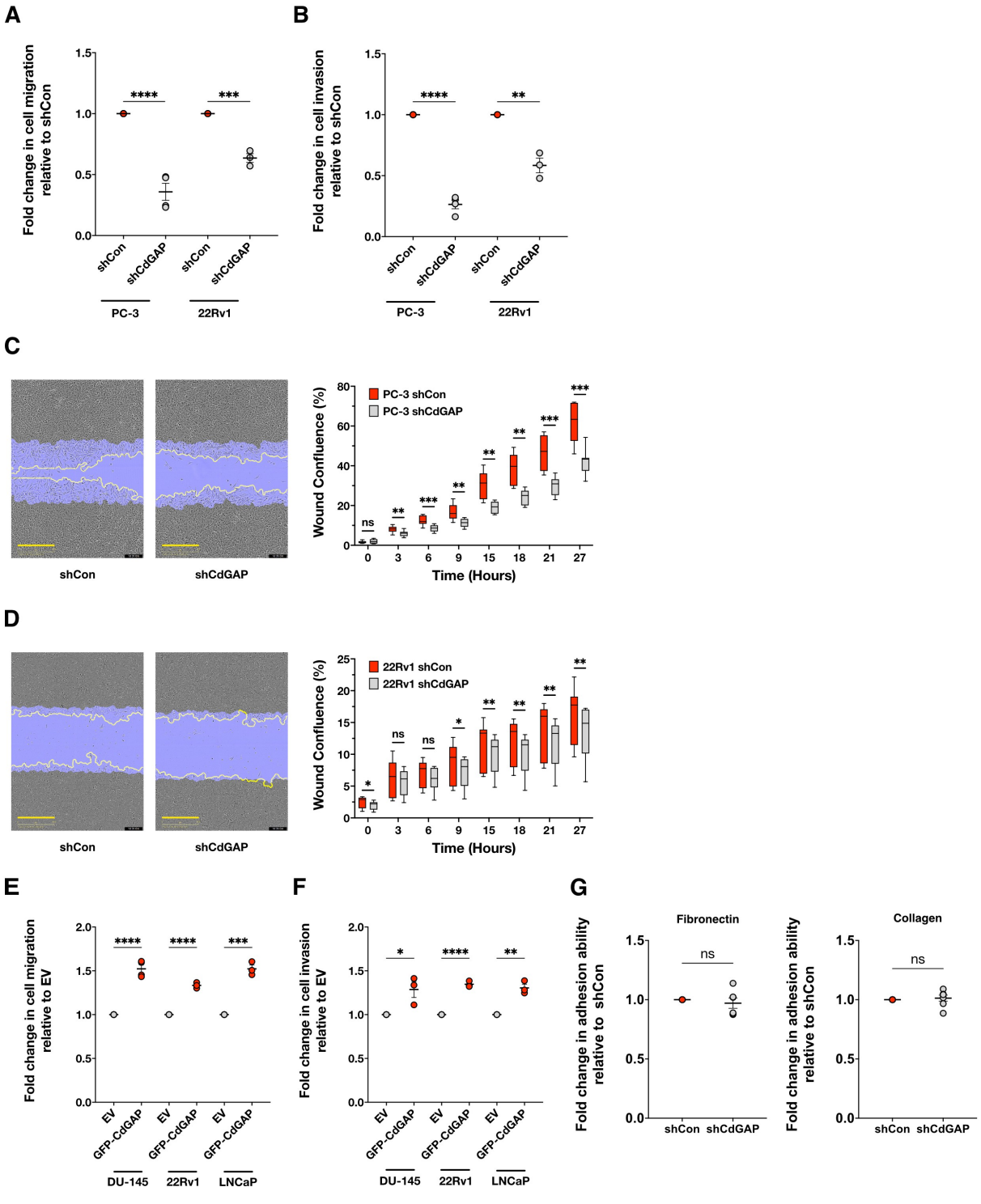
A
Fold change in cell migration relative to shCon
1.5
1.0
0.5
0.0
****
***
shCon
shCdGAP
shCon
shCdGAP
PC-3
22Rv1
B
Fold change in cell invasion relative to shCon
1.5
1.0
0.5
0.0
****
**
shCon
shCdGAP
shCon
shCdGAP
PC-3
22Rv1
C
shCon
shCdGAP
Wound Confluence (%)
80
60
40
20
0
PC-3 shCon
PC-3 shCdGAP
ns
**
***
**
**
**
***
***
0
3
6
9
15
18
21
27
Time (Hours)
D
shCon
shCdGAP
Wound Confluence (%)
25
20
15
10
5
0
22Rv1 shCon
22Rv1 shCdGAP
*
ns
ns
*
**
**
**
**
0
3
6
9
15
18
21
27
Time (Hours)
E
Fold change in cell migration relative to EV
2.0
1.5
1.0
0.5
0.0
****
****
***
EV
GFP-CdGAP
EV
GFP-CdGAP
EV
GFP-CdGAP
DU-145
22Rv1
LNCaP
F
Fold change in cell invasion relative to EV
2.0
1.5
1.0
0.5
0.0
*
****
**
EV
GFP-CdGAP
EV
GFP-CdGAP
EV
GFP-CdGAP
DU-145
22Rv1
LNCaP
G
Fold change in adhesion ability relative to shCon
Fibronectin
1.5
1.0
0.5
0.0
ns
shCon
shCdGAP
Fold change in adhesion ability relative to shCon
Collagen
1.5
1.0
0.5
0.0
ns
shCon
shCdGAP

**Figure 2.3: CdGAP promotes cell migration and invasion in CRPC cells.**

(A, B) Quantification of transwell migration (a) and invasion (b) assays of CdGAP-depleted PC-3 and 22Rv1 (shCdGAP) cells with corresponding controls (shCon) (n=3).

(C, D) Representative images from the wound healing assays of CdGAP-depleted PC-3 (C) and 22Rv1 (D) (shCdGAP) cells with corresponding controls (shCon). Scale bar, 400 μm. Quantification of the wound confluence over a period of 27 hours (n=3).

(E, F) Quantification of transwell migration (E) and invasion (F) assays of DU-145, 22Rv1, and LNCaP cells transfected with either empty vector (EV) or GFP-CdGAP (22Rv1, LNcaP: n=3; DU-145: n=4).

(G) Adhesion assays of CdGAP-depleted PC-3 (shCdGAP) and control cells (shCon) on fibronectin and collagen type 1 (n=4). Two-sample unpaired Student's t-test for comparison between two groups. Error bars indicate SEM. ****, $p < 0.0001$ ***, $p < 0.001$; **, $p < 0.01$; *, $p < 0.05$. n.s. = not significant.

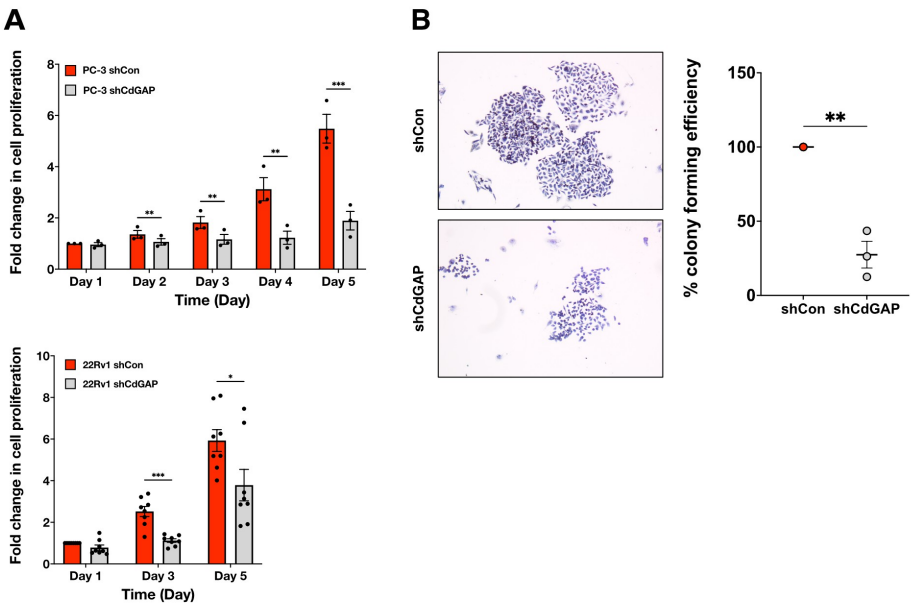


**Figure 2.4: CdGAP promotes cell proliferation in CRPC cells.**

(A) MTT assays from control (shCon) or CdGAP-depleted (shCdGAP) PC-3 and 22Rv1 cells over a period of 5 days (PC-3, n=3; 22Rv1, n=8).

(B) Representative images of an in vitro colony formation assay. Scale bar represents 100 µm. Colony forming efficiency is plotted relative to control PC-3 cells (n=3). Two-sample unpaired Student's t-test for comparison between two groups (shCon;shCdGAP). Error bars indicate SEM. ***, $p < 0.001$; **, $p < 0.01$; *, $p < 0.05$.

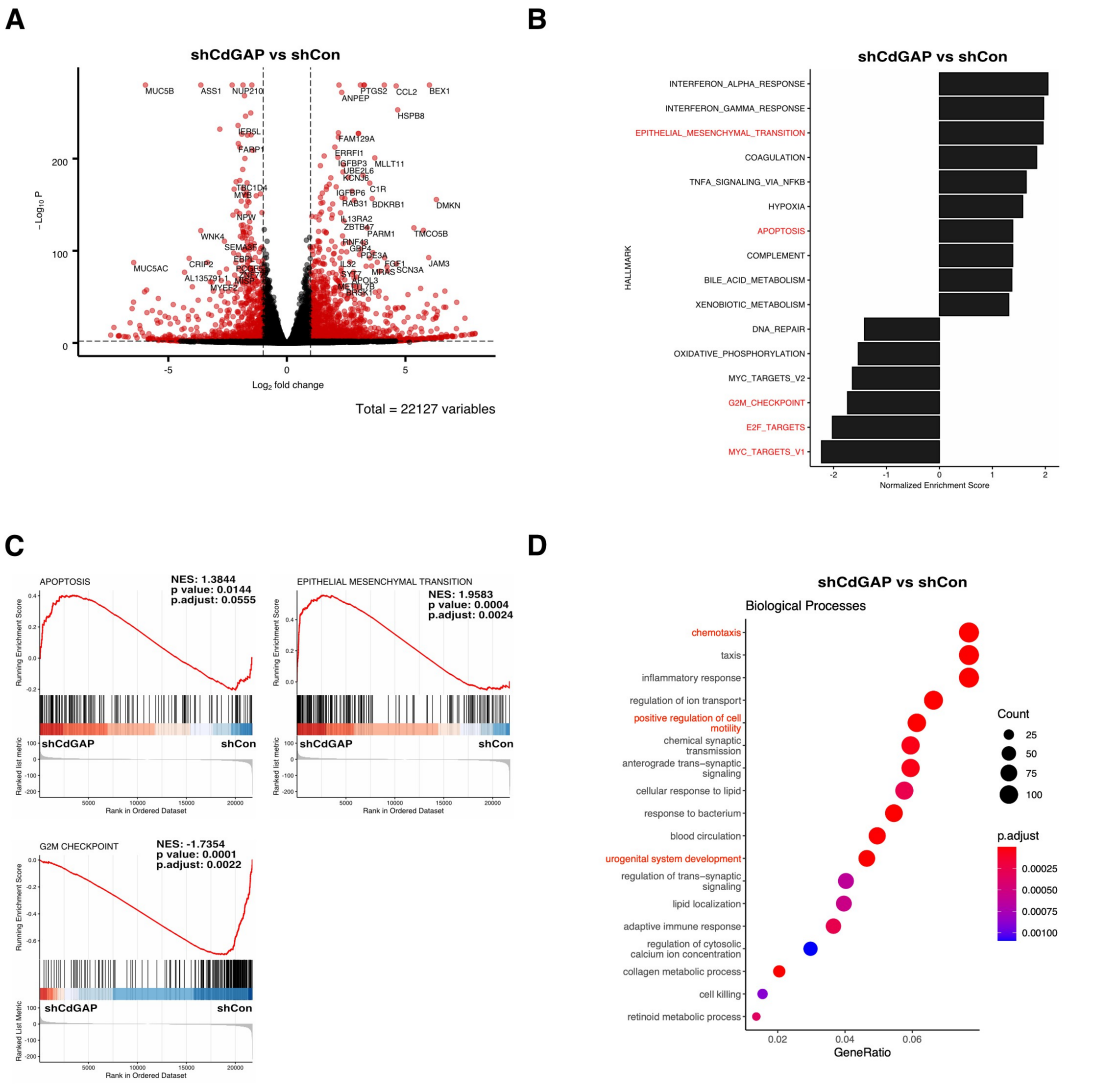
A
shCdGAP vs shCon
Total = 22127 variables
Log2 fold change
B
shCdGAP vs shCon
INTERFERON_ALPHA_RESPONSE
INTERFERON_GAMMA_RESPONSE
EPITHELIAL_MESENCHYMAL_TRANSITION
COAGULATION
TNFA_SIGNALING_VIA_NFKB
HYPOXIA
APOPTOSIS
COMPLEMENT
BILE_ACID_METABOLISM
XENOBIOTIC_METABOLISM
DNA_REPAIR
OXIDATIVE_PHOSPHORYLATION
MYC_TARGETS_V2
G2M_CHECKPOINT
E2F_TARGETS
MYC_TARGETS_V1
HALLMARK
Normalized Enrichment Score
C
APOPTOSIS
NES: 1.3844
p value: 0.0144
p.adjust: 0.0555
EPITHELIAL MESENCHYMAL TRANSITION
NES: 1.9583
p value: 0.0004
p.adjust: 0.0024
G2M CHECKPOINT
NES: -1.7354
p value: 0.0001
p.adjust: 0.0022
shCdGAP
shCon
Rank in Ordered Dataset
D
shCdGAP vs shCon
Biological Processes
chemotaxis
taxis
inflammatory response
regulation of ion transport
positive regulation of cell motility
chemical synaptic transmission
anterograde trans-synaptic signaling
cellular response to lipid
response to bacterium
blood circulation
urogenital system development
regulation of trans-synaptic signaling
lipid localization
adaptive immune response
regulation of cytosolic calcium ion concentration
collagen metabolic process
cell killing
retinoid metabolic process
GeneRatio
Count
p.adjust
E
Fold change in mRNA levels relative to shCon
shCon
shCdGAP
CDH1
SNAI1
CDH2
SNAI2
F
shCon shCdGAP
CdGAP
E-Cadherin
Snail1
N-Cadherin
Slug
Tubulin
Fold change in protein levels relative to shCon
Snail
N-Cadherin

**Figure 2.5: CdGAP controls a set of EMT, cell cycle, and apoptosis-related genes.**

(A) Volcano plot of the differentially expressed genes between shCdGAP PC-3 and shControl cells. Red dots represent genes with an absolute fold change >1 (log2FC=1) and adjusted p-value < 0.01.

(B) Normalized enrichment scores (NES) of significantly enriched and depleted Hallmark gene sets identified via GSEA in shCdGAP vs. shControl cells (p-value < 0.05).

(C) Enrichment plots depicting selected gene sets significantly enriched (apoptosis, EMT) or depleted (G2M Checkpoint) in CdGAP-depleted PC-3 cells.

(D) Top modulated biological processes enriched in CdGAP-depleted cells.

(E) qPCR analyses of the EMT-related genes after CdGAP downregulation. (CDH1, SNAI1, CDH2: n=4; SNAI2: n=6).

(F) Immunoblot analysis of the EMT-related proteins after CdGAP downregulation. Tubulin was used as a loading control. Graphs provide a densitometry analysis of the indicated protein levels represented as the fold change relative to control. (Snail1, Slug: n=4; E-Cadherin: n=5: N-Cadherin: n=6). Two-sample unpaired Student's t-test for comparison between two groups (shCon;shCdGAP). Error bars indicate SEM. ****, $p < 0.0001$ ***, $p < 0.001$; **, $p < 0.01$; *, $p < 0.05$.

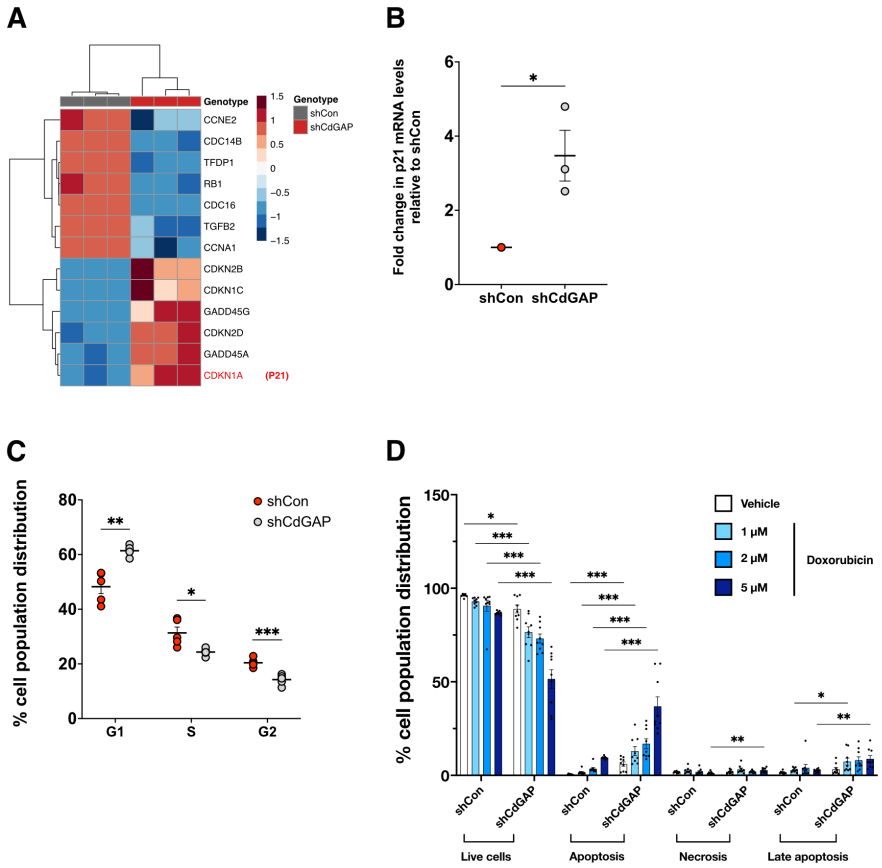


**Figure 2.6: CdGAP regulates G1 cell cycle progression and apoptosis.**

(A) Heatmap depicting cell-cycle checkpoint genes altered in CdGAP-depleted cells.

(B) p21 mRNA levels in shCon (control) and shCdGAP PC-3 cells (n=3).

(C) Flow cytometry analysis of cell cycle distribution for CdGAP-depleted (shCdGAP) and control PC-3 cells. Cell cycle distribution is represented as the percentage of cells at each phase (n=3).

(D) Flow cytometry analysis of cell death in CdGAP-depleted (shCdGAP) and control PC-3 cells treated with doxorubicin (1, 2 and 5µM) or vehicle (DMSO 0.05%) for 12h. The percentage of cell population distribution (live, apoptosis, necrosis, late apoptosis) is represented (n=3). Two-sample unpaired Student's t-test for comparison between two groups (shCon;shCdGAP). Error bars indicate SEM. ***, $p < 0.001$; **, $p < 0.01$; *, $p < 0.05$.

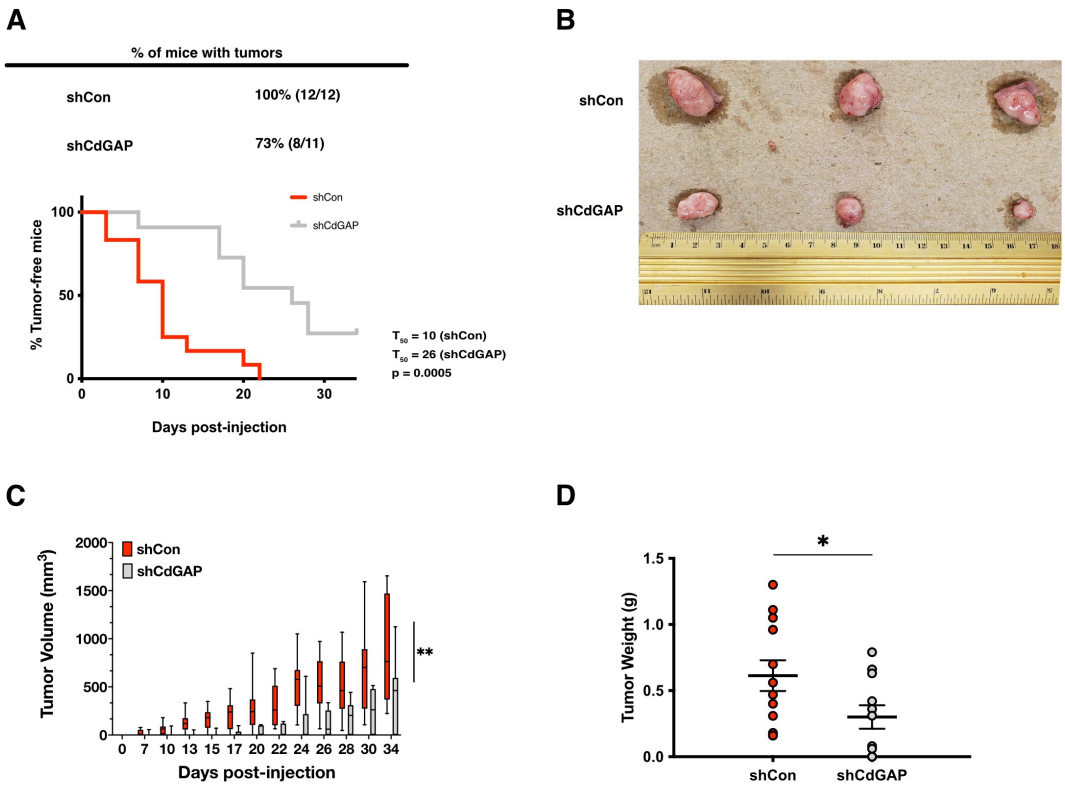


**Figure 2.7: Loss of CdGAP delays subcutaneous tumor formation of PC-3 cells *in vivo*.**
Control (shCon) or CdGAP-depleted (shCdGAP) PC-3 cells were injected into the right flanks of 7 weeks-old nude mice.

(A) Kaplan-Meier analysis of tumor-free mice using tumor initiation as end point. Time of tumor initiation was defined as when a tumor reached a volume of 20 $mm^3$.

(B) Representative photographs of endpoint tumors that formed in control (n=12) and shCdGAP (n=11) groups of mice.

(C) Growth curves of subcutaneously formed tumors. Tumor volume was measured three times a week up to 34 days and is presented as the mean volume of each group (control=12; shCdGAP=11). Error bars indicate standard deviation (SD).

(D) Tumor weight was measured at endpoint from control (n=12) and shCdGAP (n=11) groups of mice. Error bars indicate SEM. Two-sample unpaired Student's t-test for comparison between two groups (shCon;shCdGAP). **, $p < 0.001$; *, $p < 0.05$.

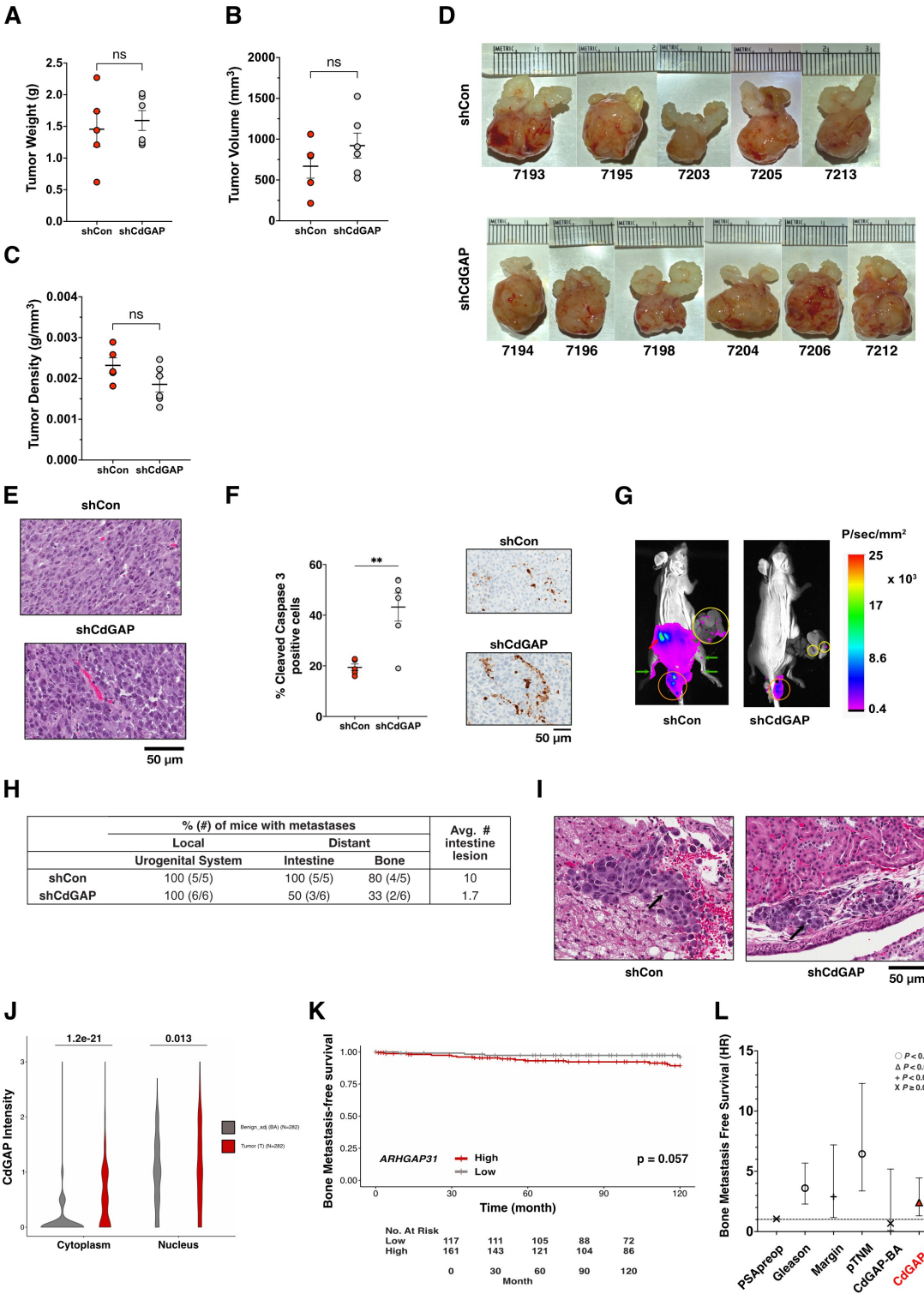
A
Tumor Weight (g)
ns
shCon shCdGAP
B
Tumor Volume (mm3)
ns
shCon shCdGAP
C
Tumor Density (g/mm3)
ns
shCon shCdGAP
D
shCon
7193 7195 7203 7205 7213
shCdGAP
7194 7196 7198 7204 7206 7212
E
shCon
shCdGAP
50 µm
F
% Cleaved Caspase 3 positive cells
**
shCon shCdGAP
shCon
shCdGAP
50 µm
G
P/sec/mm2
25
x 10³
17
8.6
0.4
shCon
shCdGAP
H
% (#) of mice with metastases
Local
Distant
Avg. # intestine lesion
Urogenital System
Intestine
Bone
shCon 100 (5/5) 100 (5/5) 80 (4/5) 10
shCdGAP 100 (6/6) 50 (3/6) 33 (2/6) 1.7
I
shCon
shCdGAP
50 µm
J
1.2e-21
0.013
CdGAP Intensity
Benign_adj (BA) (N=282)
Tumor (T) (N=282)
Cytoplasm
Nucleus
K
Bone Metastasis-free survival
ARHGAP31
High
Low
p = 0.057
Time (month)
No. At Risk
Low 117 111 105 88 72
High 161 143 121 104 86
0 30 60 90 120
Month
L
Bone Metastasis Free Survival (HR)
P < 0.001
Δ P < 0.01
+ P < 0.05
X P ≥ 0.05
PSApreop
Gleason
Margin
pTNM
CdGAP-BA
CdGAP-T

**Figure 2.8: CdGAP controls metastatic progression.**

(A - D) Weight, volume, and density of primary tumors and representative photographs of primary tumors collected from control (shCon) or CdGAP-depleted (shCdGAP) PC-3 cells-injected mice at experimental end point (28 days) (shCon: n=5; shCdGAP: n=6). Two-sample unpaired Student's t-test for comparison between two groups (shCon;shCdGAP). Error bars indicate SEM. ns = not significant.

(E) Representative images of H&E staining of primary tumors.

(F) Quantification of apoptotic cells in primary tumors by assessing the percentage of cleaved caspase-3 positive cells (shCon: n=5; shCdGAP: n=6). Representative images of IHC staining of cleaved caspase-3 in primary tumors. Two-sample unpaired Student's t-test for comparison between two groups (shCon;shCdGAP). Error bars indicate SEM. **, $p < 0.01$.

(G) Representative images of metastases found in control or CdGAP-depleted PC-3 cells-injected mice following ex vivo bioluminescent imaging at the experimental end point (28 days). Each mouse was exposed for 4 minutes after removal of the primary tumors. Yellow circle, intestine; orange circle, testis; red arrow, kidney; green arrows, legs.

(H) Percentage (number; #) of mice with local and distant metastases quantified following ex vivo bioluminescent imaging at experimental end point (28 days). The average number (#) of intestine lesions was quantified in each control and shCdGAP mice with metastases.

(I) Representative images of H&E staining of the kidneys from control (shCon) or CdGAP-depleted (shCdGAP) PC-3 cells-injected mice. Black arrows show tumor lesions.

(J) Violin plots of CdGAP intensity as scored in benign adjacent (BA) and matched tumor (T) tissue cores from the TF123 TMA (n=282; cytoplasm, p=1.2 X 10-21; nucleus, p=0.013; Wilcoxon rank-sum test).

(K) Kaplan-Meier curves of bone metastasis-free survival (10 years) based on CdGAP cytoplasmic staining in tumor cores from the TF123 TMA (p=0.057).

(L) Univariate analyses revealed that high CdGAP expression in tumor (CdGAP-T) cores is a prognostic factor for progression to bone metastasis (Supplementary Table 2).

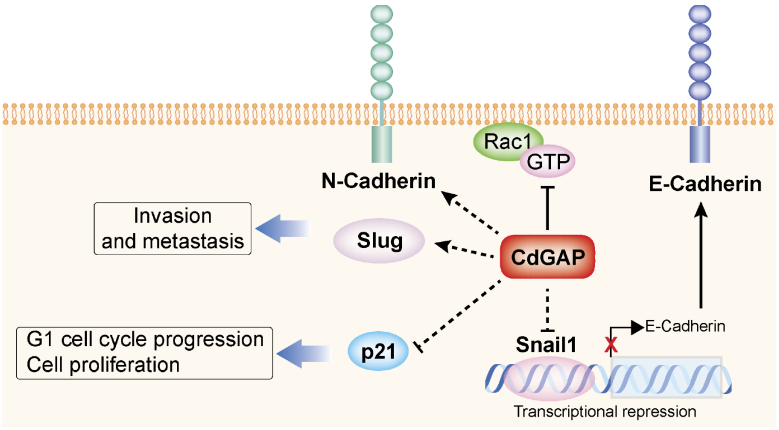


**Figure 2.9: Working model for the role of CdGAP in prostate cancer metastasis.**

High levels of CdGAP, a Rac1/Cdc42 inhibitor, are pro-oncogenic controlling cell invasion, metastasis, and proliferation. The mechanisms through which CdGAP promote cell growth and migration involve the regulation of G1 cell cycle progression, apoptosis, and EMT genes. High levels of CdGAP result in increased expression of the mesenchymal markers N-Cadherin and SLUG, promoting invasion and metastasis while reduced levels of the CDK inhibitor p21 induce G1 cell cycle progression and cell proliferation. In addition, CdGAP negatively regulates the levels of the E-cadherin transcriptional repressor SNAIL1 in PC-3 cells.

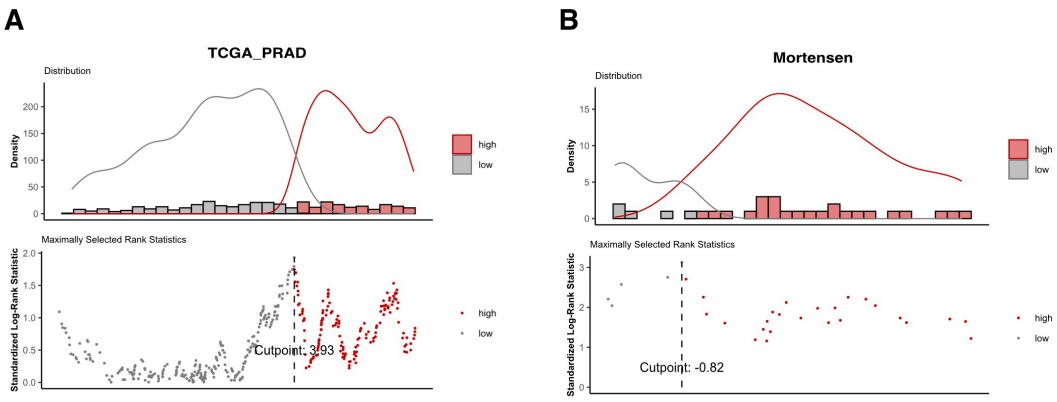


**Supplementary Figure 1**

(A, B) Dichotomization of patients in the TCGA_PRAD (A) and Mortensen datasets (B) divided into high expression and low expression groups by optimal cutpoint.

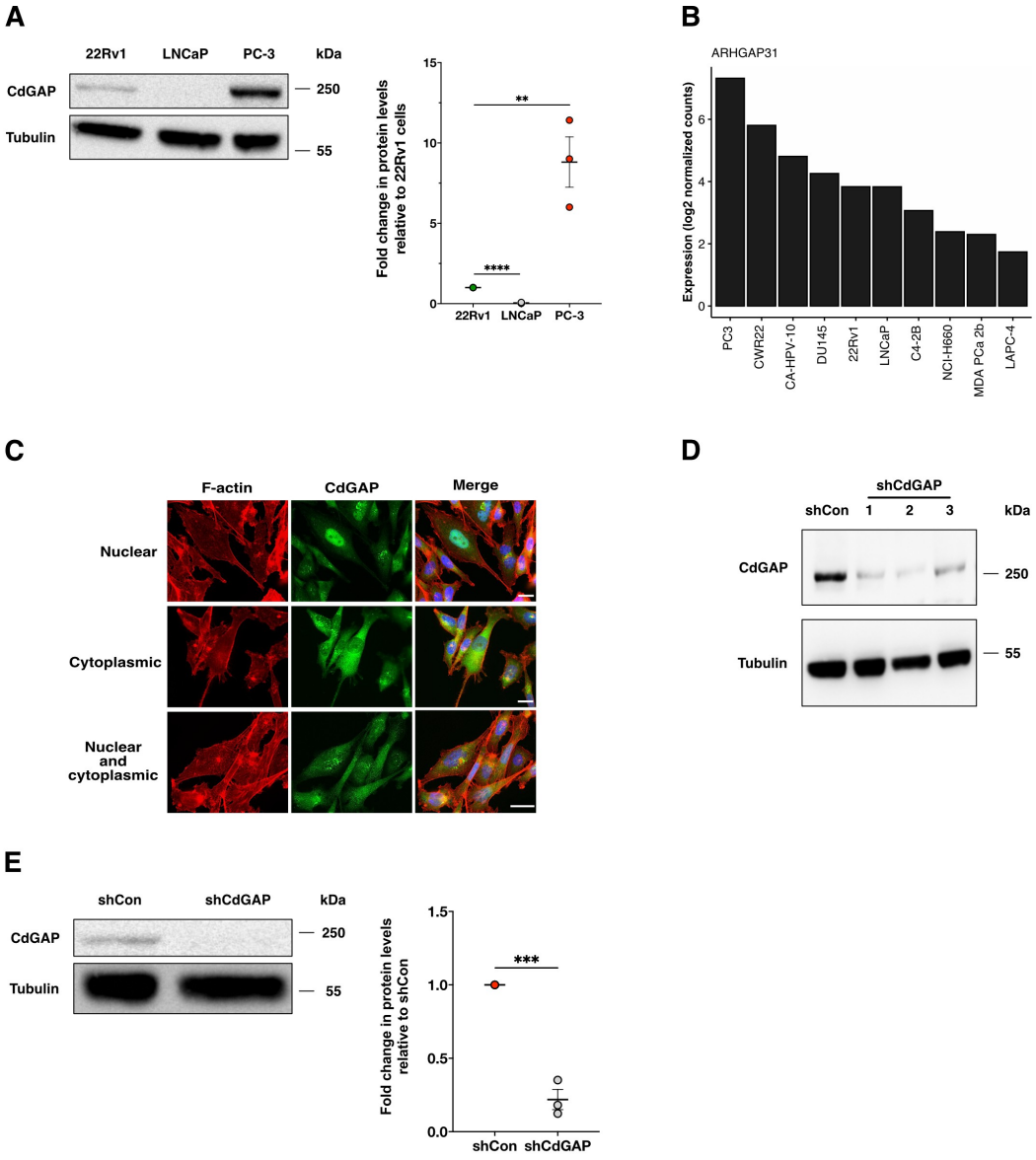
A
22Rv1
LNCaP
PC-3
kDa
CdGAP
Tubulin
250
55
Fold change in protein levels relative to 22Rv1 cells
**
****
22Rv1
LNCaP
PC-3
B
ARHGAP31
Expression (log2 normalized counts)
PC3
CWR22
CA-HPV-10
DU145
22Rv1
LNCaP
C4-2B
NCI-H660
MDA PCa 2b
LAPC-4
C
F-actin
CdGAP
Merge
Nuclear
Cytoplasmic
Nuclear and cytoplasmic
D
shCdGAP
shCon
1
2
3
kDa
CdGAP
Tubulin
250
55
E
shCon
shCdGAP
kDa
CdGAP
Tubulin
250
55
Fold change in protein levels relative to shCon
***
shCon
shCdGAP

**Supplementary Figure 2**

(A) Immunoblot analysis of CdGAP in human prostate cancer cell lines 22Rv1, LNCaP and PC-3. Tubulin was used as a loading control. Graphs provide a densitometry analysis of CdGAP protein levels relative to 22Rv1 cells (n=3).

(B) ARHGAP31 transcript abundance in prostate cancer cell lines from the Prensner RNA-seq dataset.

(C) PC-3 cells were fixed and then stained for CdGAP (green) or F-actin (red) with phalloidin. 4′,6′-diamidino-2- phenylindole (DAPI) was used to stain the nuclei. CdGAP nuclear (top panels), cytoplasmic (middle panels), or both (bottom panels) localization is represented. Scale bar represents 10 μm.

(D) Immunoblot analysis of CdGAP levels in PC-3 cells infected with scrambled control (shCon) or shRNA targeting CdGAP (shCdGAP) single clones. Tubulin was used as loading control.

(E) Immunoblot analysis of CdGAP levels in 22Rv1 cells infected with scrambled control (shCon) or shRNA targeting CdGAP (shCdGAP). Tubulin was used as loading control. Graphs provide a densitometry analysis of CdGAP protein levels in CdGAP-depleted cells relative to shCon (n=3). Two-sample unpaired Student's t-test for comparison between two groups (shCon;shCdGAP). Error bars indicate SEM. ****, $p < 0.0001$ ***, $p < 0.001$; **, $p < 0.01$.

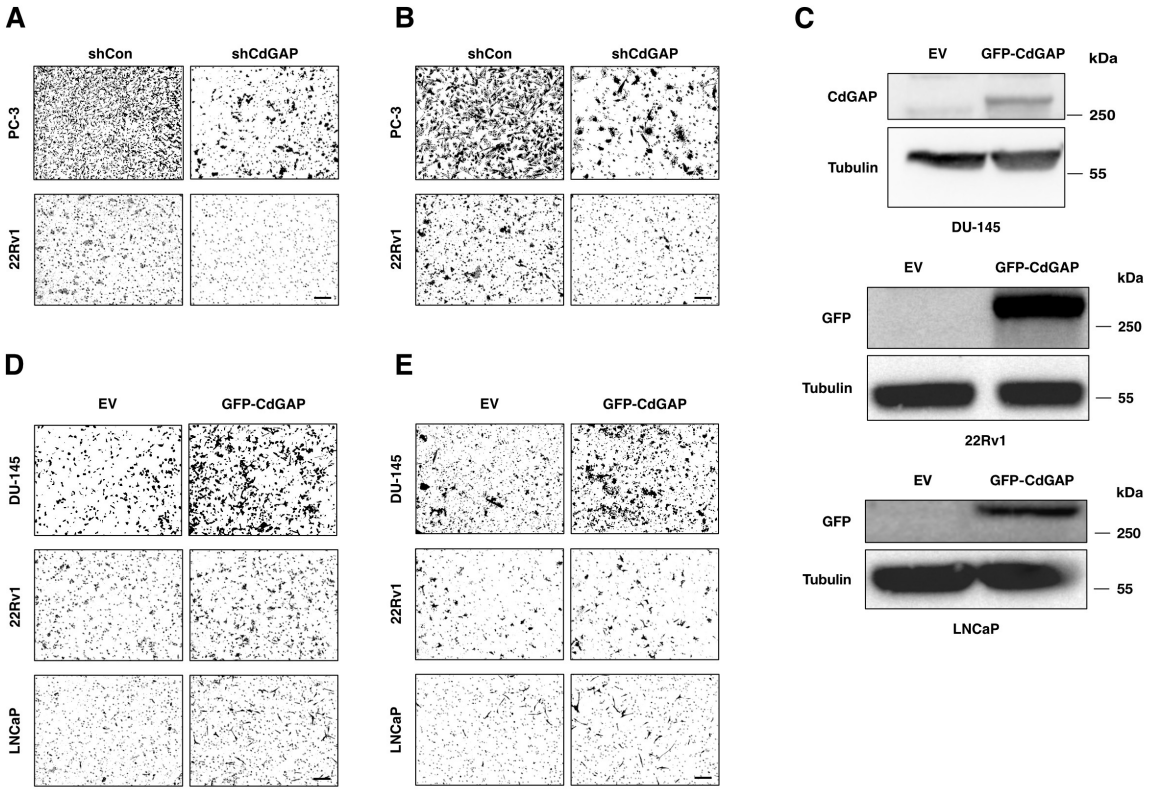
A
shCon
shCdGAP
PC-3
22Rv1
B
shCon
shCdGAP
PC-3
22Rv1
C
EV
GFP-CdGAP
kDa
CdGAP
250
Tubulin
55
DU-145
EV
GFP-CdGAP
kDa
GFP
250
Tubulin
55
22Rv1
EV
GFP-CdGAP
kDa
GFP
250
Tubulin
55
LNCaP
D
EV
GFP-CdGAP
DU-145
22Rv1
LNCaP
E
EV
GFP-CdGAP
DU-145
22Rv1
LNCaP
F
Day 1
Day 2
Day 5
shCon
shCdGAP
shCon
shCdGAP
shCon
shCdGAP
kDa
CdGAP
250
Tubulin
55
PC-3
Day 1
Day 3
Day 5
shCon
shCdGAP
shCon
shCdGAP
shCon
shCdGAP
kDa
CdGAP
250
Tubulin
55
22Rv1

**Supplementary Figure 3**

(A, B) Representative images from transwell migration and invasion assays of CdGAP- depleted PC-3 and 22Rv1 cells with corresponding controls. Scale bar represents 100 μm.

(C) Immunoblot analysis of CdGAP from protein lysates of DU-145, 22Rv1, and LNCaP cells transfected with pEGFP-C1 empty vector (EV) or pEGFP-CdGAP. Tubulin was used as loading control.

(D, E) Representative images from transwell migration (D) and invasion (E) assays of DU-145, 22Rv1, and LNCaP cells transfected with either empty vector (EV) or GFP-CdGAP. Scale bar represents 100 μm.

(F) Immunoblot analysis of CdGAP from protein lysates of CdGAP-depleted PC-3 and 22Rv1 cells with corresponding controls over a period of 5 days in culture.

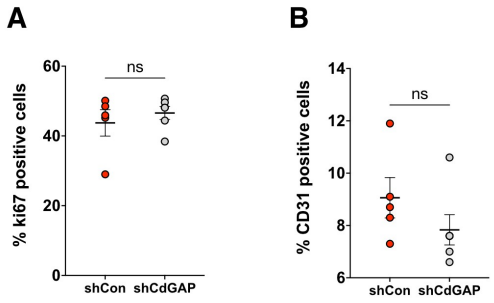


**Supplementary Figure 4**

(A, B) Quantification of Ki-67 (A) and CD-31 (B) positive cells by IHC staining in primary tumors from control (shCon) or CdGAP-depleted (shCdGAP) PC-3 cells-injected mice. Error bars indicate SEM. ns = not significant.

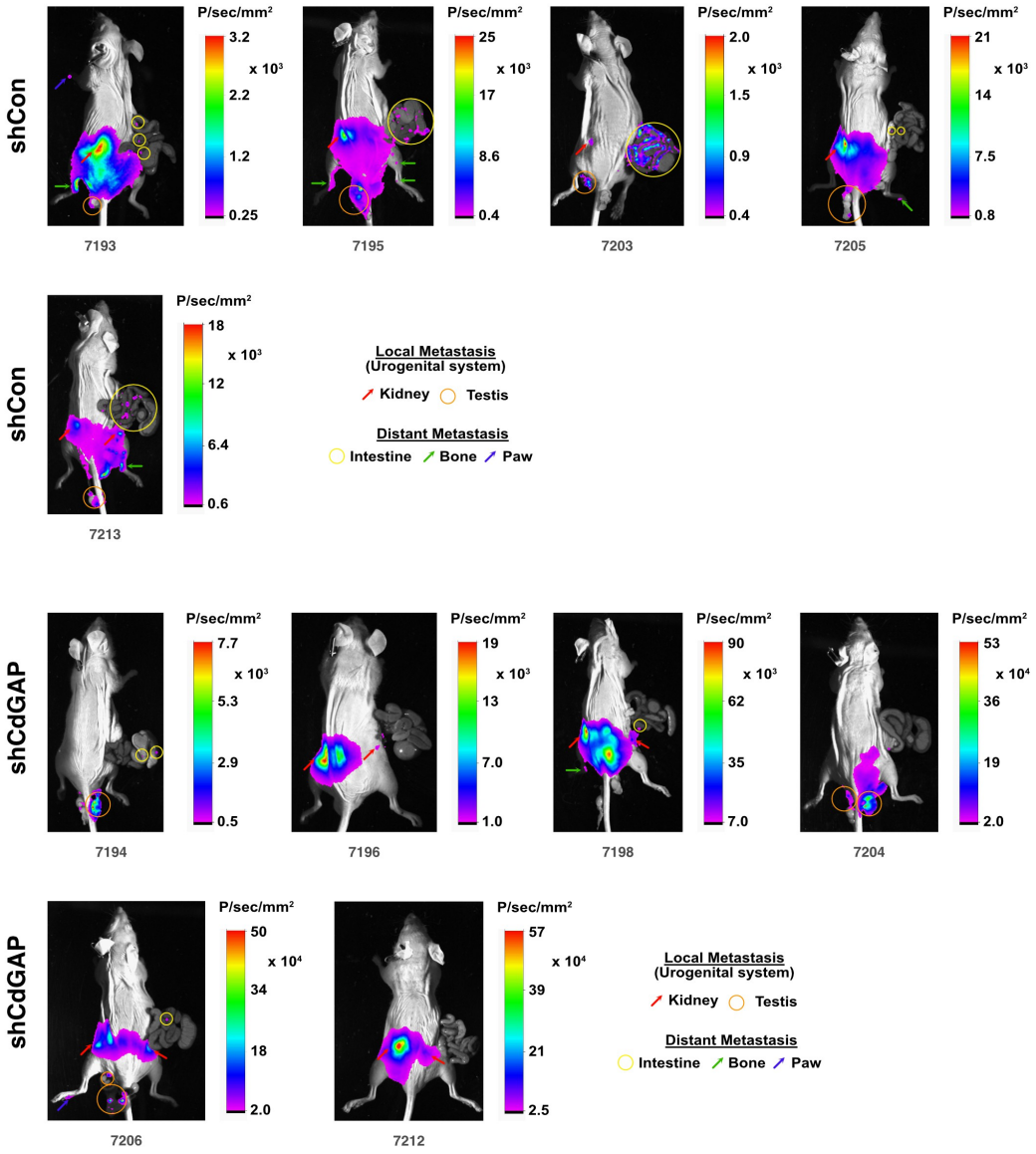


**Supplementary Figure 5**

Ex vivo imaging of mice injected with control (shCon) or CdGAP-depleted PC-3 (shCdGAP) cells. At the experimental end date (28 days), mice were euthanized, primary tumors were removed and then immediately subjected to ex vivo imaging performed on post-mortem mice to visualize metastasis. Each mouse was exposed for 4 minutes.

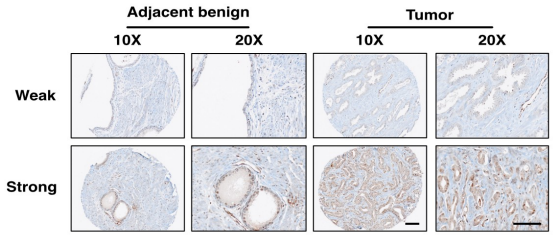


**Supplementary Figure 6**

Representative IHC of CdGAP expression on a panel of radical prostatectomy specimens from 285 prostate cancer patients using the TF123 TMA. Nuclear and cytoplasmic CdGAP staining was scored with an intensity varying from weak to strong (0 to 3) in adjacent benign and matched tumor tissue cores. Magnification, 10X and 20X. Scale bar represents 100 μm.

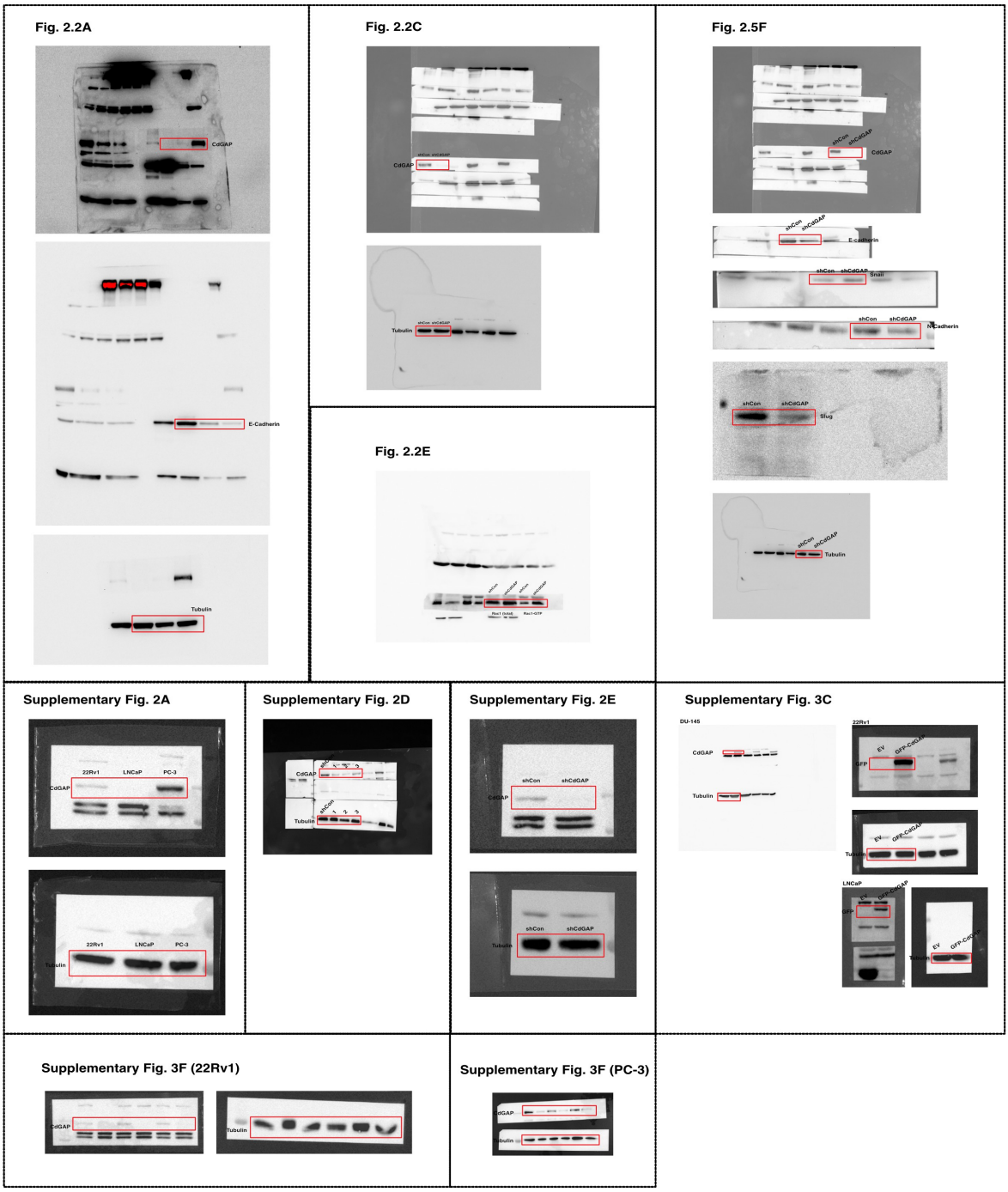


**Supplementary Figure 7: Representative western blots for each antibody used in the manuscript.**

Uncropped western blots.

| Number of Patients | | 285 | |
|---|---|---|---|
| **Age at Diagnosis** | Mean (years) | 62 | |
| **Follow-up** | Median (months) | 143 | |
| | | **N** | **%** |
| **Biochemical Relapse 60 months** | No | 190 | 67 |
| | Yes | 95 | 33 |
| **Bone Metastasis 10 years** | No | 265 | 93 |
| | Yes | 20 | 7 |
| **Castrate Resistant** | No | 259 | 91 |
| | Yes | 26 | 9 |
| **Death** | Pca specific | 20 | 7 |
| | Other cause | 45 | 16 |
| | Overall | 65 | 23 |
| **Gleason Score Radical Prostatectomy** | ≤3+3 | 139 | 49 |
| | 3+4 | 94 | 33 |
| | 4+3 | 19 | 7 |
| | ≥4+4 | 29 | 10 |
| | U | 4 | 1 |
| **pTNM** | 2 | 200 | 70 |
| | 3 | 76 | 27 |
| | 4 | 9 | 3 |
| **Lymph Node Invasion** | No | 196 | 69 |
| | Yes | 9 | 3 |
| | U | 80 | 28 |
| **Capsular Penetration** | No | 205 | 72 |
| | Yes | 80 | 28 |
| **Seminal Gland Invasion** | No | 269 | 94 |
| | Yes | 16 | 6 |
| **Margin status** | Negative | 185 | 65 |
| | Positive | 95 | 33 |
| | U | 5 | 2 |

**Supplementary Table 1**

Clinico-pathological information of the cohort of 285 prostate cancer patients participating in the Centre de Recherche du Centre Hospitalier de l'Université de Montréal prostate cancer biobank and included to the TF123 TMA.

| | Parameter | BCR free survival (5 years) | | | | Bone Metastasis free survival (10 years) | | | |
|---|---|---|---|---|---|---|---|---|---|
| | | Univariate | | | | Univariate | | | |
| | | Sig. | HR | 95.0% CI for HR | | Sig. | HR | 95.0% CI for HR | |
| | | | | Lower | Upper | | | Lower | Upper |
| Clinical data | PSApreop | **<0.001** | 1.059 | 1.032 | 1.087 | 0.055 | 1.055 | 0.999 | 1.115 |
| | GleasonScoreCat1234 | **<0.001** | 1.837 | 1.537 | 2.195 | **<0.001** | 3.606 | 2.287 | 5.686 |
| | Margin | **<0.001** | 3.396 | 2.246 | 5.136 | **0.022** | 2.893 | 1.163 | 7.193 |
| | pTNM | **<0.001** | 2.735 | 2.027 | 3.688 | **<0.001** | 6.443 | 3.376 | 12.296 |
| Continuous data | CdGAP Cytoplasm intensity in BA | 0.292 | 0.624 | 0.259 | 1.501 | 0.714 | 0.685 | 0.09 | 5.192 |
| | CdGAP Cytoplasm intensity in T | 0.615 | 1.097 | 0.764 | 1.576 | **0.005** | 2.416 | 1.31 | 4.453 |
| | BA: adjacent benign; T: Tumor; **bold** p<0.05 | | | | | | | | |

## Supplementary Table 2

Univariate analyses were used to estimate the hazard ratios (HRs) for CdGAP and other clinico-pathological parameters. The serum PSA levels prior to the radical prostatectomy, pathologic staging of the primary tumor (pT 2, 3, 4), Gleason Score category [6, 7 (3+4), 7 (4+3), 8+], and margin status (negative/positive) were included in the model.

| Antibody name | Company: Catalog number | Dilution |
|---|---|---|
| CdGAP | Sigma: HPA036380 | 1 in 1,000 |
| E-Cadherin | Cell Signaling: 3195 | 1 in 1,000 |
| Snail 1 | Cell Signaling: 3879 | 1 in 500 |
| a -Tubulin | Sigma: T5168 | 1 in 1,000 |
| Rac1 | AbCAM: 23A8 | 1 in 1,000 |
| N-Cadherin | BD Biosciences: 610920 | 1 in 1,000 |
| Slug | Cell Signaling: C19G7 | 1 in 1,000 |
| Anti-rabbit IgG | ThermoFisher: 45-000-682 | 1 in 10,000 |
| Anti-mouse IgG | ThermoFisher: 45-000-679 | 1 in 10,000 |

## Supplementary Table 3

List of antibodies used in this study.

| Gene Name | Forward Primer | Reverse Primer |
|---|---|---|
| Snail1 | CCCTCAAGATGCACATCCGAA | GACTCTTGGTGCTTGTGGAGCA |
| CDH1 | CCCGCCTTATGATTCTCTGCTCGTG | TCCGTACATGTCAGCCAGCTTCTTG |
| P21 | AGGTGGACCTGGAGACTCTCAG | TCCTCTTGGAGAAGATCAGCCG |
| N-Cadherin | CCTCCAGAGTTTACTGCCATGAC | GTAGGATCTCCGCCCTGATTC |
| Slug | TGTTGCAGTGAGGGCAAGAA | GAGCCTGGTTGCTTCAAGGA |

## Supplementary Table 4

List of primers used in this study.

## References


1. F. Bray, J. F., I. Soerjomataram, R.L Siegel, LA Torre, and A. Jemal (2018). Global cancer statistics 2018: GLOBOCAN estimates of incidence and mortality worldwide for 36 cancers in 185 countries. *CA Cancer J Clin*, *68*, 394-424.
2. DP Labbé, C. S., M. Brown, P. Galbo, S. Rosario, KM Wadosky, et al. . (2017). TOP2A and EZH2 Provide Early Detection of an Aggressive Prostate Cancer Subgroup. *Clin. Cancer Res.*, *23*, 7072-7083.
3. Haga, R. B., & Ridley, A. J. (2016). Rho GTPases: Regulation and roles in cancer cell biology. *Small GTPases*, *7*(4), 207-221. https://doi.org/10.1080/21541248.2016.1232583
4. Tcherkezian, J., & Lamarche-Vane, N. (2007). Current knowledge of the large RhoGAP family of proteins. *Biology of the Cell*, *99*(2), 67-86. https://doi.org/10.1042/BC20060086
5. RG Hodge, A. S., SV Howard, and CJ. Der. (2020). RAS and RHO family GTPase mutations in cancer: twin sons of different

mothers? *Critical Reviews in Biochemistry and Molecular Biology*, *55*, 386-407.

6. Lawson, C. D., & Der, C. J. (2018). Filling GAPs in our knowledge: ARHGAP11A and RACGAP1 act as oncogenes in basal-like breast cancers. *Small GTPases*, *9*(4), 290-296. https://doi.org/10.1080/21541248.2016.1220350
7. He, Y., Northey, J. J., Pelletier, A., Kos, Z., Meunier, L., Haibe-Kains, B., Mes-Masson, A. M., Côté, J. F., Siegel, P. M., & Lamarche-Vane, N. (2017). The Cdc42/Rac1 regulator CdGAP is a novel E-cadherin transcriptional co-repressor with Zeb2 in breast cancer. *Oncogene*, *36*(24), 3490-3503. https://doi.org/10.1038/onc.2016.492
8. He, Y., Northey, J. J., Primeau, M., Machado, R. D., Trembath, R., Siegel, P. M., & Lamarche-Vane, N. (2011). CdGAP is required for transforming growth factor β- and Neu/ErbB-2-induced breast cancer cell motility and invasion. *Oncogene*, *30*(9), 1032-1045. https://doi.org/10.1038/onc.2010.477
9. Lazarini, M., Traina, F., Machado-Neto, J. A., Barcellos, K. S., Moreira, Y. B., Brandao, M. M., Verjovski-Almeida, S., Ridley, A. J., & Saad, S. T. (2013). ARHGAP21 is a RhoGAP for RhoA and RhoC with a role in proliferation and migration of prostate adenocarcinoma cells. *Biochim Biophys Acta*, *1832*(2), 365-374. https://doi.org/10.1016/j.bbadis.2012.11.010

10. Lawson, C. D., Fan, C., Mitin, N., Baker, N. M., George, S. D., Graham, D. M., Perou, C. M., Burridge, K., Der, C. J., & Rossman, K. L. (2016). Rho GTPase Transcriptome Analysis Reveals Oncogenic Roles for Rho GTPase-Activating Proteins in Basal-like Breast Cancers. *Cancer Res*, *76*(13), 3826-3837. https://doi.org/10.1158/0008-5472.CAN-15-2923
11. Lamarche-Vane, N., & Hall, A. (1998). CdGAP, a Novel Proline-rich GTPase-activating Protein for Cdc42 and Rac *. *Journal of Biological Chemistry*, *273*(44), 29172-29177. https://doi.org/10.1074/jbc.273.44.29172
12. Bagci, H., Sriskandarajah, N., Robert, A., Boulais, J., Elkholi, I. E., Tran, V., Lin, Z. Y., Thibault, M. P., Dube, N., Faubert, D., Hipfner, D. R., Gingras, A. C., & Cote, J. F. (2020). Mapping the proximity interaction network of the Rho-family GTPases reveals signalling pathways and regulatory mechanisms. *Nat Cell Biol*, *22*(1), 120-134. https://doi.org/10.1038/s41556-019-0438-7
13. Djoudi Ouadda, A. B., He, Y., Calabrese, V., Ishii, H., Chidiac, R., Gratton, J.-P., Roux, P. P., & Lamarche-Vane, N. (2018). CdGAP/ARHGAP31 is regulated by RSK phosphorylation and binding to 14-3-3β adaptor protein. *Oncotarget*, *9*(14), 11646-11664. https://doi.org/10.18632/oncotarget.24126
14. Southgate, L., Machado, Rajiv D., Snape, Katie M., Primeau, M., Dafou, D., Ruddy, Deborah M., Branney, Peter A., Fisher, M., Lee, Grace J., Simpson, Michael A., He, Y., Bradshaw, Teisha Y., Blaumeiser, B., Winship, William S., Reardon, W., Maher, Eamonn R., FitzPatrick, David R., Wuyts, W., Zenker, M., . . . Trembath, Richard C. (2011). Gain-of-Function Mutations of ARHGAP31, a Cdc42/Rac1 GTPase Regulator, Cause Syndromic Cutis Aplasia and Limb Anomalies. *The American Journal of Human Genetics*, *88*(5), 574-585. https://doi.org/10.1016/j.ajhg.2011.04.013
15. LaLonde, D. P., Grubinger, M., Lamarche-Vane, N., & Turner, C. E. (2006). CdGAP Associates with Actopaxin to Regulate Integrin-Dependent Changes in Cell Morphology and Motility. *Current Biology*, *16*(14), 1375-1385. https://doi.org/10.1016/j.cub.2006.05.057
16. Wormer, D. B., Davis, K. A., Henderson, J. H., & Turner, C. E. (2014). The Focal Adhesion-Localized CdGAP Regulates Matrix Rigidity Sensing and Durotaxis. *PLoS One*, *9*(3), e91815. https://doi.org/10.1371/journal.pone.0091815

17. Wormer, D., Deakin, N. O., & Turner, C. E. (2012). CdGAP regulates cell migration and adhesion dynamics in two-and three-dimensional matrix environments. *Cytoskeleton*, *69*(9), 644-658. https://doi.org/10.1002/cm.21057

18. Caron, C., DeGeer, J., Fournier, P., Duquette, P. M., Luangrath, V., Ishii, H., Karimzadeh, F., Lamarche-Vane, N., & Royal, I. (2016). CdGAP/ARHGAP31, a Cdc42/Rac1 GTPase regulator, is critical for vascular development and VEGF-mediated angiogenesis. *Scientific Reports*, *6*(1), 27485. https://doi.org/10.1038/srep27485

19. McCormack, J. J., Bruche, S., Ouadda, A. B. D., Ishii, H., Lu, H., Garcia-Cattaneo, A., Chávez-Olórtegui, C., Lamarche-Vane, N., & Braga, V. M. M. (2017). The scaffold protein Ajuba suppresses CdGAP activity in epithelia to maintain stable cell-cell contacts. *Scientific Reports*, *7*(1), 9249. https://doi.org/10.1038/s41598-017-09024-4

20. Gao, J., Aksoy, B. A., Dogrusoz, U., Dresdner, G., Gross, B., Sumer, S. O., Sun, Y., Jacobsen, A., Sinha, R., Larsson, E., Cerami, E., Sander, C., & Schultz, N. (2013). Integrative Analysis of Complex Cancer Genomics and Clinical Profiles Using the cBioPortal. *Science Signaling*, *6*(269), pl1-pl1. https://doi.org/10.1126/scisignal.2004088

21. Cunningham, D., & You, Z. (2015). In vitro and in vivo model systems used in prostate cancer research. *Journal of biological methods*, *2*(1), e17. https://doi.org/10.14440/jbm.2015.63

22. JR Prensner, M. I., OA Balbin, SM Dhanasekaran, Q Cao, JC Brenner. (2011). Transcriptome sequencing across a prostate cancer cohort identifies PCAT-1, an unannotated lincRNA implicated in disease progression. *Nat Biotechnol*, *29*, 742-749.

23. Broussard, J. A., Webb, D. J., & Kaverina, I. (2008). Asymmetric focal adhesion disassembly in motile cells. *Curr Opin Cell Biol*, *20*(1), 85-90. https://doi.org/10.1016/j.ceb.2007.10.009

24. Thiery, J. P., Acloque, H., Huang, R. Y., & Nieto, M. A. (2009). Epithelial-mesenchymal transitions in development and disease. *Cell*, *139*(5), 871-890. https://doi.org/10.1016/j.cell.2009.11.007

25. Gulappa, T., Reddy, R. S., Suman, S., Nyakeriga, A. M., & Damodaran, C. (2013). Molecular interplay between cdk4 and p21 dictates G0/G1 cell cycle arrest in prostate cancer cells. *Cancer Lett*, *337*(2), 177-183. https://doi.org/10.1016/j.canlet.2013.05.014

26. Bloom, J., & Cross, F. R. (2007). Multiple levels of cyclin specificity in cell-cycle control. *Nat Rev Mol Cell Biol*, *8*(2), 149-160. https://doi.org/10.1038/nrm2105

27. S. Clairefond, B. P., V. Ouellet, V. Barrès, Z.Tian, D. Trudel, P.I. Karakiewicz, A.M. Mes-Masson, and Fred Saad. PUMA and NOXA expression in tumor-associated benign prostatic epithelial cells are predictive of prostate cancer biochemical recurrence. *Cancers*, *12*, 3187.

28. Shiao, S. L., Chu, G. C., & Chung, L. W. (2016). Regulation of prostate cancer progression by the tumor microenvironment. *Cancer Lett*, *380*(1), 340-348. https://doi.org/10.1016/j.canlet.2015.12.022

29. Laurin M, H. J., Pelletier A, Houalla T, Park M, Fukui Y, Haibe-Kains B, Muller WJ, and Côté JF. (2013). Rac-specific guanine nucleotide exchange factor DOCK1 is a critical regulator of HER2-mediated breast cancer metastasis. . *PNAS*, *110*, 7434-7439.

30. Uygur, B., & Wu, W. S. (2011). SLUG promotes prostate cancer cell migration and invasion via CXCR4/CXCL12 axis. *Mol Cancer*, *10*, 139. https://doi.org/10.1186/1476-4598-10-139

31. Hao, H., Wang, L., Chen, H., Xie, L., Bai, T., Liu, H., & Wang, D. (2017). YKL-40 promotes the migration and invasion of prostate cancer cells by regulating epithelial mesenchymal transition. *Am J Transl Res*, *9*(8), 3749-3757. https://www.ncbi.nlm.nih.gov/pubmed/28861166

32. Xu, G., Lu, X., Huang, T., & Fan, J. (2016). ARHGAP24 inhibits cell cycle progression, induces apoptosis and suppresses invasion in renal cell carcinoma. *Oncotarget*, *7*(32), 51829-51839. https://doi.org/10.18632/oncotarget.10386

33. Luo, N., Guo, J., Chen, L., Yang, W., Qu, X., & Cheng, Z. (2016). ARHGAP10, downregulated in ovarian cancer, suppresses tumorigenicity of ovarian cancer cells. *Cell Death Dis*, *7*, e2157. https://doi.org/10.1038/cddis.2015.401

34. Wang, C., Wang, W., Liu, Y., Yong, M., Yang, Y., & Zhou, H. (2018). Rac GTPase activating protein 1 promotes oncogenic progression of epithelial ovarian cancer. *Cancer Sci*, *109*(1), 84-93. https://doi.org/10.1111/cas.13434

35. Yeh, C. M., Sung, W. W., Lai, H. W., Hsieh, M. J., Yen, H. H., Su, T. C., Chang, W. H., Chen, C. Y., Ko, J. L., & Chen, C. J. (2016). Opposing prognostic roles of nuclear and

cytoplasmic RACGAP1 expression in colorectal cancer patients. *Hum Pathol*, *47*(1), 45-51. https://doi.org/10.1016/j.humpath.2015.09.002

36. Heraud, C., Pinault, M., Lagree, V., & Moreau, V. (2019). p190RhoGAPs, the ARHGAP35- and ARHGAP5-Encoded Proteins, in Health and Disease. *Cells*, *8*(4). https://doi.org/10.3390/cells8040351
37. Mortensen MM, H. S., Lynnerup AS, Ørntoft TF, Sørensen KD, Borre M and Dyrskjøt L. . (2015). Expression profiling of prostate cancer tissue delineates genes associated with recurrence after prostatectomy. *Sc. Rep.*, *5*, 160182015.
38. Davis S, M. P. (2007). GEOquery: a bridge between the Gene Expression Omnibus (GEO) and BioConductor. *Bioinformatics*, *23*, 1846-1847.
39. Network CGAR, C. G. A. R. N. (2015). The molecular taxonomy of primary prostate cancer. . *Cell*, *163*, 1011-1025.
40. Colaprico A, S. T., Olsen C, et al. (2016). TCGAbiolinks: an R/ Bioconductor package for integrative analysis of TCGA data. . *Nucleic Acids Res.*, *44*, e71.
41. Carvalho BS, I. R. (2010). A framework for oligonucleotide microarray preprocessing. . *Bioinformatics*, *26*, 2363-2367.
42. Leek JT, J. W., Parker HS, Fertig EJ, Jaffe AE, Zhang Y, Storey JD, Torres LC. (2020). sva: Surrogate Variable Analysis. R package version 3.34.0. https://bioconductor.org/packages/release/bioc/html/sva.html.
43. M., C. (2016). hgu133plus2.db: Affymetrix Human Genome U133 Plus 2.0 Array annotation data (chip hgu133plus2). R package version 3.2.3. https://bioconductor.org/packages/release/data/annotation/html/hgu133plus2.db.html.
44. Langfelder P, H. S. (2008). WGCNA: an R package for weighted correlation network analysis. *BMC Bioinformatics*, *559*.
45. Love, M. I., Huber, W. & Anders, S. . (2014). Moderated estimation of fold change and dispersion for RNA-seq data with DESeq2. *Genome Biol.*, *15*, 550.
46. Kassambara, A. (2016). Drawing Survival Curves using 'ggplot2'. R package version 0.4.6. http://CRAN.r-project.org/web/packages/survminer.
47. Therneau, T. (2020). A Package for Survival Analysis in R. R package version 3.1-12, https://CRAN.R-project.org/package=survival.

48. Huang, W., Guo, W., You, X., Pan, Y., Dong, Z., Jia, G., Yang, C., & Chen, Y. (2017). PAQR3 suppresses the proliferation, migration and tumorigenicity of human prostate cancer cells. *Oncotarget*, *8*(33), 53948-53958. https://doi.org/10.18632/oncotarget.9807

49. Yu G, W. L., Han Y, He QY. . (2012). ClusterProfiler: an R package for comparing biological themes among gene clusters. *OMICS*, *16*, 284-287.

50. J.F. Anker, H. M., A.F. Naseem, P. Thumbikat, and S.A. Abdulkadir. . (2018). A Bioluminescent and Fluorescent Orthotopic Syngeneic Murine Model of Androgen-dependent and Castration-resistant Prostate Cancer. *J. Vis. Exp.*, *133*, e57301.

# Chapter 3: Loss-of-function Adams-Oliver syndrome mutation of mouse CdGAP results in defective syncytial fusion and placental dysfunctions

Ji-Hyun Chung, Yi He, Shiva Shafei, Brian Meehan, Nadia Boufaied, Janusz Rak, David P Labbé, Daniel Dufort, and Nathalie Lamarche-Vane. Manuscript in preparation.

## Preface to Chapter 3

Currently, six genes associated with Adams-Oliver syndrome (AOS) pathogenesis have been identified, involving two critical signaling pathways: NOTCH and Rac1/Cdc42. Four identified CdGAP variants (pGln683X, p.Ser689X, p.Gln728X, and p.Lys1087Serfs*4) lead to a truncated form of CdGAP, yet their functional consequences vary significantly. Notably, the p.S689X variant only manifests as an isolated case of transverse terminal limb defects. Interestingly, multiple reports have emphasized that the placentas of AOS patients show signs of dysfunction. In women, a significant increase in CdGAP has been associated with late-onset severe preeclampsia. These observations led us to postulate that alterations in CdGAP expression or function could underpin placental dysfunction, contributing to AOS pathogenesis, aligning with the theory supporting the vascular origin of AOS. To test this hypothesis, we generated a CdGAP-AOS knock-in (KI) mouse model using the CRISPR/Cas9 strategy, introducing a truncating mutation after proline 670, corresponding to the glutamine residue at position 683 in humans. We observed an incompletely penetrant embryonic lethality at the weaning age (P21) among homozygotes (*CdGAP* $^{KI/KI}$). Intriguingly, this phenotype mirrored the effects of a global CdGAP-knockout, as reported in a previous study. Moreover, a broad range of embryonic abnormalities, including edema, pale liver, and hypovascularization, were similarly observed. Upon characterizing placentas at various gestational ages, we found that the homozygous KI mutation led to a partly penetrant onset of placental dysfunction, precipitating embryonic lethality during late gestation (> E15.5). This was largely attributed to the significantly impaired growth of the labyrinth. Furthermore, we discovered that syncytial fusion between two SynT layers was defective in *CdGAP* $^{KI/KI}$ (severe) placentas, a defect observed concurrently with congenital heart anomalies, including reduced thicknesses of ventricular walls and interventricular septum.

**Loss-of-function Adams-Oliver syndrome mutation of mouse *CdGAP* results in defective syncytial fusion and placental dysfunctions.**

Ji-Hyun Chung[1,2], Yi He[1,2], Shiva Shafei[3,4], Brian Meehan[5], Nadia Boufaied[1,4], Janusz Rak[5,6], David P Labbé[1,4], Daniel Dufort[3,4,7], and Nathalie Lamarche-Vane[1, 2]

1. Research Institute of the McGill University Health Centre (RI-MUHC), Cancer Research Program, Montréal, Québec, Canada

2. Department of Anatomy and Cell Biology, McGill University, Montréal, Québec, Canada

3. Research Institute of the McGill University Health Centre (RI-MUHC), Child Health and Human Development Program, Montréal, Québec, Canada

4. Department of Experimental Medicine, McGill University, Montréal, Québec, Canada

5. Research Institute of the McGill University Health Centre (RI-MUHC), Montréal, Québec, Canada

6. Department of Pediatrics, McGill University, Montréal, Québec, Canada

7. Department of Obstetrics and Gynecology, McGill University, Montréal, Québec, Canada

* corresponding author: Nathalie.lamarche@mcgill.ca

## Abstract

Six genes involved in the Rac1/Cdc42 and NOTCH pathways have been found associated with the Adams-Oliver syndrome (AOS), a rare inheritable congenital defect: *ARHGAP31, DOCK6, DLL4, EOGT, NOTCH1, and RBPJ*. ARHGAP31 encodes the Rac1/Cdc42 regulator CdGAP (Cdc42 GTPase-activating protein), which plays important roles in the control of cell adhesion, migration, invasion, and proliferation, central to cancer progression. Although several abnormalities, including intrauterine growth restriction, cutis marmorata telangiectatica congenita, and renal abnormalities are indicative of vascular defects, how mutations in *ARHGAP31* affect vascularization in AOS patients is unknown. Four mutations (Gln683X, Ser689X, Gln728X, and Lys187Serfs*4) in *ARHGAP31* are associated with AOS. While all mutations lead to truncated proteins, Gln683X leads to higher GAP activity *in vitro* but loss-of-function in the transcriptional regulation of E-Cadherin. To better understand the molecular function of the CdGAP variant Q683X in AOS, a CdGAP (P668T P670X) knock-in (KI) mouse, corresponding to the human *CdGAP-Q683X* variant, was generated using a CRISPR/Cas9 strategy. Here we show that CdGAP plays a role in placental development. We demonstrate that CdGAP KI mutation affects feto-maternal interaction, which leads to incompletely penetrant embryonic lethality. At E15.5, pale placentas and significant reductions in both fetal and placental weight have been identified in homozygous CdGAP KI embryos. Furthermore, embryonic abnormalities, including edema, pale liver, and hypovascularization of superficial vessels were frequently observed in homozygous embryos. Throughout late gestation, severely affected CdGAP KI/KI embryos were significantly growth-restricted, which occurred concurrently with reduced expansion of the labyrinth. By immunohistochemistry, we found significant changes in labyrinth organization, including reduced red blood cells found in vessels, enlarged vascular spaces, and defective syncytial fusion. Together, our data provide insights into understanding the vascular origin of AOS, revealing CdGAP as a major player in placental development and a candidate therapeutic target for the treatment of AOS.

## Introduction

The small GTPases of the Rho subfamily play important roles in many diverse cellular functions, including cell morphology, cell migration, differentiation, and proliferation. They act as molecular switches, cycling between inactive GDP-bound and active GTP-bound states. This GDP/GTP cycle is tightly regulated by three classes of regulators, namely guanine nucleotide exchange factors (GEFs), GTPase-activating proteins (GAPs), and guanine nucleotide dissociation inhibitors (GDIs)[1]. Rac1 and Cdc42 variants have been associated with a wide spectrum of developmental disorders. In particular, dysregulation of the Rac1/Cdc42 pathways through genetic defects in either *DOCK6*, a Cdc42 GEF, and *ARHGAP31* (also named Cdc42 GTPase-activating protein (CdGAP)), is considered to play a role in the pathogenesis of Adams-Oliver syndrome (AOS), a rare congenital disorder with familial inheritance or sporadic mutations. AOS is defined by aplasia cutis congenita (missing skin and skull tissue) and transverse terminal limb defects[2, 3]. Nevertheless, more than 50% of AOS patients remain molecularly ill-defined[4], which is largely attributed to the wide spectrum of phenotypic abnormalities seen among AOS patients. In fact, while important associated anomalies include cardiac and vascular defects[5], supporting the interruption of embryonic blood supply as a likely pathogenic mechanism for AOS[6, 7], research efforts with respect to placental dysfunctions in AOS patients have been largely deficient.

Four autosomal-dominant truncating mutations, Q683X, Ser689X, Gln728X, and Lys1087Serfs*4, in CDGAP have been found in families of patients with AOS[4, 8]. CdGAP comprises several functional domains: the N-terminal poly-basic region (PBR), GAP domain, basic-rich (BR) domain, proline-rich domain (PRD), and the C-terminus[9, 10]. Functionally, human *CDGAP-Q683X* truncating mutation leads to the loss of PRD and the C-terminus, which have been previously identified to play essential roles in transcriptional regulation of E-cadherin in breast cancer[11]. The C-terminus of CdGAP also consists of docking sites for 14-3-3β for cytoplasmic retention of CdGAP, and interaction with a scaffolding protein, Ajuba, which suppressed CdGAP activity in epithelia to maintain cell-cell contacts[10, 12]. Therefore, to better understand the molecular function of the CdGAP variant Q683X in AOS, we generated a CdGAP (P670X) knock-in (KI) mouse model, corresponding to the human *CDGAP-Q683X* variant, using a CRISPR/Cas9 strategy. Our data show that homozygous CdGAP KI embryos exhibited incompletely penetrant embryonic lethality, edema, pale liver, and vascular defects, which

resemble phenotypes that were observed in the systemic CdGAP knock-out (KO) mouse model[13]. Furthermore, we report important placental abnormalities associated with congenital heart defects. We demonstrate that CdGAP was highly expressed in the labyrinth region of E12.5 placentas. We identified labyrinth defects, which were strongly pronounced during late gestation (> E15.5), due to impaired fusion of syncytiotrophoblasts (SynTs), leading to compromised feto-maternal exchanges. *CdGAP* $^{KI/KI}$ embryos were associated with congenital heart defects, including a significant reduction in ventricular wall thickness as well as reduced myocardial compaction. Altogether, these findings support a role for CdGAP in placental development, providing novel molecular insights into the vascular origin of AOS.

## Materials and Methods

### Generation of CdGAP (P668T P670X) knock-in (KI) mice

The *CdGAP (P668T P670X) KI* mice were generated by McGill Integrated Core for Animal Modeling. CRISPR/Cas9 technology was used to generate the *CdGAP P668T P670X* allele, which encodes the truncated mutant form of CdGAP lacking the C-terminal of this protein. For targeting *CdGAP P668T P670X*, three Guide RNAs (gRNAs) were designed following the instructions at (http://crispr.mit.edu/).

| gRNA Name | Forward | Reverse |
|---|---|---|
| gRNA1 | CACCGGATTCCTGAGTCA AGCCCAG | AAACCTGGGCTTGACTCAGG AATCC |
| gRNA2 | CACCGGAGTCAAGCCCAG CCCCATT | AAACAATGGGGCTGGGCTTG ACTCC |
| gRNA3 | CACCGATTCCTGAGTCAA GCCCAGC | AAACGCTGGGCTTGACTCAG GAATC |

Mice were generated by electroporation of the three gRNAs and Cas9 protein into single-cell FVB/N mouse zygotes. Live pups born from these females were genotyped by PCR amplification of genomic DNA extracted from the tail. The targeted region was amplified using the genotyping primers (5'CAGCCATGGTTACTGAGGC3'; 5'AGTAAGAGGGGGAGAGAGATTCC3'). The products were sent for direct Sanger sequencing (Génome Québec). Instead of 5'CCGATTCCT3' in wild-type *CdGAP* sequence, two founder males had established 5'ACGATTTAA3' mutations in their two *CdGAP* alleles. Founder mutants underwent at least 2 generations of backcrossing with wild-type FVB/N mice before establishing progeny. Heterozygous $CdGAP^{wt/ki}$ mice were crossed inter se to generate $CdGAP^{wt/wt}$, heterozygous $CdGAP^{wt/ki}$, and homozygous $CdGAP^{ki/ki}$ animals. After producing 10 generations of progeny from the mating of heterozygous mice, backcrossing was performed with wild-type FVB/N (Charles River) mice before continuing with further analysis. Mice were housed in IVC cages with 12-hour light-dark cycles under ambient temperature and humidity conditions. All experimental procedures (protocol no. 7665) were approved by the McGill University Animal Care and Use Committee.

**Timed mating for collection of embryos**

7 to 12-weeks-old *CdGAP* $^{WT/KI}$ females were utilized for timed mating to collect embryos at different gestational ages (E12.5, E13.5, E15.5, E16.5, E17.5, and E18.5). To synchronize the estrous cycle utilizing the Whitten effect, an individual female mouse was introduced into the stud male's (*CdGAP* $^{WT/KI}$) cage, which had been containing soiled bedding for a minimum of 3 days[14]. Signs of successful mating (i.e., observation of vaginal plug) were monitored the next morning, and E0.5 was designated when vaginal plugs were observed. Females positive for a plug were housed separately from males. Successful pregnancy was confirmed by a weight gain of > 1.75 g by E10.5[15]. When the desired gestational ages were reached, pregnant mothers were euthanized by $CO_2$ asphyxiation followed by cervical dislocation. The tail of each mother was collected to reconfirm each mother's genotype.

**Genotyping**

Small portions of tails from embryos following dissections or tail snips from P21 litters upon weaning were digested overnight at 55 °C by incubating with 300 µL of PCR-direct tail lysis buffer (Viagen; 102-T). Proteinase K was added at 0.2mg/mL (Bioshop; PRK403) to remove proteins. The next day, the proteinase K was inactivated by incubating the tail lysates at 95 °C for 10 minutes. After inactivation, the tail lysates were centrifuged at 14,000 rpm for 5 minutes at room temperature, and the supernatants were transferred to fresh 1.5 mL Eppendorf tubes. The PCR reaction was set up by preparing a master mix using 10X PCR buffer with 15mM $MgCl_2$ (Zmtech; T207029), 10 mM dNTP (Zmtech; TD-27010), 10uM forward and reverse primers (IDT), and DMSO. 5 µL of tail lysate supernatant was used for genotyping. The PCR cycle consisted of a total of 33 cycles with the following conditions: 95 °C for 2 minutes, 94 °C for 30 seconds, 63 °C (WT primer), 60 °C (KI primer), or 58.8 °C for (Sex primer) for 30 seconds, and 72 °C for 30 seconds, followed by a final extension at 72 °C for 10 minutes (Bio-Rad, T-100). WT-specific and KI-specific primers produced amplicons at 451 bp and 254 bp, respectively. Using sex primers, flanking an 84 bp deletion of the X-linked *Rbm31x* gene, two amplicons at 269 and 353 bp were produced in male embryos, and a single amplicon at 269 bp was produced in female embryos[16]. PCR products were resolved on a 1% agarose gel (Wisent; 800-015-CG) containing Fluo-DNA/RNA gel staining solution (20,000X) (Zmtech; GS-301). Following

separation, the bands were visualized using a transilluminator (Bio-Rad, Chemidoc™ Touch imaging system).

**Collection of organs from three-months-old mice**

Heart, lung, and brain tissues of three-month-old mice were collected as follows. Age- and sex-matched *CdGAP* $^{WT/WT}$, *CdGAP* $^{WT/KI}$, and *CdGAP* $^{KI/KI}$ mice were euthanized by $CO_2$ asphyxiation followed by cervical dislocation. Prior to dissection, the abdominal fur was shaved from each mouse, and the exposed skin was cleaned with gauze soaked in 70% isopropyl alcohol. Subsequently, using sterile forceps and scissors, midline incisions were made along the abdomen. Using fine forceps, the heart, and lungs of each mouse were isolated and immediately snap-frozen. For the removal of the brain, the skull of each mouse was carefully removed using forceps and scissors to expose the brain. Using a clean spatula, the exposed brain was scooped out and immediately snap-frozen in liquid nitrogen. The isolated and snap-frozen tissues were subsequently placed in 2.0 mL cryogenic vials (CLS430488; Corning®) and stored in liquid nitrogen.

**Frequency distribution curves of fetal weights**

Frequency distribution curves of fetal weights for *CdGAP* $^{WT/WT}$, *CdGAP* $^{WT/KI}$, and *CdGAP* $^{KI/KI}$ embryos at E12.5, E13.5, E15.5, and E18.5 were plotted from a minimum of 15 litters[17]. The following bin width (g) was used for each gestational age: 0.00875g for E12.5, 0.00975g for E13.5, 0.045g for E15.5, and 0.125g for E18.5.

A non-linear regression (least squares regression with no weighting) fit of the histogram was generated for each genotype and was represented by different lines. The frequency distribution curves and $R^2$ values (goodness of fit) were presented as follows:

E12.5 and E13.5 curves:

- *CdGAP* $^{WT/WT}$: 0.9927 (E12.5), 0.9761 (E13.5)
- *CdGAP* $^{WT/KI}$: 0.9630 (E12.5), 0.9867 (E13.5)
- *CdGAP* $^{KI/KI}$: 0.9765 (E12.5), 0.9802 (E13.5)

E15.5 and E18.5 curves:

- *CdGAP* $^{WT/WT}$: 0.9995 (E15.5), 0.9821 (E18.5)
- *CdGAP* $^{WT/KI}$: 0.9960 (E15.5), 0.9643 (E18.5)

- *CdGAP* $^{KI/KI}$ (moderate): 0.9885 (E15.5), 0.9931 (E18.5)
- *CdGAP* $^{KI/KI}$ (severe): 0.9492 (E15.5), 0.9177 (E18.5)

Solid vertical lines represent the 5$^{th}$ percentile of E15.5 and E18.5 *CdGAP* $^{WT/WT}$ embryos' weight, calculated as: (- Z score x SD) + mean, where Z score = 1.645 and SD = standard deviation[18]. Embryos were considered growth-restricted if the fetal weight fell below the 5$^{th}$ percentile (solid vertical lines in Figure 3E)[17].

**Tissue fixation, processing, and embedding**

Embryos and their matching placentas were dissected in sterile, ice-cold 1X PBS (pH 7.4) and fixed using either 4% PFA for 48 hours at 4 °C with rotation or 10% neutral buffered formalin at room temperature for RNAscope. After fixation, excess fixatives were discarded, and tissues were washed three times with an excess volume of 1X PBS (pH 7.4) for 5 minutes with rotation at 4 °C. Successfully fixed tissues were then stored submerged in sterile 1X PBS (pH 7.4) at 4 °C. Prior to processing, placenta tissues were longitudinally bisected using sterile surgical blades (No. 11) with the maternal side facing up. Similarly, the heads and lower body portions of E15.5 embryos were trimmed using a sterile razor blade. Bisected placentas and trimmed E15.5 embryos were placed in cassettes with their IDs clearly labeled on the front and sides using a pencil and subsequently submerged in a beaker containing 70% ethanol for 24 hours. Subsequently, the tissues were processed through the tissue processor (Leica; TP 1050) and embedded in paraffin blocks[19].

**Microtome sectioning of FFPE blocks**

E12.5, E15.5, and E18.5 placentas were serially sectioned at 4 μm thickness using a rotary microtome (Thermo-Scientific; HM 355S), while E15.5 embryos were serially sectioned at 8 μm thickness. Individual sections were gently placed on a floatation bath (VWR; 97043-530), which was set at 42 °C and then mounted onto Superfrost™ Plus positively charged slides (Fisher Brand™; 12-550-15). The slides were placed vertically on a rack at an angle and allowed to air dry. The following day, after confirming the tissue sections were well-adhered to each slide, the slides were transferred to slide boxes and stored at 4 °C.

**Immunostaining**

Slides with individual tissue sections were first incubated at 60 °C for 1 hour. Subsequently, the slides were placed in a 12-position vertical staining rack for Easy Dip slide staining system (Diamed; DLAN1810-12DGY), de-waxed and rehydrated in a series of 5-minute steps, starting with xylene and progressing through ethanol concentrations from 100% down to 50%. Tissues were further processed by heating at 95 °C for 15 minutes using a microwave oven in an unmasking solution (Vector Labs; H3300) for antigen retrieval. Following heat-assisted antigen retrieval, slides submerged in antigen retrieval solution were cooled for 20 minutes at room temperature. Subsequently, slides were placed back in the slide holder and washed three times for 5 minutes using 1X PBS (pH 7.4). Prior to incubation with primary antibodies, tissues were blocked with 5% goat (Sigma-Aldrich; G9023) or donkey serum (Sigma-Aldrich; D6993) prepared in 1X PBS (pH 7.4). Primary antibodies, diluted in 1X PBS (pH 7.4): rabbit anti-MCT4 (EMD-Milipore; AB3314P, 1:200), chicken anti-MCT1 (EMD-Milipore; AB1286-I, 1:200), rabbit anti-E-Cadherin (Cell Signaling; 3195S, 1:100) and goat anti-CD31 (R&D Systems; AF3628, 1:20) were incubated overnight at 4 °C. As a negative control, ensuring the specificity of each antibody used, one of the slides was incubated in 5% serum overnight (18 hours) instead. On the following day, tissues were washed for 5 minutes three times in 1X PBS (pH 7.4). The respective fluorescent secondary antibodies were incubated with tissues for 45 minutes at room temperature. Secondary antibodies: goat anti-rabbit IgG Alexa Fluor 488 (Invitrogen; A11008, 1:200), donkey anti-goat Alexa Fluor Plus 594 (Invitrogen; A32758, 1:200), and donkey anti-chicken IgG Alexa Fluor 594 (Invitrogen; A78951, 1:200)[19]. Tissues were washed three times for 5 minutes then quenched to reduce autofluorescence for 2 minutes using TrueView with DAPI mounting medium, prepared as a 1:1:1 mix of reagent A, B, and C as per manufacturer's instructions (Vector Labs; VECT8500). Quenched slides were subsequently washed for 5 minutes with 1X PBS (pH 7.4), then slides were cover-slipped using the mounting medium with DAPI (Vector Labs; VECT8500). Cover-slipped slides were kept dark at 4 °C for 24 hours before image acquisition.

**In situ hybridization**

In situ hybridization assay was performed using RNAscope (Advanced Cell Diagnostics, Inc.) with the target probe for mouse CdGAP mRNA (Advanced Cell Diagnostics, Inc., 569971) according to the manufacturer's instructions[20].

**Image acquisition**

For phenotypic characterization of embryos and placentas at different gestational ages, E15.5 embryos and placentas, as well as E18.5 placentas, were imaged using a digital camera (Leica Microsystems Inc.; MC170) attached to a stereomicroscope (Leica Microsystems Inc.; M80). Embryos and placentas were placed on top of an Ergo transmitted light base (Leica Microsystems Inc.; TL5000) for illumination. H&E or fluorescently stained tissue sections at E15.5 and E18.5 were scanned with the help of Small Animal Imaging Labs (SAIL) (RI-MUHC). H&E-stained slides were scanned under a bright field using 10X objectives (Zeiss; Axioscan Z1). Similarly, fluorescent slides were imaged using 10X objectives. DAPI was used for initial focusing, where images were focused for every tile (Zeiss; Axioscan Z1). For fluorescent slides, images were further processed for correction of stitching of each tile with the following settings: use all channels for reference, edge detection, overlap (1%), and quality (best). H&E-stained E12.5 placenta sections were scanned with the help of the Histopathology Core (RI-MUHC). Slides were scanned using a Scanscope XT digital slide scanner (Aperio, Leica Biosystems Inc.).

**Histological analysis**

For histological analyses of placentas, every fifth section was routinely stained with Hematoxylin and Eosin (H&E). E12.5 placenta sections stained for H&E were analyzed using Imagescope software (Aperio, Leica Biosystems Inc.), and a freehand selection tool was employed to outline specific layers: maternal decidua, junctional zone, and the labyrinth or the entire placenta. For E15.5 and E18.5 placenta and E15.5 embryonic heart sections, analysis was conducted using QuPath for Mac (v0.4.3)[21]. Similar to E12.5 placenta sections, a closed polygon annotation tool was selected to outline the junctional zone and the labyrinth or the entire placenta. Labyrinth thickness was measured along the middle, from the base (chorionic plate), for all gestational ages, using a line tool. The thickness of the compact zone or trabeculae from both ventricles in each E15.5 embryo was measured using a line annotation tool. For the

ventricular non-compaction index, this tool was used to measure compact zone and trabecular layer thickness in a defined area (a square with a size of 100,000 $\mu m^2$; width: 316.25 μm). The ventricular non-compaction index was calculated as the ratio between the compact zone thickness and the thickness of trabeculae. For each calculation, three consecutive sections were averaged for comparison.

**Immunoblot**

Whole E18.5 placental tissues or 100mg of heart, lung, and brain tissue from three-month-old mice were homogenized using a Biomasher (9790A; TaKaRa) with 500 μL RIPA buffer. The buffer contained 50 mM HEPES (pH 7.5), 0.1% sodium dodecyl sulfate, 1% Triton X-100, 0.5% sodium deoxycholate, 50mM sodium fluoride, 150mM sodium chloride, 10mM EDTA (pH 8.0), 50mM sodium orthovanadate, 20mM leupeptin, 20mM aprotinin, and 1mM phenylmethylsulphonyl fluoride. Protein lysates were subjected to centrifugation at 10,000 x *g* for 15 min at 4 °C to remove insoluble materials, and protein concentrations were determined using the Bicinchoninic Acid Assay (BCA) protein kit (Thermo-Scientific; 23225). Equal amounts of protein samples were resolved by sodium dodecyl sulfate-polyacrylamide gel electrophoresis (SDS-PAGE) and transferred to nitrocellulose membranes for immunoblotting with the following antibodies: CdGAP (HPA036380; Sigma-Aldrich), CdGAP (14087S; Cell Signaling), and Tubulin (T5168; Sigma-Aldrich). The proteins were visualized by enhanced chemiluminescence (ECL) using Clarity™ western ECL substrate (Bio-Rad; 1705061) and ChemiDoc™ Touch imaging system (Bio-Rad).

**Analysis of pre-existing single-cell RNA-Seq data**

Expression of CdGAP in the developing mouse placenta was analyzed at various embryonic days (E9.5, E10.5, E12.5, and E14.5) using a previously published dataset by Marsh *et al.* (2020)[22]. R object of the scRNAseq data was downloaded from the figshare (https://figshare.com/projects/Single_nuclei_RNA-seq_of_mouse_placental_labyrinth_development/92354).

FeaturePlot function from the Seurat R package was used to visualize cdGAP expression in the different trophoblast populations projected in the UMAP space.

**Statistical analysis**

Student's t-test was used to compare two groups, while one-way ANOVA, followed by correction for multiple comparisons, was used for the comparison of more than three groups. Two-way ANOVA was used to first assess differences due to the row factor, column factor, or their interactions. Subsequently, Tukey's multiple comparisons tests were utilized for comparison between two genotypes within each row (simple effects within a row). For Student's t-test and one-way ANOVA, the F-test, Brown-Forsythe, or Bartlett's test were used respectively, to assess whether SDs were significantly different. When SDs were significantly different, an unpaired t-test with Welch's correction or Welch's one-way ANOVA was performed, respectively. For the comparison of the number of healthy embryos in Figure 3.2D, where data did not follow Gaussian distribution, a non-parametric test (Kruskal-Wallis) followed by Dunn's T3 correction for multiple comparisons was performed. Lastly, *Fisher's* exact tests or *Chi-square* tests were used to assess whether sex distribution or genotypic distribution of *CdGAP* $^{WT/WT}$, *CdGAP* $^{WT/KI}$, and *CdGAP* $^{KI/KI}$ embryos during embryonic development or at wean (P21) significantly differed from expectation. All statistical analyses presented in this study were performed using GraphPad Prism v9.5.1. The results were considered not significant (NS) when $P > 0.05$, or significant when $P < 0.05$ (*); $P < 0.01$ (**); $P < 0.001$ (***) and $P < 0.0001$ (****).

## Results

### *P670X truncating mutation in CdGAP causes incompletely penetrant embryonic lethality*

Despite four known causative mutations in *CDGAP* that share common traits – namely leading to a loss of the proline-rich domain (PRD) and C-terminal region, – clinical manifestations resulting from each mutation differed significantly in patients[4, 5]. Guided by these observations, we decided to examine *in vivo* the functional consequence of the p.Gln683X mutation in CDGAP, which leads to the two main AOS clinical manifestations[2, 3]: transverse terminal limb defects (TTLD) and aplasia cutis congenita (ACC) by generating a CdGAP (P670X) knock-in (KI) mouse model, corresponding to the human *CDGAP-Q683X* variant, using a CRISPR/Cas9 strategy (Figure 3.1A). In this study, CdGAP P670X knock-in (KI) mice were maintained by breeding heterozygotes. We only observed wild type (451 bp) and mutation-specific (254 bp) amplicons among *CdGAP* $^{WT/WT}$ and *CdGAP* $^{KI/KI}$ pups, respectively, with both types present in *CdGAP* $^{WT/KI}$ pups (Figure 3.1B). Incompletely penetrant lethality (9.8% (KI) observed vs 25% (WT)) was observed among *CdGAP* $^{KI/KI}$ pups at weaning (P21) (Figure 3.1C). To determine whether the source of this lethality was due to embryonic (*in utero*) or post-natal complications, we collected embryos at embryonic day (E) 15.5. They did not deviate from the expected ratio (Figure 3.1C), even though abnormal embryos were frequently observed (Figure 3.1D, E). Moreover, neither the genotype nor the sex distribution significantly differed from the expected 1:2:1 and 1:1 ratios, respectively, at any gestational ages examined from E12.5 (Supplementary Figure 1A), a point at which rapid growth starts[23].

Notably, the percentage of grossly abnormal embryos between E15.5 and at E18.5 were comparable, with significantly increased abnormalities (> 40%) associated with *CdGAP* $^{KI/KI}$, but not *CdGAP* $^{WT/KI}$ embryos (Figure 3.1D). This revealed that a significantly higher number of mutant embryos (*CdGAP* $^{WT/KI}$ and *CdGAP* $^{KI/KI}$) were affected by various abnormalities including edema, pale liver, and hypovascularization of superficial vessels (Figure 3.1E). Together, these results show that the loss of CdGAP C-terminus severely impaired CdGAP function and leads to vascular defects and edema.

### *Male CdGAP$^{KI/KI}$ mice show reduced body weights*

To demonstrate the expression of the truncated CdGAP (1-669) protein in various tissues of three-month-old mice, we used two different commercial antibodies against CdGAP. One

antibody targeting the CdGAP-basic rich (BR) domain allowed the detection of the truncated and full-length CdGAP proteins whereas the anti-CdGAP antibody targeting the C-terminus of CdGAP can detect only the full-length protein. Truncated CdGAP was observed in the brain, heart, and lung tissues of mutant mice (*CdGAP* $^{WT/KI}$ and *CdGAP* $^{KI/KI}$), while both the full-length and truncated CdGAP proteins were observed in *CdGAP* $^{WT/KI}$ mice (Supplementary Figure 1B). To investigate potential long-term physiological consequences amongst surviving *CdGAP* $^{KI/KI}$ pups, we measured the body weight of both male and female pups weekly from weaning until they reached three months of age. We observed significant body weight differences that were dependent not only on the genotype but also based on the sex. Male but not female *CdGAP* $^{KI/KI}$ pups showed a significant reduction in body weight compared to wild type littermates at all ages (Supplementary Figure 1C). This observation was reinforced by the smaller sizes of male three-month-old *CdGAP* $^{KI/KI}$ mice (Supplementary Figure 1D). Together, these results demonstrate that the truncated CdGAP protein is expressed in the *CdGAP* $^{WT/KI}$ and *CdGAP* $^{KI/KI}$ mice and that the male homozygous *CdGAP* $^{KI/KI}$ mice show reduced body weights compared to the wild type or heterozygous *CdGAP* $^{WT/KI}$ mice.

***The P670X mutation in CdGAP mice leads to placental dysfunction***

To determine whether placental dysfunction could underlie the embryonic lethality observed in *CdGAP* $^{KI/KI}$ embryos, we first crossed *CdGAP* $^{WT/KI}$ males with *CdGAP* $^{WT/WT}$, *CdGAP* $^{WT/KI}$, and *CdGAP* $^{KI/KI}$ female mice. This was performed to phenotypically characterize both the embryos and their corresponding placentas at E18.5 (Figure 3.2A). A gross morphological examination of the uterine horn revealed multiple abnormalities in the embryonic sacs of *CdGAP* $^{KI/KI}$ mothers. Specifically, the embryonic sacs were hemorrhagic (Figure 3.2B; white arrowhead) and were irregularly sized with reduced sizes (Figure 3.2B; white arrow). In addition to these morphological analyses, we observed a trend toward reduced body weight gains during late gestation (> E14.5) in *CdGAP* $^{KI/KI}$ mothers (Figure 3.2C). These trends were associated with a significant reduction in the number of total or healthy pups (those without phenotypic abnormalities, as defined in Figure 3.1E) from *CdGAP* $^{WT/KI}$ and *CdGAP* $^{KI/KI}$ mothers, respectively. Furthermore, pale placentas, which can be associated with placental dysfunction[24, 25], were observed exclusively with abnormal embryos (Figure 3.2D). To assess whether CdGAP was expressed in the placentas, we performed immunoblot analyses of E18.5 placental protein

lysates. We determined that CdGAP was expressed in wild type placentas, while both full-length and truncated CdGAP were expressed in *CdGAP* $^{WT/KI}$ placentas. Only the truncated CdGAP protein was expressed in *CdGAP* $^{KI/KI}$ placentas. Importantly, paler placentas associated with *CdGAP* $^{KI/KI}$ embryos were observed compared to wild type or heterozygous embryos (Figure 3.2E). Together, these results demonstrate that the incompletely penetrant embryonic lethality of *CdGAP* $^{KI/KI}$ embryos may be caused in part by placental dysfunction.

**Male *CdGAP* $^{KI/KI}$ *embryos with placental dysfunction were severely growth-restricted during late gestation***

During mouse gestation, the successful formation of the "definitive placenta" – comprised of maternal decidua, the junctional zone, and the labyrinth – by E12.5 (Figure 3.3A) is crucial. The intricate network of maternal and fetal blood vessels laid out in this structure supports the increasing demand for nutrient, gas, and waste exchanges, allowing for rapid fetal growth during late gestation[23, 26]. To understand the consequences of placental dysfunction, we collected both embryos and their placentas during late gestation (> E15.5) for phenotypic characterization. This highlighted considerable variability among *CdGAP* $^{KI/KI}$ placentas, with noticeable differences in placental morphology, such as paleness and poor vascularization (Figures 3.3B, C). As a result, we further categorized *CdGAP* $^{KI/KI}$ embryos into two groups of phenotypes for subsequent analyses: *CdGAP* $^{KI/KI}$ (moderate) and *CdGAP* $^{KI/KI}$ (severe) from E15.5 onward.

We investigated the functional impact of placental dysfunction on embryonic development by comparing the weights of embryos and placentas at E15.5 and E18.5. Our data showed a positive correlation between the weights of embryos and their placentas. In the *CdGAP* $^{KI/KI}$ (severe) group, a significant reduction of the placental weights was associated with significantly reduced fetal weights compared to *CdGAP* $^{WT/WT}$ embryos. Contrastingly, both fetal and placental weights of *CdGAP* $^{KI/KI}$ (moderate) embryos were comparable to those of *CdGAP* $^{WT/WT}$ and *CdGAP* $^{WT/KI}$ embryos (Figure 3.3D, Supplementary Figure 2A, C). Interestingly, despite the trend towards disproportionate sex distribution among *CdGAP* $^{KI/KI}$ (severe) embryos at E15.5 (Supplementary Figure 2B) and at E18.5 (Supplementary Figure 2D), neither fetal nor placental weights at both gestational ages significantly differed between male and female embryos (Supplementary Figure 2A, C). Importantly, the effects of placental dysfunction resulted in dramatic shifts in the body weight distribution of *CdGAP* $^{KI/KI}$ (severe) embryos, which fell

below the 5th percentile of *CdGAP* $^{WT/WT}$ embryos' body weight (Figure 3.3E). This indicated that *CdGAP* $^{KI/KI}$ (severe) embryos were severely growth-restricted (Figure 3.3F)[17]. Between E12.5 to E13.5 – when the definitive placenta begins to function, leading to a shift toward "hemotrophic" nutrition[27] – the average fetal weight of *CdGAP* $^{KI/KI}$ embryos did not significantly differ from those of *CdGAP* $^{WT/WT}$ embryos (Supplementary Figure 2E ,F).

In human studies, the fetal-to-placental weight ratio has been used as an indicator of placental efficiency and as a marker of dysfunction[28, 29]. However, despite significant growth restriction in *CdGAP* $^{KI/KI}$ (severe) embryos, placental efficiencies were comparable to *CdGAP* $^{WT/WT}$ embryos both at E15.5 and at E18.5, when considering both embryonic sexes equally. Interestingly, the placental efficiency of both *CdGAP* $^{WT/KI}$ and *CdGAP* $^{KI/KI}$ (moderate) embryos was significantly increased at E15.5 (Figure 3.3G). Further segregation of placental efficiency by embryonic sex revealed differences among E15.5 embryos, where placental efficiencies of *CdGAP* $^{KI/KI}$ (severe) embryos were significantly increased among female embryos, whereas this showed a trend towards reduction compared to *CdGAP* $^{WT/WT}$ embryos among male embryos (Supplementary Figure 2A). Nevertheless, differences in placental efficiency between males and females among *CdGAP* $^{KI/KI}$ (severe) embryos were lost at E18.5, at which point placental efficiency was reduced in both sexes (Supplementary Figure 2C). A positive correlation between placental and fetal weights was also observed at E18.5 (Figure 3.3H). These findings suggest that placental dysfunctions observed in *CdGAP* $^{KI/KI}$ (severe) embryos cause severe growth restriction, which is limited to late gestation (> E15.5).

***CdGAP*** $^{KI/KI}$ ***placentas show reduced vascular complexity and defective labyrinth***

We next conducted histological analyses of E15.5 and E18.5 placenta tissues. These analyses revealed that the vascular complexity in the labyrinth of *CdGAP* $^{KI/KI}$ (severe) placentas was significantly reduced at E15.5, but not in *CdGAP* $^{KI/KI}$ (moderate) placentas. These reductions were even more severe at E18.5, leading to visible cellular atrophy (Figure 3.4A; asterisk). Consistent with observations of pale and poorly vascularized placentas, we also noticed a significantly increased number of vacant vascular spaces in the labyrinth of *CdGAP* $^{KI/KI}$ (severe) placentas (Figure 3.4A; yellow arrowhead). Subsequent measurements revealed that the average area of the labyrinth, which comprises the majority of the definitive placenta[30, 31], was significantly reduced in *CdGAP* $^{KI/KI}$ (severe) placentas at both E15.5 and E18.5, leading to a

reduced total placental area (Figure 3.4B, C). However, the relative area of the labyrinth remained comparable between genotypes of both gestational ages (Supplementary Figure 3A).

Though the "definitive" placenta is established by E12.5, it continues to grow, reaching maximum labyrinth size by E14.5, maximizing feto-maternal exchanges[23]. We, therefore, assessed how the expansion of the labyrinth was affected in *CdGAP* $^{KI/KI}$ (moderate) and *CdGAP* $^{KI/KI}$ (severe) placentas during late gestation by measuring labyrinth thickness. Labyrinth thickness was also reduced in *CdGAP* $^{KI/KI}$ (severe) placentas at E15.5, but not at E18.5. Conversely, labyrinth thickness in *CdGAP* $^{KI/KI}$ (moderate) placentas was comparable to that in *CdGAP* $^{WT/WT}$ placentas at both gestational ages (Figure 3.4D). We further compared the average labyrinth area at E15.5 and at E18.5 to understand how its expansion was affected in *CdGAP* $^{KI/KI}$ (severe) embryos. This revealed severely compromised expansion of the labyrinth in *CdGAP* $^{KI/KI}$ (severe) placentas during late gestation, unlike in *CdGAP* $^{KI/KI}$ (moderate) placentas, which reached similar sizes to that in *CdGAP* $^{WT/WT}$ placentas by E18.5 (Figure 3.4E).

Considering the complexity of the placenta and the interdependence of each layer's development[26], we determined the labyrinth-to-junctional zone area ratio differed between genotypes, to further elucidate the compromised labyrinth expansion. Contrary to the area measurements, this ratio was not significantly reduced in *CdGAP* $^{KI/KI}$ (severe) placentas at either E15.5 or E18.5 (Figure 3.4F). Taken together, labyrinth defects, including reduced vascular complexity and limited labyrinth expansion, leading to poor placental maturation, are the primary placental dysfunctions in *CdGAP* $^{KI/KI}$ (severe) placentas, and likely contribute to embryonic lethality.

***CdGAP*$^{KI/KI}$ *placentas demonstrate a disorganized syncytium***

In mouse placenta, the maternal and embryonic circulations are separated by "hemotrichorial" structures, which consist of sinusoidal trophoblast giant cells (sTGCs) and two continuous layers of multinucleated syncytiotrophoblasts (SynTs)[27, 30]. To investigate the causes of placental dysfunction in *CdGAP* $^{KI/KI}$ embryos, we visualized the organization of SynT layers in E18.5 placentas using immunostaining with antibodies against MCT1 and MCT4 lactate transporters, which are highly expressed on the apical membrane of the SynT-I layer, which faces maternal sinusoids, and on the basal membrane of the SynT-II layer, which faces fetal blood spaces, respectively[27, 30, 32] (Figure 3.5A, G). Upon fluorescent staining of the E18.5 *CdGAP*

$^{WT/WT}$ placentas, we could see intricately organized vascular networks alongside tightly apposed SynT layers within the labyrinth (Figure 3.5B, white arrows). However, vascular complexity and syncytial fusion were noticeably altered in both *CdGAP* $^{KI/KI}$ (severe) and *CdGAP* $^{KI/KI}$ (moderate) placentas. More specifically, the tight apposition between the two SynT layers was lost in small regions towards the periphery or throughout the labyrinth in *CdGAP* $^{KI/KI}$ (moderate) and *CdGAP* $^{KI/KI}$ (severe) placentas, respectively (Figure 3.5C-F, see white arrows; Figure 3.5G). Furthermore, in the regions where the syncytia were defective, the MCT1 and MCT4 transporters were abnormally expressed, with increased non-membranous localization (Figure 3.5D, F; white arrowheads).

To further analyze the functional consequences of a disorganized syncytium, we compared fluorescently stained placental tissue sections with sections stained with hematoxylin and eosin (H&E) for histological examination at E18.5 between *CdGAP* $^{KI/KI}$ (severe) and *CdGAP* $^{WT/WT}$ placentas. This juxtaposition revealed several defects in the labyrinth of *CdGAP* $^{KI/KI}$ (severe) placentas. This included cellular atrophy (Figure 3.5H-K; asterisk), an increase in deep-purple stained red blood cells, indicative of deficient circulation (Figure 3.5I, K; black arrowheads), and significantly enlarged vascular spaces (Figure 3.5J, K; #) compared to *CdGAP* $^{WT/WT}$ placentas (Figure 3.5M-P). These alterations ultimately resulted in embryonic lethality at E18.5 (Figure 3.5L vs 5Q). Thus, these results suggest that defects in the labyrinth, particularly the impaired fusion of SynT cells, cause placental dysfunction in *CdGAP* $^{KI/KI}$ (severe) embryos.

***Defective organization of syncytium, but not placental angiogenesis is associated with labyrinth defects in E15.5 CdGAP*** $^{KI/KI}$ ***placentas***

In *CdGAP* $^{KI/KI}$ (severe) embryos, which manifested apparent embryonic abnormalities, including edema and pale liver at E15.5, compared to *CdGAP* $^{WT/WT}$ embryos (Figure 3.6A vs F; red and blue arrowheads), their matching placentas were poorly vascularized and pale (Figure 3.6B vs G). We next examined the labyrinth organization of E15.5 *CdGAP* $^{KI/KI}$ placentas (Figure 3.6H-J vs Figure 3.6C-E). Similar to E18.5 placentas, the organization of the syncytium was defective in various regions of the labyrinth of *CdGAP* $^{KI/KI}$ (severe) placentas, in particular at the extremity (Figure 3.6I; white arrowhead), as compared to the tightly apposed SynT layers with thin, membranous expression of MCT1 and MCT4 transporters in *CdGAP* $^{WT/WT}$ placentas (Figure 3.6D). Thicker interhaemal membranes were observed in the labyrinth of *CdGAP* $^{KI/KI}$

(severe) placentas (Figure 3.6K; yellow arrows), with markedly enlarged vascular spaces, filled with significantly fewer red blood cells (Figure 3.6E vs J). The increased non-membranous expression of MCT1 and MCT4 (Figure 3.6L; white arrows) and thicker interhaemal membranes (Figure 3.6K; yellow arrows) led to the significantly higher mean fluorescence intensity of MCT4, but not MCT1 transporters in *CdGAP* $^{KI/KI}$ (severe) placentas (Figure 3.6M). Furthermore, the mean fluorescence intensity of E-cadherin was significantly decreased, coinciding with the reduced complexity of vascular networks (Figure 3.6M).

Labyrinth defects, a common cause of embryonic death[33], may result from two main factors: 1) defects in placental angiogenesis[34, 35], and 2) defective syncytial fusion[32, 35]. To determine whether placental angiogenesis was impaired in *CdGAP* $^{KI/KI}$ (severe) placentas, we conducted immunostaining against endothelial cells ($CD31^{+}$). Contrary to the defective syncytia and reduced vascular complexity, the lining of fetal blood spaces by fetal endothelial cells was unaffected, with comparable morphologies of fetal blood vessels in E15.5 *CdGAP* $^{KI/KI}$ (severe) placentas compared to wild type placentas (Figure 3.6N). Therefore, these results show that defective syncytial fusion, but not placental angiogenesis may be responsible for the labyrinth defects, and consequently placental dysfunction in *CdGAP* $^{KI/KI}$ (severe) embryos.

***E15.5 male CdGAP*** $^{KI/KI}$ ***embryos are "asymmetrically" growth-restricted***

The placenta is a transient organ that forms during pregnancy and is unique in that it grows in parallel with the developing embryo, sharing several pathways[36]. Therefore, we measured the weights of the liver and brain in E15.5 embryos to examine whether organogenesis was differentially affected by placental dysfunctions. A comparison of liver and organ weights demonstrated that liver development was severely compromised in *CdGAP* $^{KI/KI}$ (severe) embryos. Interestingly, while the gross morphologies and weights of *CdGAP* $^{KI/KI}$ (moderate) embryos and their matching placentas were comparable to those of *CdGAP* $^{WT/WT}$ embryos at E15.5 (Figure 3.3B, D), the liver-to-fetal weight ratio was significantly reduced in *CdGAP* $^{KI/KI}$ (moderate) embryos, albeit to a much lesser degree than in *CdGAP* $^{KI/KI}$ (severe) embryos. However, neither the normalized liver weight nor the liver-to-fetal weight ratio significantly differed in *CdGAP* $^{WT/KI}$ embryos. Most notably, unlike the liver, overall brain development in mutant embryos appeared unaffected (Supplementary Figure 3B, C).

We next investigated whether organogenesis differed between male and female embryos at E15.5. This analysis further indicated that the development of fetal livers was not differentially affected between males and females, although liver development in *CdGAP* $^{KI/KI}$ (severe) embryos was severely compromised (Supplementary Figure 3D). However, when considering sex-specific differences, brain development was found to be differentially affected between male and female *CdGAP* $^{KI/KI}$ (severe) embryos, with the effects being strictly observed in male embryos (Supplementary Figure 3E). Interestingly, a comparison of liver-to-fetal weight ratios showed that relative liver growth was significantly more impaired in male *CdGAP* $^{KI/KI}$ (severe) embryos (Supplementary Figure 3F). Most significantly, in alignment with trends towards reduced placental efficiency in male *CdGAP* $^{KI/KI}$ (severe) embryos (Supplementary Figure 2A), the brain-to-liver-weight ratio, widely accepted as a marker for "asymmetric" growth restriction[37], was significantly increased specifically in male *CdGAP* $^{KI/KI}$ (severe) embryos (Supplementary Figure 3G). Together, the development of organs, such as the liver and brain, was differentially affected between E15.5 male and female embryos (Supplementary Figure 3H). Most significantly, liver development was more severely compromised in male *CdGAP* $^{KI/KI}$ (severe) embryos, further underscoring the asymmetric growth restriction in *CdGAP* $^{KI/KI}$ embryos.

***Placental dysfunctions are further associated with congenital heart defects in E15.5 CdGAP*** $^{KI/KI}$ ***embryos***

As E15.5 male *CdGAP* $^{KI/KI}$ (severe) embryos exhibited asymmetric growth restriction, with notably compromised liver development (Supplementary Figure 3G), we hypothesized that placental dysfunctions observed in *CdGAP* $^{KI/KI}$ (severe) placentas could also contribute to the pathogenesis of congenital heart defects (Figure 3.7A). Congenital heart defects comprise minor diagnostic criteria for AOS and affect approximately 20% of AOS patients[5]. We first examined CdGAP expression levels in mouse developing cardiomyocytes and whole hearts using a web interface built upon transcriptomic analyses of cardiomyocytes and proteomic analyses of whole heart lysates[38]. This analysis illustrated that *ARHGAP31* expression in mouse cardiomyocytes significantly increased from E14.5 to E16.5, peaking at E18.5. A similar trend was observed at the protein levels (Figure 3.7B).

Recently, placental defects have been identified as a common cause for congenital heart defects, which may begin to manifest at E14.5[32], coinciding with the peak period of feto-maternal exchanges occurring in the labyrinth[23]. Thus, to assess whether the placental dysfunctions observed in *CdGAP* $^{KI/KI}$ (severe) embryos during late gestation could also contribute to the pathogenesis of congenital heart defects, we analyzed serial sections of E15.5 embryos from the rostral-caudal axis. Histological analyses revealed significant structural changes in the hearts of *CdGAP* $^{KI/KI}$ (severe) embryos, including a reduced compact zone thickness and poor development of the interventricular septum, which separates the left and right ventricles compared to of *CdGAP* $^{WT/WT}$ embryos (Figure 3.7O - Q compared to Figure 3.7E - G and Figure 3.7R). Importantly, these changes were closely associated with placental dysfunctions, including a pale and poorly vascularized placenta (Figure 3.7M, N compared to Figure 3.7C, D). In contrast, despite the absence of dramatic structural changes in the hearts of *CdGAP* $^{KI/KI}$ (moderate) embryos (Figure 3.7J - L), the thickness of the compact zone was significantly reduced not only in *CdGAP* $^{KI/KI}$ (severe) but also in *CdGAP* $^{KI/KI}$ (moderate) embryos from both ventricles (Figure 3.7R). More importantly, the reduced compact zone thickness was inversely correlated with a trend toward increased trabeculae thickness (Figure 3.7R). In fact, the ratio between trabeculae and compact zone thickness was significantly increased in the right ventricle of *CdGAP* $^{KI/KI}$ (severe) embryos, along with a trend towards an increase in the left ventricle. Interestingly, similar trends indicative of reduced myocardial compaction were seen in both ventricles of *CdGAP* $^{KI/KI}$ (moderate) embryos (Figure 3.7S).

To provide insights into how cardiovascular functions might be affected in the long-term in "surviving" *CdGAP* $^{KI/KI}$ embryos, we further compared the thickness of the interventricular septum, a reduction or thinning of which has been shown to increase cardiovascular risks in humans[39]. Consistent with the reduced thickness of the compact zone from both ventricles (Figure 3.7R), the interventricular septum was significantly thinner in *CdGAP* $^{KI/KI}$ (moderate) embryos (Figure 3.7T). Despite this thinning, there were no apparent changes in the gross morphology of the embryo and the placenta (Figure 3.7H, I compared to Figure 3.7C, D), and no apparent structural abnormalities were observed (Figure 3.7J). In conclusion, our findings suggest that severe labyrinth defects (i.e., disorganized syncytium) as well as physiological changes, which do not result in apparent gross morphological changes but can still cause

placental dysfunction and thus hinder rapid fetal growth, may contribute to the pathogenesis of congenital heart defects in *CdGAP* $^{KI/KI}$ embryos during late gestation.

***Organization and the development of the labyrinth are specifically affected in CdGAP*** $^{KI/KI}$ ***placentas at E12.5***

To address whether the development of the labyrinth was affected at earlier stages of gestation, we compared the area of each placental layer comprising the definitive placenta: decidua, the junctional zone, and the labyrinth[23], at E12.5, across genotypes. In contrast to late gestation, due to the lack of visible gross morphological abnormalities in embryos and their placentas, *CdGAP* $^{KI/KI}$ placentas at E12.5 were not further categorized. Nevertheless, histological analyses revealed reduced vascular complexity with enlarged vascular spaces in the labyrinth in *CdGAP* $^{KI/KI}$ placentas (Supplementary Figure 4A; yellow arrows). The total placental area across genotypes was comparable at E12.5. However, the area of the labyrinth, but not the junctional zone or the decidua, was significantly reduced in E12.5 *CdGAP* $^{KI/KI}$ placentas compared to wild type embryos (Supplementary Figure 4B). Interestingly, unlike at late gestation (Supplementary Figure 3A), the relative area of the labyrinth was significantly reduced in E12.5 *CdGAP* $^{KI/KI}$ placentas, further highlighting that the growth of the labyrinth was specifically affected (Supplementary Figure 4C). No significant differences in the total placentas or the labyrinth areas between male and female embryos were observed (Supplementary Figure 4D). Moreover, junctional zone areas and the area of the decidua did not significantly differ between male and female embryos (Supplementary Figure 4E). Likewise, the labyrinth-to-the-junctional zone area ratio was comparable across genotypes and between both sexes (Supplementary Figure 4F). As well, the labyrinth thickness did not significantly differ across genotypes and between both sexes at E12.5 (Supplementary Figure 4G). Taken together, these data demonstrate that labyrinth defects were present upon the establishment of the definitive placenta by E12.5, which progressively worsened throughout gestation.

***CdGAP is expressed in the labyrinth region of the placentas during early development and E12.5 CdGAP*** $^{KI/KI}$ ***placentas show labyrinth defects***

To determine whether CdGAP is expressed in specific regions of the placenta during development, we examined the dataset from Marsh *et al* (2020), in which expression profiles in

developing placentas were analyzed by single-cell RNA-sequencing[22]. This revealed that *ARHGAP31* was enriched in various cell types of the developing placenta, including SynT-I and SynT-II, whose expression continued to increase between E9.5 and E14.5 (Figure 3.8A; red and green arrows denote SynT-I and SynT-II). We then validated the expression of *ARHGAP31* through RNAscope, which showed high expression in the labyrinth of E12.5 placentas (Figure 3.8B). We next examined the organization of vascular networks within the labyrinth between *CdGAP* $^{WT/WT}$ and *CdGAP* $^{KI/KI}$ placentas at E12.5. In line with a significant reduction in the labyrinth area (Figure 3.8D compared to Figure 3.8C; Supplementary Figure 4B), the organization of the vascular networks in *CdGAP* $^{KI/KI}$ placentas differed from that in *CdGAP* $^{WT/WT}$ placentas (Figure 3.8G compared to Figure 3.8E), showing a specific reduction in the contact surfaces between fetal blood spaces and maternal sinusoids in the labyrinth of *CdGAP* $^{KI/KI}$ placentas (Figure 3.8H compared to Figure 3.8F; white arrowheads).

We then compared the labyrinth occupancy by fetal blood spaces and maternal sinusoids between genotypes and sexes. This analysis revealed that labyrinth occupancy by fetal blood spaces, but not by maternal sinusoids, was significantly reduced in male *CdGAP* $^{KI/KI}$ placentas (Figures 3.8I, J). Occupancy by maternal sinusoids significantly differed between sexes, where a trend towards an inversely correlated increase was observed in male *CdGAP* $^{KI/KI}$ placentas (Figures 3.8I, J). Collectively, these data demonstrate that CdGAP is highly expressed in the labyrinth region during placenta development and that the C-terminus of CdGAP is required for the proper development of the vascular complexity in the labyrinth, leading to efficient feto-maternal exchanges.

## Discussion

*ARHGAP31*, encoding CdGAP, is one of the six genes found associated with Adams-Oliver syndrome, a rare familial disease[4]. Wide spectrum of how CdGAP may affect human lives therefore necessitates the need to understand the role of CdGAP beyond its pro-oncogenic roles in breast and prostate tumorigenesis[11, 40, 41]. Whereas several mutations in the *ARHGAP31* gene have been found associated with AOS, due to variable phenotypic expressivity, p.Gln683X mutation, which led to clinical manifestations of both transverse terminal limb defects and aplasia cutis congenita, two phenotypes used as the major diagnosis criteria for AOS[2, 3, 8], have been chosen to create a mouse model for AOS (CdGAP-P670X) using a CRISPR/Cas9 strategy.

Incompletely penetrant embryonic lethality was apparent with significant changes in the genotypic distribution of *CdGAP* $^{KI/KI}$ adult mice (~10% vs 25%), which was positively correlated with elevated frequency of embryonic abnormalities including pale liver and edema. Attributable to incomplete penetrance as well as largely variable phenotypic expressivity among affected individuals, a wide spectrum of abnormalities, including congenital heart defects and pregnancy-associated complications (i.e., intrauterine growth restriction) have been further reported. Interestingly, whereas several findings were indicative of placental dysfunction as a plausible pathogenic origin of AOS[42, 43], in support of the original postulation by Fryns and Hoyme[6, 7], which may further underlie the pathogenesis of congenital heart defects seen among 20% of AOS patients[5], research efforts were significantly deficient. Therefore, how truncating mutation of CdGAP affects the development of the placenta and exerts an effect on developing embryos was investigated in this study.

In this study, we found that defects in placental development were associated with incompletely penetrant embryonic lethality seen among *CdGAP* $^{KI/KI}$ embryos. Indeed, vascular complexity as well as blood-filled spaces in the labyrinth of *CdGAP* $^{KI/KI}$ (severe) placentas were significantly reduced, despite pronouncedly enlarged vascular spaces. Additionally, while cellular atrophy and increased non-membranous expression of MCT1 and MCT4 lactate transporters were found in the labyrinth of *CdGAP* $^{KI/KI}$ (severe) placentas, where the fusion between syncytiotrophoblast (SynT) layers were defective, defects in placental angiogenesis did not further underlie placental dysfunctions attributable to labyrinth defects. In fact, despite sparse fetal blood spaces, which were enlarged in size, the lining of fetal blood spaces by fetal endothelial cells was comparable to wild-type placentas. Most importantly, compromised

labyrinth function resulted in embryonic defects including asymmetric fetal growth restriction, with increased severity in the development of the liver and heart of E15.5 *CdGAP* $^{KI/KI}$ (severe) embryos. Although embryonic abnormalities reported in our study were apparent at late stages (> E15.5), vascular network organization was significantly altered at E12.5, where the "definitive" placenta completes its construction. Moreover, this change was further associated with reduced contact surfaces between fetal blood spaces and maternal sinusoids among male *CdGAP* $^{KI/KI}$ embryos. Feto-maternal exchanges might have been further compromised by the remarkable increase in interhaemal membrane thickness, which was apparent among *CdGAP* $^{KI/KI}$ (severe) placentas at E15.5, which further coincided with the manifestation of cardiac abnormalities, including increased myocardial non-compaction. While placenta sex-associated dimorphism was not observable from gross morphological analyses, specific evidence such as a noticeably smaller number of severely affected male *CdGAP* $^{KI/KI}$ embryos found at E18.5 and reduced occupancy of the labyrinth by fetal blood spaces, only among male *CdGAP* $^{KI/KI}$ placentas at E12.5, led us to speculate on an evolutionary perspective. Historically, evolutionary changes have driven males to prioritize rapid growth[44], thereby increasing their dependency on the placenta, and this adaptation may explain why male embryos are affected at an earlier stage of development.

In summary, our findings revealed labyrinth defects, attributable to defective organization of the syncytium, whose development is crucial for efficient feto-maternal exchanges[30, 31], were underlying incompletely penetrant embryonic lethality seen in *CdGAP* $^{KI/KI}$ embryos. However, as SynTs are constantly replaced throughout gestation as they get damaged from shear forces of blood transports, whether fusogenic defects were due to reduced proliferation of its progenitor, cytotrophoblasts, or due to accelerated cell death of SynTs, remains yet to be determined. Although further investigations are required, an increasing population of red blood cells, which were deep-purple in color, indicative of deficient circulation or poor oxygenation, were observed in E18.5 *CdGAP* $^{KI/KI}$ (severe) placentas, in support of the possibility that *CdGAP* $^{KI/KI}$ (severe) placentas during late gestation were poorly perfused. Besides, expression of E-cadherin was significantly reduced in E15.5 *CdGAP* $^{KI/KI}$ placentas, which might not only underlie fusogenic defects but also accelerated the loss of SynTs. In conclusion, we hereby present evidence in support of the prenatal origin of AOS, attributable to placental dysfunctions and defective syncytial fusion with a concomitant increase in interhaemal membrane thickness in placentas

with homozygous P670X truncating mutation of CdGAP. This results in compromised feto-maternal exchanges, leading to poor congenital heart developments and cardiac abnormalities.

## Acknowledgments

We thank Mr. Mathieu Simard at the Small Animal Imaging Labs (SAIL) of the Research Institute of the McGill University Health Centre (RI-MUHC) for their assistance and help with the image acquisition. We thank the Histopathology platform of the RI-MUHC for assistance with the slide scanning and technical advice. We also thank Ms. Audrey Lamoureux and Ms. Diane Kim for providing training for a rotary microtome. J.-H.C. was supported by studentships from the RI-MUHC.

D.P.L is a Lewis Katz – Young Investigator of the Prostate Cancer Foundation and is also a Research Scholar – Junior 1 from FRQS. This research was supported by a Heart and Stroke Foundation grant to N. L.V. and Canadian Institutes of Health Research (CIHR) project grants (PJT-153151) to N.L.V.

**Author contributions**

**Conception and design:** J.-H. Chung, Y. He, and N. Lamarche-Vane. **Acquisition of data:** J.-H. Chung. **Analysis and interpretation of data:** J.-H. Chung, Y. He, S. Shafei, B. Meehan, N. Boufaied, DP. Labbé, D. Dufort, N. Lamarche-Vane. **Writing, review, and/or revision of the manuscript:** J.-H. Chung and N. Lamarche-Vane.

**Competing interests**

The authors declare no competing interests.

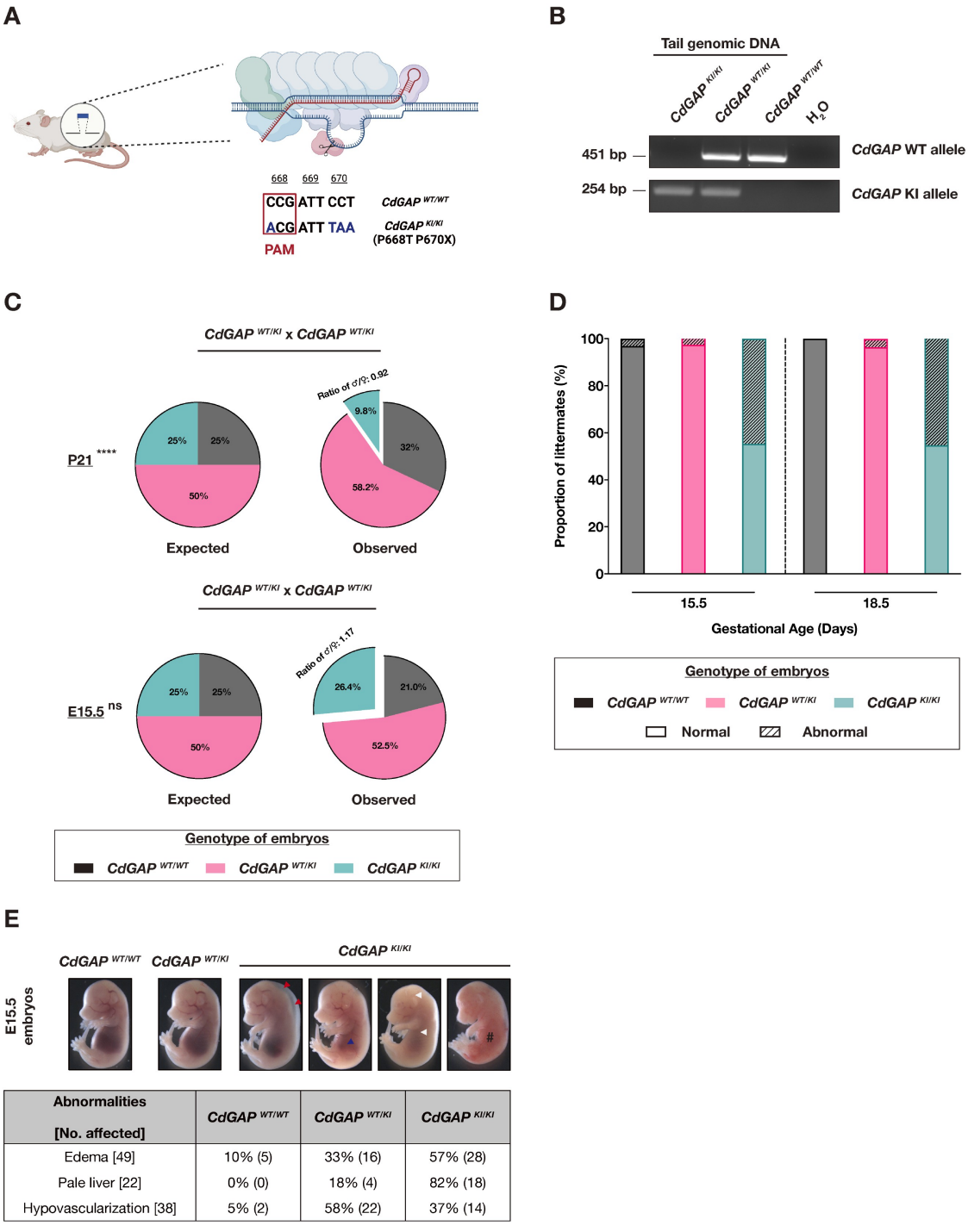


| Abnormalities [No. affected] | CdGAP WT/WT | CdGAP WT/KI | CdGAP KI/KI |
|---|---|---|---|
| Edema [49] | 10% (5) | 33% (16) | 57% (28) |
| Pale liver [22] | 0% (0) | 18% (4) | 82% (18) |
| Hypovascularization [38] | 5% (2) | 58% (22) | 37% (14) |

**Figure 3.1: P670X truncating mutation in CdGAP leads in incompletely penetrant embryonic lethality.**

(A) Schematic diagram illustrates how CdGAP-AOS KI mouse model was created by CRISPR-Cas9 strategy.

(B) Agarose gel-resolved PCR amplicons using WT or KI mutation-specific primers are shown. While only WT or mutation-specific amplicons, with amplicon sizes of 451 bp and 254 bp, were observed in *CdGAP* $^{WT/WT}$ and *CdGAP* $^{KI/KI}$ pups, both amplicons were observed in *CdGAP* $^{WT/KI}$ pups.

(C) Graphic illustrations of the observed genotype distribution at weaning (P21) and at E15.5 are shown, compared against the expected distribution. The notion in superscripts indicates statistical significance. *Chi-square* tests were used to assess the significance for E15.5 and P21, respectively (ns: no significance, ****: $p < 0.0001$).

The number of pups from each genotype at P21 was as the following: *CdGAP* $^{WT/WT}$: 320, *CdGAP* $^{WT/KI}$: 582, *CdGAP* $^{KI/KI}$: 98. At E15.5, the following number of embryos was observed: *CdGAP* $^{WT/WT}$: 62, *CdGAP* $^{WT/KI}$: 155, and *CdGAP* $^{KI/KI}$: 78.

(D) Summary of gross abnormalities across different genotypes of embryos at E15.5 and at E18.5, gestational ages representative of late gestation. The gross morphology of each embryo was noted blindly, prior to genotyping. A notable population (> 40%) of *CdGAP* $^{KI/KI}$ embryos was abnormal.

(E) Phenotypic characterization of E15.5 embryos is presented, using the stereomicroscope. The characterization was conducted blindly, prior to genotyping. Several embryonic abnormalities were observed including edema, seen behind the head and along the spine (red arrowhead), a pale or poorly developed liver (blue arrowhead), and hypovascularization of superficial vessels (white arrowhead). Frequently, embryos exhibiting several abnormalities were observed, and these abnormalities were strongly pronounced (#).

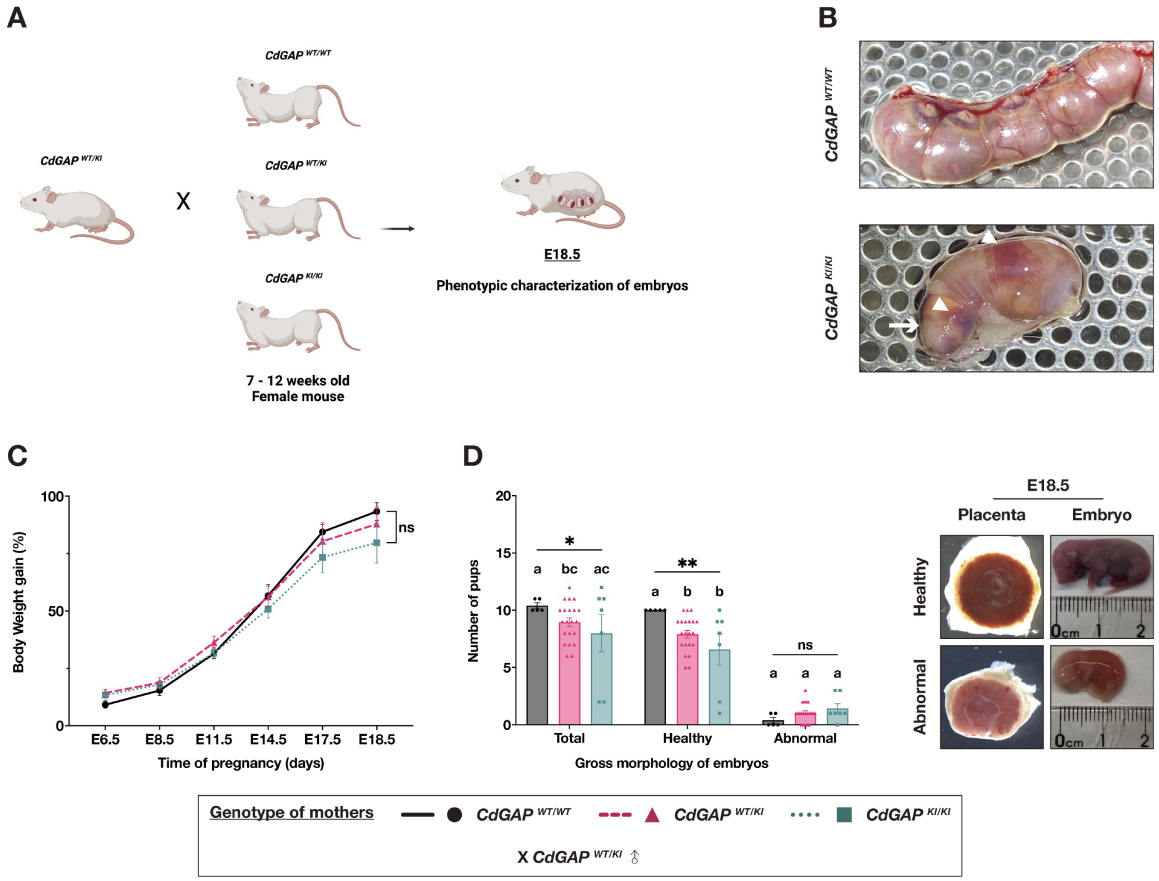
A
CdGAP WT/WT
CdGAP WT/KI
X
CdGAP WT/KI
CdGAP KI/KI
7 - 12 weeks old
Female mouse
E18.5
Phenotypic characterization of embryos
B
CdGAP WT/WT
CdGAP KI/KI
C
Body Weight gain (%)
100
50
0
ns
E6.5
E8.5
E11.5
E14.5
E17.5
E18.5
Time of pregnancy (days)
D
Number of pups
20
15
10
5
0
*
a
bc
ac
**
a
b
b
ns
a
a
a
Total
Healthy
Abnormal
Gross morphology of embryos
E18.5
Placenta
Embryo
Healthy
Abnormal
0cm
1
2
Genotype of mothers
CdGAP WT/WT
CdGAP WT/KI
CdGAP KI/KI
X CdGAP WT/KI
E
Genotype of embryos
kDa
CdGAP WT/WT
CdGAP WT/KI
CdGAP KI/KI
250
CdGAP (full-length)
95
CdGAP (truncated form)
55
Tubulin
Genotype of embryos
CdGAP WT/WT
CdGAP WT/KI
CdGAP KI/KI
E18.5
Placenta

**Figure 3.2: The P670X mutation in CdGAP mice leads to placental dysfunction.**

(A) Schematic diagram illustrates the mating of female mice with stud *CdGAP* $^{WT/KI}$ males for phenotypic characterization of embryos and their placentas at E18.5.

(B) Representative images of embryonic sacs from wild type and *CdGAP* $^{KI/KI}$ mothers at E18.5 are shown. Compared to embryonic sacs from a wild type mother, those from a *CdGAP* $^{KI/KI}$ mother appear hemorrhagic (indicated by the white arrowhead). Additionally, the sizes of the embryonic sacs are uneven and significantly reduced (denoted by the white arrow).

(C) Changes in body weight gain among pregnant mothers of different genotypes are illustrated. Body weight gain was measured relative to the starting body weight of a virgin female mouse. The average weight gain is plotted for *CdGAP* $^{WT/WT}$ (n = 5), *CdGAP* $^{WT/KI}$ (n = 4), and *CdGAP* $^{KI/KI}$ (n= 7). Variations in body weight gain across genotypes were analyzed using one-way ANOVA at each gestational age.

(D) Comparison of the total, healthy, or abnormal embryo count at E18.5 from different genotypes of pregnant mothers is presented. Embryos were categorized as healthy or abnormal based on the gross morphology, and any co-occurrence of embryonic abnormalities and placental morphological changes, such as paleness and reduced vascularity, marked an embryo as abnormal. Welch's one-way ANOVA followed by Dunnett's T3 multiple comparison tests were used for the total embryo count across genotypes. For healthy or abnormal embryo counts, the Kruskal-Wallis test followed by Dunn's multiple comparison test and ordinary one-way ANOVA with Tukey's multiple comparison tests were respectively applied. Horizontal lines represent significance across genotypes, while different letters indicate significance between genotypes for each comparison.

(E) Immunoblot of whole placenta lysate (E18.5) shows the detection of both full-length and truncated forms of CdGAP using two different antibodies. Weak signals for the truncated and full-length CdGAP are observed in *CdGAP* $^{WT/WT}$ and *CdGAP* $^{KI/KI}$ placentas; these signals originate from the maternal placental tissue. Tubulin is used as a loading control. Beside the immunoblot, representative photographs of placentas from each genotype are shown, displaying noticeable changes in the gross morphology of the placenta (pale placenta) in *CdGAP* $^{KI/KI}$ embryos.

For panels (C and D), data are presented as mean ± SEM (ns: no significance, *: $p < 0.05$, **: $p < 0.01$).

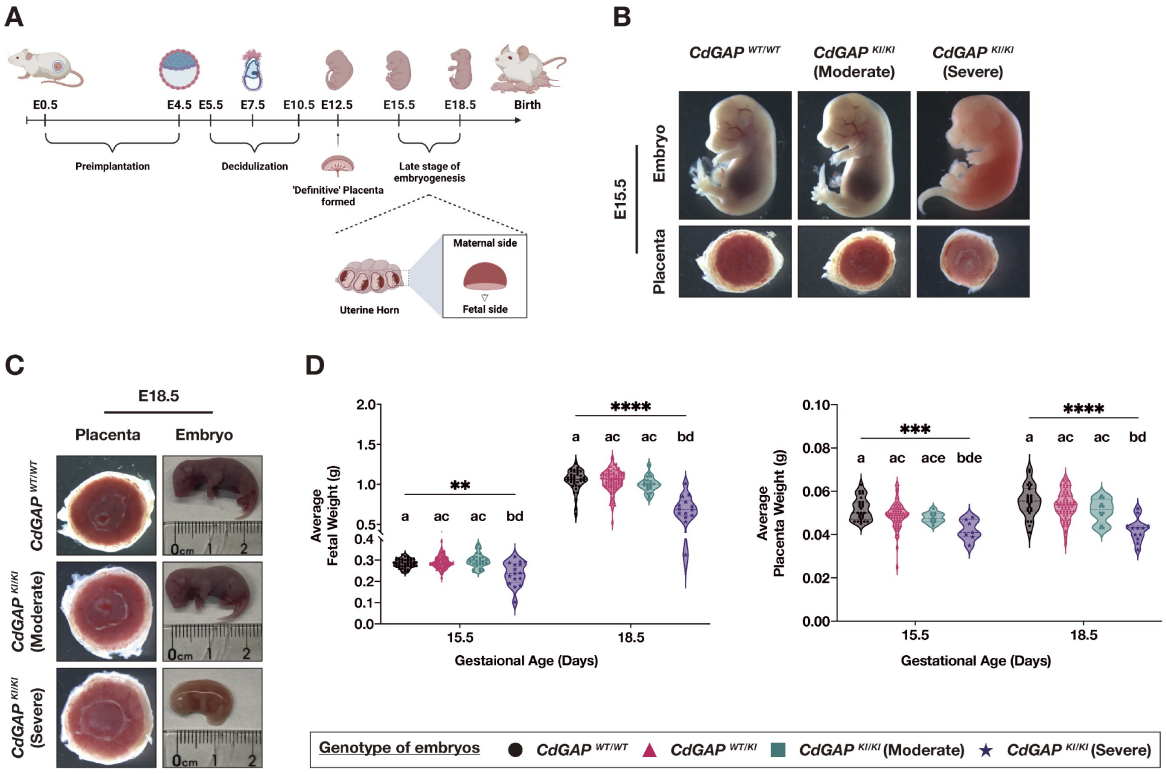
A
E0.5
E4.5
E5.5
E7.5
E10.5
E12.5
E15.5
E18.5
Birth
Preimplantation
Decidulization
Late stage of embryogenesis
'Definitive' Placenta formed
Maternal side
Fetal side
Uterine Horn
B
CdGAP WT/WT
CdGAP KI/KI (Moderate)
CdGAP KI/KI (Severe)
E15.5
Embryo
Placenta
C
E18.5
Placenta
Embryo
CdGAP WT/WT
CdGAP KI/KI (Moderate)
CdGAP KI/KI (Severe)
D
Average Fetal Weight (g)
Gestaional Age (Days)
Average Placenta Weight (g)
Gestational Age (Days)
Genotype of embryos
CdGAP WT/WT
CdGAP WT/KI
CdGAP KI/KI (Moderate)
CdGAP KI/KI (Severe)
E
E15.5
E18.5
% of population
Fetal Weight (g)
F
Average Fetal Weight (g)
Gestational Age (Days)
Genotype of embryos
CdGAP WT/WT
CdGAP WT/KI
CdGAP KI/KI (Moderate)
CdGAP KI/KI (Severe)
G
Fetal/Placenta (Weight)
Gestational Age (Days)
H
Fetal Weight (g)
Placenta Weight (g)
Genotype of embryos
CdGAP WT/WT
CdGAP WT/KI
CdGAP KI/KI (Moderate)
CdGAP KI/KI (Severe)

**Figure 3.3: Male *CdGAP* $^{KI/KI}$ embryos with placental dysfunction were severely growth-restricted during late gestation.**

(A) The schematic diagram illustrates mouse gestation, with a detailed graphic below that represents the observational plane used for the phenotypic characterization of placentas during late gestation (> E15.5.).

(B and C) Representative images of embryos and corresponding placentas at E15.5 and at E18.5 are shown, focusing on the fetal side of each placenta.

(D) Comparisons of average fetal and placental weights are shown. For fetal weight comparisons at E15.5, the numbers of embryos were: *CdGAP* $^{WT/WT}$ = 44, *CdGAP* $^{WT/KI}$ = 115, *CdGAP* $^{KI/KI}$ (moderate) = 29, *CdGAP* $^{KI/KI}$ (severe) = 16. At E18.5, the numbers were: *CdGAP* $^{WT/WT}$ = 36, *CdGAP* $^{WT/KI}$ = 97, *CdGAP* $^{KI/KI}$ (moderate) = 21, *CdGAP* $^{KI/KI}$ (severe) = 14. For placental weight comparisons at E15.5, the numbers of embryos were: *CdGAP* $^{WT/WT}$ = 27, *CdGAP* $^{WT/KI}$ = 71, *CdGAP* $^{KI/KI}$ (moderate) = 12, *CdGAP* $^{KI/KI}$ (severe) = 7. At E18.5, the numbers were: *CdGAP* $^{WT/WT}$ = 26, *CdGAP* $^{WT/KI}$ = 69, *CdGAP* $^{KI/KI}$ (moderate) = 12, *CdGAP* $^{KI/KI}$ (severe) = 12. Ordinary one-way ANOVA followed by Tukey's multiple comparisons tests were used for each comparison, except for the comparison of E15.5 placental weights, where Welch's ANOVA followed by Dunnett's T3 multiple comparisons test was used.

(E) A non-linear regression fit illustrates the distribution of embryos' body weights across genotypes. Solid vertical lines mark the 5$^{th}$ percentile of *CdGAP* $^{WT/WT}$ embryos' body weight at each gestational age.

(F) Changes in the average fetal weight of embryos across genotypes during late gestation are shown. The number of embryos at different gestational ages was as follows: E15.5: *CdGAP* $^{WT/WT}$ = 44 *CdGAP* $^{WT/KI}$ = 115, *CdGAP* $^{KI/KI}$ (moderate) = 29, *CdGAP* $^{KI/KI}$ (severe) = 16; E16.5: *CdGAP* $^{WT/WT}$ = 5 *CdGAP* $^{WT/KI}$ = 6, *CdGAP* $^{KI/KI}$ (moderate) = 5, *CdGAP* $^{KI/KI}$ (severe) = 4; E17.5: *CdGAP* $^{WT/WT}$ = 4 *CdGAP* $^{WT/KI}$ = 12, *CdGAP* $^{KI/KI}$ (moderate) = 7, *CdGAP* $^{KI/KI}$ (severe) = 4; E18.5: *CdGAP* $^{WT/WT}$ = 36, *CdGAP* $^{WT/KI}$ = 97, *CdGAP* $^{KI/KI}$ (moderate) = 21, *CdGAP* $^{KI/KI}$ (severe) = 14. For comparisons at all gestational ages, ordinary one-way ANOVA was utilized, except for E15.5, where Welch's ANOVA was applied. At all gestational ages, fetal weights significantly differ across genotypes.

(G) Comparison of average placental efficiency (defined as fetal/placental weight ratio) across genotypes is shown. Welch's ANOVA followed by Dunnett's T3 multiple comparisons test was conducted at both gestational ages.

(H) A correlation plot of fetal and placental weight at E18.5 across genotypes is displayed. Data are presented as mean ± SEM, except in panels (E) and (H) (*: $p < 0.05$, **: $p < 0.01$, ****: $p < 0.0001$). For panels (D and G), horizontal lines in each panel denote significance across genotypes, while different letters indicate significance between genotypes for each comparison.

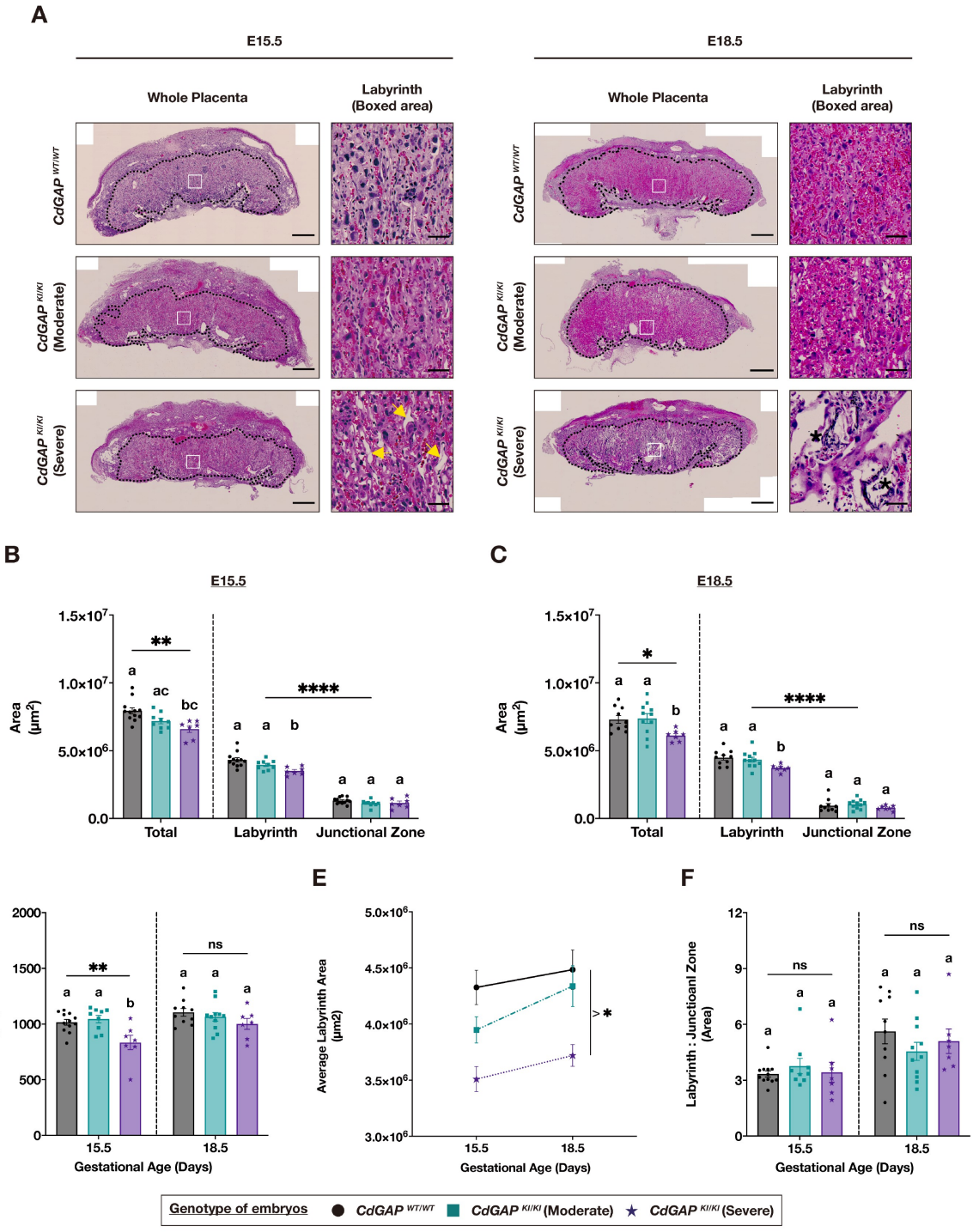
A
E15.5
E18.5
Whole Placenta
Labyrinth (Boxed area)
CdGAP WT/WT
CdGAP KI/KI (Moderate)
CdGAP KI/KI (Severe)
B
E15.5
Area (µm²)
1.5x10⁷
1.0x10⁷
5.0x10⁶
0.0
**
****
a
ac
bc
a
a
b
a
a
a
Total
Labyrinth
Junctional Zone
C
E18.5
*
****
Total
Labyrinth
Junctional Zone
D
Labyrinth thickness (µm)
2000
1500
1000
500
0
**
ns
15.5
18.5
Gestational Age (Days)
E
Average Labyrinth Area (µm2)
5.0x10⁶
4.5x10⁶
4.0x10⁶
3.5x10⁶
3.0x10⁶
> *
F
Labyrinth : Junctioanl Zone (Area)
12
9
6
3
0
Genotype of embryos
CdGAP WT/WT
CdGAP KI/KI (Moderate)
CdGAP KI/KI (Severe)

**Figure 3.4: Reduced vascular complexity as well as the expansion of the labyrinth underlie placental dysfunction among *CdGAP* $^{KI/KI}$ (severe) placentas.**

(A) Representative cross-sections of E15.5 and E18.5 placentas from different genotypes, stained with H&E, are shown. The labyrinth is outlined (dashed line), and abnormal features in E15.5 or E18.5 *CdGAP* $^{KI/KI}$ (severe) placentas are indicated (yellow arrows for vacant vascular spaces, asterisks for cellular atrophies). Scale bar: 200 μm (whole placenta), 50 μm (boxed area).

(B and C) Total placental area or area of placental layers (labyrinth, junctional zone) from H&E stained sections at E15.5 or E18.5 is quantified. Differences in the total placental area across genotypes were assessed by ordinary one-way ANOVA followed by Tukey's multiple comparison tests. For each gestational age, two-way ANOVA was utilized to examine differences by placental layer. Subsequently, Tukey's multiple comparisons tests were applied to evaluate differences between genotypes for each placental layer.

(D) The average labyrinth thickness across genotypes at E15.5 and at E18.5 is compared. An ordinary one-way ANOVA followed by Tukey's multiple comparison tests was used at each gestational age to compare between genotypes.

(E) Changes in the average labyrinth area across genotypes from E15.5 to E18.5 are shown, analyzed similarly to the methods described in (D).

(F) The average ratio between the labyrinth and the junctional zone area across genotypes at E15.5 and at E18.5 is compared, following a similar method as described in (D).

Data are presented as mean ± SEM (*: $p < 0.05$, **: $p < 0.01$, ****: $p < 0.0001$). At E15.5, the numbers of placentas were as follows: *CdGAP* $^{WT/WT}$ = 12, *CdGAP* $^{KI/KI}$ (moderate) = 9, *CdGAP* $^{KI/KI}$ (severe) = 7. At E18.5, the numbers were: *CdGAP* $^{WT/WT}$ = 10, *CdGAP* $^{KI/KI}$ (moderate) = 11, *CdGAP* $^{KI/KI}$ (severe) = 7.

For panels (B) to (F), when one-way ANOVA was performed, lines above or beside represent significance across genotypes, while different letters denote significance between genotypes for each comparison. In the two-way ANOVA performed for (B and C), the horizontal line in each panel indicates significance due to the row factor (placental layer), while different letters denote significance between genotypes for each placental layer.

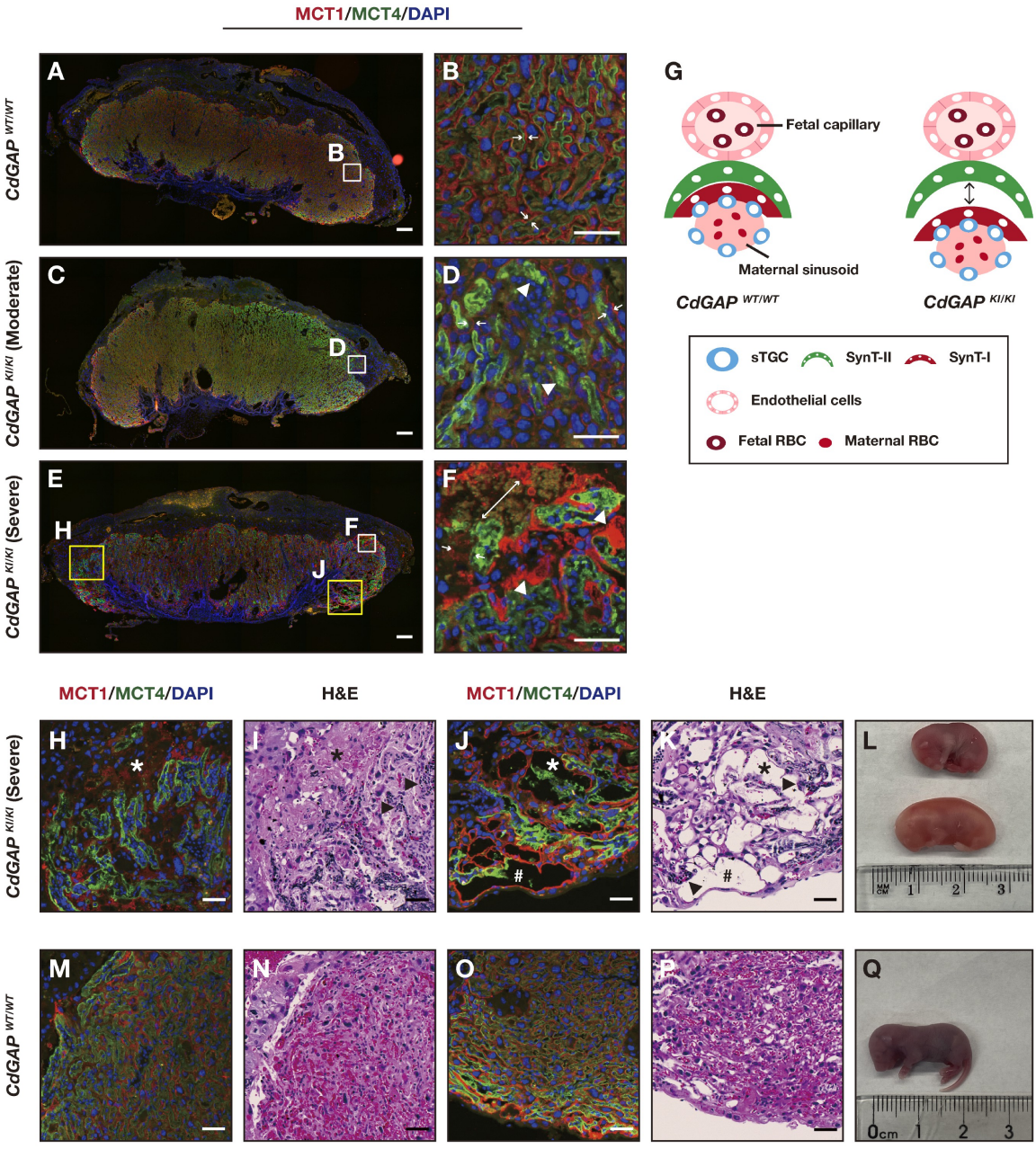
MCT1/MCT4/DAPI
CdGAP WT/WT
CdGAP KI/KI (Moderate)
CdGAP KI/KI (Severe)
A
B
C
D
E
F
H
J
G
Fetal capillary
Maternal sinusoid
CdGAP WT/WT
CdGAP KI/KI
sTGC
SynT-II
SynT-I
Endothelial cells
Fetal RBC
Maternal RBC
MCT1/MCT4/DAPI
H&E
MCT1/MCT4/DAPI
H&E
CdGAP KI/KI (Severe)
CdGAP WT/WT
H
I
J
K
L
M
N
O
P
Q
0cm 1 2 3

**Figure 3.5: *CdGAP* $^{KI/KI}$ placentas demonstrate a disorganized syncytium.**

(A - F) Representative images of E18.5 placenta sections are shown, fluorescently stained for SynT-I (MCT1$^{+}$; red) and SynT-II (MCT4$^{+}$; green). The images include both whole and magnified views (indicated by white boxes in A, C, and E) of the labyrinth. Nuclei are visualized with DAPI staining (blue). The apposition of SynT layers is highlighted by white arrows, while areas showing defective syncytial fusion are marked by white arrowheads. The scale bar corresponds to 200 μm for the whole view and 50 μm for the magnified view. At least three samples were examined for each genotype.

(G) Schematic diagram of SynT layer organization. The loss of tight apposition is highlighted by the black arrow. The white circle in each cell type represents the nucleus.

(H - K) Representative images of peripheral tissue damage in E18.5 *CdGAP* $^{KI/KI}$ (severe) placentas are shown. H&E staining of corresponding regions of affected areas is provided for histological comparisons. Characteristic changes, such as cellular atrophy (marked by an asterisk), poorly oxygenated red blood cells (identified by black arrowheads), and enlarged vascular spaces (denoted by #), are emphasized. Their relative positions within the whole placenta are indicated by yellow boxes in (C). The scale bar represents 50 μm.

(L) Representative images show lethal E18.5 *CdGAP* $^{KI/KI}$ (severe) embryos with severe placental defects.

(M - P) Corresponding regions to those shown in (H – K) are presented in E18.5 *CdGAP* $^{WT/WT}$ placentas. The scale bar corresponds to 50 μm.

(Q) Representative images of *CdGAP* $^{WT/WT}$ embryos at E18.5 are shown.

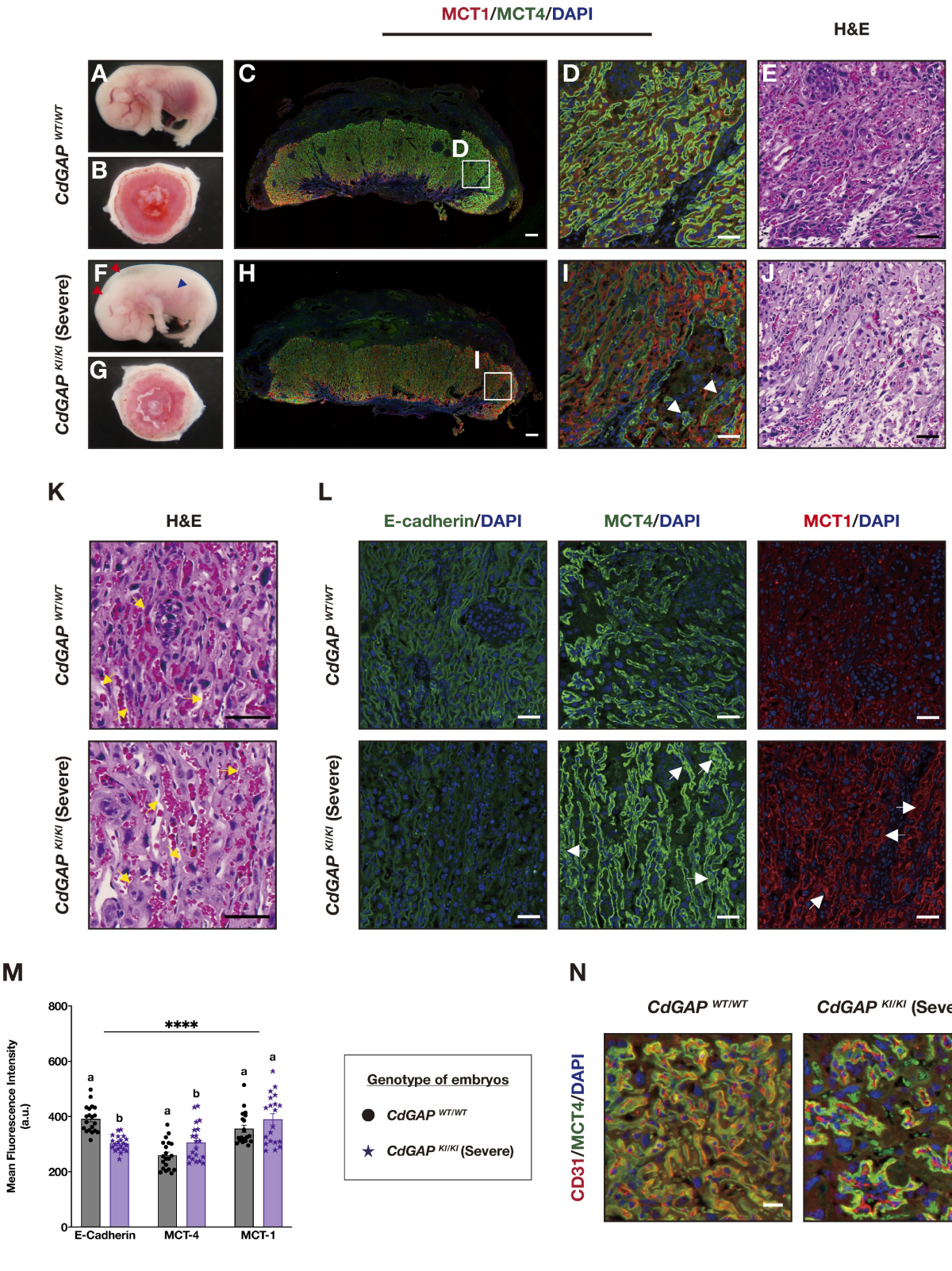
MCT1/MCT4/DAPI
H&E
CdGAP WT/WT
CdGAP KI/KI (Severe)
A
B
C
D
E
F
G
H
I
J
K
H&E
L
E-cadherin/DAPI
MCT4/DAPI
MCT1/DAPI
M
Mean Fluorescence Intensity (a.u.)
800
600
400
200
0
****
a
b
a
b
a
a
E-Cadherin
MCT-4
MCT-1
Genotype of embryos
CdGAP WT/WT
CdGAP KI/KI (Severe)
N
CdGAP WT/WT
CdGAP KI/KI (Severe)
CD31/MCT4/DAPI

**Figure 3.6: Defective organization of syncytium, but not placental angiogenesis is associated with labyrinth defects in E15.5 *CdGAP* $^{KI/KI}$ placentas.**

(A - J) Representative images of E15.5 placenta sections, fluorescently stained for SynT-I (MCT1$^{+}$; red) and SynT-II (MCT4$^{+}$; green), are shown in (D and I), along with corresponding embryos and placentas for *CdGAP* $^{WT/WT}$ (A, B) and *CdGAP* $^{KI/KI}$ (severe) (F, G). Notable embryonic abnormalities, such as edema and pale liver (comparing F to A), are marked by red and blue arrowheads, respectively. Regions, where tight apposition between SynTs is lost, are indicated by white arrowheads in (I). Corresponding regions that were stained with H&E for histological comparisons are presented in (E and J). The scale bar corresponds to 50 μm, and each genotype is represented by at least three samples.

(K) Representative images comparing interhaemal membrane thickness between E15.5 *CdGAP* $^{WT/WT}$ and *CdGAP* $^{KI/KI}$ (severe) placentas. Increased thickness in the latter is denoted by yellow arrows, compared to *CdGAP* $^{WT/WT}$ placentas. The scale bar represents 50 μm.

(L) Representative images of E15.5 placenta sections, stained for E-cadherin, SynT-II (MCT4$^{+}$; green), and SynT-I (MCT1$^{+}$; red) are shown. Non-membranous expression of MCT4 and MCT1 transporters in *CdGAP* $^{KI/KI}$ (severe) placentas is highlighted by white arrows. The scale bar corresponds to 50 μm.

(M) Mean fluorescence intensity between E15.5 *CdGAP* $^{WT/WT}$ and *CdGAP* $^{KI/KI}$ (severe) placentas for E-cadherin, MCT4, or MCT1 lactate transporters is shown. Differences were analyzed using two-way ANOVA and Šídak's tests, with four placenta sections quantified per genotype. Per the placenta section, five measurements were performed throughout the whole labyrinth. Data are presented as mean ± SEM (****: $p < 0.0001$). The horizontal line represents significance due to the row factor (labeling target), while different letters denote significance between genotypes for each target.

(N) Representative images of E15.5 placenta sections, stained for fetal endothelial cells (CD31$^{+}$; red) and SynT-II (MCT4$^{+}$; green) are shown. A representative region in E15.5 *CdGAP* $^{KI/KI}$ (severe) placentas and corresponding regions in *CdGAP* $^{WT/WT}$ placentas are presented. Nuclei were labeled with DAPI staining (blue). The scale bar corresponds to 20 μm, and for each genotype, at least three samples were examined.

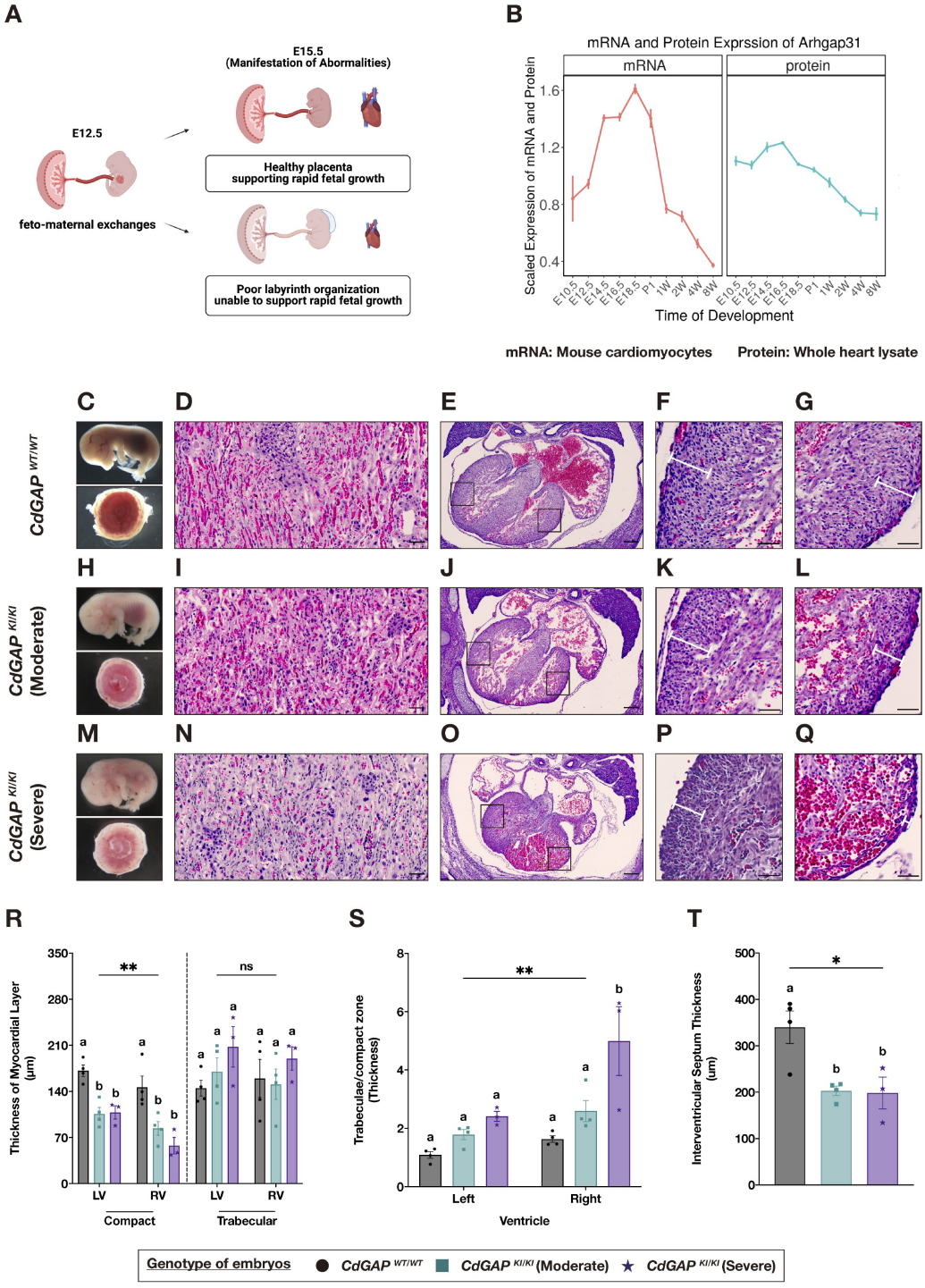
A
E15.5
(Manifestation of Abormalities)
E12.5
Healthy placenta
supporting rapid fetal growth
feto-maternal exchanges
Poor labyrinth organization
unable to support rapid fetal growth
B
mRNA and Protein Exprssion of Arhgap31
mRNA
protein
Scaled Expression of mRNA and Protein
Time of Development
mRNA: Mouse cardiomyocytes
Protein: Whole heart lysate
C
D
E
F
G
H
I
J
K
L
M
N
O
P
Q
CdGAP WT/WT
CdGAP KI/KI (Moderate)
CdGAP KI/KI (Severe)
R
Thickness of Myocardial Layer (um)
LV
RV
Compact
Trabecular
S
Trabeculae/compact zone (Thickness)
Left
Right
Ventricle
T
Interventricular Septum Thickness (um)
Genotype of embryos
CdGAP WT/WT
CdGAP KI/KI (Moderate)
CdGAP KI/KI (Severe)

**Figure 3.7: Placental dysfunctions are further associated with congenital heart defects in E15.5 *CdGAP* $^{KI/KI}$ embryos.**

(A) Schematic diagram depicting the placental-cardiovascular axis. Compared to *CdGAP* $^{WT/WT}$ embryos, *CdGAP* $^{KI/KI}$ (severe) embryos exhibit dysfunctional placentas that may compromise rapid fetal growth and organogenesis, including heart development.

(B) Graphic representation illustrates changes in CdGAP mRNA and protein expression in mice from embryonic stages (E10.5) to adulthood (8 weeks old), based on data from Gu *et al.* (2022)[38].

(C - Q) Representative images of E15.5 embryos' transverse cross-sections along the rostral-to-caudal axis are shown. Included are corresponding images of embryos and placentas (C, H, M), a magnified view of the labyrinth (D, I, N), overall views of E15.5 embryonic hearts (E, J, O), and magnified views (outlined by black boxes in E, J, O) of the left (F, K, P) and right ventricles (G, L, Q). The compact zone thicknesses of the left and right ventricles are marked by white lines. Scale bar: 200 μm (E, J, O) and 50 μm (D, F, G, I, K, L, N, P, Q).

(R) Comparisons of compact or trabecular myocardial layer thickness across genotypes for left and right ventricles are shown.

(S) Comparisons of myocardial compaction (represented by the ratio between trabeculae and compact zone thickness) across genotypes for left and right ventricles.

(T) Comparisons of interventricular septum thickness across different genotypes are shown.

Data are presented as mean ± SEM (*: $p < 0.05$, **: $p < 0.01$, ****: $p < 0.0001$). The number of E15.5 embryos examined were: *CdGAP* $^{WT/WT}$ = 4, *CdGAP* $^{KI/KI}$ (moderate) = 4, *CdGAP* $^{KI/KI}$ (severe) = 3.

For panels (R and S), a two-way ANOVA is first applied to assess differences between left and right ventricles. Following this, Tukey's multiple comparisons tests are used to evaluate differences between genotypes within the left or right ventricles individually. Horizontal lines in each panel represent significance due to the row factor (ventricles), while different letters denote significance between genotypes for each ventricle.

For panel (T), differences are analyzed using an ordinary one-way ANOVA followed by Tukey's multiple comparisons test. A horizontal line represents significance across genotypes, while different letters denote significance between genotypes.

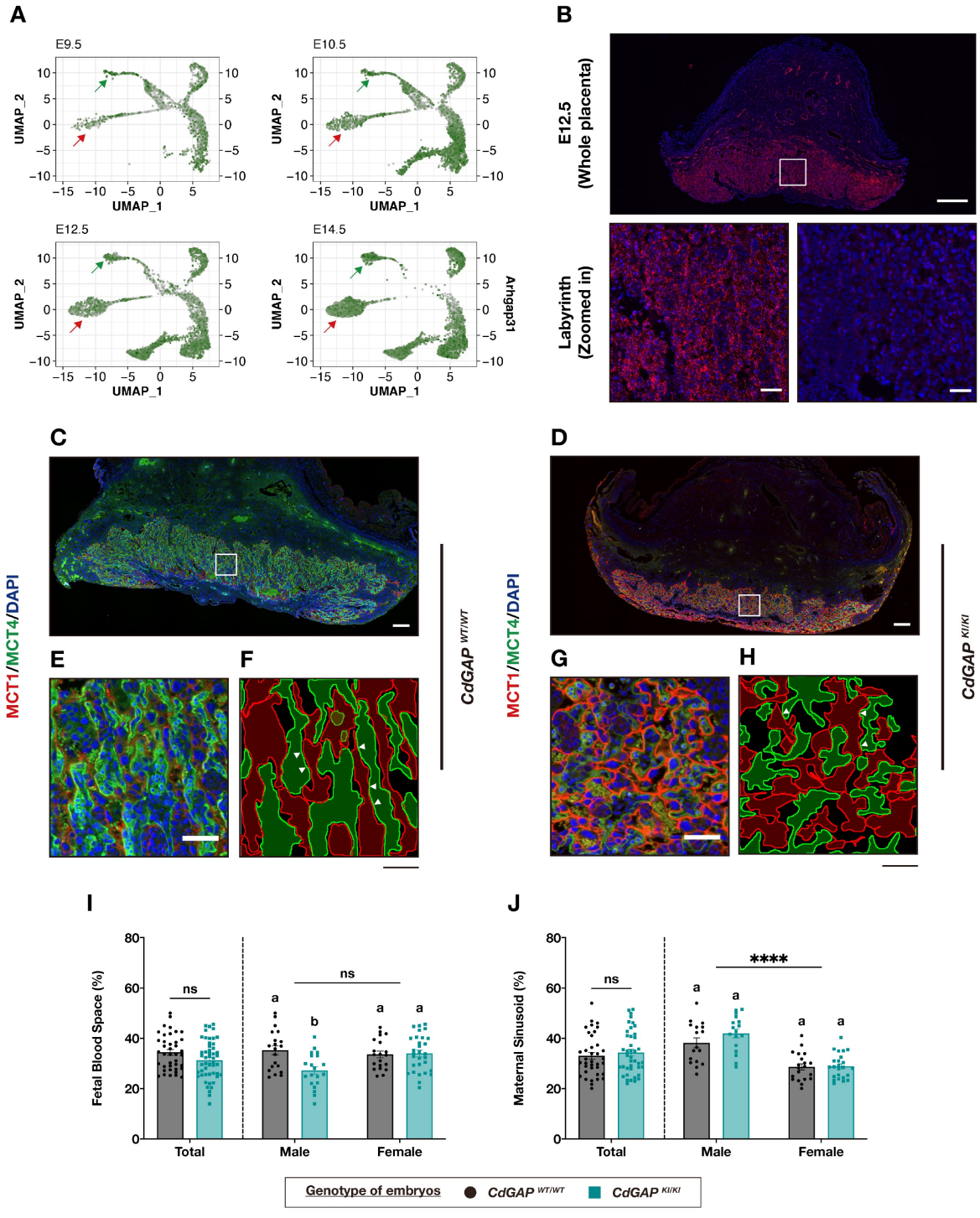
A
E9.5
E10.5
E12.5
E14.5
UMAP_1
UMAP_2
Arhgap31
B
E12.5 (Whole placenta)
Labyrinth (Zoomed in)
C
D
MCT1/MCT4/DAPI
CdGAP WT/WT
CdGAP KI/KI
E
F
G
H
I
J
Fetal Blood Space (%)
Maternal Sinusoid (%)
Total
Male
Female
ns
****
Genotype of embryos
CdGAP WT/WT
CdGAP KI/KI

**Figure 3.8: CdGAP is expressed in the labyrinth region of the placentas during early development and E12.5 *CdGAP* $^{KI/KI}$ placentas show labyrinth defects.**

(A) Graphic illustration of changes in CdGAP expression in the developing mouse placenta from E9.5 to E14.5. Two types of SynTs, SynT-I and SynT-II, are highlighted by red and green arrows, respectively.

(B) Representative images from RNAscope show *ARHGAP31* probed in E12.5 *CdGAP* $^{WT/WT}$ placentas. Red dots indicate positive signals. Images include a whole view of the E12.5 placenta and a magnified view (white box in the whole view). Adjacent to these, a placental section probed against non-specific probes is shown.

(C - H) Comparisons of vascular network organizations in E12.5 *CdGAP* $^{WT/WT}$ and *CdGAP* $^{KI/KI}$ placentas are depicted. Images of the whole placenta (C and D) and magnified views of the labyrinth (marked by the white box in C and D) are shown in (E and G). Pictographic illustrations of the vascular network organization in (E and G) are presented beside these in (F and H). E12.5 placenta cross-sections were fluorescently labeled to visualize SynTs, and nuclei were visualized using DAPI staining (blue). Contact points between two SynT layers are emphasized by white arrowheads. Scale bars are set at 200 μm for (C and D), and 50 μm for (E, F, G, H). At least three placenta sections for each genotype were examined.

(I and J) Comparisons of fetal blood spaces or maternal sinusoid occupation in the labyrinth are presented. The areas of fetal blood spaces or maternal blood sinusoids within a square (62,500μm$^2$ or a width of 250μm) were measured five times across the whole labyrinth per placental section. *Student's* t-tests (unpaired) were utilized for genotype comparison for both sexes combined (total). In contrast, two-way ANOVA followed by Šídak's multiple comparisons tests were employed to investigate significant differences in fetal blood spaces or maternal sinusoids occupancy by sex and between genotypes. Horizontal lines in each panel indicate significance due to the row factor (sex), while different letters denote significance between genotypes for each sex. Data are presented as mean ± SEM (ns: no significance; ****: $p < 0.0001$). For *CdGAP* $^{WT/WT}$ placentas, 20 measurements from five placental sections were conducted for both sexes. For male and female *CdGAP* $^{KI/KI}$ placentas, 20 or 30 measurements were conducted from five or six placentas, respectively.

**A**

| Age | *CdGAP* $^{WT/WT}$ | | | | *CdGAP* $^{WT/KI}$ | | | | *CdGAP* $^{KI/KI}$ | | | | *Chi-square* (significance) |
|---|---|---|---|---|---|---|---|---|---|---|---|---|---|
| | Male [A] | Female [B] | Ratio [A/B] | Total | Male [A] | Female [B] | Ratio [A/B] | Total | Male [A] | Female [B] | Ratio [A/B] | Total | |
| **E12.5** | 30 (48.4%) | 32 (51.6%) | $0.94^{ns}$ | 62 (28.1%) | 43 (43.4%) | 56 (56.6%) | $0.77^{ns}$ | 99 (44.8%) | 26 (43.3%) | 34 (56.7%) | $0.76^{ns}$ | 60 (27.1%) | ns |
| **E13.5** | 9 (45%) | 11 (55%) | $0.82^{ns}$ | 20 (16.4%) | 37 (52.9%) | 33 (47.1%) | $1.12^{ns}$ | 70 (57.4%) | 16 (50%) | 16 (50%) | $1^{ns}$ | 32 (26.2%) | ns |
| **E15.5** | 34 (54.8%) | 28 (45.2%) | $1.21^{ns}$ | 62 (21.0%) | 84 (54.2%) | 71 (45.8%) | $1.18^{ns}$ | 155 (52.5%) | 42 (53.8%) | 36 (46.2%) | $1.17^{ns}$ | 78 (26.4%) | ns |
| **E18.5** | 18 (46.2%) | 21 (53.8%) | $0.86^{ns}$ | 39 (22.0%) | 44 (44.4%) | 55 (55.6%) | $0.80^{ns}$ | 99 (55.9%) | 17 (43.6%) | 22 (56.4%) | $0.77^{ns}$ | 39 (22.0%) | ns |
| **P21** | 159 (49.7%) | 161 (50.3%) | $0.99^{ns}$ | 320 (32%) | 279 (47.9%) | 303 (52.1%) | $0.92^{ns}$ | 582 (58.2%) | 47 (48.0%) | 51 (52.0%) | $0.92^{ns}$ | 98 (9.8%) | **** |

**B**

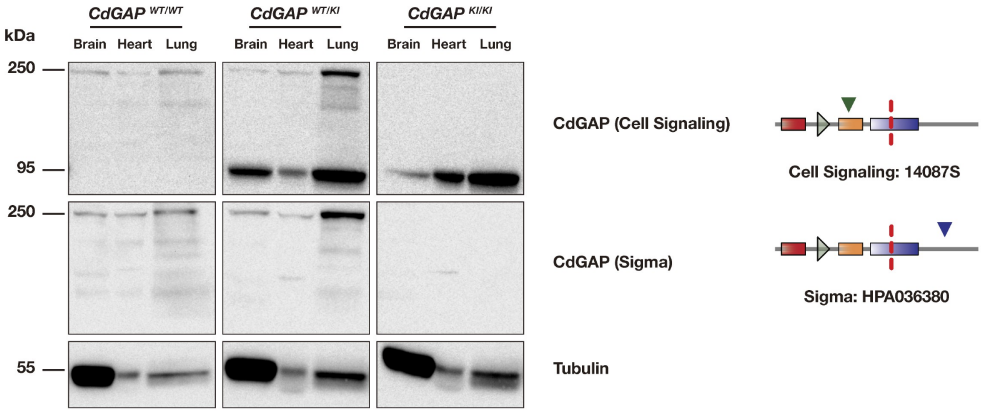


**C**

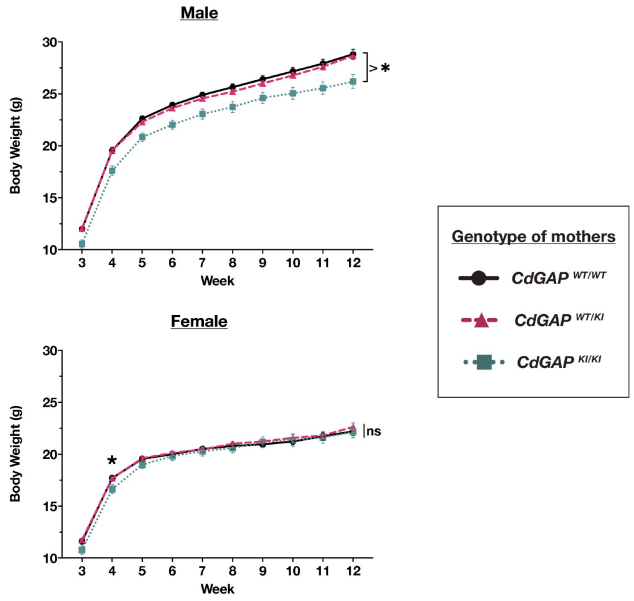


**D**

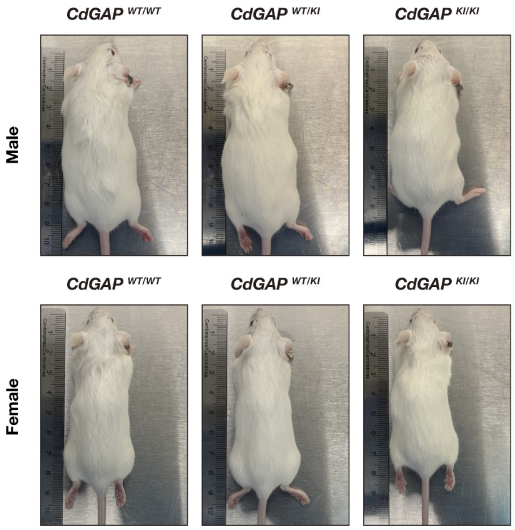

**Supplementary Figure 1**

(A) Distribution of genotype and sex of embryos at various gestational ages (E12.5, E13.5, E15.5, and E18.5) or pups at weaning (P21) is summarized. The ratio [A/B] represents the sex distribution between males [A] and females [B], while the "total" refers to the number of embryos or pups of the corresponding genotype, including both sexes. The relative proportion (represented by %) of males and females, as compared to the total number at each stage, is indicated in brackets. *Fisher's* exact tests or *Chi-square* tests were employed to analyze whether the distribution of sex or genotype significantly diverged from expectations, respectively. Notations in superscripts indicate statistical significance following *Fisher's* exact tests, while *Chi-square* significances are summarized for each gestational age (ns: no significance, ****: $p < 0.0001$).

(B) Representative immunoblots of brain, heart, and lung tissue lysates from 3-month-old mice of different genotypes are shown. The Sigma antibody was able to detect only the full-length CdGAP, approximately 250 kDa in size, while the Cell Signaling antibody could detect both the full-length and truncated forms of CdGAP.

(C) Average body weight changes in male and female mice from 3 to 12 weeks of age are depicted. Pup body weights from weaning (P21) were recorded weekly, and the averages are plotted. For male mice, over 41 *CdGAP* $^{WT/WT}$, 97 *CdGAP* $^{WT/KI}$, and 20 *CdGAP* $^{KI/KI}$ mice were measured, while for female mice, over 39 *CdGAP* $^{WT/WT}$, 68 *CdGAP* $^{WT/KI}$, and 16 *CdGAP* $^{KI/KI}$ mice were measured. Ordinary one-way ANOVA was used for comparisons each week. Significant differences in body weights were found across genotypes for males at all time points, while for females, significance was only noted at week 4.

(D) Representative photographs of 3-month-old male and female mice across different genotypes are shown.

Data are presented as mean ± SEM (*: $p < 0.05$, **: $p < 0.01$, ****: $p < 0.0001$).

**A**

| Sex [A] | Genotypes [B] | Fetal weight (g) | Placenta weight (g) | Placental efficiency |
|---|---|---|---|---|
| Male | CdGAP $^{WT/WT}$ | 0.293 ± 0.004 $^{a}$ | 0.053 ± 0.001 $^{a}$ | 5.5 ± 0.1 $^{a}$ |
| | CdGAP $^{WT/KI}$ | 0.294 ± 0.003 $^{ac}$ | 0.050 ± 0.001 $^{ac}$ | 5.9 ± 0.1 $^{ac}$ |
| | CdGAP $^{KI/KI}$ (Moderate) | 0.307 ± 0.010 $^{ac}$ | 0.048 ± 0.001 $^{ac}$ | 6.4 ± 0.2 $^{bc}$ |
| | CdGAP $^{KI/KI}$ (Severe) | 0.226 ± 0.023 $^{bd}$ | 0.044 ± 0.002 $^{bc}$ | 5.1 ± 0.5 $^{ad}$ |
| Female | CdGAP $^{WT/WT}$ | 0.274 ± 0.004 $^{a}$ | 0.051 ± 0.001 $^{a}$ | 5.4 ± 0.1 $^{a}$ |
| | CdGAP $^{WT/KI}$ | 0.283 ± 0.004 $^{ab}$ | 0.048 ± 0.001 $^{ac}$ | 5.9 ± 0.1 $^{bc}$ |
| | CdGAP $^{KI/KI}$ (Moderate) | 0.289 ± 0.006 $^{ab}$ | 0.048 ± 0.001 $^{ac}$ | 6.0 ± 0.1 $^{bc}$ |
| | CdGAP $^{KI/KI}$ (Severe) | 0.245 ± 0.019 $^{ac}$ | 0.038 ± 0.003 $^{bc}$ | 6.5 ± 0.5 $^{bc}$ |
| Significance | Sex [A] | ns | ns | ns |
| | Genotypes [B] | **** | *** | **** |
| | Interactions [AxB] | ns | ns | ** |

**B**

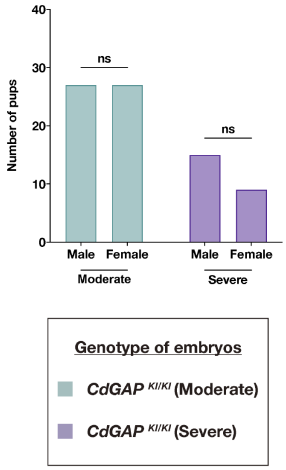


**C**

| Sex [A] | Genotypes [B] | Fetal weight (g) | Placenta weight (g) | Placental efficiency |
|---|---|---|---|---|
| Male | CdGAP $^{WT/WT}$ | 1.076 ± 0.036 $^{a}$ | 0.061 ± 0.002 $^{a}$ | 18 ± 0.58 $^{a}$ |
| | CdGAP $^{WT/KI}$ | 1.091 ± 0.018 $^{ac}$ | 0.056 ± 0.001 $^{ac}$ | 19 ± 0.33 $^{ab}$ |
| | CdGAP $^{KI/KI}$ (Moderate) | 1.029 ± 0.027 $^{ac}$ | 0.054 ± 0.002 $^{ac}$ | 19 ± 0.51 $^{abd}$ |
| | CdGAP $^{KI/KI}$ (Severe) | 0.652 ± 0.040 $^{bd}$ | 0.043 ± 0.004 $^{bd}$ | 15 ± 1.1 $^{acd}$ |
| Female | CdGAP $^{WT/WT}$ | 1.022 ± 0.028 $^{a}$ | 0.053 ± 0.002 $^{a}$ | 19 ± 0.56 $^{a}$ |
| | CdGAP $^{WT/KI}$ | 0.998 ± 0.019 $^{ac}$ | 0.052 ± 0.001 $^{ac}$ | 19 ± 0.37 $^{ac}$ |
| | CdGAP $^{KI/KI}$ (Moderate) | 0.948 ± 0.027 $^{ac}$ | 0.049 ± 0.002 $^{ace}$ | 19 ± 0.57 $^{ace}$ |
| | CdGAP $^{KI/KI}$ (Severe) | 0.698 ± 0.051 $^{bd}$ | 0.042 ± 0.002 $^{bde}$ | 17 ± 1.3 $^{bde}$ |
| Significance | Sex [A] | ns | ** | ns |
| | Genotypes [B] | **** | **** | ** |
| | Interactions [AxB] | ns | ns | ns |

**D**

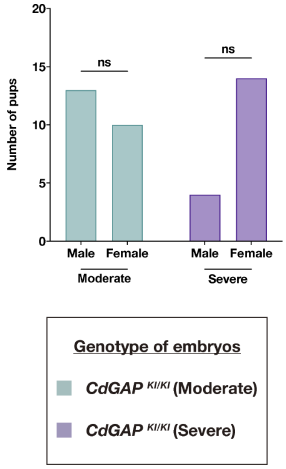


**E**

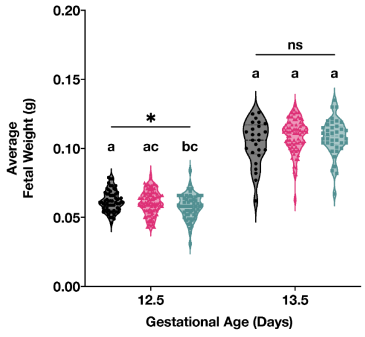


**F**

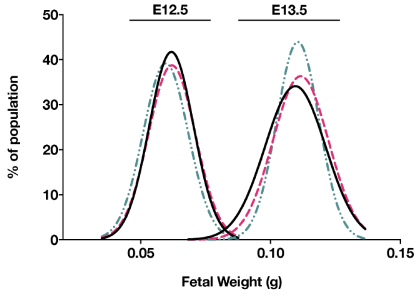


**Supplementary Figure 2**

(A) Comparisons of fetal and placental weight or placental efficiency between sexes among E15.5 embryos across genotypes are shown. The initial assessment utilized two-way ANOVA to examine differences by sex. Subsequently, Tukey's multiple comparisons tests were applied to evaluate differences between genotypes for each sex. Differences due to the row (sex) or column factor (genotype), as well as due to their interaction, are summarized. Different letters denote significance between genotypes for each sex. For fetal weights, the male and female embryo counts are (respectively): *CdGAP* $^{WT/WT}$ (n = 22, n =22), *CdGAP* $^{WT/KI}$ (n =63, n = 51), *CdGAP* $^{KI/KI}$ (moderate) (n =13, n = 16), *CdGAP* $^{KI/KI}$ (severe) = (n = 8, n = 7). For placental weights, the male and female embryo counts are (respectively): *CdGAP* $^{WT/WT}$ (n = 14, n = 13), *CdGAP* $^{WT/KI}$ (n = 36, n = 34), *CdGAP* $^{KI/KI}$ (moderate) (n = 4, n = 8), *CdGAP* $^{KI/KI}$ (severe) (n = 5, n = 2). Placental efficiency for male and female embryos is calculated by the ratio between average fetal weight and average placental weight.

(B) Comparisons of sex distribution in *CdGAP* $^{KI/KI}$ (moderate) and *CdGAP* $^{KI/KI}$ (severe) embryos at E15.5 are shown. *Fisher's* exact tests were used to examine whether the sex distribution in each group significantly deviated from the expected 1:1 ratio.

(C) Comparisons of fetal and placental weight, along with placental efficiency, between sexes among E18.5 embryos across genotypes are shown. The analysis was performed in a manner similar to that described in (A). For fetal weights, the male and female embryo counts are: *CdGAP* $^{WT/WT}$ (n = 17, n = 19), *CdGAP* $^{WT/KI}$ (n = 46, n = 51), *CdGAP* $^{KI/KI}$ (moderate) = (n = 13, n = 8), *CdGAP* $^{KI/KI}$ (severe) = (n = 2, n = 12). For placental weights, the male and female embryo counts are: *CdGAP* $^{WT/WT}$ (n = 12, n = 16), *CdGAP* $^{WT/KI}$ (n = 31, n = 34), *CdGAP* $^{KI/KI}$ (moderate) (n = 6, n = 5), *CdGAP* $^{KI/KI}$ (severe) (n = 3, n = 9).

(D) Comparisons of sex distribution in *CdGAP* $^{KI/KI}$ (moderate) and *CdGAP* $^{KI/KI}$ (severe) embryos at E18.5 are shown. *Fisher's* exact tests were used to examine whether the sex distribution in each group significantly deviated from the expected 1:1 ratio.

(E) Comparisons of average fetal weights at E12.5 and E13.5 are shown. The numbers of embryos studied were 61 for *CdGAP* $^{WT/WT}$, 99 and 75 for *CdGAP* $^{WT/KI}$, and 61 and 39 for *CdGAP* $^{KI/KI}$, respectively, at these stages. An ordinary one-way ANOVA was followed by Tukey's multiple comparisons tests for each gestational age. Horizontal lines represent

significance across genotypes, while different letters indicate significance between genotypes for each comparison.

(F) A non-linear regression fit showcases the distribution of embryos' body weights across genotypes for each gestational age.

Data are presented as mean ± SEM (ns: no significance, *: $p < 0.05$, **: $p < 0.01$, ***: $p < 0.001$, ****: $p < 0.0001$).

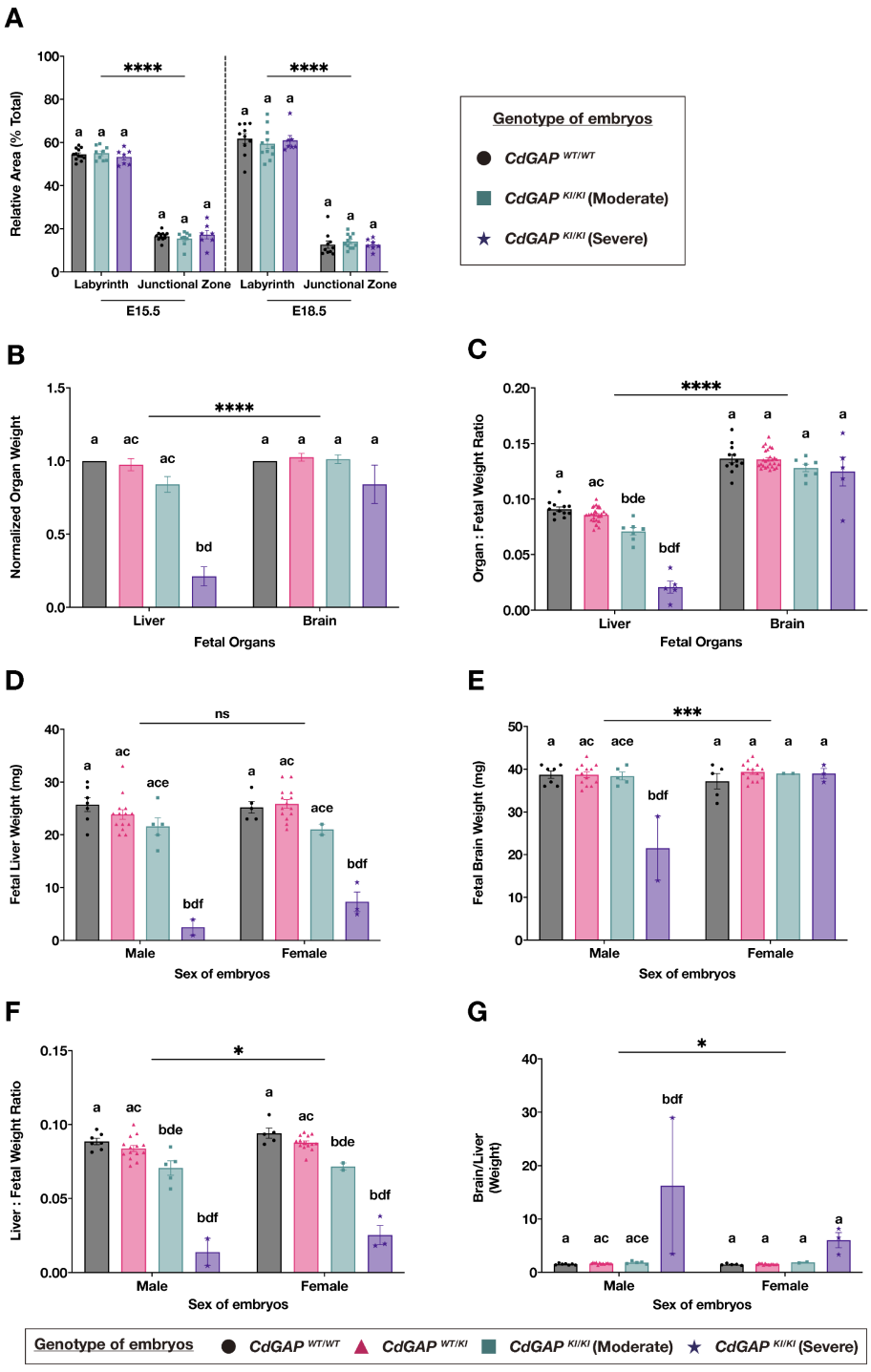


H

| Source of Variation | Liver Weight | Brain Weight | Liver : Fetal Weight | Brain : Liver |
|---|---|---|---|---|
| Sex [A] | ns | *** | * | * |
| Genotypes [B] | **** | **** | **** | **** |
| Interactions [AxB] | ns | **** | ns | ** |

**Supplementary Figure 3**

(A) Analysis of the relative area of the labyrinth and the junctional zone at E15.5 and at E18.5 is presented. Initial analysis with two-way ANOVA was performed to determine significant differences by placental layer, and then genotypic differences for each placental layer were compared using Tukey's multiple comparisons tests. Horizontal lines for each gestational age indicate significance due to the row factor (placental layer), while different letters represent significance between genotypes for each placental layer. The numbers of placental sections examined at E15.5 for each genotype were as follows: *CdGAP* $^{WT/WT}$ = 12, *CdGAP* $^{KI/KI}$ (moderate) = 9, *CdGAP* $^{KI/KI}$ (severe) = 7. Similarly, the counts at E18.5 were: *CdGAP* $^{WT/WT}$ = 10, *CdGAP* $^{KI/KI}$ (moderate) = 11, *CdGAP* $^{KI/KI}$ (severe) = 7.

(B – C) A comparison of normalized organ weights and organ-to-fetal weight ratios in E15.5 embryos is presented. Analyses were conducted similarly to the method described in (A). Horizontal lines in each panel indicate significance due to the row factor (fetal organs), while different letters denote significance between genotypes for each organ. Fetal organ weights are normalized to those in *CdGAP* $^{WT/WT}$ embryos. Organ-to-fetal weight ratios are calculated by dividing the weight of the liver or brain by the corresponding fetal weight. The E15.5 embryo counts for fetal weights are as follows: *CdGAP* $^{WT/WT}$ = 12, *CdGAP* $^{WT/KI}$ = 28, *CdGAP* $^{KI/KI}$ (moderate) = 7, *CdGAP* $^{KI/KI}$ (severe) = 5. The counts for fetal brain weights are: *CdGAP* $^{WT/WT}$ = 12, *CdGAP* $^{WT/KI}$ = 27, *CdGAP* $^{KI/KI}$ (moderate) = 7, *CdGAP* $^{KI/KI}$ (severe) = 5.

(D - G) Comparisons of fetal liver weight (D), brain weight (E), liver-to-fetal weight ratio (F), and brain-to-liver weight ratio (G) across embryonic sexes are presented. Analyses were conducted similarly to the method described in (A). Horizontal lines in each panel indicate significance due to the row factor (embryonic sex), while different letters denote significance between genotypes for each sex. Male and female embryo counts for fetal liver weight and liver-to-fetal weight ratio comparisons were, respectively: *CdGAP* $^{WT/WT}$ (n = 7, n = 5), *CdGAP* $^{WT/KI}$ (n = 14, n = 14), *CdGAP* $^{KI/KI}$ (moderate) (n = 5, n = 2), *CdGAP* $^{KI/KI}$ (severe) (n = 2, n = 3). Male and female embryo counts for fetal brain weight and brain-to-liver weight ratio comparisons were, respectively: *CdGAP* $^{WT/WT}$ (n = 7, n = 5), *CdGAP* $^{WT/KI}$ (n = 13, n = 14), *CdGAP* $^{KI/KI}$ (moderate) (n = 5, n = 2), *CdGAP* $^{KI/KI}$ (severe) (n = 2, n = 3).

(H) Summary of the significance from sources of variation following two-way ANOVA analyses in (D - G).

Data are presented as mean ± SEM (ns: no significance, *: $p < 0.05$, **: $p < 0.01$, ***: $p < 0.001$, ****: $p < 0.0001$).

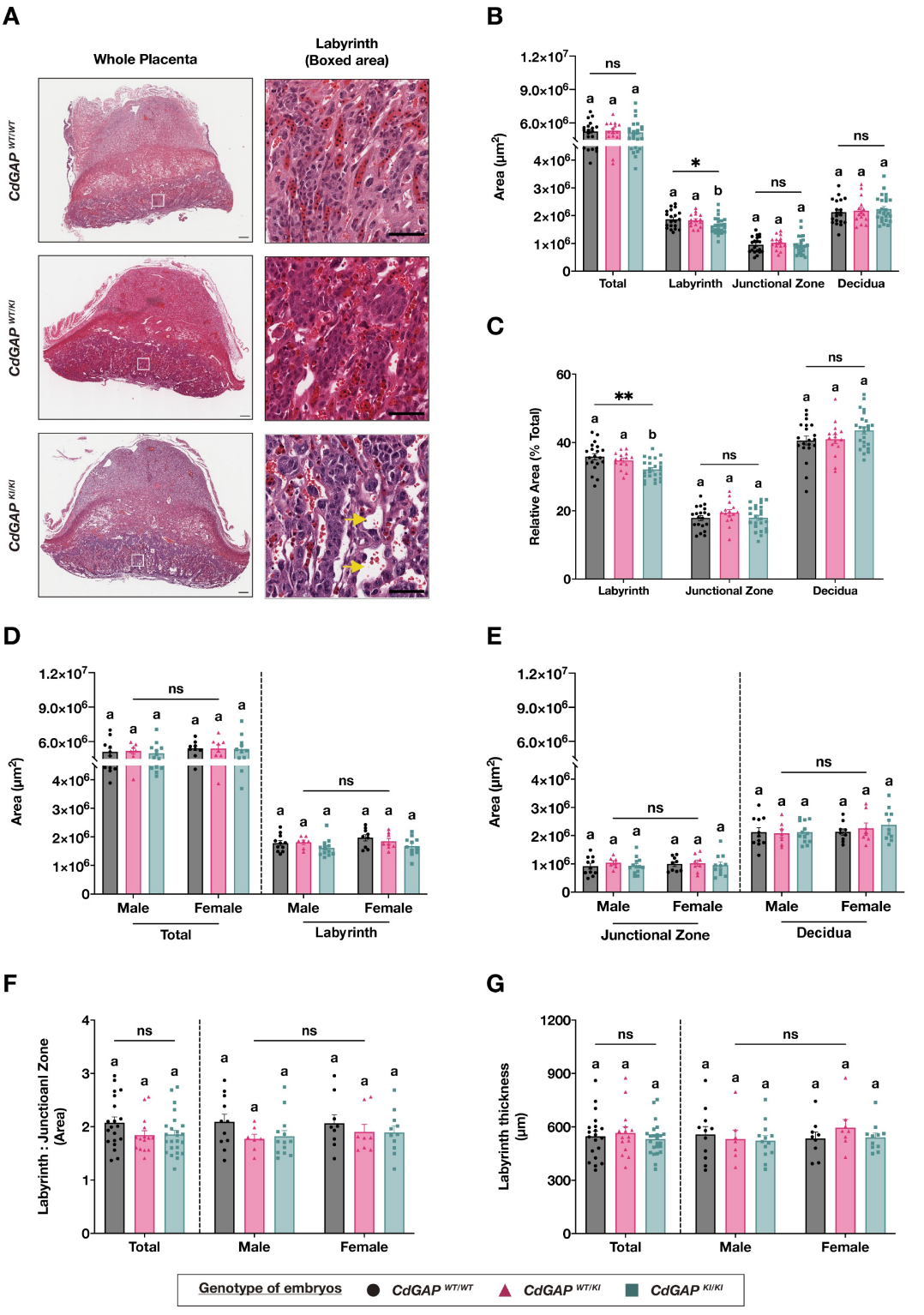
A
Whole Placenta
Labyrinth (Boxed area)
CdGAP WT/WT
CdGAP WT/KI
CdGAP KI/KI
B
Area (µm²)
Total
Labyrinth
Junctional Zone
Decidua
C
Relative Area (% Total)
Labyrinth
Junctional Zone
Decidua
D
Area (µm²)
Male
Female
Total
Labyrinth
E
Area (µm²)
Junctional Zone
Decidua
F
Labyrinth : Junctioanl Zone (Area)
G
Labyrinth thickness (µm)
Genotype of embryos
CdGAP WT/WT
CdGAP WT/KI
CdGAP KI/KI

**Supplementary Figure 4**

(A) Representative images of E12.5 placentas, stained with H&E across genotypes, are shown. Magnified views of the labyrinth (marked by white boxes) are presented next to the whole view of the placenta. Enlarged vascular spaces in *CdGAP* $^{KI/KI}$ placentas are pinpointed by yellow arrows. Scale bars correspond to 200 μm and 50 μm.

(B - C) Comparisons of the absolute area (B) or relative area (C) of placental layers (compared against the total placental area) in E12.5 embryos are shown. Initial analyses employed ordinary one-way ANOVA to assess differences across genotypes. Subsequent analyses used Tukey's multiple comparisons tests to examine differences between genotypes. Horizontal lines in each panel represent significance across genotypes, while different letters denote significance between genotypes for each comparison. Placenta counts were as follows: *CdGAP* $^{WT/WT}$ = 20, *CdGAP* $^{WT/KI}$ = 15, *CdGAP* $^{KI/KI}$ = 24.

(D – G) Comparisons of total placental area, the area of different placental layers, labyrinth to junctional zone ratio, and labyrinth thickness between placental sexes are shown. Two-way ANOVA was followed by Tukey's multiple comparisons tests to evaluate differences by placental sex and differences between genotypes, respectively. Horizontal lines in each panel represent significance due to the row factor (placental sex), while different letters denote significance between genotypes for each sex. Placenta counts for males and females were as follows: *CdGAP* $^{WT/WT}$ (n = 11, n = 9), *CdGAP* $^{WT/KI}$ (n = 7, n = 8), *CdGAP* $^{KI/KI}$ (n = 13, n = 11).

Data are presented as mean ± SEM (ns: no significance, *: $p < 0.05$, **: $p < 0.01$).

| Antibody | Company: Catalog number | Dilution |
|---|---|---|
| **Immunoblot** | | |
| Rabbit anti-CdGAP (Polyclonal) | Sigma-Aldrich: HPA036380 | 1 in 1,000 |
| Rabbit anti-CdGAP (Monoclonal) | Cell Signaling: 14087S | 1 in 1,000 |
| Mouse anti-α -Tubulin (Monoclonal) | Sigma-Aldrich: T5168 | 1 in 1,000 |
| Anti-rabbit IgG | Thermo-Fisher: 45-000-682 | 1 in 10,000 |
| Anti-mouse IgG | Thermo-Fisher: 45-000-679 | 1 in 10,000 |
| **Immunostaining** | | |
| Goat anti-CD31 (Polyclonal) | R&D Systems: AF3628 | 1 in 20 |
| Rabbit anti-E-Cadherin (Monoclonal) | Cell Signaling: 3195S | 1 in 100 |
| Chicken anti-MCT1 (Polyclonal) | EMD-Milipore: AB1286-I | 1 in 200 |
| Rabbit anti-MCT4 (Polyclonal) | EMD-Milipore: AB3314P | 1 in 200 |
| Goat anti-rabbit IgG Alexa Fluor 488 | Invitrogen; A11008 | 1 in 200 |
| Donkey anti-goat Alexa Fluor Plus 594 | Invitrogen: A32758 | 1 in 200 |
| Donkey anti-chicken IgG Alexa Fluor 594 | Invitrogen; A78951 | 1 in 200 |

**Supplementary Table 1**

List of antibodies used in this study.

| Gene Name | Forward Primer | Reverse Primer |
|---|---|---|
| *CdGAP* (wildtype) | 5'-GGCTAAGGATGGGGGTCAGA-3' | 5'-GGGCTTGACTCAGGAATCGG-3' |
| *CdGAP* (knock-in) | 5'-GAAGACAAGCACGATTTAAG-3' | 5'-TCTCAAACAGAAGCATTTCC -3' |
| *Rbm31x/y* (sex) | 5'-CACCTTAAGAACAAGCCAATACA-3' | 5'-GGCTTGTCCTGAAAACATTTGG-3' |

**Supplementary Table 2**

List of primers used in this study.

## References


1. Dvorsky, R., & Ahmadian, M. R. (2004). Always look on the bright site of Rho: structural implications for a conserved intermolecular interface. *EMBO Rep*, *5*(12), 1130-1136. https://doi.org/10.1038/sj.embor.7400293
2. Sankhyan, N., Kaushal, R. K., & Jaswal, R. S. (2006). Adams–Oliver syndrome: A case with complete expression. *The Journal of Dermatology*, *33*(6), 435-436. https://doi.org/10.1111/j.1346-8138.2006.00104.x
3. Bonafede, R. P., & Beighton, P. (1979). Autosomal dominant inheritance of scalp defects with ectrodactyly. *American Journal of Medical Genetics*, *3*(1), 35-41. https://doi.org/10.1002/ajmg.1320030109
4. Meester, J. A. N., Sukalo, M., Schröder, K. C., Schanze, D., Baynam, G., Borck, G., Bramswig, N. C., Duman, D., Gilbert-Dussardier, B., Holder-Espinasse, M., Itin, P., Johnson, D. S., Joss, S., Koillinen, H., McKenzie, F., Morton, J., Nelle, H., Reardon, W., Roll, C., . . . Wuyts, W. (2018). Elucidating the genetic architecture of Adams–Oliver syndrome in a large European cohort. *Human Mutation*, *39*(9), 1246-1261. https://doi.org/10.1002/humu.23567
5. Southgate, L., & Trembath, R. C. (2016). 1203ARHGAP31, DOCK6, RBPJ, EOGT, and Adams-Oliver Syndrome. In *Epstein's Inborn Errors of Development: The Molecular Basis of Clinical Disorders of Morphogenesis* (pp. 0). Oxford University Press. https://doi.org/10.1093/med/9780199934522.003.0183
6. Fryns, J. P., Legius, E., Demaerel, P., & van den Berghe, H. (1996). Congenital scalp defect, distal limb reduction anomalies, right spastic hemiplegia and hypoplasia of the left arteria cerebri media: Further evidence that interruption of early embryonic blood supply may result in Adams-Oliver (plus) syndrome. *Clinical Genetics*, *50*(6), 505-509. https://doi.org/10.1111/j.1399-0004.1996.tb02723.x
7. Hoyme, H. E., Jones, K. L., Allen, M. I. V., Saunders, B. S., & Benirschke, K. (1982). Vascular pathogenesis of transverse limb reduction defects. *The Journal of Pediatrics*, *101*(5), 839-843. https://doi.org/10.1016/S0022-3476(82)80343-0
8. Southgate, L., Machado, Rajiv D., Snape, Katie M., Primeau, M., Dafou, D., Ruddy, Deborah M., Branney, Peter A., Fisher, M., Lee, Grace J., Simpson, Michael A., He, Y., Bradshaw, Teisha Y., Blaumeiser, B., Winship, William S., Reardon, W., Maher,

Eamonn R., FitzPatrick, David R., Wuyts, W., Zenker, M., . . . Trembath, Richard C. (2011). Gain-of-Function Mutations of ARHGAP31, a Cdc42/Rac1 GTPase Regulator, Cause Syndromic Cutis Aplasia and Limb Anomalies. *The American Journal of Human Genetics*, *88*(5), 574-585. https://doi.org/10.1016/j.ajhg.2011.04.013

9. Karimzadeh, F., Primeau, M., Mountassif, D., Rouiller, I., & Lamarche-Vane, N. (2012). A Stretch of Polybasic Residues Mediates Cdc42 GTPase-activating Protein (CdGAP) Binding to Phosphatidylinositol 3,4,5-Trisphosphate and Regulates Its GAP Activity *<sup> </sup>. *Journal of Biological Chemistry*, *287*(23), 19610-19621. https://doi.org/10.1074/jbc.M112.344606
10. Djoudi Ouadda, A. B., He, Y., Calabrese, V., Ishii, H., Chidiac, R., Gratton, J.-P., Roux, P. P., & Lamarche-Vane, N. (2018). CdGAP/ARHGAP31 is regulated by RSK phosphorylation and binding to 14-3-3β adaptor protein. *Oncotarget*, *9*(14), 11646-11664. https://doi.org/10.18632/oncotarget.24126
11. He, Y., Northey, J. J., Pelletier, A., Kos, Z., Meunier, L., Haibe-Kains, B., Mes-Masson, A. M., Côté, J. F., Siegel, P. M., & Lamarche-Vane, N. (2017). The Cdc42/Rac1 regulator CdGAP is a novel E-cadherin transcriptional co-repressor with Zeb2 in breast cancer. *Oncogene*, *36*(24), 3490-3503. https://doi.org/10.1038/onc.2016.492
12. McCormack, J. J., Bruche, S., Ouadda, A. B. D., Ishii, H., Lu, H., Garcia-Cattaneo, A., Chávez-Olórtegui, C., Lamarche-Vane, N., & Braga, V. M. M. (2017). The scaffold protein Ajuba suppresses CdGAP activity in epithelia to maintain stable cell-cell contacts. *Scientific Reports*, *7*(1), 9249. https://doi.org/10.1038/s41598-017-09024-4
13. Caron, C., DeGeer, J., Fournier, P., Duquette, P. M., Luangrath, V., Ishii, H., Karimzadeh, F., Lamarche-Vane, N., & Royal, I. (2016). CdGAP/ARHGAP31, a Cdc42/Rac1 GTPase regulator, is critical for vascular development and VEGF-mediated angiogenesis. *Scientific Reports*, *6*(1), 27485. https://doi.org/10.1038/srep27485
14. Whitten, W. K. (1956). MODIFICATION OF THE OESTROUS CYCLE OF THE MOUSE BY EXTERNAL STIMULI ASSOCIATED WITH THE MALE. *Journal of Endocrinology*, *13*(4), 399-404. https://doi.org/10.1677/joe.0.0130399
15. Heyne, G. W., Plisch, E. H., Melberg, C. G., Sandgren, E. P., Peter, J. A., & Lipinski, R. J. (2015). A Simple and Reliable Method for Early Pregnancy Detection in Inbred Mice.

*Journal of the American Association for Laboratory Animal Science*, *54*(4), 368-371. https://www.ingentaconnect.com/content/aalas/jaalas/2015/00000054/00000004/art00005

16. Tunster, S. J. (2017). Genetic sex determination of mice by simplex PCR. *Biology of Sex Differences*, *8*(1), 31. https://doi.org/10.1186/s13293-017-0154-6
17. Dilworth, M. R., Kusinski, L. C., Baker, B. C., Renshall, L. J., Greenwood, S. L., Sibley, C. P., & Wareing, M. (2011). Defining fetal growth restriction in mice: A standardized and clinically relevant approach. *Placenta*, *32*(11), 914-916. https://doi.org/10.1016/j.placenta.2011.08.007
18. Zar, J. H. (1984). Statistical Significance of Mutation Frequencies, and the Power of Statistical Testing, Using the Poisson Distribution. *Biometrical Journal*, *26*(1), 83-88. https://doi.org/10.1002/bimj.4710260116
19. Adnani, L., Kassouf, J., Meehan, B., Spinelli, C., Tawil, N., Nakano, I., & Rak, J. (2022). Angiocrine extracellular vesicles impose mesenchymal reprogramming upon proneural glioma stem cells. *Nature Communications*, *13*(1), 5494. https://doi.org/10.1038/s41467-022-33235-7
20. Matsuda, J., Greenberg, D., Ibrahim, S., Maier, M., Aoudjit, L., Chapelle, J., Baldwin, C., He, Y., Lamarche-Vane, N., & Takano, T. (2022). CdGAP maintains podocyte function and modulates focal adhesions in a Src kinase-dependent manner. *Scientific Reports*, *12*(1), 18657. https://doi.org/10.1038/s41598-022-21634-1
21. Bankhead, P., Loughrey, M. B., Fernández, J. A., Dombrowski, Y., McArt, D. G., Dunne, P. D., McQuaid, S., Gray, R. T., Murray, L. J., Coleman, H. G., James, J. A., Salto-Tellez, M., & Hamilton, P. W. (2017). QuPath: Open source software for digital pathology image analysis. *Scientific Reports*, *7*(1), 16878. https://doi.org/10.1038/s41598-017-17204-5
22. Marsh, B., & Blelloch, R. (2020). Single nuclei RNA-seq of mouse placental labyrinth development. *eLife*, *9*, e60266. https://doi.org/10.7554/eLife.60266
23. Elmore, S. A., Cochran, R. Z., Bolon, B., Lubeck, B., Mahler, B., Sabio, D., & Ward, J. M. (2021). Histology Atlas of the Developing Mouse Placenta. *Toxicologic Pathology*, *50*(1), 60-117. https://doi.org/10.1177/01926233211042270
24. Faye-Petersen, O. M., Heller, D. S., & Joshi, V. V. (2005). *Handbook of Placental Pathology* (2nd ed.). CRC Press. https://doi.org/10.3109/9780203489567

25. Narasimha, A., & Vasudeva, D. (2011). Spectrum of changes in placenta in toxemia of pregnancy. *Indian Journal of Pathology and Microbiology*, *54*(1), 15-20. https://doi.org/10.4103/0377-4929.77317

26. Simmons, D. G. (2014). 12 - Postimplantation Development of the Chorioallantoic Placenta. In B. A. Croy, A. T. Yamada, F. J. DeMayo, & S. L. Adamson (Eds.), *The Guide to Investigation of Mouse Pregnancy* (pp. 143-161). Academic Press. https://doi.org/10.1016/B978-0-12-394445-0.00012-6

27. Bolon, B. W., J. M. (2015). 4 - Anatomy and Physiology of the Developing Mouse and Placenta. In B. Bolon (Ed.), *Pathology of the Developing Mouse* (pp. 39-98). CRC Press. https://doi-org.proxy3.library.mcgill.ca/10.1201/b18160

28. Wilson, M. E., & Ford, S. P. (2001). Comparative aspects of placental efficiency. *Reproduction (Cambridge, England). Supplement*, *58*, 223-232.

29. Fowden, A. L., Sferruzzi-Perri, A. N., Coan, P. M., Constancia, M., & Burton, G. J. (2009). Placental efficiency and adaptation: endocrine regulation. *The Journal of Physiology*, *587*(14), 3459-3472. https://doi.org/10.1113/jphysiol.2009.173013

30. Simmons, D. G., Natale, D. R. C., Begay, V., Hughes, M., Leutz, A., & Cross, J. C. (2008). Early patterning of the chorion leads to the trilaminar trophoblast cell structure in the placental labyrinth. *Development*, *135*(12), 2083-2091. https://doi.org/10.1242/dev.020099

31. Coan, P. M., Ferguson-Smith, A. C., & Burton, G. J. (2004). Developmental Dynamics of the Definitive Mouse Placenta Assessed by Stereology1. *Biology of Reproduction*, *70*(6), 1806-1813. https://doi.org/10.1095/biolreprod.103.024166

32. Radford, B. N., Zhao, X., Glazer, T., Eaton, M., Blackwell, D., Mohammad, S., Lo Vercio, L. D., Devine, J., Shalom-Barak, T., Hallgrimsson, B., Cross, J. C., Sucov, H. M., Barak, Y., Dean, W., & Hemberger, M. (2023). Defects in placental syncytiotrophoblast cells are a common cause of developmental heart disease. *Nature Communications*, *14*(1), 1174. https://doi.org/10.1038/s41467-023-36740-5

33. Woods, L., Perez-Garcia, V., & Hemberger, M. (2018). Regulation of Placental Development and Its Impact on Fetal Growth—New Insights From Mouse Models. *Frontiers in Endocrinology*, *9*, 570. https://doi.org/10.3389/fendo.2018.00570

34. Watson, E. D., & Cross, J. C. (2005). Development of Structures and Transport Functions in the Mouse Placenta. *Physiology*, *20*(3), 180-193. https://doi.org/10.1152/physiol.00001.2005

35. Wang, Y.-N., Ye, Y., Zhou, D., Guo, Z.-W., Xiong, Z., Gong, X.-X., Jiang, S.-W., & Chen, H. (2022). The Role of Syncytin in Placental Angiogenesis and Fetal Growth. *Frontiers in Cell and Developmental Biology*, *10*, 852561. https://doi.org/10.3389/fcell.2022.852561

36. Courtney, J. A., Cnota, J. F., & Jones, H. N. (2018). The Role of Abnormal Placentation in Congenital Heart Disease; Cause, Correlate, or Consequence? *Frontiers in Physiology*, *9*, 1045. https://doi.org/10.3389/fphys.2018.01045

37. Marton, T., Hargitai, B., Bowen, C., & Cox, P. M. (2013). Elevated Brain Weight/Liver Weight Ratio in Normal Body Weight Centile Term Perinatal Deaths: An Indicator of Terminal Intrauterine Malnourishment. *Pediatric and Developmental Pathology*, *16*(4), 267-271. https://doi.org/10.2350/12-11-1278-OA.1

38. Gu, Y., Zhou, Y., Ju, S., Liu, X., Zhang, Z., Guo, J., Gao, J., Zang, J., Sun, H., Chen, Q., Wang, J., Xu, J., Xu, Y., Chen, Y., Guo, Y., Dai, J., Ma, H., Wang, C., Jin, G., . . . Hu, Z. (2022). Multi-omics profiling visualizes dynamics of cardiac development and functions. *Cell Reports*, *41*(13), 111891. https://doi.org/10.1016/j.celrep.2022.111891

39. Iturriagagoitia, A., Meert, V., De Cocker, J., Penicka, M., Heggermont, W., & Vanderheyden, M. (2020). Progressive Thinning of the Basal Interventricular Septum by Giant Cell Myocarditis. *JACC: Case Reports*, *2*(2), 180-185. https://doi.org/10.1016/j.jaccas.2019.11.036

40. He, Y., Northey, J. J., Primeau, M., Machado, R. D., Trembath, R., Siegel, P. M., & Lamarche-Vane, N. (2011). CdGAP is required for transforming growth factor β- and Neu/ErbB-2-induced breast cancer cell motility and invasion. *Oncogene*, *30*(9), 1032-1045. https://doi.org/10.1038/onc.2010.477

41. Mehra, C., Chung, J.-H., He, Y., Lara-Márquez, M., Goyette, M.-A., Boufaied, N., Barrès, V., Ouellet, V., Guérard, K.-P., Delliaux, C., Saad, F., Lapointe, J., Côté, J.-F., Labbé, D. P., & Lamarche-Vane, N. (2021). CdGAP promotes prostate cancer metastasis by regulating epithelial-to-mesenchymal transition, cell cycle progression, and apoptosis. *Communications Biology*, *4*(1), 1042. https://doi.org/10.1038/s42003-021-02520-4

42. Sevilla-Montoya, R., Ríos-Flores, B., Moreno-Verduzco, E., Domínguez-Castro, M., Rivera-Pedroza, C. I., & Aguinaga-Ríos, D. M. (2014). Severe phenotype in two half-sibs with Adams Oliver syndrome. *Archivos argentinos de pediatria*, *112*(3), e108–e112. https://doi.org/10.5546/aap.2014.eng.e108

43. Schröder, K. C., Duman, D., Tekin, M., Schanze, D., Sukalo, M., Meester, J., Wuyts, W., & Zenker, M. (2019). Adams–Oliver syndrome caused by mutations of the EOGT gene. *American Journal of Medical Genetics Part A*, *179*(11), 2246-2251. https://doi.org/10.1002/ajmg.a.61313

44. Meakin, A. S., Cuffe, J. S. M., Darby, J. R. T., Morrison, J. L., & Clifton, V. L. (2021). Let's Talk about Placental Sex, Baby: Understanding Mechanisms That Drive Female- and Male-Specific Fetal Growth and Developmental Outcomes. *International Journal of Molecular Sciences*, *22*(12), 6386. https://doi.org/10.3390/ijms22126386

# Chapter 4: General Discussion and Conclusion

## *4.1 Major Findings*

### *4.1.1 CdGAP functions as an oncogene in prostate cancer*

CdGAP, through its proline-rich domain (PRD), has been implicated in the transcriptional repression of the E-cadherin gene in breast cancer cells, thereby promoting increased tumor growth and metastases to the lung[1]. This loss of E-cadherin, a well-established epithelial marker, and a hallmark of epithelial-to-mesenchymal transition (EMT), provides a convincing molecular mechanism indicating how CdGAP may function as an oncogene in a wide array of human cancers. However, this question remained unexplored. In the research presented in Chapter 2, we demonstrated that aberrantly elevated expression levels of CdGAP were associated with an increased likelihood of biochemical recurrence in prostate cancer (PCa) patients. Employing knockdown or overexpression approaches, we provided robust evidence of how CdGAP's impact on cellular migration and invasion, which was significantly impaired upon knockdown. Further, using subcutaneous and orthotopic xenografts, we revealed that the loss of CdGAP severely impairs PCa, in terms of both tumorigenesis and its ability to metastasize to distant organs, such as the bone and intestine. Collectively, our data strengthen the argument that CdGAP acts as an oncogene in human cancer by conferring enhanced proliferative, migratory, and invasive capacities.

### *4.1.2 CdGAP is crucial for mouse placenta development*

Numerous compelling pieces of evidence prompted an investigation into the role of CdGAP during embryonic development. Previously, the knock-out of both Rac1 and Cdc42 was shown to result in severe embryonic deaths during the early stages of embryonic development[2-4]. Furthermore, *ARHGAP31*, the gene encoding CdGAP, has been identified as the first causative gene associated with the Adams-Oliver syndrome (AOS). Two distinct mutations initially discovered from pedigree analyses shared similarities regarding the partial loss of PRD[5]. While we underscored the essential role of CdGAP during mouse embryonic development using CdGAP-knock-out mouse models, which resulted in incompletely penetrant embryonic lethality and a wide range of embryonic abnormalities[6], the pathological mechanism linked to truncation mutations in CdGAP seen in AOS patients remained unexplored. In the study presented in

Chapter 3, we demonstrated that incomplete embryonic lethality occurred strictly among homozygous CdGAP-AOS knock-in (KI) mice, with significant defects in placental development localized to the labyrinth. Furthermore, we highlighted that the fusion of syncytiotrophoblast (SynT) layers in the mouse labyrinth was markedly affected, with frequent observation of areas where the tight apposition between two SynT layers was lost. Together, our data provide new insight into how CdGAP might influence embryonic development through the regulation of placental development.

#### *4.1.3 Homozygous CdGAP-AOS mice suffer from congenital heart defects*

While AOS is frequently characterized by clinical manifestations of transverse terminal limb defects (TTLD) and aplasia cutis congenita (ACC)[7], the expanding list of phenotypic abnormalities further supports its vascular origin[8-10]. In fact, congenital heart defects, often co-occuring with cutis marmorata telangiectatica (CMTC), are observed in around 20% of AOS patients[7]. Despite relatively sparse investigative efforts, several clinical reports have suggested the possibility of placental dysfunction contributing to the pathogenesis of AOS[11, 12]. Given the vital importance of the placenta, which grows in parallel with the embryo and shares numerous developmental pathways[554], we sought to investigate whether congenital heart development might be affected in homozygous CdGAP-AOS KI mice. In the study presented in Chapter 3, we demonstrated that homozygous CdGAP-AOS KI placentas, exhibiting pronounced histological abnormalities in the labyrinth, led to changes in congenital heart development. These changes included a significant reduction in the ventricular wall and interventricular septum thickness, as well as a pronounced reduction in the compaction of myocardial layers. Collectively, our data further support the placental-cardiovascular axis, providing new insights into how placental dysfunction – a factor that has been largely overlooked in clinical investigations among AOS-affected families – can directly contribute to the pathogenesis of embryonic abnormalities observed in AOS patients.

## *4.2 CdGAP functions as an oncogene in prostate cancer*

In these studies, we spotlighted the oncogenic function of CdGAP in PCa, thereby reinforcing our earlier findings in breast cancer. Like breast cancer, PCa is the most frequently

diagnosed cancer among men and stands as the fifth leading cause of cancer-related deaths[13]. Although localized PCa can be effectively treated with a 5-year survival rate exceeding 99%, the survival rate drops dramatically to approximately 32% when the tumor metastasizes to distant organs[14]. A notable characteristic of this transition is resistance against castration therapy, aimed at controlling androgen receptor signaling[15-18]. Thus, our investigation was focused on whether CdGAP plays an oncogenic role in PCa tumorigenesis and progression, which could greatly enrich therapeutic alternatives by targeting its function.

In PCa patients, we observed that both increased expression of *ARHGAP31* and the presence of mutations were linked to higher risks of biochemical recurrence. This aligns with prior reports in which Rac1 mutations, analogous to KRAS mutation[19], were observed in PCa and a positive correlation between Cdc42 expression levels and PCa metastasis, via regulation of β1-integrin expression, essential for cancer cell and endothelial cell interactions[20]. Moreover, prior studies have identified the key role of CdGAP in regulating cellular migration[21, 22] and durotaxis[23]. Consequently, we investigated transcript levels of *ARHGAP31* across various PCa cell lines and found the highest expression in the highly aggressive and metastatic PC-3 cell line. High protein-level expression was further confirmed in PC-3 cells, which were then selected as the model system for further exploration of oncogenic mechanisms of CdGAP in PCa.

In this study, we successfully employed short hairpin (shRNA) to knock down CdGAP, resulting in a significant decrease in the migratory and invasive potential of CRPC cells. Furthermore, we validated the oncogenic role of CdGAP in various PCa cell lines, including DU-145, LNCaP, and 22Rv1. In these lines, overexpression of CdGAP substantially increased their migratory and invasive potential. However, at the molecular level, we observed a stark contrast to our earlier findings in breast cancer cells. Specifically, while CdGAP knockdown in ErbB2-expressing breast cancer cells was inversely correlated with E-cadherin levels, which further correlated with reduced expression levels of Snail 1 and Zeb2[1], this was not the case in PC-3 cells, where CdGAP knockdown did not result in an inverse increase in E-cadherin expression. Moreover, unlike in breast cancer cells, both mRNA and protein levels of Snail 1, a well-known E-cadherin repressor, increased in shCdGAP PC-3 cells. These findings suggested that the PRD of CdGAP-mediated transcriptional regulation of E-cadherin observed in breast cancer cells did not drive the regulation of E-cadherin gene expression in PC-3 cells. However, CdGAP did play an essential role in positive regulation of cell proliferation in CRPC cells, an ability that was

significantly compromised in both PC-3 and 22Rv1 cells when CdGAP was depleted. Therefore, we performed RNA-sequencing to capture changes in gene signature that underpin the oncogenic roles of CdGAP in PC-3 cells.

In the current study, we observed remarkable changes in numerous molecular pathways following CdGAP knockdown in PC-3 cells. Notably, there was a significant increase in genes related to EMT and apoptosis, concurrently with a significant decrease in genes associated with cellular proliferation. We further confirmed our findings from the transcriptomics analysis using quantitative PCR (qPCR) and immunoblotting. We demonstrated that expression levels of N-cadherin and Slug, EMT mesenchymal markers, were reduced in shCdGAP PC-3 cells. Moreover, regarding changes in gene signatures indicative of reduced cell proliferation but increased cell death (i.e., apoptosis), we showed a significant increase in p21 mRNA levels, a cell cycle inhibitor. Importantly, we observed a higher proportion of shCdGAP PC-3 cells in the G1 phase, with a significant reduction in cells in S and G2 phases. Additionally, we evidenced a significant increase in cell death following CdGAP depletion, in response to doxorubicin, which increased not only apoptotic but also necrotic cell death. These observations further align with our previous findings in breast cancer, where CdGAP played vital roles in breast cancer tumorigenesis and lung metastasis by conferring increased proliferative, migratory, and invasive potential to breast cancer cells[1, 21]. To examine the therapeutic potential of inhibiting CdGAP to improve PCa patient survival, we initiated *in vivo* studies using xenograft mouse models.

In subcutaneous xenografts to male nude mice, we showed that both tumor initiation and growth were severely impaired when CdGAP was knocked down in PC-3 cells. Notably, nearly 30% of mice (8/11) injected with shCdGAP PC-3 cells did not form tumors. In line with our *in vitro* observations, PCa tumorigenesis was significantly compromised, leading to a substantial reduction in tumor volume and primary tumor weight. This observation further aligns with our previous findings in breast cancer, where CdGAP depletion in ErbB2-expressing breast cancer cells led to a significant reduction in primary tumor volume, associated with reduced Ki-67 hybridization, a proliferative marker[1]. Collectively, our findings from subcutaneous xenograft mice suggest that CdGAP depletion may inhibit CRPC progression by blocking cellular proliferation while increasing cell death via apoptosis and necrosis.

While no single cell line can fully mirror the complex heterogeneity of human cancer, our study faced constraints due to the CRPC cell line selection for *in vivo* experiment. Notably,

acinar adenocarcinomas make up over 90% of PCa cases, often originating from prostatic intraepithelial neoplasia (PIN) of the benign epithelium of the acini or ducts within the prostatic gland[24-26]. In contrast, the PC-3 cells used in our study, isolated from the bone metastasis of a CRPC patient, represent a rare, neuroendocrine cell type[27, 28]. Importantly, while CRPC emerges from androgen deprivation therapy (ADT)[16-18], ultimately leading to an androgen-independent growth[16-18, 29, 30], PC-3 cells lack androgen receptor (AR) expression[28]. As a result, additional validation using other PCa cell lines, which better represent the human PCa physiology, will be necessary for future studies to yield translational benefits enhancing patient survival. In this vein, the 22Rv1 CRPC cell line, exhibiting variable androgen sensitivity due to the expression of numerous AR splice variants, might provide valuable insights as it better portrays the PCa heterogeneity in patients[28, 31, 32]. Alternatively, LNCaP cells, derived from a lymph node metastasis of human prostate adenocarcinoma, could be employed to decipher the early stages of PCa tumorigenesis. These cells are not only androgen-sensitive but also retain functional AR signaling (Table 4.1)[28, 33]. Nevertheless, we found nearly undetectable mRNA and protein expression of CdGAP in LNCaP cells in our study, suggesting that a stable LNCaP cell line overexpressing CdGAP could be useful in future investigations.

Our study, utilizing subcutaneous xenograft models, faced an inherent limitations regarding the absence of tumor microenvironment, a pivotal factor in tumorigenesis and cancer metastasis[34]. Considering that metastases rather than the primary tumor, are largely responsible for cancer-related deaths[35], we further probed whether CdGAP depletion in the CRPC cell, PC-3, would impede PCa metastasis. For our study, shCon and shCdGAP PC-3 cells were orthotopically injected into the right dorsal lobe of athymic nude mice. These cells were modified to express luciferase prior to injection, facilitating non-invasive bioluminescence imaging (BLI) of xenografted mice for PCa progression monitoring.

Interestingly, we observed comparable growth of primary tumors in mice injected with shCon and shCdGAP PC-3 cells, contrasting our findings from subcutaneous xenograft models. This observation was substantiated by the similar sizes of primary tumors collected at the experimental endpoint, with no significant disparities in tumor weight and volume. This finding from the orthotopic xenograft models diverged from our observations in the subcutaneous xenograft models of PCa and from breast cancer cells, where a notable Ki-67 signal reduction was observed upon immunohistochemistry (IHC)[1]. On the contrary, through *ex vivo* carcass

imaging post-primary tumor removal, we demonstrated a substantial metastasis reduction when CdGAP was depleted in PC-3 cells. Specifically, we observed marked metastasis reductions to the intestine and bone in mice injected with shCdGAP PC-3 cells. These observations, underscoring the oncogenic role of CdGAP in CRPC cells, in conferring increased migratory and invasive potential leading to the enhanced ability to distantly metastasize, validated our findings from the TMA analysis where high levels of CdGAP were associated with an elevated bone metastasis risk.

Our study effectively illustrated numerous oncogenic roles of CdGAP underpinning PCa tumorigenesis, promoting cellular proliferation, facilitating cell death evasion (i.e., apoptosis), and increasing migratory and invasive potential. Despite our current findings underscoring the pivotal role of CdGAP in human cancer, where high expression levels have been linked to poor patient survival in breast cancer[1], the extent to which targeted CdGAP inhibition can benefit CRPC patients remains uncertain. This is mainly due to the absence of an ideal cell line that can accurately depict the complex and heterogenous nature of PCa[32]. Although PC-3 cells expressed significantly higher CdGAP levels compared to DU-145 and 22Rv1, they are cytologically distinct with their neuroendocrine origin[27], in contrast to the adenocarcinoma originating from epithelial origin, which represent over 90% of PCa patients[24-26]. This difference likely explains PC-3 cells forming osteolytic rather than the more common osteoblastic metastasis seen in in castration-resistant, metastatic prostate adenocarcinoma[28]. Hence, future studies employing orthotopic injection of a stable LNCaP cell line, modified to overexpress CdGAP and gain ADT resistance, may offer tremendous value. Despite the lengthy, time-consuming processes involved in these modifications, this approach would more accurately represent the molecular changes in human CRPC, validating our findings and assessing the therapeutic benefit of CdGAP targeting in PCa patients.

| Cell Line | Origin | Bone metastasis* | Genetic ancestry | AR expression (Protein) | PSA expression (Protein) | CdGAP expression (Protein) |
|---|---|---|---|---|---|---|
| LNCaP | Lymph node metastasis | Osteoblastic | EA | Yes | Yes | Very low |
| 22Rv1 | Xenograft | Osteolytic | N/A | Yes | Yes | Low |
| DU-145 | Brain metastasis | Osteolytic | EA | No | No | Low |
| PC-3 | Bone (vertebral) metastasis | Osteolytic | EA | No | No | High |

**Table 4.1: Characteristics of PCa cell lines utilized in Chapter 2.**

The origin of each cell line, mode of bone metastasis formed *in vivo* (mouse xenografts), ethnicity, and expression levels of AR, prostate-specific antigen (PSA), and CdGAP are summarized. The 22Rv1 cell line was initially reported to carry a mixed genetic ancestry, but a more comprehensive analysis performed later determined its European ancestry (EA). With the exception of LNCaP, CRPC cell lines utilized in our study have been reported to form osteolytic bone metastasis in mice.

This table was created based on findings presented in this study as well as information from Cunningham *et al.* (2015)[28], Woods-Burnham *et al*. (2017)[36], and Hooker *et al.* (2019)[37].

## *4.3 CdGAP is crucial for mouse placenta development*

In this study, we highlighted the crucial role of CdGAP in development and its potential contribution to the pathogenesis of AOS in humans. Despite significant advancements in large cohort studies, the molecular diagnosis of AOS remains challenging due to a rising number of sporadic cases not attributable to mutations in the six known genes. Thus, we generated a CdGAP-AOS KI mouse model to investigate how truncation mutations in CdGAP, as seen in CdGAP-AOS patients, lead to a range of embryonic abnormalities that underpin the pathogenesis of AOS.

Heterozygous mating resulted in incompletely penetrant lethality, causing a significant deviation in the genotype ratio of homozygous litters at wean from the expected Mendelian ratio (~10% vs 25%). This finding is in line with our previous research, where a global knockout of CdGAP led to incompletely penetrant embryonic lethality[6]. In this study, we observed a trend towards reduced body weight gain in homozygous pregnant mothers carrying the CdGAP truncation mutation during late gestation (> E15.5). This trend correlated with a decreased number of total or healthy pups at E18.5. We also noted significant changes in the gross morphology of the placenta along with abnormal embryos (i.e., resorbing).

In humans, dysfunctional placentas often underpin the pathogenesis of prenatal complications, such as intrauterine growth restriction (IUGR), stillbirth, and neonatal death. Such dysfunction often accompanies marked changes in placental morphology, including color, diameter, and weight[38, 39]. Despite some evidence suggesting a link between AOS pathogenesis and placental dysfunctions[11, 12], research has largely overlooked the role of the placenta in AOS patients. Therefore, this study considered not only the fetal weights at various gestational ages but also the weights of placentas across genotypes. We also compared placental efficiency, represented by the ratio of the embryo to placental weight[40, 41]. Along with changes in the gross morphology of the placenta, which were pale and poorly vascularized, we found that the placentas of severely affected homozygous embryos were dysfunctional during late gestation (> E15.0). This dysfunction was evidenced by significant reductions in embryonic weights, indicating severe growth restriction, starting at E15.5 and worsening until E18.5. Although the truncation mutation in CdGAP in mice correlated positively with an increased frequency of embryonic abnormalities, including pale liver, hypovascularization of superficial vessels on the skin, and edema, TTLD, characterized by limb defects, and ACC, often associated with scalp

defects – both major diagnostic criteria of AOS and frequently observed in human CdGAP-AOS patients[5, 42, 43] – were not observed. However, the pathogenic changes underlying placental defects in homozygous embryos warrant further investigation, as a wide array of embryonic abnormalities affecting various sites and incomplete embryonic lethality among these embryos, which led to pale and poorly vascularized placentas, support the vascular origin of AOS.

Before this study, it was widely accepted that embryonic lethality in mutant mouse models was primarily due to labyrinth defects, often summed up by the simple phrase, "small labyrinth"[44, 45]. However, the definitive mouse placenta is a complex, multi-layered structure, and its layers are interdependent[46]. Prior findings have indicated that labyrinth defects could occur as a secondary result of primary defects in the junctional zone[47]. In this study, we examined late-gestation (> E15.5) placentas histologically to gain further insight into the pathological changes underlying placental defects. From this analysis, we demonstrated not only that the labyrinth area was significantly reduced in placentas from severely affected homozygotes, but also that the fusion of SynTs, a major constituent of the labyrinth, was defective. The hemotrichorial organization of the placenta was frequently disrupted, as evidenced by the loss of tight apposition between the two SynT layers.

Using RNAscope, we demonstrated that CdGAP was highly expressed in the placenta, particularly in the labyrinth. Interestingly, although neither embryonic nor placental abnormalities were apparent at E12.5 when the definitive placenta completes its construction and begins to function[46, 48], vascular complexity was significantly affected in the placentas of male homozygous embryos. In these placentas, occupancy of the labyrinth by fetal blood spaces was reduced. Collectively, these observations emphasize that a truncation mutation in CdGAP, leading to the loss of a functional PRD, compromises the development and maturation of the labyrinth. This failure to meet increasing demands from the embryo during late gestation leads to embryonic deaths. Given the complexity of these processes, future studies will be needed to unravel the molecular mechanism by which CdGAP governs syncytial fusion. One potential avenue to explore involves CdGAP's role in regulating syncytin-2 expression. This regulation may be mediated by Glial Cells Missing Homolog 1 (GCM1) and p21, while p21 acting as a key player in ensuring that fusion occurs only in non-proliferative cells[49]. Our hypothesis gains credibility from our observation in Chapter 2 that p21 mRNA expression was significantly upregulated upon CdGAP knockdown in PC-3 cells. This led to increased apoptosis and cell

cycle arrests, highlighting the ability of CdGAP to modulate cell cycle regulation and apoptosis. The link between CdGAP and P21 presents an intriguing possibility, suggesting that CdGAP could be a crucial factor in guiding cellular decisions related to fusion through interaction with cell cycle regulators like p21.

The current consensus is that placental defects may arise from either defective syncytial fusion or defective placental angiogenesis. In previous studies, knocking out the fusogen *syncytin* led to severe placental defects during late gestation. These defects were due to not just defective syncytial fusion, but also to abnormal fetal endothelial cell morphologies, which suggest defective placental angiogenesis[50]. To better define the roles governed by CdGAP during placental development, we examined the distribution and morphologies of fetal endothelial cells in moderately or severely affected homozygous placentas in this study. However, contrary to the findings of Wang *et al.*, we found the morphologies of fetal endothelial cells to be comparable between homozygous and wild-type placentas. Furthermore, we demonstrated that even with reduced vascular complexity and defective syncytia, the lining of each fetal blood space by fetal endothelial cells remained comparable. Taken together, these observations suggest that truncation mutations in CdGAP predominantly influence syncytial fusion, resulting in labyrinth defects during late gestation.

Last, but certainly not least, in the field of placenta research, the consideration of placental sex has largely been overlooked. However, numerous pieces of evidence emphasize its significance. For instance, evolutionary changes have led males to prioritize growth pathways, ensuring the greatest chance of reproductive success. Yet, this emphasis has made males less adaptable to changes in the *in-utero* environment[51]. This notion is further bolstered by a growing body of findings that reveal an increased risk of adverse outcomes for males in relation to pregnancy complications, including conditions like preeclampsia, which can lead to growth restriction, preterm birth, and neonatal deaths[52-54]. In the current study, despite observing 1) pronounced effects on the development of the liver and brain among male *CdGAP* $^{KI/KI}$ (severe) embryos, and 2) reduced vascular complexity solely in male placentas at E12.5, there were generally no dimorphic changes evident in the gross morphologies or weights of the embryos and placentas. Interestingly, while not reaching statistical significance, we did observe a noticeably lower count of severely affected homozygous male embryos at E18.5.

Although additional research regarding placental sex may be beneficial, further investigation using our current experimental model, where embryos were obtained by crossing heterozygotes, will be challenging. This perspective aligns with previous findings from studies examining the association between changes in glycogen contents—a factor linked to prenatal complications like IUGR—and placental sex[44]. However, as noted by Roberts *et al.*, since litters share the same maternal circulation, correlative studies targeting metabolic changes with respect to placental sex in affected embryos may be difficult as they could be masked by the placental functions of unaffected littermates, which may confound the interpretation[55]. Therefore, in the current study, it may be possible that dimorphic responses due to placental sex were obscured by the effects of homozygous embryos sharing the same maternal circulation with their wild-type littermates.

## *4.4 Homozygous CdGAP-AOS mice show congenital heart defects*

In humans, CdGAP-AOS patients demonstrate an autosomal-dominant mode of inheritance, reflecting similarities with *NOTCH1, RBPJ*, and *DLL4*[56]. In sharp contrast, phenotypic abnormalities associated with TTLD and ACC were largely absent from the embryos examined in our study. Despite the detection of several embryonic abnormalities in heterozygous embryos – such as a pale liver, hypovascularization of superficial vessels on the skin, and edema – we did not encounter embryonic lethality, unlike in homozygous embryos. Additionally, placental dysfunction resulting from labyrinth defects was mostly absent, barring a few isolated incidents. Although further studies are necessary to unravel the molecular roles of CdGAP in placental development, it is plausible that the differences in placental structures between humans and mice could be the root of these observed discrepancies. SynTs, which oversee nutrient, gas, and waste exchanges between the developing embryo and the mother in both species, play pivotal roles from the early stages of human embryonic development by aiding the implantation process[57-59], unlike in mice. Hence, the functional implications of a truncation mutation in CdGAP, leading to suboptimal development of the syncytia, could potentially result in late-onset embryonic lethality in mice, with fewer embryonic abnormalities compared to humans.

Historically, clinical investigations of AOS patients have largely overlooked the placenta. Nonetheless, a growing body of research continues to underline its significance, given that this temporary organ can exert long-lasting effects on both the baby and the mother[60-62]. We were

particularly drawn to the existence of several axes between the placenta and the embryo, such as the extensively documented “placental-cardiovascular” or “placenta-heart” axis[63]. Similar to AOS, our molecular understanding of congenital heart defects, which are responsible for the majority of neonatal deaths, remains inadequate[64, 65]. This shortfall could be due to a limited research scope, primarily confined to the heart tissue[66, 67]. Therefore, we aimed to explore whether placental abnormalities, which are seldom reported among AOS patients, underpin the pathogenesis of congenital heart defects, impacting approximately 20% of AOS patients[7].

Using E15.5 embryos, a point at which both embryonic and placental abnormalities become evident, we demonstrated that the development of congenital hearts in severely affected homozygotes, with identifiable severe placental defects, was compromised. The thickness of the left and right ventricular walls and the interventricular septum was reduced, alongside an increase in myocardial layer non-compaction. Intriguingly, similar congenital anomalies were observed in moderately affected homozygous embryos, despite the absence of any overt gross morphological or histological abnormalities in the placenta. This discrepancy might stem from changes in placental blood flow. Indeed, Thornburg *et al.*, emphasized that since the direction of blood flow differs between the heart and the placenta, congenital hearts are exposed to shear stress from maternal blood flow[68].

Our study provides evidence suggesting that the CdGAP mutation leads to defective syncytial fusion, a characteristic finding in preeclamptic placentas[69, 70]. As preeclamptic women often experience hypertension[71-73], physiological changes relating to maternal blood flow could potentially underpin the pathogenesis of congenital heart defects. Supporting this hypothesis, we demonstrated, using placentas at E15.5 and at E18.5, that syncytial defects in the placentas of homozygous embryos appeared as regional defects, often observed towards the periphery or outer extremities within the labyrinth. These defects became more pronounced with increasing cellular atrophy until E18.5. Collectively, these observations align with various research findings, where regional variations in placental perfusions were associated with congenital heart defects[74], and defective organization of syncytia was observed concurrently with congenital heart defects and embryonic abnormalities[66, 75, 76]. This supports the notion that placental defects due to truncation mutations in CdGAP could underlie congenital heart defects. However, further studies are necessary to fully elucidate whether physiological changes in the mother, such as the onset of

hypertension and damage to renal or cardiac tissues, also result from placental dysfunctions in mothers carrying homozygous embryos.

The findings of our study contrast with previous clinical findings, which reported an almost complete absence of clinical manifestations of cardiac anomalies among AOS patients with mutations in *CDGAP* and *RBPJ*[5, 77, 78]. This discrepancy could be attributed to the lack of thorough prenatal diagnosis of AOS, where prenatal deaths potentially resulting from fatal congenital heart defects may have been overlooked. Supporting this idea, a mother from an AOS family experienced a stillbirth and prior placental dysfunctions. Her newborn baby, who was diagnosed with AOS, also exhibited a congenital heart defect and a hypertrophic placenta[11]. However, our current experimental design does not allow for a clear determination of the causality of congenital heart defects. Although our findings strongly resemble those from *ATP11a*-KO mice, which result in congenital heart defects and display severely disrupted syncytia[66, 75], we cannot conclusively attribute the observed placental defects to the congenital heart defects without further investigations using trophoblast-specific and epiblast or cardiomyocyte-specific mutant mouse models. Another limitation of our experimental design is the lack of spatiotemporal regulation of mutant CdGAP. CdGAP expression levels vary in both the placenta and cardiomyocytes. In the placenta, CdGAP expression levels continue to increase until E14.5, while in cardiomyocytes, they peak at E15.5. The importance of spatiotemporal regulation may be highlighted by differential effects that could result from α-Major Histocompatibility Complex (MHC)-Cre and β-MHC-Cre-driven genetic ablation in cardiomyocytes. Compared to α-MHC-Cre, β-MHC-Cre affects earlier stages of congenital heart development, with expression occurring as early as E8.0[79]. Future studies could implement a conditional knock-in system to better define the window of pathogenic events, thereby significantly enhancing clinical interventions.

In examining embryos at various gestational ages, we found that embryonic abnormalities appeared during late gestation, leading to incomplete penetrance of embryonic lethality. This observation aligns with reports by Woods *et al.*, who documented a common onset of embryonic lethality during the late stages of gestation (> E15.5), following the manifestation of labyrinth defects[44]. Whether earlier stages of placental development, such as chorioallantoic fusion, governing labyrinth formation through branching morphogenesis[80-82], were moderately comprised remains largely unknown. In light of this limitation, while E12.5 and E13.5 embryos

displayed comparable gross morphologies, pale yolk sacs were frequently observed among severely affected homozygous embryos at E15.5 (Figure 4.1). Though it is unlikely that chorioallantoic fusion was significantly comprised among homozygous embryos, as mouse models with defective chorioallantoic fusion exhibit embryonic lethality at earlier stages[83], further study, focused on understanding the role of CdGAP in chorioallantoic fusion may be beneficial.

Lastly, we have found that congenital hearts among moderately affected homozygotes exhibited similar issues, including a reduction in the thickness of the ventricular walls and interventricular septum. These changes often underpin cardiomyopathy[84]. Given that many of these moderately affected homozygotes often survive into adulthood, it becomes essential to delve deeper into the long-term physiological consequences of these abnormalities. Critically, it remains unknown whether these changes in the heart recover by adulthood or if they pose an increased risk for cardiac complications. Unearthing answers to these questions may be pivotal in identifying asymptomatic carriers, whose offspring could be at heightened risk.

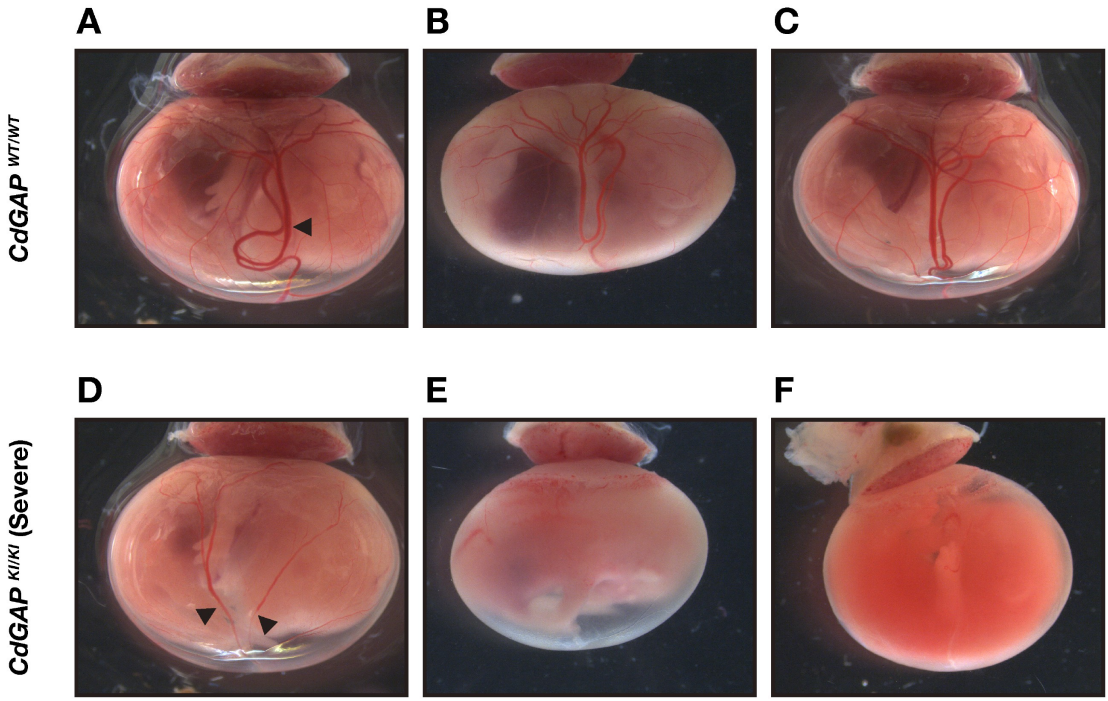


**Figure 4.1: Development of the yolk sac vasculature is defective among homozygous CdGAP AOS-KI embryos at E15.5.**

Dramatic changes in the gross morphology of the embryonic yolk sac are observed among *CdGAP* $^{KI/KI}$ (Severe) embryos at E15.5 (D - F). Compared to *CdGAP* $^{WT/WT}$ embryos (A - C), the blood vessels on the periphery of the yolk sac are markedly thinner (black arrowheads) or absent (E, F), leading to pale appearance of the yolk sac.

## *4.5 Conclusion and Perspectives*

As technology continues to advance at an extraordinary pace, an expanding body of research underscores the vital roles that CdGAP plays in various aspects of human life, including cancer and embryonic development. This thesis has illuminated two primary biological functions of CdGAP, specifically focusing on its aberrant functions linked to PCa tumorigenesis and developmental anomalies.

Our research, through a combination of *in vtiro* and *in vivo* studies, has underscored the oncogenic roles of CdGAP in prostate cancer. This function spans diverse aspects such as cellular proliferation, survival, and the capacity for metastasis to distant organs, including the bone. Furthermore, we have revealed a novel function of CdGAP in placental development using the first humanized mouse model of AOS. Notably, we uncovered that CdGAP mediates the fusion of two SynT layers within the labyrinth of the mouse placenta. Despite these significant findings, further research is necessary to assess the therapeutic potential of targeting CdGAP in prostate cancer patients. Furthermore, more exploration is needed to unravel the molecular mechanisms through which CdGAP regulates syncytial fusion. In summary, this thesis has not only deepened our understanding of CdGAP as an oncogene in human cancer but also provided substantial insights into its role in placental development.

Considering that placental defects can lead to embryonic abnormalities, including congenital heart defects, a leading cause of neonatal deaths, our findings hold substantial promise. They may provide the foundation for discovering common treatments for a range of rare diseases and could also improve the molecular diagnosis of individuals affected by these conditions. Pursuing these research avenues could yield substantial benefits, advancing our understanding of these diseases and fostering the development of more effective therapeutic strategies.

# Chapter 5: References

## Chapter 1: Literature Review


1. Hanahan, D. (2022). Hallmarks of Cancer: New Dimensions. *Cancer Discovery*, *12*(1), 31-46. https://doi.org/10.1158/2159-8290.CD-21-1059
2. Lee, M. Y. (2022). Embryonic Programs in Cancer and Metastasis—Insights From the Mammary Gland. *Frontiers in Cell and Developmental Biology*, *10*. https://www.frontiersin.org/articles/10.3389/fcell.2022.938625
3. Ferreira, C. R. (2019). The burden of rare diseases. *American Journal of Medical Genetics Part A*, *179*(6), 885-892. https://doi.org/10.1002/ajmg.a.61124
4. Wennerberg, K., Rossman, K. L., & Der, C. J. (2005). The Ras superfamily at a glance. *J Cell Sci*, *118*(Pt 5), 843-846. https://doi.org/10.1242/jcs.01660
5. Ellenbroek, S. I., & Collard, J. G. (2007). Rho GTPases: functions and association with cancer. *Clin Exp Metastasis*, *24*(8), 657-672. https://doi.org/10.1007/s10585-007-9119-1
6. Jaffe, A. B., & Hall, A. (2005). Rho GTPases: biochemistry and biology. *Annu Rev Cell Dev Biol*, *21*, 247-269. https://doi.org/10.1146/annurev.cellbio.21.020604.150721
7. Dvorsky, R., & Ahmadian, M. R. (2004). Always look on the bright site of Rho: structural implications for a conserved intermolecular interface. *EMBO Rep*, *5*(12), 1130-1136. https://doi.org/10.1038/sj.embor.7400293
8. Cherfils, J., & Zeghouf, M. (2013). Regulation of small GTPases by GEFs, GAPs, and GDIs. *Physiol Rev*, *93*(1), 269-309. https://doi.org/10.1152/physrev.00003.2012
9. Jaiswal, M., Dvorsky, R., & Ahmadian, M. R. (2013). Deciphering the molecular and functional basis of Dbl family proteins: a novel systematic approach toward classification of selective activation of the Rho family proteins. *J Biol Chem*, *288*(6), 4486-4500. https://doi.org/10.1074/jbc.M112.429746
10. Etienne-Manneville, S., & Hall, A. (2002). Rho GTPases in cell biology. *Nature*, *420*(6916), 629-635. https://doi.org/10.1038/nature01148
11. Ridley, A. J., & Hall, A. (1992). The small GTP-binding protein rho regulates the assembly of focal adhesions and actin stress fibers in response to growth factors. *Cell*, *70*(3), 389-399. https://doi.org/10.1016/0092-8674(92)90163-7
12. Nobes, C. D., & Hall, A. (1995). Rho, Rac, and Cdc42 GTPases regulate the assembly of multimolecular focal complexes associated with actin stress fibers, lamellipodia, and filopodia. *Cell*, *81*(1), 53-62. https://doi.org/10.1016/0092-8674(95)90370-4

13. Ridley, A. J., & Hall, A. (1992). Distinct patterns of actin organization regulated by the small GTP-binding proteins Rac and Rho. *Cold Spring Harbor symposia on quantitative biology*, *57*, 661–671. https://doi.org/10.1101/sqb.1992.057.01.072
14. Kozma, R., Ahmed, S., Best, A., & Lim, L. (1995). The Ras-Related Protein Cdc42Hs and Bradykinin Promote Formation of Peripheral Actin Microspikes and Filopodia in Swiss 3T3 Fibroblasts. *Molecular and Cellular Biology*, *15*(4), 1942-1952. https://doi.org/10.1128/MCB.15.4.1942
15. Haga, R. B., & Ridley, A. J. (2016). Rho GTPases: Regulation and roles in cancer cell biology. *Small GTPases*, *7*(4), 207-221. https://doi.org/10.1080/21541248.2016.1232583
16. Troeger, A., Chae, H. D., Senturk, M., Wood, J., & Williams, D. A. (2013). A unique carboxyl-terminal insert domain in the hematopoietic-specific, GTPase-deficient Rho GTPase RhoH regulates post-translational processing. *J Biol Chem*, *288*(51), 36451-36462. https://doi.org/10.1074/jbc.M113.505727
17. Garavini, H., Riento, K., Phelan, J. P., McAlister, M. S. B., Ridley, A. J., & Keep, N. H. (2002). Crystal Structure of the Core Domain of RhoE/Rnd3: A Constitutively Activated Small G Protein. *Biochemistry*, *41*(20), 6303-6310. https://doi.org/10.1021/bi025651h
18. Zubor, P., Dankova, Z., Kolkova, Z., Holubekova, V., Brany, D., Mersakova, S., Samec, M., Liskova, A., Koklesova, L., Kubatka, P., Bujnak, J., Kajo, K., Mlyncek, M., Giordano, F. A., & Golubnitschaja, O. (2020). Rho GTPases in Gynecologic Cancers: In-Depth Analysis toward the Paradigm Change from Reactive to Predictive, Preventive, and Personalized Medical Approach Benefiting the Patient and Healthcare. *Cancers (Basel)*, *12*(5). https://doi.org/10.3390/cancers12051292
19. Hodge, R. G., & Ridley, A. J. (2016). Regulating Rho GTPases and their regulators. *Nat Rev Mol Cell Biol*, *17*(8), 496-510. https://doi.org/10.1038/nrm.2016.67
20. Knyphausen, P., Kuhlmann, N., de Boor, S., & Lammers, M. (2015). Lysine-acetylation as a fundamental regulator of Ran function: Implications for signaling of proteins of the Ras-superfamily. *Small GTPases*, *6*(4), 189-195. https://doi.org/10.1080/21541248.2015.1103399
21. Wittinghofer, A., & Vetter, I. R. (2011). Structure-function relationships of the G domain, a canonical switch motif. *Annu Rev Biochem*, *80*, 943-971. https://doi.org/10.1146/annurev-biochem-062708-134043

22. Winter-Vann, A. M., & Casey, P. J. (2005). Post-prenylation-processing enzymes as new targets in oncogenesis. *Nature Reviews Cancer*, *5*(5), 405-412. https://doi.org/10.1038/nrc1612

23. Lang, P., Gesbert, F., Delespine-Carmagnat, M., Stancou, R., Pouchelet, M., & Bertoglio, J. (1996). Protein kinase A phosphorylation of RhoA mediates the morphological and functional effects of cyclic AMP in cytotoxic lymphocytes. *The EMBO Journal*, *15*(3), 510-519. https://doi.org/10.1002/j.1460-2075.1996.tb00383.x

24. Forget, M.-A., Desrosiers, R. R., Gingras, D., & BÉLiveau, R. (2002). Phosphorylation states of Cdc42 and RhoA regulate their interactions with Rho GDP dissociation inhibitor and their extraction from biological membranes. *Biochemical Journal*, *361*(2), 243-254. https://doi.org/10.1042/bj3610243

25. Bustelo, X. R., Sauzeau, V., & Berenjeno, I. M. (2007). GTP-binding proteins of the Rho/Rac family: regulation, effectors and functions in vivo. *Bioessays*, *29*(4), 356-370. https://doi.org/10.1002/bies.20558

26. Houssa, B., de Widt, J., Kranenburg, O., Moolenaar, W. H., & van Blitterswijk, W. J. (1999). Diacylglycerol Kinase θ Binds to and Is Negatively Regulated by Active RhoA*. *Journal of Biological Chemistry*, *274*(11), 6820-6822. https://doi.org/10.1074/jbc.274.11.6820

27. Illenberger, D., Schwald, F., Pimmer, D., Binder, W., Maier, G., Dietrich, A., & Gierschik, P. (1998). Stimulation of phospholipase C-beta2 by the Rho GTPases Cdc42Hs and Rac1. *EMBO J*, *17*(21), 6241-6249. https://doi.org/10.1093/emboj/17.21.6241

28. Mosaddeghzadeh, N., Kazemein Jasemi, N. S., Majolee, J., Zhang, S. C., Hordijk, P. L., Dvorsky, R., & Ahmadian, M. R. (2021). Electrostatic Forces Mediate the Specificity of RHO GTPase-GDI Interactions. *Int J Mol Sci*, *22*(22). https://doi.org/10.3390/ijms222212493

29. Garcia-Mata, R., Boulter, E., & Burridge, K. (2011). The 'invisible hand': regulation of RHO GTPases by RHOGDIs. *Nat Rev Mol Cell Biol*, *12*(8), 493-504. https://doi.org/10.1038/nrm3153

30. Moissoglu, K., & Schwartz, M. A. (2014). Spatial and temporal control of Rho GTPase functions. *Cell Logist*, *4*(2), e943618. https://doi.org/10.4161/21592780.2014.943618

31. DerMardirossian, C., & Bokoch, G. M. (2005). GDIs: central regulatory molecules in Rho GTPase activation. *Trends Cell Biol*, *15*(7), 356-363. https://doi.org/10.1016/j.tcb.2005.05.001

32. Xie, F., Shao, S., Aziz, A. U. R., Zhang, B., Wang, H., & Liu, B. (2017). Role of Rho-specific guanine nucleotide dissociation inhibitor alpha regulation in cell migration. *Acta Histochem*, *119*(3), 183-189. https://doi.org/10.1016/j.acthis.2017.01.008

33. Griner, E. M., & Theodorescu, D. (2012). The faces and friends of RhoGDI2. *Cancer Metastasis Rev*, *31*(3-4), 519-528. https://doi.org/10.1007/s10555-012-9376-6

34. de Leon-Bautista, M. P., Cardenas-Aguayo, M. D., Casique-Aguirre, D., Almaraz-Salinas, M., Parraguirre-Martinez, S., Olivo-Diaz, A., Thompson-Bonilla, M. D., & Vargas, M. (2016). Immunological and Functional Characterization of RhoGDI3 and Its Molecular Targets RhoG and RhoB in Human Pancreatic Cancerous and Normal Cells. *PLoS One*, *11*(11), e0166370. https://doi.org/10.1371/journal.pone.0166370

35. Brunet, N., Morin, A., & Olofsson, B. (2002). RhoGDI-3 regulates RhoG and targets this protein to the Golgi complex through its unique N-terminal domain. *Traffic*, *3*(5), 342-357. https://doi.org/10.1034/j.1600-0854.2002.30504.x

36. Cherfils, J., & Chardin, P. (1999). GEFs: structural basis for their activation of small GTP-binding proteins. *Trends in Biochemical Sciences*, *24*(8), 306-311. https://doi.org/10.1016/S0968-0004(99)01429-2

37. Guo, Z., Ahmadian, M. R., & Goody, R. S. (2005). Guanine Nucleotide Exchange Factors Operate by a Simple Allosteric Competitive Mechanism. *Biochemistry*, *44*(47), 15423-15429. https://doi.org/10.1021/bi0518601

38. Hutchinson, J. P., & Eccleston, J. F. (2000). Mechanism of Nucleotide Release from Rho by the GDP Dissociation Stimulator Protein. *Biochemistry*, *39*(37), 11348-11359. https://doi.org/10.1021/bi0007573

39. Rossman, K. L., Der, C. J., & Sondek, J. (2005). GEF means go: turning on RHO GTPases with guanine nucleotide-exchange factors. *Nat Rev Mol Cell Biol*, *6*(2), 167-180. https://doi.org/10.1038/nrm1587

40. Kunimura, K., Uruno, T., & Fukui, Y. (2020). DOCK family proteins: key players in immune surveillance mechanisms. *Int Immunol*, *32*(1), 5-15. https://doi.org/10.1093/intimm/dxz067

41. Srivastava, S. K., Wheelock, R. H., Aaronson, S. A., & Eva, A. (1986). Identification of the protein encoded by the human diffuse B-cell lymphoma (dbl) oncogene. *Proceedings of the National Academy of Sciences*, *83*(23), 8868-8872. https://doi.org/10.1073/pnas.83.23.8868

42. Hart, M. J., Eva, A., Evans, T., Aaronson, S. A., & Cerione, R. A. (1991). Catalysis of guanine nucleotide exchange on the CDC42Hs protein by the dbloncogene product. *Nature*, *354*(6351), 311-314. https://doi.org/10.1038/354311a0

43. Jaiswal, M., Dubey, B. N., Koessmeier, K. T., Gremer, L., & Ahmadian, M. R. (2012). Biochemical Assays to Characterize Rho GTPases. In F. Rivero (Ed.), *Rho GTPases: Methods and Protocols* (pp. 37-58). Springer New York. https://doi.org/10.1007/978-1-61779-442-1_3

44. Jaiswal, M., Gremer, L., Dvorsky, R., Haeusler, L. C., Cirstea, I. C., Uhlenbrock, K., & Ahmadian, M. R. (2011). Mechanistic insights into specificity, activity, and regulatory elements of the regulator of G-protein signaling (RGS)-containing Rho-specific guanine nucleotide exchange factors (GEFs) p115, PDZ-RhoGEF (PRG), and leukemia-associated RhoGEF (LARG). *J Biol Chem*, *286*(20), 18202-18212. https://doi.org/10.1074/jbc.M111.226431

45. Riento, K., Totty, N., Villalonga, P., Garg, R., Guasch, R., & Ridley, A. J. (2005). RhoE function is regulated by ROCK I-mediated phosphorylation. *EMBO J*, *24*(6), 1170-1180. https://doi.org/10.1038/sj.emboj.7600612

46. Kazemein Jasemi, N. S., Herrmann, C., Magdalena Estirado, E., Gremer, L., Willbold, D., Brunsveld, L., Dvorsky, R., & Ahmadian, M. R. (2021). The intramolecular allostery of GRB2 governing its interaction with SOS1 is modulated by phosphotyrosine ligands. *Biochem J*, *478*(14), 2793-2809. https://doi.org/10.1042/BCJ20210105

47. DiNitto, J. P., & Lambright, D. G. (2006). Membrane and juxtamembrane targeting by PH and PTB domains. *Biochim Biophys Acta*, *1761*(8), 850-867. https://doi.org/10.1016/j.bbalip.2006.04.008

48. Cook, D. R., Rossman, K. L., & Der, C. J. (2014). Rho guanine nucleotide exchange factors: regulators of Rho GTPase activity in development and disease. *Oncogene*, *33*(31), 4021-4035. https://doi.org/10.1038/onc.2013.362

49. Shi, L. (2013). Dock protein family in brain development and neurological disease. *Commun Integr Biol*, *6*(6), e26839. https://doi.org/10.4161/cib.26839

50. Chang, L., Yang, J., Jo, C. H., Boland, A., Zhang, Z., McLaughlin, S. H., Abu-Thuraia, A., Killoran, R. C., Smith, M. J., Cote, J. F., & Barford, D. (2020). Structure of the DOCK2-ELMO1 complex provides insights into regulation of the auto-inhibited state. *Nat Commun*, *11*(1), 3464. https://doi.org/10.1038/s41467-020-17271-9

51. Li, H., Yang, L., Fu, H., Yan, J., Wang, Y., Guo, H., Hao, X., Xu, X., Jin, T., & Zhang, N. (2013). Association between Galphai2 and ELMO1/Dock180 connects chemokine signalling with Rac activation and metastasis. *Nat Commun*, *4*, 1706. https://doi.org/10.1038/ncomms2680

52. Cimino, P. J., Sokal, I., Leverenz, J., Fukui, Y., & Montine, T. J. (2009). DOCK2 is a microglial specific regulator of central nervous system innate immunity found in normal and Alzheimer's disease brain. *Am J Pathol*, *175*(4), 1622-1630. https://doi.org/10.2353/ajpath.2009.090443

53. Cimino, P. J., Yang, Y., Li, X., Hemingway, J. F., Cherne, M. K., Khademi, S. B., Fukui, Y., Montine, K. S., Montine, T. J., & Keene, C. D. (2013). Ablation of the microglial protein DOCK2 reduces amyloid burden in a mouse model of Alzheimer's disease. *Exp Mol Pathol*, *94*(2), 366-371. https://doi.org/10.1016/j.yexmp.2013.01.002

54. Laurin, M., & Cote, J. F. (2014). Insights into the biological functions of Dock family guanine nucleotide exchange factors. *Genes Dev*, *28*(6), 533-547. https://doi.org/10.1101/gad.236349.113

55. Cote, J. F., & Vuori, K. (2002). Identification of an evolutionarily conserved superfamily of DOCK180-related proteins with guanine nucleotide exchange activity. *J Cell Sci*, *115*(Pt 24), 4901-4913. https://doi.org/10.1242/jcs.00219

56. Eberth, A., Dvorsky, R., Becker, C. F., Beste, A., Goody, R. S., & Ahmadian, M. R. (2005). Monitoring the real-time kinetics of the hydrolysis reaction of guanine nucleotide-binding proteins. *Biol Chem*, *386*(11), 1105-1114. https://doi.org/10.1515/BC.2005.127

57. Fidyk, N. J., & Cerione, R. A. (2002). Understanding the Catalytic Mechanism of GTPase-Activating Proteins: Demonstration of the Importance of Switch Domain

Stabilization in the Stimulation of GTP Hydrolysis. *Biochemistry*, *41*(52), 15644-15653. https://doi.org/10.1021/bi026413p

58. Tcherkezian, J., & Lamarche-Vane, N. (2007). Current knowledge of the large RhoGAP family of proteins. *Biology of the Cell*, *99*(2), 67-86. https://doi.org/10.1042/BC20060086

59. Amin, E., Jaiswal, M., Derewenda, U., Reis, K., Nouri, K., Koessmeier, K. T., Aspenstrom, P., Somlyo, A. V., Dvorsky, R., & Ahmadian, M. R. (2016). Deciphering the Molecular and Functional Basis of RHOGAP Family Proteins: A SYSTEMATIC APPROACH TOWARD SELECTIVE INACTIVATION OF RHO FAMILY PROTEINS. *J Biol Chem*, *291*(39), 20353-20371. https://doi.org/10.1074/jbc.M116.736967

60. Scheffzek, K., & Ahmadian, M. R. (2005). GTPase activating proteins: structural and functional insights 18 years after discovery. *Cell Mol Life Sci*, *62*(24), 3014-3038. https://doi.org/10.1007/s00018-005-5136-x

61. Barrett, T., Xiao, B., Dodson, E. J., Dodson, G., Ludbrook, S. B., Nurmahomed, K., Gamblin, S. J., Musacchio, A., Smerdon, S. J., & Eccleston, J. F. (1997). The structure of the GTPase-activating domain from p50rhoGAP. *Nature*, *385*(6615), 458-461. https://doi.org/10.1038/385458a0

62. Garrett, M. D., Self, A. J., van Oers, C., & Hall, A. (1989). Identification of distinct cytoplasmic targets for ras/R-ras and rho regulatory proteins. *Journal of Biological Chemistry*, *264*(1), 10-13. https://doi.org/10.1016/s0021-9258(17)31215-2

63. Diekmann, D., Brill, S., Garrett, M. D., Totty, N., Hsuan, J., Monfries, C., Hall, C., Lim, L., & Hall, A. (1991). Bcr encodes a GTPase-activating protein for p21rac. *Nature*, *351*(6325), 400-402. https://doi.org/10.1038/351400a0

64. Lancaster, C. A., Taylor-Harris, P. M., Self, A. J., Brill, S., van Erp, H. E., & Hall, A. (1994). Characterization of rhoGAP. A GTPase-activating protein for rho-related small GTPases. *Journal of Biological Chemistry*, *269*(2), 1137-1142. https://doi.org/10.1016/s0021-9258(17)42232-0

65. Trahey, M., & McCormick, F. (1987). A Cytoplasmic Protein Stimulates Normal N-ras p21 GTPase, But Does Not Affect Oncogenic Mutants. *Science*, *238*(4826), 542-545. https://doi.org/10.1126/science.2821624

66. Longenecker, K., Read, P., Derewenda, U., Dauter, Z., Liu, X., Garrard, S., Walker, L., Somlyo, A. V., Nakamoto, R. K., Somlyo, A. P., & Derewenda, Z. S. (1999). How

RhoGDI binds Rho. *Acta Crystallogr D Biol Crystallogr*, *55*(Pt 9), 1503-1515. https://doi.org/10.1107/s090744499900801x

67. Rittinger, K., Walker, P. A., Eccleston, J. F., Nurmahomed, K., Owen, D., Laue, E., Gamblin, S. J., & Smerdon, S. J. (1997). Crystal structure of a small G protein in complex with the GTPase-activating protein rhoGAP. *Nature*, *388*(6643), 693-697. https://doi.org/10.1038/41805
68. Vetter, I. R., & Wittinghofer, A. (2001). The Guanine Nucleotide-Binding Switch in Three Dimensions. *Science*, *294*(5545), 1299-1304. https://doi.org/10.1126/science.1062023
69. Scheffzek, K., Ahmadian, M. R., & Wittinghofer, A. (1998). GTPase-activating proteins: helping hands to complement an active site. *Trends in Biochemical Sciences*, *23*(7), 257-262. https://doi.org/10.1016/S0968-0004(98)01224-9
70. Rittinger, K., Walker, P. A., Eccleston, J. F., Smerdon, S. J., & Gamblin, S. J. (1997). Structure at 1.65 Å of RhoA and its GTPase-activating protein in complex with a transition-state analogue. *Nature*, *389*(6652), 758-762. https://doi.org/10.1038/39651
71. Rittinger, K., Taylor, W. R., Smerdon, S. J., & Gamblin, S. J. (1998). Support for shared ancestry of GAPs. *Nature*, *392*(6675), 448-448. https://doi.org/10.1038/33043
72. Scheffzek, K., Lautwein, A., Kabsch, W., Reza Ahmadian, M., & Wittinghofer, A. (1996). Crystal structure of the GTPase-activating domain of human p120GAP and implications for the interaction with Ras. *Nature*, *384*(6609), 591-596. https://doi.org/10.1038/384591a0
73. Graham, D. L., Eccleston, J. F., & Lowe, P. N. (1999). The Conserved Arginine in Rho-GTPase-Activating Protein Is Essential for Efficient Catalysis but Not for Complex Formation with Rho·GDP and Aluminum Fluoride. *Biochemistry*, *38*(3), 985-991. https://doi.org/10.1021/bi9821770
74. Eberth, A., Lundmark, R., Gremer, L., Dvorsky, R., Koessmeier, K. T., McMahon, H. T., & Ahmadian, M. R. (2009). A BAR domain-mediated autoinhibitory mechanism for RhoGAPs of the GRAF family. *Biochem J*, *417*(1), 371-377. https://doi.org/10.1042/BJ20081535
75. Minoshima, Y., Kawashima, T., Hirose, K., Tonozuka, Y., Kawajiri, A., Bao, Y. C., Deng, X., Tatsuka, M., Narumiya, S., May, W. S., Jr., Nosaka, T., Semba, K., Inoue, T., Satoh,

T., Inagaki, M., & Kitamura, T. (2003). Phosphorylation by Aurora B Converts MgcRacGAP to a RhoGAP during Cytokinesis. *Developmental Cell*, *4*(4), 549-560. https://doi.org/10.1016/S1534-5807(03)00089-3

76. Jaiswal, M., Dvorsky, R., Amin, E., Risse, S. L., Fansa, E. K., Zhang, S. C., Taha, M. S., Gauhar, A. R., Nakhaei-Rad, S., Kordes, C., Koessmeier, K. T., Cirstea, I. C., Olayioye, M. A., Haussinger, D., & Ahmadian, M. R. (2014). Functional cross-talk between ras and rho pathways: a Ras-specific GTPase-activating protein (p120RasGAP) competitively inhibits the RhoGAP activity of deleted in liver cancer (DLC) tumor suppressor by masking the catalytic arginine finger. *J Biol Chem*, *289*(10), 6839-6849. https://doi.org/10.1074/jbc.M113.527655
77. Yang, X. Y., Guan, M., Vigil, D., Der, C. J., Lowy, D. R., & Popescu, N. C. (2009). p120Ras-GAP binds the DLC1 Rho-GAP tumor suppressor protein and inhibits its RhoA GTPase and growth-suppressing activities. *Oncogene*, *28*(11), 1401-1409. https://doi.org/10.1038/onc.2008.498
78. Jefferson, A. B., & Majerus, P. W. (1995). Properties of type II inositol polyphosphate 5-phosphatase. *J Biol Chem*, *270*(16), 9370-9377. https://doi.org/10.1074/jbc.270.16.9370
79. Amin, E., Dubey, B. N., Zhang, S. C., Gremer, L., Dvorsky, R., Moll, J. M., Taha, M. S., Nagel-Steger, L., Piekorz, R. P., Somlyo, A. V., & Ahmadian, M. R. (2013). Rho-kinase: regulation, (dys)function, and inhibition. *Biol Chem*, *394*(11), 1399-1410. https://doi.org/10.1515/hsz-2013-0181
80. Narumiya, S., Tanji, M., & Ishizaki, T. (2009). Rho signaling, ROCK and mDia1, in transformation, metastasis and invasion. *Cancer Metastasis Rev*, *28*(1-2), 65-76. https://doi.org/10.1007/s10555-008-9170-7
81. Zhao, Z.-s., & Manser, E. (2005). PAK and other Rho-associated kinases – effectors with surprisingly diverse mechanisms of regulation. *Biochemical Journal*, *386*(2), 201-214. https://doi.org/10.1042/BJ20041638
82. Hedman, A. C., Smith, J. M., & Sacks, D. B. (2015). The biology of IQGAP proteins: beyond the cytoskeleton. *EMBO Rep*, *16*(4), 427-446. https://doi.org/10.15252/embr.201439834

83. Liu, C. A., Wang, M. J., Chi, C. W., Wu, C. W., & Chen, J. Y. (2004). Rho/Rhotekin-mediated NF-kappaB activation confers resistance to apoptosis. *Oncogene*, *23*(54), 8731-8742. https://doi.org/10.1038/sj.onc.1208106

84. Lamarche, N., Tapon, N., Stowers, L., Burbelo, P. D., Aspenström, P., Bridges, T., Chant, J., & Hall, A. (1996). Rac and Cdc42 Induce Actin Polymerization and G1 Cell Cycle Progression Independently of p65<sup>PAK</sup> and the JNK/SAPK MAP Kinase Cascade. *Cell*, *87*(3), 519-529. https://doi.org/10.1016/S0092-8674(00)81371-9

85. Dvorsky, R., Blumenstein, L., Vetter, I. R., & Ahmadian, M. R. (2004). Structural insights into the interaction of ROCKI with the switch regions of RhoA. *J Biol Chem*, *279*(8), 7098-7104. https://doi.org/10.1074/jbc.M311911200

86. Abdul-Manan, N., Aghazadeh, B., Liu, G. A., Majumdar, A., Ouerfelli, O., Siminovitch, K. A., & Rosen, M. K. (1999). Structure of Cdc42 in complex with the GTPase-binding domain of the 'Wiskott–Aldrich syndrome' protein. *Nature*, *399*(6734), 379-383. https://doi.org/10.1038/20726

87. Gizachew, D., Guo, W., Chohan, K. K., Sutcliffe, M. J., & Oswald, R. E. (2000). Structure of the Complex of Cdc42Hs with a Peptide Derived from P-21 Activated Kinase. *Biochemistry*, *39*(14), 3963-3971. https://doi.org/10.1021/bi992646d

88. Garrard, S. M., Capaldo, C. T., Gao, L., Rosen, M. K., Macara, I. G., & Tomchick, D. R. (2003). Structure of Cdc42 in a complex with the GTPase-binding domain of the cell polarity protein, Par6. *EMBO J*, *22*(5), 1125-1133. https://doi.org/10.1093/emboj/cdg110

89. Hemsath, L., Dvorsky, R., Fiegen, D., Carlier, M. F., & Ahmadian, M. R. (2005). An electrostatic steering mechanism of Cdc42 recognition by Wiskott-Aldrich syndrome proteins. *Mol Cell*, *20*(2), 313-324. https://doi.org/10.1016/j.molcel.2005.08.036

90. Martinelli, S., Krumbach, O. H. F., Pantaleoni, F., Coppola, S., Amin, E., Pannone, L., Nouri, K., Farina, L., Dvorsky, R., Lepri, F., Buchholzer, M., Konopatzki, R., Walsh, L., Payne, K., Pierpont, M. E., Vergano, S. S., Langley, K. G., Larsen, D., Farwell, K. D., . . . Mirzaa, G. M. (2018). Functional Dysregulation of CDC42 Causes Diverse Developmental Phenotypes. *Am J Hum Genet*, *102*(2), 309-320. https://doi.org/10.1016/j.ajhg.2017.12.015

91. Morreale, A., Venkatesan, M., Mott, H. R., Owen, D., Nietlispach, D., Lowe, P. N., & Laue, E. D. (2000). Structure of Cdc42 bound to the GTPase binding domain of PAK. *Nature Structural Biology*, *7*(5), 384-388. https://doi.org/10.1038/75158

92. Diebold, B. A., & Bokoch, G. M. (2001). Molecular basis for Rac2 regulation of phagocyte NADPH oxidase. *Nature Immunology*, *2*(3), 211-215. https://doi.org/10.1038/85259

93. Hoffman, G. R., & Cerione, R. A. (2001). Rac inserts its way into the immune response. *Nature Immunology*, *2*(3), 194-196. https://doi.org/10.1038/85240

94. Kinch, M. S., Clark, G. J., Der, C. J., & Burridge, K. (1995). Tyrosine phosphorylation regulates the adhesions of ras-transformed breast epithelia. *Journal of Cell Biology*, *130*(2), 461-471. https://doi.org/10.1083/jcb.130.2.461

95. Crosas-Molist, E., Samain, R., Kohlhammer, L., Orgaz, J. L., George, S. L., Maiques, O., Barcelo, J., & Sanz-Moreno, V. (2021). Rho GTPase signaling in cancer progression and dissemination. *Physiological Reviews*, *102*(1), 455-510. https://doi.org/10.1152/physrev.00045.2020

96. Khosravi-Far, R., Solski, P. A., Clark, G. J., Kinch, M. S., & Der, C. J. (1995). Activation of Rac1, RhoA, and mitogen-activated protein kinases is required for Ras transformation. *Mol Cell Biol*, *15*(11), 6443-6453. https://doi.org/10.1128/MCB.15.11.6443

97. Qiu, R.-G., Abo, A., McCormick, F., & Symons, M. (1997). Cdc42 Regulates Anchorage-Independent Growth and Is Necessary for Ras Transformation. *Molecular and Cellular Biology*, *17*(6), 3449-3458. https://doi.org/10.1128/MCB.17.6.3449

98. Murphy, G. A., Solski, P. A., Jillian, S. A., de la Ossa, P. P., D'Eustachio, P., Der, C. J., & Rush, M. G. (1999). Cellular functions of TC10, a Rho family GTPase: regulation of morphology, signal transduction and cell growth. *Oncogene*, *18*(26), 3831-3845. https://doi.org/10.1038/sj.onc.1202758

99. Shutes, A., Berzat, A. C., Cox, A. D., & Der, C. J. (2004). Atypical mechanism of regulation of the Wrch-1 Rho family small GTPase. *Curr Biol*, *14*(22), 2052-2056. https://doi.org/10.1016/j.cub.2004.11.011

100. Chenette, E. J., Abo, A., & Der, C. J. (2005). Critical and Distinct Roles of Amino- and Carboxyl-terminal Sequences in Regulation of the Biological Activity of the Chp

Atypical Rho GTPase *. *Journal of Biological Chemistry*, *280*(14), 13784-13792. https://doi.org/10.1074/jbc.M411300200

101. Crosas-Molist, E., Bertran, E., Rodriguez-Hernandez, I., Herraiz, C., Cantelli, G., Fabra, À., Sanz-Moreno, V., & Fabregat, I. (2017). The NADPH oxidase NOX4 represses epithelial to amoeboid transition and efficient tumour dissemination. *Oncogene*, *36*(21), 3002-3014. https://doi.org/10.1038/onc.2016.454

102. López-Luque, J., Bertran, E., Crosas-Molist, E., Maiques, O., Malfettone, A., Caja, L., Serrano, T., Ramos, E., Sanz-Moreno, V., & Fabregat, I. (2019). Downregulation of Epidermal Growth Factor Receptor in hepatocellular carcinoma facilitates Transforming Growth Factor-β-induced epithelial to amoeboid transition. *Cancer Letters*, *464*, 15-24. https://doi.org/10.1016/j.canlet.2019.08.011

103. Lin, R., Cerione, R. A., & Manor, D. (1999). Specific Contributions of the Small GTPases Rho, Rac, and Cdc42 to Dbl Transformation *. *Journal of Biological Chemistry*, *274*(33), 23633-23641. https://doi.org/10.1074/jbc.274.33.23633

104. Orgaz, J. L., Herraiz, C., & Sanz-Moreno, V. (2014). Rho GTPases modulate malignant transformation of tumor cells. *Small GTPases*, *5*(4), e983867. https://doi.org/10.4161/sgtp.29019

105. Lorenzo-Martín, L. F., Fernández-Parejo, N., Menacho-Márquez, M., Rodríguez-Fdez, S., Robles-Valero, J., Zumalave, S., Fabbiano, S., Pascual, G., García-Pedrero, J. M., Abad, A., García-Macías, M. C., González, N., Lorenzano-Menna, P., Pavón, M. A., González-Sarmiento, R., Segrelles, C., Paramio, J. M., Tubío, J. M. C., Rodrigo, J. P., . . . Bustelo, X. R. (2020). VAV2 signaling promotes regenerative proliferation in both cutaneous and head and neck squamous cell carcinoma. *Nature Communications*, *11*(1), 4788. https://doi.org/10.1038/s41467-020-18524-3

106. Khan, I., Rhett, J. M., & O'Bryan, J. P. (2020). Therapeutic targeting of RAS: New hope for drugging the “undruggable”. *Biochimica et Biophysica Acta (BBA) - Molecular Cell Research*, *1867*(2), 118570. https://doi.org/10.1016/j.bbamcr.2019.118570

107. Fritz, G., Brachetti, C., Bahlmann, F., Schmidt, M., & Kaina, B. (2002). Rho GTPases in human breast tumours: expression and mutation analyses and correlation with clinical parameters. *British Journal of Cancer*, *87*(6), 635-644. https://doi.org/10.1038/sj.bjc.6600510

108. del Pulgar, T. G., Benitah, S. A., Valerón, P. F., Espina, C., & Lacal, J. C. (2005). Rho GTPase expression in tumourigenesis: Evidence for a significant link. *Bioessays*, *27*(6), 602-613. https://doi.org/10.1002/bies.20238

109. Kamai, T., Yamanishi, T., Shirataki, H., Takagi, K., Asami, H., Ito, Y., & Yoshida, K.-I. (2004). Overexpression of RhoA, Rac1, and Cdc42 GTPases Is Associated with Progression in Testicular Cancer. *Clinical Cancer Research*, *10*(14), 4799-4805. https://doi.org/10.1158/1078-0432.CCR-0436-03

110. Prendergast, G. C., Khosravi-Far, R., Solski, P. A., Kurzawa, H., Lebowitz, P. F., & Der, C. J. (1995). Critical role of Rho in cell transformation by oncogenic Ras. *Oncogene*, *10*(12), 2289-2296.

111. Roux, P., Gauthier-Rouvière, C., Doucet-Brutin, S., & Fort, P. (1997). The small GTPases Cdc42Hs, Rac1 and RhoG delineate Raf-independent pathways that cooperate to transform NIH3T3 cells. *Current Biology*, *7*(9), 629-637. https://doi.org/10.1016/S0960-9822(06)00289-2

112. Sahai, E., Olson, M. F., & Marshall, C. J. (2001). Cross-talk between Ras and Rho signalling pathways in transformation favours proliferation and increased motility. *The EMBO Journal*, *20*(4), 755-766. https://doi.org/10.1093/emboj/20.4.755

113. Li, Z., Dong, X., Wang, Z., Liu, W., Deng, N., Ding, Y., Tang, L., Hla, T., Zeng, R., Li, L., & Wu, D. (2005). Regulation of PTEN by Rho small GTPases. *Nature Cell Biology*, *7*(4), 399-404. https://doi.org/10.1038/ncb1236

114. Bass, A. J., Thorsson, V., Shmulevich, I., Reynolds, S. M., Miller, M., Bernard, B., Hinoue, T., Laird, P. W., Curtis, C., Shen, H., Weisenberger, D. J., Schultz, N., Shen, R., Weinhold, N., Kelsen, D. P., Bowlby, R., Chu, A., Kasaian, K., Mungall, A. J., . . . Center, U. N. C. L. C. C. (2014). Comprehensive molecular characterization of gastric adenocarcinoma. *Nature*, *513*(7517), 202-209. https://doi.org/10.1038/nature13480

115. Nagata, Y., Kontani, K., Enami, T., Kataoka, K., Ishii, R., Totoki, Y., Kataoka, T. R., Hirata, M., Aoki, K., Nakano, K., Kitanaka, A., Sakata-Yanagimoto, M., Egami, S., Shiraishi, Y., Chiba, K., Tanaka, H., Shiozawa, Y., Yoshizato, T., Suzuki, H., . . . Ogawa, S. (2016). Variegated RHOA mutations in adult T-cell leukemia/lymphoma. *Blood*, *127*(5), 596-604. https://doi.org/10.1182/blood-2015-06-644948

116. Svensmark, J. H., & Brakebusch, C. (2019). Rho GTPases in cancer: friend or foe? *Oncogene*, *38*(50), 7447-7456. https://doi.org/10.1038/s41388-019-0963-7

117. Lawson, A. R. J., Abascal, F., Coorens, T. H. H., Hooks, Y., O'Neill, L., Latimer, C., Raine, K., Sanders, M. A., Warren, A. Y., Mahbubani, K. T. A., Bareham, B., Butler, T. M., Harvey, L. M. R., Cagan, A., Menzies, A., Moore, L., Colquhoun, A. J., Turner, W., Thomas, B., . . . Martincorena, I. (2020). Extensive heterogeneity in somatic mutation and selection in the human bladder. *Science*, *370*(6512), 75-82. https://doi.org/10.1126/science.aba8347

118. Benton, D., & Chernoff, J. (2020). A New Rho(d) Map to Diffuse Gastric Cancer. *Cancer Discovery*, *10*(2), 182-184. https://doi.org/10.1158/2159-8290.CD-19-1327

119. O'Hayre, M., Inoue, A., Kufareva, I., Wang, Z., Mikelis, C. M., Drummond, R. A., Avino, S., Finkel, K., Kalim, K. W., DiPasquale, G., Guo, F., Aoki, J., Zheng, Y., Lionakis, M. S., Molinolo, A. A., & Gutkind, J. S. (2016). Inactivating mutations in GNA13 and RHOA in Burkitt's lymphoma and diffuse large B-cell lymphoma: a tumor suppressor function for the Gα13/RhoA axis in B cells. *Oncogene*, *35*(29), 3771-3780. https://doi.org/10.1038/onc.2015.442

120. Kakiuchi, M., Nishizawa, T., Ueda, H., Gotoh, K., Tanaka, A., Hayashi, A., Yamamoto, S., Tatsuno, K., Katoh, H., Watanabe, Y., Ichimura, T., Ushiku, T., Funahashi, S., Tateishi, K., Wada, I., Shimizu, N., Nomura, S., Koike, K., Seto, Y., . . . Ishikawa, S. (2014). Recurrent gain-of-function mutations of RHOA in diffuse-type gastric carcinoma. *Nature Genetics*, *46*(6), 583-587. https://doi.org/10.1038/ng.2984

121. Wang, K., Yuen, S. T., Xu, J., Lee, S. P., Yan, H. H. N., Shi, S. T., Siu, H. C., Deng, S., Chu, K. M., Law, S., Chan, K. H., Chan, A. S. Y., Tsui, W. Y., Ho, S. L., Chan, A. K. W., Man, J. L. K., Foglizzo, V., Ng, M. K., Chan, A. S., . . . Leung, S. Y. (2014). Whole-genome sequencing and comprehensive molecular profiling identify new driver mutations in gastric cancer. *Nature Genetics*, *46*(6), 573-582. https://doi.org/10.1038/ng.2983

122. Zhang, H., Schaefer, A., Wang, Y., Hodge, R. G., Blake, D. R., Diehl, J. N., Papageorge, A. G., Stachler, M. D., Liao, J., Zhou, J., Wu, Z., Akarca, F. G., de Klerk, L. K., Derks, S., Pierobon, M., Hoadley, K. A., Wang, T. C., Church, G., Wong, K.-K., . . . Bass, A. J. (2020). Gain-of-Function RHOA Mutations Promote Focal Adhesion Kinase Activation

and Dependency in Diffuse Gastric Cancer. *Cancer Discovery*, *10*(2), 288-305. https://doi.org/10.1158/2159-8290.CD-19-0811

123. Palomero, T., Couronné, L., Khiabanian, H., Kim, M.-Y., Ambesi-Impiombato, A., Perez-Garcia, A., Carpenter, Z., Abate, F., Allegretta, M., Haydu, J. E., Jiang, X., Lossos, I. S., Nicolas, C., Balbin, M., Bastard, C., Bhagat, G., Piris, M. A., Campo, E., Bernard, O. A., . . . Ferrando, A. A. (2014). Recurrent mutations in epigenetic regulators, RHOA and FYN kinase in peripheral T cell lymphomas. *Nature Genetics*, *46*(2), 166-170. https://doi.org/10.1038/ng.2873

124. Sakata-Yanagimoto, M., Enami, T., Yoshida, K., Shiraishi, Y., Ishii, R., Miyake, Y., Muto, H., Tsuyama, N., Sato-Otsubo, A., Okuno, Y., Sakata, S., Kamada, Y., Nakamoto-Matsubara, R., Tran, N. B., Izutsu, K., Sato, Y., Ohta, Y., Furuta, J., Shimizu, S., . . . Chiba, S. (2014). Somatic RHOA mutation in angioimmunoblastic T cell lymphoma. *Nature Genetics*, *46*(2), 171-175. https://doi.org/10.1038/ng.2872

125. Yoo, H. Y., Sung, M. K., Lee, S. H., Kim, S., Lee, H., Park, S., Kim, S. C., Lee, B., Rho, K., Lee, J.-E., Cho, K.-H., Kim, W., Ju, H., Kim, J., Kim, S. J., Kim, W. S., Lee, S., & Ko, Y. H. (2014). A recurrent inactivating mutation in RHOA GTPase in angioimmunoblastic T cell lymphoma. *Nature Genetics*, *46*(4), 371-375. https://doi.org/10.1038/ng.2916

126. Cortes, J. R., Ambesi-Impiombato, A., Couronné, L., Quinn, S. A., Kim, C. S., da Silva Almeida, A. C., West, Z., Belver, L., Martin, M. S., Scourzic, L., Bhagat, G., Bernard, O. A., Ferrando, A. A., & Palomero, T. (2018). RHOA G17V Induces T Follicular Helper Cell Specification and Promotes Lymphomagenesis. *Cancer Cell*, *33*(2), 259-273.e257. https://doi.org/10.1016/j.ccell.2018.01.001

127. Davis, M. J., Ha, B. H., Holman, E. C., Halaban, R., Schlessinger, J., & Boggon, T. J. (2013). RAC1P29S is a spontaneously activating cancer-associated GTPase. *Proceedings of the National Academy of Sciences*, *110*(3), 912-917. https://doi.org/10.1073/pnas.1220895110

128. Cerami, E., Gao, J., Dogrusoz, U., Gross, B. E., Sumer, S. O., Aksoy, B. A., Jacobsen, A., Byrne, C. J., Heuer, M. L., Larsson, E., Antipin, Y., Reva, B., Goldberg, A. P., Sander, C., & Schultz, N. (2012). The cBio Cancer Genomics Portal: An Open Platform for

Exploring Multidimensional Cancer Genomics Data. *Cancer Discovery*, *2*(5), 401-404. https://doi.org/10.1158/2159-8290.CD-12-0095

129. Gao, J., Aksoy, B. A., Dogrusoz, U., Dresdner, G., Gross, B., Sumer, S. O., Sun, Y., Jacobsen, A., Sinha, R., Larsson, E., Cerami, E., Sander, C., & Schultz, N. (2013). Integrative Analysis of Complex Cancer Genomics and Clinical Profiles Using the cBioPortal. *Science Signaling*, *6*(269), pl1-pl1. https://doi.org/10.1126/scisignal.2004088
130. Hodis, E., Watson, Ian R., Kryukov, Gregory V., Arold, Stefan T., Imielinski, M., Theurillat, J.-P., Nickerson, E., Auclair, D., Li, L., Place, C., DiCara, D., Ramos, Alex H., Lawrence, Michael S., Cibulskis, K., Sivachenko, A., Voet, D., Saksena, G., Stransky, N., Onofrio, Robert C., . . . Chin, L. (2012). A Landscape of Driver Mutations in Melanoma. *Cell*, *150*(2), 251-263. https://doi.org/10.1016/j.cell.2012.06.024
131. Krauthammer, M., Kong, Y., Ha, B. H., Evans, P., Bacchiocchi, A., McCusker, J. P., Cheng, E., Davis, M. J., Goh, G., Choi, M., Ariyan, S., Narayan, D., Dutton-Regester, K., Capatana, A., Holman, E. C., Bosenberg, M., Sznol, M., Kluger, H. M., Brash, D. E., . . . Halaban, R. (2012). Exome sequencing identifies recurrent somatic RAC1 mutations in melanoma. *Nature Genetics*, *44*(9), 1006-1014. https://doi.org/10.1038/ng.2359
132. Lionarons, D. A., Hancock, D. C., Rana, S., East, P., Moore, C., Murillo, M. M., Carvalho, J., Spencer-Dene, B., Herbert, E., Stamp, G., Damry, D., Calado, D. P., Rosewell, I., Fritsch, R., Neubig, R. R., Molina-Arcas, M., & Downward, J. (2019). RAC1<sup>P29S</sup> Induces a Mesenchymal Phenotypic Switch via Serum Response Factor to Promote Melanoma Development and Therapy Resistance. *Cancer Cell*, *36*(1), 68-83.e69. https://doi.org/10.1016/j.ccell.2019.05.015
133. Watson, I. R., Li, L., Cabeceiras, P. K., Mahdavi, M., Gutschner, T., Genovese, G., Wang, G., Fang, Z., Tepper, J. M., Stemke-Hale, K., Tsai, K. Y., Davies, M. A., Mills, G. B., & Chin, L. (2014). The RAC1 P29S Hotspot Mutation in Melanoma Confers Resistance to Pharmacological Inhibition of RAF. *Cancer Research*, *74*(17), 4845-4852. https://doi.org/10.1158/0008-5472.CAN-14-1232-T
134. Vu, H. L., Rosenbaum, S., Purwin, T. J., Davies, M. A., & Aplin, A. E. (2015). RAC1 P29S regulates PD-L1 expression in melanoma. *Pigment Cell & Melanoma Research*, *28*(5), 590-598. https://doi.org/10.1111/pcmr.12392

135. Clark, E. A., Golub, T. R., Lander, E. S., & Hynes, R. O. (2000). Genomic analysis of metastasis reveals an essential role for RhoC. *Nature*, *406*(6795), 532-535. https://doi.org/10.1038/35020106

136. Hakem, A., Sanchez-Sweatman O Fau - You-Ten, A., You-Ten A Fau - Duncan, G., Duncan G Fau - Wakeham, A., Wakeham A Fau - Khokha, R., Khokha R Fau - Mak, T. W., & Mak, T. W. (2005). RhoC is dispensable for embryogenesis and tumor initiation but essential for metastasis. *Genes & development*, *19*(17), 1974–1979. https://doi.org/10.1101/gad.1310805

137. Lambert, A. W., Pattabiraman, D. R., & Weinberg, R. A. (2017). Emerging Biological Principles of Metastasis. *Cell*, *168*(4), 670-691. https://doi.org/10.1016/j.cell.2016.11.037

138. Bolado-Carrancio, A., Rukhlenko, O. S., Nikonova, E., Tsyganov, M. A., Wheeler, A., Garcia-Munoz, A., Kolch, W., von Kriegsheim, A., & Kholodenko, B. N. (2020). Periodic propagating waves coordinate RhoGTPase network dynamics at the leading and trailing edges during cell migration. *eLife*, *9*, e58165. https://doi.org/10.7554/eLife.58165

139. Sanz-Moreno, V., Gadea, G., Ahn, J., Paterson, H., Marra, P., Pinner, S., Sahai, E., & Marshall, C. J. (2008). Rac Activation and Inactivation Control Plasticity of Tumor Cell Movement. *Cell*, *135*(3), 510-523. https://doi.org/10.1016/j.cell.2008.09.043

140. Sahai, E., & Marshall, C. J. (2003). Differing modes of tumour cell invasion have distinct requirements for Rho/ROCK signalling and extracellular proteolysis. *Nature Cell Biology*, *5*(8), 711-719. https://doi.org/10.1038/ncb1019

141. Friedl, P., & Alexander, S. (2011). Cancer Invasion and the Microenvironment: Plasticity and Reciprocity. *Cell*, *147*(5), 992-1009. https://doi.org/10.1016/j.cell.2011.11.016

142. Pandya, P., Orgaz, J. L., & Sanz-Moreno, V. (2017). Modes of invasion during tumour dissemination. *Molecular Oncology*, *11*(1), 5-27. https://doi.org/10.1002/1878-0261.12019

143. Wolf, K., Mazo, I., Leung, H., Engelke, K., von Andrian, U. H., Deryugina, E. I., Strongin, A. Y., Bröcker, E.-B., & Friedl, P. (2003). Compensation mechanism in tumor cell migration : mesenchymal–amoeboid transition after blocking of pericellular proteolysis. *Journal of Cell Biology*, *160*(2), 267-277. https://doi.org/10.1083/jcb.200209006

144. Orgaz, J. L., Pandya, P., Dalmeida, R., Karagiannis, P., Sanchez-Laorden, B., Viros, A., Albrengues, J., Nestle, F. O., Ridley, A. J., Gaggioli, C., Marais, R., Karagiannis, S. N., & Sanz-Moreno, V. (2014). Diverse matrix metalloproteinase functions regulate cancer amoeboid migration. *Nature Communications*, *5*(1), 4255. https://doi.org/10.1038/ncomms5255

145. Lehmann, S., te Boekhorst, V., Odenthal, J., Bianchi, R., van Helvert, S., Ikenberg, K., Ilina, O., Stoma, S., Xandry, J., Jiang, L., Grenman, R., Rudin, M., & Friedl, P. (2017). Hypoxia Induces a HIF-1-Dependent Transition from Collective-to-Amoeboid Dissemination in Epithelial Cancer Cells. *Current Biology*, *27*(3), 392-400. https://doi.org/10.1016/j.cub.2016.11.057

146. Vennin, C., Chin, V. T., Warren, S. C., Lucas, M. C., Herrmann, D., Magenau, A., Melenec, P., Walters, S. N., del Monte-Nieto, G., Conway, J. R. W., Nobis, M., Allam, A. H., McCloy, R. A., Currey, N., Pinese, M., Boulghourjian, A., Zaratzian, A., Adam, A. A. S., Heu, C., . . . Timpson, P. (2017). Transient tissue priming via ROCK inhibition uncouples pancreatic cancer progression, sensitivity to chemotherapy, and metastasis. *Science Translational Medicine*, *9*(384), eaai8504. https://doi.org/10.1126/scitranslmed.aai8504

147. Croft, D. R., Sahai, E., Mavria, G., Li, S., Tsai, J., Lee, W. M. F., Marshall, C. J., & Olson, M. F. (2004). Conditional ROCK Activation In vivo Induces Tumor Cell Dissemination and Angiogenesis. *Cancer Research*, *64*(24), 8994-9001. https://doi.org/10.1158/0008-5472.CAN-04-2052

148. Georgouli, M., Herraiz, C., Crosas-Molist, E., Fanshawe, B., Maiques, O., Perdrix, A., Pandya, P., Rodriguez-Hernandez, I., Ilieva, K. M., Cantelli, G., Karagiannis, P., Mele, S., Lam, H., Josephs, D. H., Matias-Guiu, X., Marti, R. M., Nestle, F. O., Orgaz, J. L., Malanchi, I., . . . Sanz-Moreno, V. (2019). Regional Activation of Myosin II in Cancer Cells Drives Tumor Progression via a Secretory Cross-Talk with the Immune Microenvironment. *Cell*, *176*(4), 757-774.e723. https://doi.org/10.1016/j.cell.2018.12.038

149. Higashida, C., Miyoshi, T., Fujita, A., Oceguera-Yanez, F., Monypenny, J., Andou, Y., Narumiya, S., & Watanabe, N. (2004). Actin Polymerization-Driven Molecular

Movement of mDia1 in Living Cells. *Science*, *303*(5666), 2007-2010. https://doi.org/10.1126/science.1093923

150. Hetmanski, J. H. R., de Belly, H., Busnelli, I., Waring, T., Nair, R. V., Sokleva, V., Dobre, O., Cameron, A., Gauthier, N., Lamaze, C., Swift, J., del Campo, A., Starborg, T., Zech, T., Goetz, J. G., Paluch, E. K., Schwartz, J.-M., & Caswell, P. T. (2019). Membrane Tension Orchestrates Rear Retraction in Matrix-Directed Cell Migration. *Developmental Cell*, *51*(4), 460-475.e410. https://doi.org/10.1016/j.devcel.2019.09.006
151. Vicente-Manzanares, M., Ma, X., Adelstein, R. S., & Horwitz, A. R. (2009). Non-muscle myosin II takes centre stage in cell adhesion and migration. *Nature Reviews Molecular Cell Biology*, *10*(11), 778-790. https://doi.org/10.1038/nrm2786
152. Liu, Y.-J., Le Berre, M., Lautenschlaeger, F., Maiuri, P., Callan-Jones, A., Heuzé, M., Takaki, T., Voituriez, R., & Piel, M. (2015). Confinement and Low Adhesion Induce Fast Amoeboid Migration of Slow Mesenchymal Cells. *Cell*, *160*(4), 659-672. https://doi.org/10.1016/j.cell.2015.01.007
153. Bergert, M., Erzberger, A., Desai, R. A., Aspalter, I. M., Oates, A. C., Charras, G., Salbreux, G., & Paluch, E. K. (2015). Force transmission during adhesion-independent migration. *Nature Cell Biology*, *17*(4), 524-529. https://doi.org/10.1038/ncb3134
154. Ruprecht, V., Wieser, S., Callan-Jones, A., Smutny, M., Morita, H., Sako, K., Barone, V., Ritsch-Marte, M., Sixt, M., Voituriez, R., & Heisenberg, C.-P. (2015). Cortical Contractility Triggers a Stochastic Switch to Fast Amoeboid Cell Motility. *Cell*, *160*(4), 673-685. https://doi.org/10.1016/j.cell.2015.01.008
155. Sahai, E., Garcia-Medina, R., Pouysségur, J., & Vial, E. (2006). Smurf1 regulates tumor cell plasticity and motility through degradation of RhoA leading to localized inhibition of contractility. *Journal of Cell Biology*, *176*(1), 35-42. https://doi.org/10.1083/jcb.200605135
156. Gong, X., Didan, Y., Lock, J. G., & Strömblad, S. (2018). KIF13A-regulated RhoB plasma membrane localization governs membrane blebbing and blebby amoeboid cell migration. *The EMBO Journal*, *37*(17), e98994. https://doi.org/10.15252/embj.201898994

157. Kitzing, T. M., Wang, Y., Pertz, O., Copeland, J. W., & Grosse, R. (2010). Formin-like 2 drives amoeboid invasive cell motility downstream of RhoC. *Oncogene*, *29*(16), 2441-2448. https://doi.org/10.1038/onc.2009.515

158. Stoletov, K., Montel, V., Lester, R. D., Gonias, S. L., & Klemke, R. (2007). High-resolution imaging of the dynamic tumor cell–vascular interface in transparent zebrafish. *Proceedings of the National Academy of Sciences*, *104*(44), 17406-17411. https://doi.org/10.1073/pnas.0703446104

159. Roh-Johnson, M., Bravo-Cordero, J. J., Patsialou, A., Sharma, V. P., Guo, P., Liu, H., Hodgson, L., & Condeelis, J. (2014). Macrophage contact induces RhoA GTPase signaling to trigger tumor cell intravasation. *Oncogene*, *33*(33), 4203-4212. https://doi.org/10.1038/onc.2013.377

160. Zhou, Y., Liao, Q., Han, Y., Chen, J., Liu, Z., Ling, H., Zhang, J., Yang, W., Oyang, L., Xia, L., Wang, L., Wang, H., Xue, L., Wang, H., & Hu, B. (2016). Rac1 overexpression is correlated with epithelial mesenchymal transition and predicts poor prognosis in non-small cell lung cancer. *Journal of Cancer*, *7*(14), 2100-2109. https://doi.org/10.7150/jca.16198

161. Fang, D., Chen, H., Zhu, J. Y., Wang, W., Teng, Y., Ding, H. F., Jing, Q., Su, S. B., & Huang, S. (2017). Epithelial–mesenchymal transition of ovarian cancer cells is sustained by Rac1 through simultaneous activation of MEK1/2 and Src signaling pathways. *Oncogene*, *36*(11), 1546-1558. https://doi.org/10.1038/onc.2016.323

162. Shin, S., Buel, G. R., Nagiec, M. J., Han, M.-J., Roux, P. P., Blenis, J., & Yoon, S.-O. (2019). ERK2 regulates epithelial-to-mesenchymal plasticity through DOCK10-dependent Rac1/FoxO1 activation. *Proceedings of the National Academy of Sciences*, *116*(8), 2967-2976. https://doi.org/10.1073/pnas.1811923116

163. Herraiz, C., Calvo, F., Pandya, P., Cantelli, G., Rodriguez-Hernandez, I., Orgaz, J. L., Kang, N., Chu, T., Sahai, E., & Sanz-Moreno, V. (2016). Reactivation of p53 by a Cytoskeletal Sensor to Control the Balance Between DNA Damage and Tumor Dissemination. *JNCI: Journal of the National Cancer Institute*, *108*(1), djv289. https://doi.org/10.1093/jnci/djv289

164. Le Gal, K., Ibrahim, M. X., Wiel, C., Sayin, V. I., Akula, M. K., Karlsson, C., Dalin, M. G., Akyürek, L. M., Lindahl, P., Nilsson, J., & Bergo, M. O. (2015). Antioxidants can

increase melanoma metastasis in mice. *Science Translational Medicine*, *7*(308), 308re308-308re308. https://doi.org/10.1126/scitranslmed.aad3740

165. Cai, D., Chen, S.-C., Prasad, M., He, L., Wang, X., Choesmel-Cadamuro, V., Sawyer, Jessica K., Danuser, G., & Montell, Denise J. (2014). Mechanical Feedback through E-Cadherin Promotes Direction Sensing during Collective Cell Migration. *Cell*, *157*(5), 1146-1159. https://doi.org/10.1016/j.cell.2014.03.045
166. Wang, X., He, L., Wu, Y. I., Hahn, K. M., & Montell, D. J. (2010). Light-mediated activation reveals a key role for Rac in collective guidance of cell movement in vivo. *Nature Cell Biology*, *12*(6), 591-597. https://doi.org/10.1038/ncb2061
167. Holle, A. W., Govindan Kutty Devi, N., Clar, K., Fan, A., Saif, T., Kemkemer, R., & Spatz, J. P. (2019). Cancer Cells Invade Confined Microchannels via a Self-Directed Mesenchymal-to-Amoeboid Transition. *Nano Letters*, *19*(4), 2280-2290. https://doi.org/10.1021/acs.nanolett.8b04720
168. Ladhani, O., Sánchez-Martinez, C., Orgaz, J. L., Jimenez, B., & Volpert, O. V. (2011). Pigment Epithelium-Derived Factor Blocks Tumor Extravasation by Suppressing Amoeboid Morphology and Mesenchymal Proteolysis. *Neoplasia*, *13*(7), 633-IN611. https://doi.org/10.1593/neo.11446
169. Yang, W.-H., Lan, H.-Y., Huang, C.-H., Tai, S.-K., Tzeng, C.-H., Kao, S.-Y., Wu, K.-J., Hung, M.-C., & Yang, M.-H. (2012). RAC1 activation mediates Twist1-induced cancer cell migration. *Nature Cell Biology*, *14*(4), 366-374. https://doi.org/10.1038/ncb2455
170. Kwong, C. H., Adams, A. G., & Leto, T. L. (1995). Characterization of the Effector-specifying Domain of Rac Involved in NADPH Oxidase Activation (*). *Journal of Biological Chemistry*, *270*(34), 19868-19872. https://doi.org/10.1074/jbc.270.34.19868
171. Lapouge, K., Smith, S. J. M., Walker, P. A., Gamblin, S. J., Smerdon, S. J., & Rittinger, K. (2000). Structure of the TPR Domain of p67<sup>phox</sup> in Complex with Rac·GTP. *Molecular Cell*, *6*(4), 899-907. https://doi.org/10.1016/S1097-2765(05)00091-2
172. Diekmann, D., Abo, A., Johnston, C., Segal, A. W., & Hall, A. (1994). Interaction of Rac with p67phox and Regulation pf Phagocytic NADPH Oxidase Activity. *Science*, *265*(5171), 531-533. https://doi.org/10.1126/science.8036496

173. Revach, O.-Y., Winograd-Katz, S. E., Samuels, Y., & Geiger, B. (2016). The involvement of mutant Rac1 in the formation of invadopodia in cultured melanoma cells. *Experimental Cell Research*, *343*(1), 82-88. https://doi.org/10.1016/j.yexcr.2016.02.003

174. Block, J., Breitsprecher, D., Kühn, S., Winterhoff, M., Kage, F., Geffers, R., Duwe, P., Rohn, Jennifer L., Baum, B., Brakebusch, C., Geyer, M., Stradal, Theresia E. B., Faix, J., & Rottner, K. (2012). FMNL2 Drives Actin-Based Protrusion and Migration Downstream of Cdc42. *Current Biology*, *22*(11), 1005-1012. https://doi.org/10.1016/j.cub.2012.03.064

175. Kutys, M. L., & Yamada, K. M. (2014). An extracellular-matrix-specific GEF–GAP interaction regulates Rho GTPase crosstalk for 3D collagen migration. *Nature Cell Biology*, *16*(9), 909-917. https://doi.org/10.1038/ncb3026

176. Farrugia, A. J., Rodríguez, J., Orgaz, J. L., Lucas, M., Sanz-Moreno, V., & Calvo, F. (2020). CDC42EP5/BORG3 modulates SEPT9 to promote actomyosin function, migration, and invasion. *Journal of Cell Biology*, *219*(9), e201912159. https://doi.org/10.1083/jcb.201912159

177. Plutoni, C., Bazellieres, E., Le Borgne-Rochet, M., Comunale, F., Brugues, A., Séveno, M., Planchon, D., Thuault, S., Morin, N., Bodin, S., Trepat, X., & Gauthier-Rouvière, C. (2016). P-cadherin promotes collective cell migration via a Cdc42-mediated increase in mechanical forces. *Journal of Cell Biology*, *212*(2), 199-217. https://doi.org/10.1083/jcb.201505105

178. Gligorijevic, B., Wyckoff, J., Yamaguchi, H., Wang, Y., Roussos, E. T., & Condeelis, J. (2012). N-WASP-mediated invadopodium formation is involved in intravasation and lung metastasis of mammary tumors. *Journal of Cell Science*, *125*(3), 724-734. https://doi.org/10.1242/jcs.092726

179. Ju, J. A., & Gilkes, D. M. (2018). RhoB: Team Oncogene or Team Tumor Suppressor? *Genes*, *9*(2), 67. https://doi.org/10.3390/genes9020067

180. Liu, A.-x., Cerniglia, G. J., Bernhard, E. J., & Prendergast, G. C. (2001). RhoB is required to mediate apoptosis in neoplastically transformed cells after DNA damage. *Proceedings of the National Academy of Sciences*, *98*(11), 6192-6197. https://doi.org/10.1073/pnas.111137198

181. Liu, A.-X., Rane, N., Liu, J.-P., & Prendergast, G. C. (2001). RhoB Is Dispensable for Mouse Development, but It Modifies Susceptibility to Tumor Formation as Well as Cell

Adhesion and Growth Factor Signaling in Transformed Cells. *Molecular and Cellular Biology*, *21*(20), 6906-6912. https://doi.org/10.1128/MCB.21.20.6906-6912.2001

182. Jiang, K., Sun, J., Cheng, J., Djeu, J. Y., Wei, S., & Sebti, S. (2004). Akt Mediates Ras Downregulation of RhoB, a Suppressor of Transformation, Invasion, and Metastasis. *Molecular and Cellular Biology*, *24*(12), 5565-5576. https://doi.org/10.1128/MCB.24.12.5565-5576.2004

183. Villalonga, P., Guasch, R. M., Riento, K., & Ridley, A. J. (2004). RhoE Inhibits Cell Cycle Progression and Ras-Induced Transformation. *Molecular and Cellular Biology*, *24*(18), 7829-7840. https://doi.org/10.1128/MCB.24.18.7829-7840.2004

184. Zhang, C.-S., Liu, Q., Li, M., Lin, S.-Y., Peng, Y., Wu, D., Li, T. Y., Fu, Q., Jia, W., Wang, X., Ma, T., Zong, Y., Cui, J., Pu, C., Lian, G., Guo, H., Ye, Z., & Lin, S.-C. (2015). RHOBTB3 promotes proteasomal degradation of HIFα through facilitating hydroxylation and suppresses the Warburg effect. *Cell Research*, *25*(9), 1025-1042. https://doi.org/10.1038/cr.2015.90

185. Alexander, K., Yang, H.-S., & Hinds, P. W. (2004). Cellular Senescence Requires CDK5 Repression of Rac1 Activity. *Molecular and Cellular Biology*, *24*(7), 2808-2819. https://doi.org/10.1128/MCB.24.7.2808-2819.2004

186. Yang, H.-S., & Hinds, P. W. (2006). Phosphorylation of Ezrin by Cyclin-Dependent Kinase 5 Induces the Release of Rho GDP Dissociation Inhibitor to Inhibit Rac1 Activity in Senescent Cells. *Cancer Research*, *66*(5), 2708-2715. https://doi.org/10.1158/0008-5472.CAN-05-3141

187. Yoshizaki, H., Ohba, Y., Parrini, M.-C., Dulyaninova, N. G., Bresnick, A. R., Mochizuki, N., & Matsuda, M. (2004). Cell Type-specific Regulation of RhoA Activity during Cytokinesis *<sup></sup>. *Journal of Biological Chemistry*, *279*(43), 44756-44762. https://doi.org/10.1074/jbc.M402292200

188. Canman, J. C., Lewellyn, L., Laband, K., Smerdon, S. J., Desai, A., Bowerman, B., & Oegema, K. (2008). Inhibition of Rac by the GAP Activity of Centralspindlin Is Essential for Cytokinesis. *Science*, *322*(5907), 1543-1546. https://doi.org/10.1126/science.1163086

189. Joneson, T., & Bar-Sagi, D. (1999). Suppression of Ras-Induced Apoptosis by the Rac GTPase. *Molecular and Cellular Biology*, *19*(9), 5892-5901. https://doi.org/10.1128/MCB.19.9.5892

190. Friedland, J. C., Lakins, J. N., Kazanietz, M. G., Chernoff, J., Boettiger, D., & Weaver, V. M. (2007). α6β4 integrin activates Rac-dependent p21-activated kinase 1 to drive NF-κB-dependent resistance to apoptosis in 3D mammary acini. *Journal of Cell Science*, *120*(20), 3700-3712. https://doi.org/10.1242/jcs.03484

191. Faruqi, T. R., Gomez, D., Bustelo, X. R., Bar-Sagi, D., & Reich, N. C. (2001). Rac1 mediates STAT3 activation by autocrine IL-6. *Proceedings of the National Academy of Sciences*, *98*(16), 9014-9019. https://doi.org/10.1073/pnas.161281298

192. Normand, G., & King, R. W. (2010). Understanding Cytokinesis Failure. In R. Y. C. Poon (Ed.), *Polyploidization and Cancer* (pp. 27-55). Springer New York. https://doi.org/10.1007/978-1-4419-6199-0_3

193. Watanabe, S., Ando, Y., Yasuda, S., Hosoya, H., Watanabe, N., Ishizaki, T., & Narumiya, S. (2008). mDia2 Induces the Actin Scaffold for the Contractile Ring and Stabilizes Its Position during Cytokinesis in NIH 3T3 Cells. *Molecular Biology of the Cell*, *19*(5), 2328-2338. https://doi.org/10.1091/mbc.e07-10-1086

194. Serrano, M., Lin, A. W., McCurrach, M. E., Beach, D., & Lowe, S. W. (1997). Oncogenic ras Provokes Premature Cell Senescence Associated with Accumulation of p53 and p16<sup>INK4a</sup>. *Cell*, *88*(5), 593-602. https://doi.org/10.1016/S0092-8674(00)81902-9

195. Ogrunc, M., Di Micco, R., Liontos, M., Bombardelli, L., Mione, M., Fumagalli, M., Gorgoulis, V. G., & d'Adda di Fagagna, F. (2014). Oncogene-induced reactive oxygen species fuel hyperproliferation and DNA damage response activation. *Cell Death & Differentiation*, *21*(6), 998-1012. https://doi.org/10.1038/cdd.2014.16

196. Debidda, M., Williams, D. A., & Zheng, Y. (2006). Rac1 GTPase Regulates Cell Genomic Stability and Senescence *. *Journal of Biological Chemistry*, *281*(50), 38519-38528. https://doi.org/10.1074/jbc.M604607200

197. Biran, A., Perelmutter, M., Gal, H., Burton, D. G., Ovadya, Y., Vadai, E., Geiger, T., & Krizhanovsky, V. (2015). Senescent cells communicate via intercellular protein transfer. *Genes & development*, *29*(8), 791–802. https://doi.org/10.1101/gad.259341.115

198. Wang, L., Yang, L., Debidda, M., Witte, D., & Zheng, Y. (2007). Cdc42 GTPase-activating protein deficiency promotes genomic instability and premature aging-like

phenotypes. *Proceedings of the National Academy of Sciences*, *104*(4), 1248-1253. https://doi.org/10.1073/pnas.0609149104

199. Nguyen, T. H., Ralbovska, A., & Kugler, J.-M. (2020). RhoBTB Proteins Regulate the Hippo Pathway by Antagonizing Ubiquitination of LKB1. *G3 Genes|Genomes|Genetics*, *10*(4), 1319-1325. https://doi.org/10.1534/g3.120.401038
200. Valentijn, L. J., Koppen, A., van Asperen, R., Root, H. A., Haneveld, F., & Versteeg, R. (2005). Inhibition of a New Differentiation Pathway in Neuroblastoma by Copy Number Defects of N-myc, Cdc42, and nm23 Genes. *Cancer Research*, *65*(8), 3136-3145. https://doi.org/10.1158/0008-5472.CAN-04-2469
201. Yang, L., Wang, L., Kalfa, T. A., Cancelas, J. A., Shang, X., Pushkaran, S., Mo, J., Williams, D. A., & Zheng, Y. (2007). Cdc42 critically regulates the balance between myelopoiesis and erythropoiesis. *Blood*, *110*(12), 3853-3861. https://doi.org/10.1182/blood-2007-03-079582
202. Stengel, K., & Zheng, Y. (2011). Cdc42 in oncogenic transformation, invasion, and tumorigenesis. *Cellular Signalling*, *23*(9), 1415-1423. https://doi.org/10.1016/j.cellsig.2011.04.001
203. Martin-Belmonte, F., & Perez-Moreno, M. (2012). Epithelial cell polarity, stem cells and cancer. *Nature Reviews Cancer*, *12*(1), 23-38. https://doi.org/10.1038/nrc3169
204. Gudipaty, S. A., & Rosenblatt, J. (2017). Epithelial cell extrusion: Pathways and pathologies. *Seminars in Cell & Developmental Biology*, *67*, 132-140. https://doi.org/10.1016/j.semcdb.2016.05.010
205. Wu, S. K., Lagendijk, A. K., Hogan, B. M., Gomez, G. A., & Yap, A. S. (2015). Active contractility at E-cadherin junctions and its implications for cell extrusion in cancer. *Cell Cycle*, *14*(3), 315-322. https://doi.org/10.4161/15384101.2014.989127
206. Hogan, C., Dupré-Crochet, S., Norman, M., Kajita, M., Zimmermann, C., Pelling, A. E., Piddini, E., Baena-López, L. A., Vincent, J.-P., Itoh, Y., Hosoya, H., Pichaud, F., & Fujita, Y. (2009). Characterization of the interface between normal and transformed epithelial cells. *Nature Cell Biology*, *11*(4), 460-467. https://doi.org/10.1038/ncb1853
207. Rosenblatt, J., Raff, M. C., & Cramer, L. P. (2001). An epithelial cell destined for apoptosis signals its neighbors to extrude it by an actin- and myosin-dependent

mechanism. *Current Biology*, *11*(23), 1847-1857. https://doi.org/10.1016/S0960-9822(01)00587-5

208. Toivanen, R., & Shen, M. M. (2017). Prostate organogenesis: tissue induction, hormonal regulation and cell type specification. *Development*, *144*(8), 1382-1398. https://doi.org/10.1242/dev.148270

209. Murray, T. (2021). The Pathogenesis of Prostate Cancer. In B. S. N. KL (Ed.), *Prostate Cancer*. Exon Publications. https://doi.org/10.36255/exonpublications.prostatecancer.pathogenesis.2021

210. Lee, S. H., & Shen, M. M. (2015). Cell types of origin for prostate cancer. *Current Opinion in Cell Biology*, *37*, 35-41. https://doi.org/10.1016/j.ceb.2015.10.002

211. Blagoev, K. B., Iordanov, R., Zhou, M., Fojo, T., & Bates, S. E. (2020). Drug resistant cells with very large proliferative potential grow exponentially in metastatic prostate cancer. *Oncotarget*, *12*(1), 15-21. https://doi.org/10.18632/oncotarget.27855

212. Rebello, R. J., Oing, C., Knudsen, K. E., Loeb, S., Johnson, D. C., Reiter, R. E., Gillessen, S., Van der Kwast, T., & Bristow, R. G. (2021). Prostate cancer. *Nature Reviews Disease Primers*, *7*(1), 9. https://doi.org/10.1038/s41572-020-00243-0

213. Belkahla, S., Nahvi, I., Biswas, S., Nahvi, I., & Ben Amor, N. (2022). Advances and development of prostate cancer, treatment, and strategies: A systemic review. *Frontiers in Cell and Developmental Biology*, *10*, 991330. https://doi.org/10.3389/fcell.2022.991330

214. Buyyounouski, M. K., Choyke, P. L., McKenney, J. K., Sartor, O., Sandler, H. M., Amin, M. B., Kattan, M. W., & Lin, D. W. (2017). Prostate cancer – major changes in the American Joint Committee on Cancer eighth edition cancer staging manual. *CA: A Cancer Journal for Clinicians*, *67*(3), 245-253. https://doi.org/10.3322/caac.21391

215. Yap, T. A., Smith, A. D., Ferraldeschi, R., Al-Lazikani, B., Workman, P., & de Bono, J. S. (2016). Drug discovery in advanced prostate cancer: translating biology into therapy. *Nature Reviews Drug Discovery*, *15*(10), 699-718. https://doi.org/10.1038/nrd.2016.120

216. Society, A. C. *Cancer Facts & Figures 2023*. American Cancer Society. Retrieved June 30, 2023 from http://cancerstatisticscenter.cancer.org

217. Dasgupta, S., Srinidhi S Fau - Vishwanatha, J. K., & Vishwanatha, J. K. (2012). Oncogenic activation in prostate cancer progression and metastasis: Molecular insights

and future challenges. *Journal of carcinogenesis*, *11*, 4. https://doi.org/10.4103/1477-3163.93001

218. Humphrey, P. A., Moch, H., Cubilla, A. L., Ulbright, T. M., & Reuter, V. E. (2016). The 2016 WHO Classification of Tumours of the Urinary System and Male Genital Organs—Part B: Prostate and Bladder Tumours. *European Urology*, *70*(1), 106-119. https://doi.org/10.1016/j.eururo.2016.02.028
219. Epstein, J. I., Egevad, L., Amin, M. B., Delahunt, B., Srigley, J. R., Humphrey, P. A., & the Grading, C. (2016). The 2014 International Society of Urological Pathology (ISUP) Consensus Conference on Gleason Grading of Prostatic Carcinoma: Definition of Grading Patterns and Proposal for a New Grading System. *The American Journal of Surgical Pathology*, *40*(2), 244-252. https://doi.org/10.1097/PAS.0000000000000530
220. Barakzai, M. A. (2019). Prostatic Adenocarcinoma: A Grading from Gleason to the New Grade-Group System: A Historical and Critical Review. *Asian Pacific Journal of Cancer Prevention*, *20*(3), 661-666. https://doi.org/10.31557/APJCP.2019.20.3.661
221. Alizadeh, M., & Alizadeh, S. (2014). Survey of clinical and pathological characteristics and outcomes of patients with prostate cancer. *Global journal of health science*, *6*(7), 49-57. https://doi.org/10.5539/gjhs.v6n7p49
222. Brawer, M. K. Prostatic intraepithelial neoplasia: an overview. *Reviews in urology*, *7*(Suppl 3), S11–S18.
223. Kim, H. L., & Yang, X. J. (2002). Prevalence of high-grade prostatic intraepithelial neoplasia and its relationship to serum prostate specific antigen. *International braz j urol : official journal of the Brazilian Society of Urology*, *28*(5), 413-417.
224. Alexander, E. E., Qian, J., Wollan, P. C., Myers, R. P., & Bostwick, D. G. (1996). Prostatic intraepithelial neoplasia does not appear to raise serum prostate-specific antigen concentration. *Urology*, *47*(5), 693-698. https://doi.org/10.1016/S0090-4295(96)00004-0
225. Bostwick, D. G., & Qian, J. (2004). High-grade prostatic intraepithelial neoplasia. *Modern Pathology*, *17*(3), 360-379. https://doi.org/10.1038/modpathol.3800053
226. Dai, C., Heemers, H., & Sharifi, N. Androgen Signaling in Prostate Cancer. *Cold Spring Harbor perspectives in medicine*, *7*(9), a030452. https://doi.org/10.1101/cshperspect.a030452

227. Huggins, C., & Hodges, C. V. (1941). Studies on Prostatic Cancer. I. The Effect of Castration, of Estrogen and of Androgen Injection on Serum Phosphatases in Metastatic Carcinoma of the Prostate*. *Cancer Research*, *1*(4), 293-297.

228. Nadal, M., Prekovic, S., Gallastegui, N., Helsen, C., Abella, M., Zielinska, K., Gay, M., Vilaseca, M., Taulès, M., Houtsmuller, A. B., van Royen, M. E., Claessens, F., Fuentes-Prior, P., & Estébanez-Perpiñá, E. (2017). Structure of the homodimeric androgen receptor ligand-binding domain. *Nature Communications*, *8*(1), 14388. https://doi.org/10.1038/ncomms14388

229. van Royen, M. E., van Cappellen, W. A., de Vos, C., Houtsmuller, A. B., & Trapman, J. (2012). Stepwise androgen receptor dimerization. *Journal of Cell Science*, *125*(8), 1970-1979. https://doi.org/10.1242/jcs.096792

230. Van der Steen, T., Tindall, D. J., & Huang, H. (2013). Posttranslational Modification of the Androgen Receptor in Prostate Cancer. *International Journal of Molecular Sciences*, *14*(7), 14833-14859. https://doi.org/10.3390/ijms140714833

231. Faus, H., & Haendler, B. (2006). Post-translational modifications of steroid receptors. *Biomedicine & Pharmacotherapy*, *60*(9), 520-528. https://doi.org/10.1016/j.biopha.2006.07.082

232. Wadosky, K. M., & Koochekpour, S. (2016). Molecular mechanisms underlying resistance to androgen deprivation therapy in prostate cancer. *Oncotarget*, *7*, 64447-64470. https://doi.org/10.18632/oncotarget.10901

233. Sumanasuriya, S., & De Bono, J. (2018). Treatment of Advanced Prostate Cancer-A Review of Current Therapies and Future Promise. *Cold Spring Harbor perspectives in medicine*, *8*(6), a030635. https://doi.org/10.1101/cshperspect.a030635

234. De Maeseneer, D. J., Van Praet, C., Lumen, N., & Rottey, S. (2015). Battling resistance mechanisms in antihormonal prostate cancer treatment: Novel agents and combinations. *Urologic Oncology: Seminars and Original Investigations*, *33*(7), 310-321. https://doi.org/10.1016/j.urolonc.2015.01.008

235. Girling, J. S., Whitaker, H. C., Mills, I. G., & Neal, D. E. (2007). Pathogenesis of prostate cancer and hormone refractory prostate cancer. *Indian Journal of Urology*, *23*(1), 35-42. https://doi.org/10.4103/0970-1591.30265

236. Perdana, N. R., Mochtar Ca Fau - Umbas, R., Umbas R Fau - Hamid, A. R. A., & Hamid, A. R. The Risk Factors of Prostate Cancer and Its Prevention: A Literature Review. *Acta medica Indonesiana*, *48*(3), 228–238.

237. Ina, W., & Charles, S. M. (2012). Disparities in prostate cancer in African American men: What primary care physicians can do. *Cleveland Clinic Journal of Medicine*, *79*(5), 313. https://doi.org/10.3949/ccjm.79a.11001

238. DeSantis, C. E., Siegel, R. L., Sauer, A. G., Miller, K. D., Fedewa, S. A., Alcaraz, K. I., & Jemal, A. (2016). Cancer statistics for African Americans, 2016: Progress and opportunities in reducing racial disparities. *CA: A Cancer Journal for Clinicians*, *66*(4), 290-308. https://doi.org/10.3322/caac.21340

239. Nair, S. S., Chakravarty, D., Dovey, Z. S., Zhang, X., & Tewari, A. K. (2022). Why do African–American men face higher risks for lethal prostate cancer? *Current Opinion in Urology*, *32*(1), 96-101. https://doi.org/10.1097/MOU.0000000000000951

240. Darst, B. F., Wan, P., Sheng, X., Bensen, J. T., Ingles, S. A., Rybicki, B. A., Nemesure, B., John, E. M., Fowke, J. H., Stevens, V. L., Berndt, S. I., Huff, C. D., Strom, S. S., Park, J. Y., Zheng, W., Ostrander, E. A., Walsh, P. C., Srivastava, S., Carpten, J., . . . Haiman, C. A. (2020). A Germline Variant at 8q24 Contributes to Familial Clustering of Prostate Cancer in Men of African Ancestry. *European Urology*, *78*(3), 316-320. https://doi.org/10.1016/j.eururo.2020.04.060

241. Sridhar, G., Masho, S. W., Adera, T., Ramakrishnan, V., & Roberts, J. D. (2010). Association between family history of cancers and risk of prostate cancer. *Journal of Men's Health*, *7*(1), 45-54. https://doi.org/10.1016/j.jomh.2009.10.006

242. Vietri, M. T., D'Elia, G., Caliendo, G., Resse, M., Casamassimi, A., Passariello, L., Albanese, L., Cioffi, M., & Molinari, A. M. (2021). Hereditary Prostate Cancer: Genes Related, Target Therapy and Prevention. *International Journal of Molecular Sciences*, *22*(7), 3753. https://doi.org/10.3390/ijms22073753

243. Vickers, A. J., Cronin, A. M., Björk, T., Manjer, J., Nilsson, P. M., Dahlin, A., Bjartell, A., Scardino, P. T., Ulmert, D., & Lilja, H. (2010). Prostate specific antigen concentration at age 60 and death or metastasis from prostate cancer: case-control study. *BMJ*, *341*, c4521. https://doi.org/10.1136/bmj.c4521

244. Howlader, N., Noone, A. M., Krapcho, M., Garshell, J., Neyman, N., Altekruse, S. F., Kosary, C. L., Yu, M., Ruhl, J., Tatalovich, Z., Cho, Mariotto, A., Lewis, D. R., Chen, H. S. F. E. J., & Cronin, K. A. (2013). *SEER cancer statistics review, 1975-2010*. http://seer.cancer.gov/csr/1975_2010/

245. Jayadevappa, R., Chhatre, S., Johnson, J. C., & Malkowicz, S. B. (2011). Association between ethnicity and prostate cancer outcomes across hospital and surgeon volume groups. *Health Policy*, *99*(2), 97-106. https://doi.org/10.1016/j.healthpol.2010.07.014

246. Siegel, R. L., Miller, K. D., & Jemal, A. (2018). Cancer statistics, 2018. *CA: A Cancer Journal for Clinicians*, *68*(1), 7-30. https://doi.org/10.3322/caac.21442

247. Boeing, H. (2013). Obesity and cancer – The update 2013. *Best Practice & Research Clinical Endocrinology & Metabolism*, *27*(2), 219-227. https://doi.org/10.1016/j.beem.2013.04.005

248. Hu, M.-B., Xu, H., Bai, P.-D., Jiang, H.-W., & Ding, Q. (2014). Obesity has multifaceted impact on biochemical recurrence of prostate cancer: a dose–response meta-analysis of 36,927 patients. *Medical Oncology*, *31*(2), 829. https://doi.org/10.1007/s12032-013-0829-8

249. Huncharek, M., Haddock, K. S., Reid, R., & Kupelnick, B. (2010). Smoking as a Risk Factor for Prostate Cancer: A Meta-Analysis of 24 Prospective Cohort Studies. *American Journal of Public Health*, *100*(4), 693-701. https://doi.org/10.2105/AJPH.2008.150508

250. Baird, W. M., Hooven, L. A., & Mahadevan, B. (2005). Carcinogenic polycyclic aromatic hydrocarbon-DNA adducts and mechanism of action. *Environmental and Molecular Mutagenesis*, *45*(2-3), 106-114. https://doi.org/10.1002/em.20095

251. Gutt, R., Tonlaar, N., Kunnavakkam, R., Karrison, T., Weichselbaum, R. R., & Liauw, S. L. (2010). Statin Use and Risk of Prostate Cancer Recurrence in Men Treated With Radiation Therapy. *Journal of Clinical Oncology*, *28*(16), 2653-2659. https://doi.org/10.1200/JCO.2009.27.3003

252. Pauwels, E. K. J. (2011). The Protective Effect of the Mediterranean Diet: Focus on Cancer and Cardiovascular Risk. *Medical Principles and Practice*, *20*(2), 103-111. https://doi.org/10.1159/000321197

253. Bojková, B., Winklewski, P. J., & Wszedybyl-Winklewska, M. (2020). Dietary Fat and Cancer—Which Is Good, Which Is Bad, and the Body of Evidence. *International Journal of Molecular Sciences*, *21*(11), 4114. https://doi.org/10.3390/ijms21114114

254. Schultz, C., Meier, M., & Schmid, H.-P. (2011). Nutrition, dietary supplements and adenocarcinoma of the prostate. *Maturitas*, *70*(4), 339-342. https://doi.org/10.1016/j.maturitas.2011.08.007

255. Wilson, K. M., Shui, I. M., Mucci, L. A., & Giovannucci, E. (2015). Calcium and phosphorus intake and prostate cancer risk: a 24-y follow-up study2. *The American Journal of Clinical Nutrition*, *101*(1), 173-183. https://doi.org/10.3945/ajcn.114.088716

256. Corona, G., Baldi, E., & Maggi, M. (2011). Androgen regulation of prostate cancer: Where are we now? *Journal of Endocrinological Investigation*, *34*(3), 232-243. https://doi.org/10.1007/BF03347072

257. Taplin, M.-E., Bubley, G. J., Shuster, T. D., Frantz, M. E., Spooner, A. E., Ogata, G. K., Keer, H. N., & Balk, S. P. (1995). Mutation of the Androgen-Receptor Gene in Metastatic Androgen-Independent Prostate Cancer. *New England Journal of Medicine*, *332*(21), 1393-1398. https://doi.org/10.1056/NEJM199505253322101

258. Chen, C. D., Welsbie, D. S., Tran, C., Baek, S. H., Chen, R., Vessella, R., Rosenfeld, M. G., & Sawyers, C. L. (2004). Molecular determinants of resistance to antiandrogen therapy. *Nature Medicine*, *10*(1), 33-39. https://doi.org/10.1038/nm972

259. Visakorpi, T., Hyytinen, E., Koivisto, P., Tanner, M., Keinänen, R., Palmberg, C., Palotie, A., Tammela, T., Isola, J., & Kallioniemi, O.-P. (1995). In vivo amplification of the androgen receptor gene and progression of human prostate cancer. *Nature Genetics*, *9*(4), 401-406. https://doi.org/10.1038/ng0495-401

260. Gottlieb, B., Beitel, L. K., Nadarajah, A., Paliouras, M., & Trifiro, M. (2012). The androgen receptor gene mutations database: 2012 update. *Human Mutation*, *33*(5), 887-894. https://doi.org/10.1002/humu.22046

261. Koivisto, P., Kononen J Fau - Palmberg, C., Palmberg C Fau - Tammela, T., Tammela T Fau - Hyytinen, E., Hyytinen E Fau - Isola, J., Isola J Fau - Trapman, J., Trapman J Fau - Cleutjens, K., Cleutjens K Fau - Noordzij, A., Noordzij A Fau - Visakorpi, T., Visakorpi T Fau - Kallioniemi, O. P., & Kallioniemi, O. P. (1997). Androgen receptor gene

amplification: a possible molecular mechanism for androgen deprivation therapy failure in prostate cancer. *Cancer Research*, *57*(2), 314-319.

262. Tan, M. H. E., Li, J., Xu, H. E., Melcher, K., & Yong, E.-l. (2015). Androgen receptor: structure, role in prostate cancer and drug discovery. *Acta Pharmacologica Sinica*, *36*(1), 3-23. https://doi.org/10.1038/aps.2014.18

263. Heinlein, C. A., & Chang, C. (2004). Androgen Receptor in Prostate Cancer. *Endocrine Reviews*, *25*(2), 276-308. https://doi.org/10.1210/er.2002-0032

264. Craft, N., Shostak, Y., Carey, M., & Sawyers, C. L. (1999). A mechanism for hormone-independent prostate cancer through modulation of androgen receptor signaling by the HER-2/neu tyrosine kinase. *Nature Medicine*, *5*(3), 280-285. https://doi.org/10.1038/6495

265. Sarker, D., Reid, A. H. M., Yap, T. A., & de Bono, J. S. (2009). Targeting the PI3K/AKT Pathway for the Treatment of Prostate Cancer. *Clinical Cancer Research*, *15*(15), 4799-4805. https://doi.org/10.1158/1078-0432.CCR-08-0125

266. Shorning, B. Y., Dass, M. S., Smalley, M. J., & Pearson, H. B. (2020). The PI3K-AKT-mTOR Pathway and Prostate Cancer: At the Crossroads of AR, MAPK, and WNT Signaling. *International Journal of Molecular Sciences*, *21*(12), 4507. https://doi.org/10.3390/ijms21124507

267. MacGrogan, D., & Bookstein, R. (1997). Tumour suppressor genes in prostate cancer. *Seminars in Cancer Biology*, *8*(1), 11-19. https://doi.org/10.1006/scbi.1997.0048

268. Thienger, P., & Rubin, M. A. (2021). Prostate cancer hijacks the microenvironment. *Nature Cell Biology*, *23*(1), 3-5. https://doi.org/10.1038/s41556-020-00616-3

269. Moose, D. L., Krog, B. L., Kim, T.-H., Zhao, L., Williams-Perez, S., Burke, G., Rhodes, L., Vanneste, M., Breheny, P., Milhem, M., Stipp, C. S., Rowat, A. C., & Henry, M. D. (2020). Cancer Cells Resist Mechanical Destruction in Circulation via RhoA/Actomyosin-Dependent Mechano-Adaptation. *Cell Reports*, *30*(11), 3864-3874.e3866. https://doi.org/10.1016/j.celrep.2020.02.080

270. Reymond, N., Im, J. H., Garg, R., Vega, F. M., Borda d'Agua, B., Riou, P., Cox, S., Valderrama, F., Muschel, R. J., & Ridley, A. J. (2012). Cdc42 promotes transendothelial migration of cancer cells through β1 integrin. *Journal of Cell Biology*, *199*(4), 653-668. https://doi.org/10.1083/jcb.201205169

271. Goel, Hira L., Pursell, B., Shultz, Leonard D., Greiner, Dale L., Brekken, Rolf A., Vander Kooi, Craig W., & Mercurio, Arthur M. (2016). P-Rex1 Promotes Resistance to VEGF/VEGFR-Targeted Therapy in Prostate Cancer. *Cell Reports*, *14*(9), 2193-2208. https://doi.org/10.1016/j.celrep.2016.02.016

272. Bektic, J., Pfeil, K., Berger, A. P., Ramoner, R., Pelzer, A., Schäfer, G., Kofler, K., Bartsch, G., & Klocker, H. (2005). Small G-protein RhoE is underexpressed in prostate cancer and induces cell cycle arrest and apoptosis. *The Prostate*, *64*(4), 332-340. https://doi.org/10.1002/pros.20243

273. Lee, H. J., Diaz, M. F., Price, K. M., Ozuna, J. A., Zhang, S., Sevick-Muraca, E. M., Hagan, J. P., & Wenzel, P. L. (2017). Fluid shear stress activates YAP1 to promote cancer cell motility. *Nature Communications*, *8*(1), 14122. https://doi.org/10.1038/ncomms14122

274. Chang, M. T., Asthana, S., Gao, S. P., Lee, B. H., Chapman, J. S., Kandoth, C., Gao, J., Socci, N. D., Solit, D. B., Olshen, A. B., Schultz, N., & Taylor, B. S. (2016). Identifying recurrent mutations in cancer reveals widespread lineage diversity and mutational specificity. *Nature Biotechnology*, *34*(2), 155-163. https://doi.org/10.1038/nbt.3391

275. Li, Z., Liu, Q., Piao, J., Hua, F., Wang, J., Jin, G., Lin, Z., & Zhang, Y. (2016). Clinicopathological implications of Tiam1 overexpression in invasive ductal carcinoma of the breast. *BMC Cancer*, *16*(1), 681. https://doi.org/10.1186/s12885-016-2724-0

276. Gao, Y., Dickerson, J. B., Guo, F., Zheng, J., & Zheng, Y. (2004). Rational design and characterization of a Rac GTPase-specific small molecule inhibitor. *Proceedings of the National Academy of Sciences*, *101*(20), 7618-7623. https://doi.org/10.1073/pnas.0307512101

277. Zins, K., Lucas, T., Reichl, P., Abraham, D., & Aharinejad, S. (2013). A Rac1/Cdc42 GTPase-Specific Small Molecule Inhibitor Suppresses Growth of Primary Human Prostate Cancer Xenografts and Prolongs Survival in Mice. *PLoS One*, *8*(9), e74924. https://doi.org/10.1371/journal.pone.0074924

278. Friesland, A., Zhao, Y., Chen, Y.-H., Wang, L., Zhou, H., & Lu, Q. (2013). Small molecule targeting Cdc42–intersectin interaction disrupts Golgi organization and suppresses cell motility. *Proceedings of the National Academy of Sciences*, *110*(4), 1261-1266. https://doi.org/10.1073/pnas.1116051110

279. Rath, N., & Olson, M. F. (2012). Rho-associated kinases in tumorigenesis: re-considering ROCK inhibition for cancer therapy. *EMBO reports*, *13*(10), 900-908. https://doi.org/10.1038/embor.2012.127

280. Somlyo, A. V., Bradshaw, D., Ramos, S., Murphy, C., Myers, C. E., & Somlyo, A. P. (2000). Rho-Kinase Inhibitor Retards Migration and in Vivo Dissemination of Human Prostate Cancer Cells. *Biochemical and Biophysical Research Communications*, *269*(3), 652-659. https://doi.org/10.1006/bbrc.2000.2343

281. Duquette, P. M., & Lamarche-Vane, N. (2014). Rho GTPases in embryonic development. *Small GTPases*, *5*(2), e972857. https://doi.org/10.4161/sgtp.29716

282. Sugihara, K., Nakatsuji, N., Nakamura, K., Nakao, K., Hashimoto, R., Otani, H., Sakagami, H., Kondo, H., Nozawa, S., Aiba, A., & Katsuki, M. (1998). Rac1 is required for the formation of three germ layers during gastrulation. *Oncogene*, *17*(26), 3427-3433. https://doi.org/10.1038/sj.onc.1202595

283. Chen, F., Ma, L., Parrini, M. C., Mao, X., Lopez, M., Wu, C., Marks, P. W., Davidson, L., Kwiatkowski, D. J., Kirchhausen, T., Orkin, S. H., Rosen, F. S., Mayer, B. J., Kirschner, M. W., & Alt, F. W. (2000). Cdc42 is required for PIP2-induced actin polymerization and early development but not for cell viability. *Current Biology*, *10*(13), 758-765. https://doi.org/10.1016/S0960-9822(00)00571-6

284. Pedersen, E., & Brakebusch, C. (2012). Rho GTPase function in development: How in vivo models change our view. *Experimental Cell Research*, *318*(14), 1779-1787. https://doi.org/10.1016/j.yexcr.2012.05.004

285. Southgate, L., Machado, Rajiv D., Snape, Katie M., Primeau, M., Dafou, D., Ruddy, Deborah M., Branney, Peter A., Fisher, M., Lee, Grace J., Simpson, Michael A., He, Y., Bradshaw, Teisha Y., Blaumeiser, B., Winship, William S., Reardon, W., Maher, Eamonn R., FitzPatrick, David R., Wuyts, W., Zenker, M., . . . Trembath, Richard C. (2011). Gain-of-Function Mutations of ARHGAP31, a Cdc42/Rac1 GTPase Regulator, Cause Syndromic Cutis Aplasia and Limb Anomalies. *The American Journal of Human Genetics*, *88*(5), 574-585. https://doi.org/10.1016/j.ajhg.2011.04.013

286. Sankhyan, N., Kaushal, R. K., & Jaswal, R. S. (2006). Adams–Oliver syndrome: A case with complete expression. *The Journal of Dermatology*, *33*(6), 435-436. https://doi.org/10.1111/j.1346-8138.2006.00104.x

287. Bonafede, R. P., & Beighton, P. (1979). Autosomal dominant inheritance of scalp defects with ectrodactyly. *American Journal of Medical Genetics*, *3*(1), 35-41. https://doi.org/10.1002/ajmg.1320030109

288. Wu, X., Tu, X., Joeng, K. S., Hilton, M. J., Williams, D. A., & Long, F. (2008). Rac1 Activation Controls Nuclear Localization of β-catenin during Canonical Wnt Signaling. *Cell*, *133*(2), 340-353. https://doi.org/10.1016/j.cell.2008.01.052

289. Aizawa, R., Yamada, A., Suzuki, D., Iimura, T., Kassai, H., Harada, T., Tsukasaki, M., Yamamoto, G., Tachikawa, T., Nakao, K., Yamamoto, M., Yamaguchi, A., Aiba, A., & Kamijo, R. (2012). Cdc42 is required for chondrogenesis and interdigital programmed cell death during limb development. *Mechanisms of Development*, *129*(1), 38-50. https://doi.org/10.1016/j.mod.2012.02.002

290. Migeotte, I., Grego-Bessa, J., & Anderson, K. V. (2011). Rac1 mediates morphogenetic responses to intercellular signals in the gastrulating mouse embryo. *Development*, *138*(14), 3011-3020. https://doi.org/10.1242/dev.059766

291. Migeotte, I., Omelchenko, T., Hall, A., & Anderson, K. V. (2010). Rac1-Dependent Collective Cell Migration Is Required for Specification of the Anterior-Posterior Body Axis of the Mouse. *PLOS Biology*, *8*(8), e1000442. https://doi.org/10.1371/journal.pbio.1000442

292. Arnold, S. J., & Robertson, E. J. (2009). Making a commitment: cell lineage allocation and axis patterning in the early mouse embryo. *Nature Reviews Molecular Cell Biology*, *10*(2), 91-103. https://doi.org/10.1038/nrm2618

293. Wu, X., Li, S., Chrostek-Grashoff, A., Czuchra, A., Meyer, H., Yurchenco, P. D., & Brakebusch, C. (2007). Cdc42 is crucial for the establishment of epithelial polarity during early mammalian development. *Developmental Dynamics*, *236*(10), 2767-2778. https://doi.org/10.1002/dvdy.21309

294. Bryant, D. M., & Mostov, K. E. (2008). From cells to organs: building polarized tissue. *Nature Reviews Molecular Cell Biology*, *9*(11), 887-901. https://doi.org/10.1038/nrm2523

295. Mellman, I., & Nelson, W. J. (2008). Coordinated protein sorting, targeting and distribution in polarized cells. *Nature Reviews Molecular Cell Biology*, *9*(11), 833-845. https://doi.org/10.1038/nrm2525

296. Martin-Belmonte, F., Gassama, A., Datta, A., Yu, W., Rescher, U., Gerke, V., & Mostov, K. (2007). PTEN-Mediated Apical Segregation of Phosphoinositides Controls Epithelial Morphogenesis through Cdc42. *Cell*, *128*(2), 383-397. https://doi.org/10.1016/j.cell.2006.11.051

297. Marchiando, A. M., Graham, W. V., & Turner, J. R. (2010). Epithelial Barriers in Homeostasis and Disease. *Annual Review of Pathology: Mechanisms of Disease*, *5*(1), 119-144. https://doi.org/10.1146/annurev.pathol.4.110807.092135

298. Kesavan, G., Sand, F. W., Greiner, T. U., Johansson, J. K., Kobberup, S., Wu, X., Brakebusch, C., & Semb, H. (2009). Cdc42-Mediated Tubulogenesis Controls Cell Specification. *Cell*, *139*(4), 791-801. https://doi.org/10.1016/j.cell.2009.08.049

299. Wan, H., Liu, C., Wert, S. E., Xu, W., Liao, Y., Zheng, Y., & Whitsett, J. A. (2013). CDC42 is required for structural patterning of the lung during development. *Developmental Biology*, *374*(1), 46-57. https://doi.org/10.1016/j.ydbio.2012.11.030

300. Scott, R. P., Hawley, S. P., Ruston, J., Du, J., Brakebusch, C., Jones, N., & Pawson, T. (2012). Podocyte-Specific Loss of Cdc42 Leads to Congenital Nephropathy. *Journal of the American Society of Nephrology*, *23*(7), 1149-1154. https://doi.org/10.1681/ASN.2011121206

301. Lamarche-Vane, N., & Hall, A. (1998). CdGAP, a Novel Proline-rich GTPase-activating Protein for Cdc42 and Rac *. *Journal of Biological Chemistry*, *273*(44), 29172-29177. https://doi.org/10.1074/jbc.273.44.29172

302. Tcherkezian, J., Triki, I., Stenne, R., Danek, E. I., & Lamarche-Vane, N. (2006). The human orthologue of CdGAP is a phosphoprotein and a GTPase-activating protein for Cdc42 and Rac1 but not RhoA. *Biology of the Cell*, *98*(8), 445-456. https://doi.org/10.1042/BC20050101

303. Tcherkezian, J., Danek, E. I., Jenna, S., Triki, I., & Lamarche-Vane, N. (2005). Extracellular Signal-Regulated Kinase 1 Interacts with and Phosphorylates CdGAP at an Important Regulatory Site. *Molecular and Cellular Biology*, *25*(15), 6314-6329. https://doi.org/10.1128/MCB.25.15.6314-6329.2005

304. Jenna, S., Hussain, N. K., Danek, E. I., Triki, I., Wasiak, S., McPherson, P. S., & Lamarche-Vane, N. (2002). The Activity of the GTPase-activating Protein CdGAP Is

Regulated by the Endocytic Protein Intersectin *. *Journal of Biological Chemistry*, *277*(8), 6366-6373. https://doi.org/10.1074/jbc.M105516200

305. LaLonde, D. P., Grubinger, M., Lamarche-Vane, N., & Turner, C. E. (2006). CdGAP Associates with Actopaxin to Regulate Integrin-Dependent Changes in Cell Morphology and Motility. *Current Biology*, *16*(14), 1375-1385. https://doi.org/10.1016/j.cub.2006.05.057

306. Danek, E. I., Tcherkezian, J., Triki, I., Meriane, M., & Lamarche-Vane, N. (2007). Glycogen Synthase Kinase-3 Phosphorylates CdGAP at a Consensus ERK 1 Regulatory Site *. *Journal of Biological Chemistry*, *282*(6), 3624-3631. https://doi.org/10.1074/jbc.M610073200

307. Djoudi Ouadda, A. B., He, Y., Calabrese, V., Ishii, H., Chidiac, R., Gratton, J.-P., Roux, P. P., & Lamarche-Vane, N. (2018). CdGAP/ARHGAP31 is regulated by RSK phosphorylation and binding to 14-3-3β adaptor protein. *Oncotarget*, *9*(14), 11646-11664. https://doi.org/10.18632/oncotarget.24126

308. Primeau, M., Ouadda, A. B. D., & Lamarche-Vane, N. (2011). Cdc42 GTPase-activating protein (CdGAP) interacts with the SH3D domain of Intersectin through a novel basic-rich motif. *FEBS Letters*, *585*(6), 847-853. https://doi.org/10.1016/j.febslet.2011.02.022

309. McCormack, J. J., Bruche, S., Ouadda, A. B. D., Ishii, H., Lu, H., Garcia-Cattaneo, A., Chávez-Olórtegui, C., Lamarche-Vane, N., & Braga, V. M. M. (2017). The scaffold protein Ajuba suppresses CdGAP activity in epithelia to maintain stable cell-cell contacts. *Scientific Reports*, *7*(1), 9249. https://doi.org/10.1038/s41598-017-09024-4

310. Karimzadeh, F., Primeau, M., Mountassif, D., Rouiller, I., & Lamarche-Vane, N. (2012). A Stretch of Polybasic Residues Mediates Cdc42 GTPase-activating Protein (CdGAP) Binding to Phosphatidylinositol 3,4,5-Trisphosphate and Regulates Its GAP Activity *<sup> </sup>. *Journal of Biological Chemistry*, *287*(23), 19610-19621. https://doi.org/10.1074/jbc.M112.344606

311. He, Y., Northey, J. J., Pelletier, A., Kos, Z., Meunier, L., Haibe-Kains, B., Mes-Masson, A. M., Côté, J. F., Siegel, P. M., & Lamarche-Vane, N. (2017). The Cdc42/Rac1 regulator CdGAP is a novel E-cadherin transcriptional co-repressor with Zeb2 in breast cancer. *Oncogene*, *36*(24), 3490-3503. https://doi.org/10.1038/onc.2016.492

312. Ouadda, A. B. D. (2016). *Identification of novel regulatory mechanisms for Cdc42 GTPase-activating protein CdGAP/ARHGAP31, a protein involved in development and cancer* [Doctoral thesis, McGill University]. https://escholarship.mcgill.ca/concern/theses/70795b314

313. Erlmann, P., Schmid, S., Horenkamp, F. A., Geyer, M., Pomorski, T. G., & Olayioye, M. A. (2009). DLC1 Activation Requires Lipid Interaction through a Polybasic Region Preceding the RhoGAP Domain. *Molecular Biology of the Cell*, *20*(20), 4400-4411. https://doi.org/10.1091/mbc.e09-03-0247

314. Lévay, M., Settleman, J., & Ligeti, E. (2009). Regulation of the Substrate Preference of p190RhoGAP by Protein Kinase C-Mediated Phosphorylation of a Phospholipid Binding Site. *Biochemistry*, *48*(36), 8615-8623. https://doi.org/10.1021/bi900667y

315. Ligeti, E., Dagher, M.-C., Hernandez, S. E., Koleske, A. J., & Settleman, J. (2004). Phospholipids Can Switch the GTPase Substrate Preference of a GTPase-activating Protein*. *Journal of Biological Chemistry*, *279*(7), 5055-5058. https://doi.org/10.1074/jbc.C300547200

316. Pechstein, A., Shupliakov, O., & Haucke, V. (2010). Intersectin 1: a versatile actor in the synaptic vesicle cycle. *Biochemical Society Transactions*, *38*(1), 181-186. https://doi.org/10.1042/BST0380181

317. Yamabhai, M., Hoffman, N. G., Hardison, N. L., McPherson, P. S., Castagnoli, L., Cesareni, G., & Kay, B. K. (1998). Intersectin, a Novel Adaptor Protein with Two Eps15 Homology and Five Src Homology 3 Domains*. *Journal of Biological Chemistry*, *273*(47), 31401-31407. https://doi.org/10.1074/jbc.273.47.31401

318. Hussain, N. K., Jenna, S., Glogauer, M., Quinn, C. C., Wasiak, S., Guipponi, M., Antonarakis, S. E., Kay, B. K., Stossel, T. P., Lamarche-Vane, N., & McPherson, P. S. (2001). Endocytic protein intersectin-l regulates actin assembly via Cdc42 and N-WASP. *Nature Cell Biology*, *3*(10), 927-932. https://doi.org/10.1038/ncb1001-927

319. Roos, J., & Kelly, R. B. (1998). Dap160, a Neural-specific Eps15 Homology and Multiple SH3 Domain-containing Protein That Interacts with DrosophilaDynamin*. *Journal of Biological Chemistry*, *273*(30), 19108-19119. https://doi.org/10.1074/jbc.273.30.19108

320. Simpson, F., Hussain, N. K., Qualmann, B., Kelly, R. B., Kay, B. K., McPherson, P. S., & Schmid, S. L. (1999). SH3-domain-containing proteins function at distinct steps in clathrin-coated vesicle formation. *Nature Cell Biology*, *1*(2), 119-124. https://doi.org/10.1038/10091

321. Nishimura, T., Yamaguchi, T., Tokunaga, A., Hara, A., Hamaguchi, T., Kato, K., Iwamatsu, A., Okano, H., & Kaibuchi, K. (2006). Role of Numb in Dendritic Spine Development with a Cdc42 GEF Intersectin and EphB2. *Molecular Biology of the Cell*, *17*(3), 1273-1285. https://doi.org/10.1091/mbc.e05-07-0700

322. Tong, X.-K., Hussain, N. K., Adams, A. G., O'Bryan, J. P., & McPherson, P. S. (2000). Intersectin Can Regulate the Ras/MAP Kinase Pathway Independent of Its Role in Endocytosis *. *Journal of Biological Chemistry*, *275*(38), 29894-29899. https://doi.org/10.1074/jbc.M004096200

323. Songyang, Z., Lu, K. P., Kwon, Y. T., Tsai, L.-H., Filhol, O., Cochet, C., Brickey, D. A., Soderling, T. R., Bartleson, C., Graves, D. J., DeMaggio, A. J., Hoekstra, M. F., Blenis, J., Hunter, T., & Cantley, L. C. (1996). A Structural Basis for Substrate Specificities of Protein Ser/Thr Kinases: Primary Sequence Preference of Casein Kinases I and II, NIMA, Phosphorylase Kinase, Calmodulin-Dependent Kinase II, CDK5, and Erk1. *Molecular and Cellular Biology*, *16*(11), 6486-6493. https://doi.org/10.1128/MCB.16.11.6486

324. Chidiac, R., Zhang, Y., Tessier, S., Faubert, D., Delisle, C., & Gratton, J.-P. (2016). Comparative Phosphoproteomics Analysis of VEGF and Angiopoietin-1 Signaling Reveals ZO-1 as a Critical Regulator of Endothelial Cell Proliferation *<sup></sup>. *Molecular & Cellular Proteomics*, *15*(5), 1511-1525. https://doi.org/10.1074/mcp.M115.053298

325. He, Y., Northey, J. J., Primeau, M., Machado, R. D., Trembath, R., Siegel, P. M., & Lamarche-Vane, N. (2011). CdGAP is required for transforming growth factor β- and Neu/ErbB-2-induced breast cancer cell motility and invasion. *Oncogene*, *30*(9), 1032-1045. https://doi.org/10.1038/onc.2010.477

326. Wormer, D., Deakin, N. O., & Turner, C. E. (2012). CdGAP regulates cell migration and adhesion dynamics in two-and three-dimensional matrix environments. *Cytoskeleton*, *69*(9), 644-658. https://doi.org/10.1002/cm.21057

327. Wormer, D. B., Davis, K. A., Henderson, J. H., & Turner, C. E. (2014). The Focal Adhesion-Localized CdGAP Regulates Matrix Rigidity Sensing and Durotaxis. *PLoS One*, *9*(3), e91815. https://doi.org/10.1371/journal.pone.0091815

328. Northey, J. J., Chmielecki, J., Ngan, E., Russo, C., Annis, M. G., Muller, W. J., & Siegel, P. M. (2008). Signaling through ShcA Is Required for Transforming Growth Factor β- and Neu/ErbB-2-Induced Breast Cancer Cell Motility and Invasion. *Molecular and Cellular Biology*, *28*(10), 3162-3176. https://doi.org/10.1128/MCB.01734-07

329. He, Y., Goyette, M.-A., Chapelle, J., Boufaied, N., Al Rahbani, J., Schonewolff, M., Danek, E. I., Muller, W. J., Labbé, D. P., Côté, J.-F., & Lamarche-Vane, N. (2023). CdGAP is a talin-binding protein and a target of TGF-β signaling that promotes HER2-positive breast cancer growth and metastasis. *Cell Reports*, *42*(8). https://doi.org/10.1016/j.celrep.2023.112936

330. Kuo, J.-C., Han, X., Hsiao, C.-T., Yates Iii, J. R., & Waterman, C. M. (2011). Analysis of the myosin-II-responsive focal adhesion proteome reveals a role for β-Pix in negative regulation of focal adhesion maturation. *Nature Cell Biology*, *13*(4), 383-393. https://doi.org/10.1038/ncb2216

331. Bristow, J. M., Sellers, M. H., Majumdar, D., Anderson, B., Hu, L., & Webb, D. J. (2009). The Rho-family GEF Asef2 activates Rac to modulate adhesion and actin dynamics and thereby regulate cell migration. *Journal of Cell Science*, *122*(24), 4535-4546. https://doi.org/10.1242/jcs.053728

332. Delorme-Walker, V. D., Peterson, J. R., Chernoff, J., Waterman, C. M., Danuser, G., DerMardirossian, C., & Bokoch, G. M. (2011). Pak1 regulates focal adhesion strength, myosin IIA distribution, and actin dynamics to optimize cell migration. *Journal of Cell Biology*, *193*(7), 1289-1303. https://doi.org/10.1083/jcb.201010059

333. Plotnikov, S. V., & Waterman, C. M. (2013). Guiding cell migration by tugging. *Current Opinion in Cell Biology*, *25*(5), 619-626. https://doi.org/10.1016/j.ceb.2013.06.003

334. Plotnikov, Sergey V., Pasapera, Ana M., Sabass, B., & Waterman, Clare M. (2012). Force Fluctuations within Focal Adhesions Mediate ECM-Rigidity Sensing to Guide Directed Cell Migration. *Cell*, *151*(7), 1513-1527. https://doi.org/10.1016/j.cell.2012.11.034

335. Adams, F. H., & Oliver, C. P. (1945). HEREDITARY DEFORMITIES IN MAN: Due to Arrested Development. *Journal of Heredity*, *36*(1), 3-7. https://doi.org/10.1093/oxfordjournals.jhered.a105415

336. Lehman, A., Wuyts, W., & Patel, M. S. (2016). Adams-Oliver Syndrome – RETIRED CHAPTER, FOR HISTORICAL REFERENCE ONLY. In M. G. Adam MP, Pagon RA, et al. (Ed.), *GeneReviews®*. University of Washington, Seattle. https://www.ncbi.nlm.nih.gov/books/NBK355754/

337. Meester, J. A. N., Sukalo, M., Schröder, K. C., Schanze, D., Baynam, G., Borck, G., Bramswig, N. C., Duman, D., Gilbert-Dussardier, B., Holder-Espinasse, M., Itin, P., Johnson, D. S., Joss, S., Koillinen, H., McKenzie, F., Morton, J., Nelle, H., Reardon, W., Roll, C., . . . Wuyts, W. (2018). Elucidating the genetic architecture of Adams–Oliver syndrome in a large European cohort. *Human Mutation*, *39*(9), 1246-1261. https://doi.org/10.1002/humu.23567

338. Southgate, L., & Trembath, R. C. (2016). 1203ARHGAP31, DOCK6, RBPJ, EOGT, and Adams-Oliver Syndrome. In *Epstein's Inborn Errors of Development: The Molecular Basis of Clinical Disorders of Morphogenesis* (pp. 0). Oxford University Press. https://doi.org/10.1093/med/9780199934522.003.0183

339. Kutlubay, Z., & Pehlivan, Ö. (2014). Adams–Oliver syndrome. *International Journal of Dermatology*, *53*(3), 352-354. https://doi.org/10.1111/j.1365-4632.2012.05533.x

340. Snape, K. M. G., Ruddy, D., Zenker, M., Wuyts, W., Whiteford, M., Johnson, D., Lam, W., & Trembath, R. C. (2009). The spectra of clinical phenotypes in aplasia cutis congenita and terminal transverse limb defects. *American Journal of Medical Genetics Part A*, *149A*(8), 1860-1881. https://doi.org/10.1002/ajmg.a.32708

341. Tröbs, R.-B., Barenberg, K., Hemminghaus, M., Günther, M., & Neid, M. (2010). Herniation of the brain after conservative treatment of a large congenital skull defect in an infant with Adams-Oliver syndrome. *Journal of Pediatric Surgery*, *45*(10), 2064-2067. https://doi.org/10.1016/j.jpedsurg.2010.06.029

342. Zapata, H. H., Sletten, L. J., & Pierpont, M. E. M. (1995). Congenital cardiac malformations in Adams-Oliver syndrome. *Clinical Genetics*, *47*(2), 80-84. https://doi.org/10.1111/j.1399-0004.1995.tb03928.x

343. Atasoy, H. I., Tug, E., Yavuz, T., & Cine, N. (2013). Unique variant of Adams–Oliver syndrome with dilated cardiomyopathy and heart block. *Pediatrics International*, *55*(4), 508-512. https://doi.org/10.1111/ped.12011

344. Becker, R., Kunze, J., Horn, D., Gasiorek-Wiens, A., Entezami, M., Rossi, R., Guschmann, M., & Sarioglu, N. (2002). Autosomal recessive type of Adams–Oliver syndrome: prenatal diagnosis. *Ultrasound in Obstetrics & Gynecology*, *20*(5), 506-510. https://doi.org/10.1046/j.1469-0705.2002.00839.x

345. Jaeggi, E., Kind, C., & Morger, R. (1990). Congenital scalp and skull defects with terminal transverse limb anomalies (Adams-Oliver syndrome): Report of three additional cases. *European Journal of Pediatrics*, *149*(8), 565-566. https://doi.org/10.1007/BF01957693

346. Silva, G., Braga, A., Leitão, B., Mesquita, A., Reis, A., Duarte, C., Barbot, J., & Silva, E. S. (2012). Adams–Oliver syndrome and portal hypertension: Fortuitous association or common mechanism? *American Journal of Medical Genetics Part A*, *158A*(3), 648-651. https://doi.org/10.1002/ajmg.a.34435

347. Patel, M. S., Taylor, G. P., Bharya, S., Al-Sanna'a, N., Adatia, I., Chitayat, D., Suzanne Lewis, M. E., & Human, D. G. (2004). Abnormal pericyte recruitment as a cause for pulmonary hypertension in Adams–Oliver syndrome. *American Journal of Medical Genetics Part A*, *129A*(3), 294-299. https://doi.org/10.1002/ajmg.a.30221

348. Gridley, T. (2007). Notch signaling in vascular development and physiology. *Development*, *134*(15), 2709-2718. https://doi.org/10.1242/dev.004184

349. Balasubramanian, M., & Collins, A. L. (2009). Aplasia cutis congenita, terminal limb defects and periventricular leukomalacia in one sibling with minor findings in the other-probable autosomal recessive Adams-Oliver Syndrome. *European Journal of Medical Genetics*, *52*(4), 234-238. https://doi.org/10.1016/j.ejmg.2009.04.005

350. Hassed, Susan J., Wiley, Graham B., Wang, S., Lee, J.-Y., Li, S., Xu, W., Zhao, Zhizhuang J., Mulvihill, John J., Robertson, J., Warner, J., & Gaffney, Patrick M. (2012). RBPJ Mutations Identified in Two Families Affected by Adams-Oliver Syndrome. *The American Journal of Human Genetics*, *91*(2), 391-395. https://doi.org/10.1016/j.ajhg.2012.07.005

351. Alsulaiman, A. M., Alsulaiman, H. M., Almousa, A., & Alsulaiman, S. M. (2020). Adams Oliver syndrome: A mimicker of familial exudative vitreoretinopathy. *American Journal of Ophthalmology Case Reports*, *19*, 100715. https://doi.org/10.1016/j.ajoc.2020.100715

352. Sukalo, M., Tilsen, F., Kayserili, H., Müller, D., Tüysüz, B., Ruddy, D. M., Wakeling, E., Ørstavik, K. H., Snape, K. M., Trembath, R., De Smedt, M., van der Aa, N., Skalej, M., Mundlos, S., Wuyts, W., Southgate, L., & Zenker, M. (2015). DOCK6 Mutations Are Responsible for a Distinct Autosomal-Recessive Variant of Adams–Oliver Syndrome Associated with Brain and Eye Anomalies. *Human Mutation*, *36*(6), 593-598. https://doi.org/10.1002/humu.22795

353. Shaheen, R., Aglan, M., Keppler-Noreuil, K., Faqeih, E., Ansari, S., Horton, K., Ashour, A., Zaki, Maha S., Al-Zahrani, F., Cueto-González, Anna M., Abdel-Salam, G., Temtamy, S., & Alkuraya, Fowzan S. (2013). Mutations in EOGT Confirm the Genetic Heterogeneity of Autosomal-Recessive Adams-Oliver Syndrome. *The American Journal of Human Genetics*, *92*(4), 598-604. https://doi.org/10.1016/j.ajhg.2013.02.012

354. Southgate, L., Sukalo, M., Karountzos, A. S. V., Taylor, E. J., Collinson, C. S., Ruddy, D., Snape, K. M., Dallapiccola, B., Tolmie, J. L., Joss, S., Brancati, F., Digilio, M. C., Graul-Neumann, L. M., Salviati, L., Coerdt, W., Jacquemin, E., Wuyts, W., Zenker, M., Machado, R. D., & Trembath, R. C. (2015). Haploinsufficiency of the NOTCH1 Receptor as a Cause of Adams–Oliver Syndrome With Variable Cardiac Anomalies. *Circulation: Cardiovascular Genetics*, *8*(4), 572-581. https://doi.org/10.1161/CIRCGENETICS.115.001086

355. Küster, W., Lenz, W., Kääriäinen, H., Majewski, F., Opitz, J. M., & Reynolds, J. F. (1988). Congenital scalp defects with distal limb anomalies (Adams-Oliver syndrome): Report of ten cases and review of the literature. *American Journal of Medical Genetics*, *31*(1), 99-115. https://doi.org/10.1002/ajmg.1320310112

356. Khajavi, M., Inoue, K., & Lupski, J. R. (2006). Nonsense-mediated mRNA decay modulates clinical outcome of genetic disease. *European Journal of Human Genetics*, *14*(10), 1074-1081. https://doi.org/10.1038/sj.ejhg.5201649

357. Isrie, M., Wuyts, W., Van Esch, H., & Devriendt, K. (2014). Isolated terminal limb reduction defects: Extending the clinical spectrum of Adams–Oliver syndrome and

ARHGAP31 mutations. *American Journal of Medical Genetics Part A*, *164*(6), 1576-1579. https://doi.org/10.1002/ajmg.a.36486

358. High, F. A., & Epstein, J. A. (2008). The multifaceted role of Notch in cardiac development and disease. *Nature Reviews Genetics*, *9*(1), 49-61. https://doi.org/10.1038/nrg2279

359. Meester, Josephina A. N., Southgate, L., Stittrich, A.-B., Venselaar, H., Beekmans, Sander J. A., den Hollander, N., Bijlsma, Emilia K., Helderman-van den Enden, A., Verheij, Joke B. G. M., Glusman, G., Roach, Jared C., Lehman, A., Patel, Millan S., de Vries, Bert B. A., Ruivenkamp, C., Itin, P., Prescott, K., Clarke, S., Trembath, R., . . . Wuyts, W. (2015). Heterozygous Loss-of-Function Mutations in DLL4 Cause Adams-Oliver Syndrome. *The American Journal of Human Genetics*, *97*(3), 475-482. https://doi.org/10.1016/j.ajhg.2015.07.015

360. Chillakuri, C. R., Sheppard, D., Lea, S. M., & Handford, P. A. (2012). Notch receptor–ligand binding and activation: Insights from molecular studies. *Seminars in Cell & Developmental Biology*, *23*(4), 421-428. https://doi.org/10.1016/j.semcdb.2012.01.009

361. Luca, V. C., Jude, K. M., Pierce, N. W., Nachury, M. V., Fischer, S., & Garcia, K. C. (2015). Structural basis for Notch1 engagement of Delta-like 4. *Science*, *347*(6224), 847-853. https://doi.org/10.1126/science.1261093

362. Yamamizu, K., Matsunaga, T., Uosaki, H., Fukushima, H., Katayama, S., Hiraoka-Kanie, M., Mitani, K., & Yamashita, J. K. (2010). Convergence of Notch and β-catenin signaling induces arterial fate in vascular progenitors. *Journal of Cell Biology*, *189*(2), 325-338. https://doi.org/10.1083/jcb.200904114

363. Rand, M. D., Lindblom, A., Carlson, J., Villoutreix, B. O., & Stenflo, J. (1997). Calcium binding to tandem repeats of EGF-like modules. Expression and characterization of the EGF-like modules of human Notch-1 implicated in receptor-ligand interactions. *Protein Science*, *6*(10), 2059-2071. https://doi.org/10.1002/pro.5560061002

364. Bray, S. J. (2006). Notch signalling: a simple pathway becomes complex. *Nature Reviews Molecular Cell Biology*, *7*(9), 678-689. https://doi.org/10.1038/nrm2009

365. Jarriault, S., Brou, C., Logeat, F., Schroeter, E. H., Kopan, R., & Israel, A. (1995). Signalling downstream of activated mammalian Notch. *Nature*, *377*(6547), 355-358. https://doi.org/10.1038/377355a0

366. Stittrich, A.-B., Lehman, A., Bodian, Dale L., Ashworth, J., Zong, Z., Li, H., Lam, P., Khromykh, A., Iyer, Ramaswamy K., Vockley, Joseph G., Baveja, R., Silva, Ermelinda S., Dixon, J., Leon, Eyby L., Solomon, Benjamin D., Glusman, G., Niederhuber, John E., Roach, Jared C., & Patel, Millan S. (2014). Mutations in NOTCH1 Cause Adams-Oliver Syndrome. *The American Journal of Human Genetics*, *95*(3), 275-284. https://doi.org/10.1016/j.ajhg.2014.07.011

367. Sabria, J., Benassar, M., Laborda, A., Pérez, M. A., Arca, G., Muñoz, E., Gómez, O. P., & Martínez, J. M. (2021). Fetoscopic Diagnosis of Adams-Oliver Syndrome. *Clinics in Surgery*, *6*(1), 3152. https://doi.org/10.25107/2474-1647.3152

368. Algaze, C., Esplin, E. D., Lowenthal, A., Hudgins, L., Tacy, T. A., & Selamet Tierney, E. S. (2013). Expanding the phenotype of cardiovascular malformations in Adams–Oliver syndrome. *American Journal of Medical Genetics Part A*, *161*(6), 1386-1389. https://doi.org/10.1002/ajmg.a.35864

369. Gale, N. W., Dominguez, M. G., Noguera, I., Pan, L., Hughes, V., Valenzuela, D. M., Murphy, A. J., Adams, N. C., Lin, H. C., Holash, J., Thurston, G., & Yancopoulos, G. D. (2004). Haploinsufficiency of delta-like 4 ligand results in embryonic lethality due to major defects in arterial and vascular development. *Proceedings of the National Academy of Sciences*, *101*(45), 15949-15954. https://doi.org/10.1073/pnas.0407290101

370. Nagasaka, M., Taniguchi-Ikeda, M., Inagaki, H., Ouchi, Y., Kurokawa, D., Yamana, K., Harada, R., Nozu, K., Sakai, Y., Mishra, S. K., Yamaguchi, Y., Morioka, I., Toda, T., Kurahashi, H., & Iijima, K. (2017). Novel missense mutation in DLL4 in a Japanese sporadic case of Adams–Oliver syndrome. *Journal of Human Genetics*, *62*(9), 851-855. https://doi.org/10.1038/jhg.2017.48

371. Miyamoto, Y., Yamauchi, J., Sanbe, A., & Tanoue, A. (2007). Dock6, a Dock-C subfamily guanine nucleotide exchanger, has the dual specificity for Rac1 and Cdc42 and regulates neurite outgrowth. *Experimental Cell Research*, *313*(4), 791-804. https://doi.org/10.1016/j.yexcr.2006.11.017

372. Sakaidani, Y., Ichiyanagi, N., Saito, C., Nomura, T., Ito, M., Nishio, Y., Nadano, D., Matsuda, T., Furukawa, K., & Okajima, T. (2012). O-linked-N-acetylglucosamine modification of mammalian Notch receptors by an atypical O-GlcNAc transferase Eogt1.

*Biochemical and Biophysical Research Communications*, *419*(1), 14-19. https://doi.org/10.1016/j.bbrc.2012.01.098

373. Müller, R., Jenny, A., & Stanley, P. (2013). The EGF Repeat-Specific O-GlcNAc-Transferase Eogt Interacts with Notch Signaling and Pyrimidine Metabolism Pathways in Drosophila. *PLoS One*, *8*(5), e62835. https://doi.org/10.1371/journal.pone.0062835
374. Sawaguchi, S., Varshney, S., Ogawa, M., Sakaidani, Y., Yagi, H., Takeshita, K., Murohara, T., Kato, K., Sundaram, S., Stanley, P., & Okajima, T. (2017). O-GlcNAc on NOTCH1 EGF repeats regulates ligand-induced Notch signaling and vascular development in mammals. *eLife*, *6*, e24419. https://doi.org/10.7554/eLife.24419
375. Cohen, I., Silberstein, E., Perez, Y., Landau, D., Elbedour, K., Langer, Y., Kadir, R., Volodarsky, M., Sivan, S., Narkis, G., & Birk, O. S. (2014). Autosomal recessive Adams–Oliver syndrome caused by homozygous mutation in EOGT, encoding an EGF domain-specific O-GlcNAc transferase. *European Journal of Human Genetics*, *22*(3), 374-378. https://doi.org/10.1038/ejhg.2013.159
376. Schröder, K. C., Duman, D., Tekin, M., Schanze, D., Sukalo, M., Meester, J., Wuyts, W., & Zenker, M. (2019). Adams–Oliver syndrome caused by mutations of the EOGT gene. *American Journal of Medical Genetics Part A*, *179*(11), 2246-2251. https://doi.org/10.1002/ajmg.a.61313
377. Machado, R. D., Southgate, L., Eichstaedt, C. A., Aldred, M. A., Austin, E. D., Best, D. H., Chung, W. K., Benjamin, N., Elliott, C. G., Eyries, M., Fischer, C., Gräf, S., Hinderhofer, K., Humbert, M., Keiles, S. B., Loyd, J. E., Morrell, N. W., Newman, J. H., Soubrier, F., . . . Grünig, E. (2015). Pulmonary Arterial Hypertension: A Current Perspective on Established and Emerging Molecular Genetic Defects. *Human Mutation*, *36*(12), 1113-1127. https://doi.org/10.1002/humu.22904
378. Yang, X.-F., Shi, S.-W., & Chen, K. (2023). Case report: Recombinant human epidermal growth factor gel plus kangfuxin solution in the treatment of aplasia cutis congenita in a case with Adams–Oliver syndrome. *Frontiers in Surgery*, *9*, 1072021. https://doi.org/10.3389/fsurg.2022.1072021
379. Wadhwa, B., Karambelkar, V. H. Sindal, D. K., Paranjpe, G. (2017). A case report on Adams oliver symdrome. *MedPulse International Journal of Ophtalmology*, *3*(1), 04-07. https://www.medpulse.in/Ophthlmology/

380. Kahn, E. A., & Olmedo, L. (1950). CONGENITAL DEFECT OF THE SCALP: WITH A NOTE ON THE CLOSURE OF LARGE SCALP DEFECTS IN GENERAL. *Plastic and Reconstructive Surgery*, *6*(6), 435-440. https://journals.lww.com/plasreconsurg/Fulltext/1950/12000/CONGENITAL_DEFECT_OF_THE_SCALP__WITH_A_NOTE_ON_THE.3.aspx

381. Swartz, E. N., Sanatani, S., Sandor, G. G. S., & Schreiber, R. A. (1999). Vascular abnormalities in Adams-Oliver syndrome: Cause or effect? *American Journal of Medical Genetics*, *82*(1), 49-52. https://doi.org/10.1002/(SICI)1096-8628(19990101)82:1<49::AID-AJMG10>3.0.CO;2-M

382. Peralta-Calvo, J., Pastora, N., Casa-Ventura, Y. G., Hernandez-Serrano, R., & Abelairas, J. (2012). Peripheral Ischemic Retinopathy in Adams-Oliver Syndrome. *Archives of Ophthalmology*, *130*(8), 1078-1080. https://doi.org/10.1001/archophthalmol.2012.531

383. Krebs, L. T., Shutter Jr Fau - Tanigaki, K., Tanigaki K Fau - Honjo, T., Honjo T Fau - Stark, K. L., Stark Kl Fau - Gridley, T., & Gridley, T. (2004). Haploinsufficient lethality and formation of arteriovenous malformations in Notch pathway mutants. *Genes & development*, *18*(20), 2469–2473. https://doi.org/10.1101/gad.1239204

384. Digilio, M. C., Marino, B., & Dallapiccola, B. (2008). Autosomal dominant inheritance of aplasia cutis congenita and congenital heart defect: A possible link to the Adams–Oliver syndrome. *American Journal of Medical Genetics Part A*, *146A*(21), 2842-2844. https://doi.org/10.1002/ajmg.a.32526

385. Fryns, J. P., Legius, E., Demaerel, P., & van den Berghe, H. (1996). Congenital scalp defect, distal limb reduction anomalies, right spastic hemiplegia and hypoplasia of the left arteria cerebri media: Further evidence that interruption of early embryonic blood supply may result in Adams-Oliver (plus) syndrome. *Clinical Genetics*, *50*(6), 505-509. https://doi.org/10.1111/j.1399-0004.1996.tb02723.x

386. Hoyme, H. E., Jones, K. L., Allen, M. I. V., Saunders, B. S., & Benirschke, K. (1982). Vascular pathogenesis of transverse limb reduction defects. *The Journal of Pediatrics*, *101*(5), 839-843. https://doi.org/10.1016/S0022-3476(82)80343-0

387. Suarez, E., Bertoli, M. J., Eloy, J. D., & Shah, S. P. (2021). Case report and review of literature of a rare congenital disorder: Adams-Oliver syndrome. *BMC Anesthesiology*, *21*(1), 117. https://doi.org/10.1186/s12871-021-01339-0

388. Ishihara, N., Matsuo, H., Murakoshi, H., Laoag-Fernandez, J. B., Samoto, T., & Maruo, T. (2002). Increased apoptosis in the syncytiotrophoblast in human term placentas complicated by either preeclampsia or intrauterine growth retardation. *American Journal of Obstetrics and Gynecology*, *186*(1), 158-166. https://doi.org/10.1067/mob.2002.119176

389. Kaufmann, P., Black, S., & Huppertz, B. (2003). Endovascular Trophoblast Invasion: Implications for the Pathogenesis of Intrauterine Growth Retardation and Preeclampsia. *Biology of Reproduction*, *69*(1), 1-7. https://doi.org/10.1095/biolreprod.102.014977

390. Woods, L., Perez-Garcia, V., & Hemberger, M. (2018). Regulation of Placental Development and Its Impact on Fetal Growth—New Insights From Mouse Models. *Frontiers in Endocrinology*, *9*, 570. https://doi.org/10.3389/fendo.2018.00570

391. Dehdashtian, A., & Dehdashtian, M. (2016). Adams-Oliver Syndrome: A Case With Full Expression. *Pediatric Reports*, *8*(2), 6517. https://doi.org/10.4081/pr.2016.6517

392. Sevilla-Montoya, R., Ríos-Flores, B., Moreno-Verduzco, E., Domínguez-Castro, M., Rivera-Pedroza, C. I., & Aguinaga-Ríos, D. M. (2014). Severe phenotype in two half-sibs with Adams Oliver syndrome. *Archivos argentinos de pediatria*, *112*(3), e108–e112. https://doi.org/10.5546/aap.2014.eng.e108

393. Hypertension in Pregnancy: Executive Summary. (2013). *Obstetrics & Gynecology*, *122*(5), 1122-1131. https://doi.org/10.1097/01.AOG.0000437382.03963.88

394. Albrecht, E. D., & Pepe, G. J. (2020). Regulation of Uterine Spiral Artery Remodeling: a Review. *Reproductive Sciences*, *27*(10), 1932-1942. https://doi.org/10.1007/s43032-020-00212-8

395. Brennan, L. J., Morton, J. S., & Davidge, S. T. (2014). Vascular Dysfunction in Preeclampsia. *Microcirculation*, *21*(1), 4-14. https://doi.org/10.1111/micc.12079

396. Roland, C. S., Hu, J., Ren, C.-E., Chen, H., Li, J., Varvoutis, M. S., Leaphart, L. W., Byck, D. B., Zhu, X., & Jiang, S.-W. (2016). Morphological changes of placental syncytium and their implications for the pathogenesis of preeclampsia. *Cellular and Molecular Life Sciences*, *73*(2), 365-376. https://doi.org/10.1007/s00018-015-2069-x

397. Beck, S., Wojdyla D Fau - Say, L., Say L Fau - Betran, A. P., Betran Ap Fau - Merialdi, M., Merialdi M Fau - Requejo, J. H., Requejo Jh Fau - Rubens, C., Rubens C Fau - Menon, R., Menon R Fau - Van Look, P. F. A., & Van Look, P. F. (2010). The worldwide

incidence of preterm birth: a systematic review of maternal mortality and morbidity. *Bulletin of the World Health Organization*, *88*(1), 31-38. https://doi.org/10.2471/BLT.08.062554

398. Mercuro, G., Bassareo, P. P., Flore, G., Fanos, V., Dentamaro, I., Scicchitano, P., Laforgia, N., & Ciccone, M. M. (2013). Prematurity and low weight at birth as new conditions predisposing to an increased cardiovascular risk. *European Journal of Preventive Cardiology*, *20*(2), 357-367. https://doi.org/10.1177/2047487312437058
399. Moster, D., Lie, R. T., & Markestad, T. (2008). Long-Term Medical and Social Consequences of Preterm Birth. *New England Journal of Medicine*, *359*(3), 262-273. https://doi.org/10.1056/NEJMoa0706475
400. Enquobahrie, D. A., Abetew, D. F., Sorensen, T. K., Willoughby, D., Chidambaram, K., & Williams, M. A. (2011). Placental microRNA expression in pregnancies complicated by preeclampsia. *American Journal of Obstetrics & Gynecology*, *204*(2), 178.e112-178.e121. https://doi.org/10.1016/j.ajog.2010.09.004
401. Huang, Q., Chen, H., Li, J., Oliver, M., Ma, X., Byck, D., Gao, Y., & Jiang, S.-W. (2014). Epigenetic and non-epigenetic regulation of syncytin-1 expression in human placenta and cancer tissues. *Cellular Signalling*, *26*(3), 648-656. https://doi.org/10.1016/j.cellsig.2013.11.002
402. Goulopoulou, S., & Davidge, S. T. (2015). Molecular mechanisms of maternal vascular dysfunction in preeclampsia. *Trends in Molecular Medicine*, *21*(2), 88-97. https://doi.org/10.1016/j.molmed.2014.11.009
403. Khalil, R. A., & Granger, J. P. (2002). Vascular mechanisms of increased arterial pressure in preeclampsia: lessons from animal models. *American Journal of Physiology-Regulatory, Integrative and Comparative Physiology*, *283*(1), R29-R45. https://doi.org/10.1152/ajpregu.00762.2001
404. Faye-Petersen, O. M., Heller, D. S., & Joshi, V. V. (2005). *Handbook of Placental Pathology* (2nd ed.). CRC Press. https://doi.org/10.3109/9780203489567
405. Narasimha, A., & Vasudeva, D. (2011). Spectrum of changes in placenta in toxemia of pregnancy. *Indian Journal of Pathology and Microbiology*, *54*(1), 15-20. https://doi.org/10.4103/0377-4929.77317

406. Khong, T. Y., De Wolf, F., Robertson, W. B., & Brosens, I. (1986). Inadequate maternal vascular response to placentation in pregnancies complicated by pre-eclampsia and by small-for-gestational age infants. *BJOG: An International Journal of Obstetrics & Gynaecology*, *93*(10), 1049-1059. https://doi.org/10.1111/j.1471-0528.1986.tb07830.x

407. Tenney, B., & Parker, F. (1940). The placenta in toxemia of pregnancy. *American Journal of Obstetrics and Gynecology*, *39*(6), 1000-1005. https://doi.org/10.1016/S0002-9378(40)90458-6

408. Soma, H., Yoshida, K., Mukaida, T., & Tabuchi, Y. (1982). Morphologic Changes in the Hypertensive Placenta1. In *Morphological and Functional Aspects of Placental Dysfunction* (Vol. 9, pp. 0). S.Karger AG. https://doi.org/10.1159/000406845

409. Hammer, A. (2011). Immunological regulation of trophoblast invasion. *Journal of Reproductive Immunology*, *90*(1), 21-28. https://doi.org/10.1016/j.jri.2011.05.001

410. Soares, M., Chakraborty, D., Kubota, K., Renaud, S., & Rumi, M. A. K. (2014). Adaptive mechanisms controlling uterine spiral artery remodeling during the establishment of pregnancy. *The International Journal of Developmental Biology*, *58*(2-3-4), 247-259. https://doi.org/10.1387/ijdb.140083ms

411. Hamilton, W. J., & Boyd, J. D. (1960). Development of the human placenta in the first three months of gestation. *Journal of anatomy*, *94*, 297-328.

412. Ramsey, E. M., Houston, M. L., & Harris, J. W. S. (1976). Interactions of the trophoblast and maternal tissues in three closely related primate species. *American Journal of Obstetrics and Gynecology*, *124*(6), 647-652. https://doi.org/10.1016/0002-9378(76)90068-5

413. Pijnenborg, R., Dixon, G., Robertson, W. B., & Brosens, I. (1980). Trophoblastic invasion of human decidua from 8 to 18 weeks of pregnancy. *Placenta*, *1*(1), 3-19. https://doi.org/10.1016/S0143-4004(80)80012-9

414. Enders, A. C., & King, B. F. (1991). Early stages of trophoblastic invasion of the maternal vascular system during implantation in the macaque and baboon. *American Journal of Anatomy*, *192*(4), 329-346. https://doi.org/10.1002/aja.1001920403

415. Pollheimer, J., Vondra, S., Baltayeva, J., Beristain, A. G., & Knöfler, M. (2018). Regulation of Placental Extravillous Trophoblasts by the Maternal Uterine Environment. *Frontiers in Immunology*, *9*, 2597. https://doi.org/10.3389/fimmu.2018.02597

416. Moser, G., Windsperger, K., Pollheimer, J., de Sousa Lopes, S. C., & Huppertz, B. (2018). Human trophoblast invasion: new and unexpected routes and functions. *Histochemistry and Cell Biology*, *150*(4), 361-370. https://doi.org/10.1007/s00418-018-1699-0

417. Chakraborty, D., Rumi, M. A. K., Konno, T., & Soares, M. J. (2011). Natural killer cells direct hemochorial placentation by regulating hypoxia-inducible factor dependent trophoblast lineage decisions. *Proceedings of the National Academy of Sciences*, *108*(39), 16295-16300. https://doi.org/10.1073/pnas.1109478108

418. Knöfler, M. (2010). Critical growth factors and signalling pathways controlling human trophoblast invasion. *The International Journal of Developmental Biology*, *54*(2-3), 269-280. https://doi.org/10.1387/ijdb.082769mk

419. Zhou, Y., Fisher, S. J., Janatpour, M., Genbacev, O., Dejana, E., Wheelock, M., & Damsky, C. H. (1997). Human cytotrophoblasts adopt a vascular phenotype as they differentiate. A strategy for successful endovascular invasion? *The Journal of Clinical Investigation*, *99*(9), 2139-2151. https://doi.org/10.1172/JCI119387

420. Zhou, Y., Damsky, C. H., & Fisher, S. J. (1997). Preeclampsia is associated with failure of human cytotrophoblasts to mimic a vascular adhesion phenotype. One cause of defective endovascular invasion in this syndrome? *The Journal of Clinical Investigation*, *99*(9), 2152-2164. https://doi.org/10.1172/JCI119388

421. Gauster, M., Moser, G., Orendi, K., & Huppertz, B. (2009). Factors Involved in Regulating Trophoblast Fusion: Potential Role in the Development of Preeclampsia. *Placenta*, *30*, 49-54. https://doi.org/10.1016/j.placenta.2008.10.011

422. Mayhew, T. M. (2014). Turnover of human villous trophoblast in normal pregnancy: What do we know and what do we need to know? *Placenta*, *35*(4), 229-240. https://doi.org/10.1016/j.placenta.2014.01.011

423. Askelund, K. J., & Chamley, L. W. (2011). Trophoblast deportation part I: Review of the evidence demonstrating trophoblast shedding and deportation during human pregnancy. *Placenta*, *32*(10), 716-723. https://doi.org/10.1016/j.placenta.2011.07.081

424. Lu, X., Wang, R., Zhu, C., Wang, H., Lin, H.-Y., Gu, Y., Cross, J. C., & Wang, H. (2017). Fine-Tuned and Cell-Cycle-Restricted Expression of Fusogenic Protein Syncytin-2

Maintains Functional Placental Syncytia. *Cell Reports*, *21*(5), 1150-1159. https://doi.org/10.1016/j.celrep.2017.10.019

425. Aguilar, P. S., Baylies, M. K., Fleissner, A., Helming, L., Inoue, N., Podbilewicz, B., Wang, H., & Wong, M. (2013). Genetic basis of cell–cell fusion mechanisms. *Trends in Genetics*, *29*(7), 427-437. https://doi.org/10.1016/j.tig.2013.01.011

426. Simpson, R. A., Mayhew, T. M., & Barnes, P. R. (1992). From 13 weeks to term, the trophoblast of human placenta grows by the continuous recruitment of new proliferative units: A study of nuclear number using the disector. *Placenta*, *13*(5), 501-512. https://doi.org/10.1016/0143-4004(92)90055-X

427. Gauster, M., Moser, G., Wernitznig, S., Kupper, N., & Huppertz, B. (2022). Early human trophoblast development: from morphology to function. *Cellular and Molecular Life Sciences*, *79*(6), 345. https://doi.org/10.1007/s00018-022-04377-0

428. Spencer, T. E., & Bazer, F. W. (2004). Conceptus signals for establishment and maintenance of pregnancy. *Reproductive Biology and Endocrinology*, *2*(1), 49. https://doi.org/10.1186/1477-7827-2-49

429. Staun-Ram, E., & Shalev, E. (2005). Human trophoblast function during the implantation process. *Reproductive Biology and Endocrinology*, *3*(1), 56. https://doi.org/10.1186/1477-7827-3-56

430. Hertig, A. T., Rock, J., & Adams, E. C. (1956). A description of 34 human ova within the first 17 days of development. *American Journal of Anatomy*, *98*(3), 435-493. https://doi.org/10.1002/aja.1000980306

431. Simmons, D. G., Natale, D. R. C., Begay, V., Hughes, M., Leutz, A., & Cross, J. C. (2008). Early patterning of the chorion leads to the trilaminar trophoblast cell structure in the placental labyrinth. *Development*, *135*(12), 2083-2091. https://doi.org/10.1242/dev.020099

432. Bolon, B. W., J. M. (2015). 4 - Anatomy and Physiology of the Developing Mouse and Placenta. In B. Bolon (Ed.), *Pathology of the Developing Mouse* (pp. 39-98). CRC Press. https://doi-org.proxy3.library.mcgill.ca/10.1201/b18160

433. Georgiades, P., Ferguson-Smith, A. C., & Burton, G. J. (2002). Comparative Developmental Anatomy of the Murine and Human Definitive Placentae. *Placenta*, *23*(1), 3-19. https://doi.org/10.1053/plac.2001.0738

434. Placental Development and Anatomy. (2021). In D. J. Roberts & C. Polizzano (Eds.), *Atlas of Placental Pathology* (Vol. 6, pp. 0). American Registry of Pathology. https://doi.org/10.55418/9781933477091-ch01

435. Cross, J. C., Simmons, D. G., & Watson, E. D. (2003). Chorioallantoic Morphogenesis and Formation of the Placental Villous Tree. *Annals of the New York Academy of Sciences*, *995*(1), 84-93. https://doi.org/10.1111/j.1749-6632.2003.tb03212.x

436. Rinkenberger, J., & Werb, Z. (2000). The labyrinthine placenta. *Nature Genetics*, *25*(3), 248-250. https://doi.org/10.1038/76985

437. Elmore, S. A., Cochran, R. Z., Bolon, B., Lubeck, B., Mahler, B., Sabio, D., & Ward, J. M. (2021). Histology Atlas of the Developing Mouse Placenta. *Toxicologic Pathology*, *50*(1), 60-117. https://doi.org/10.1177/01926233211042270

438. Silva, J. F., & Serakides, R. (2016). Intrauterine trophoblast migration: A comparative view of humans and rodents. *Cell Adhesion & Migration*, *10*(1-2), 88-110. https://doi.org/10.1080/19336918.2015.1120397

439. LaMarca, B. B. D., Bennett, W. A., Alexander, B. T., Cockrell, K., & Granger, J. P. (2005). Hypertension Produced by Reductions in Uterine Perfusion in the Pregnant Rat. *Hypertension*, *46*(4), 1022-1025. https://doi.org/10.1161/01.HYP.0000175476.26719.36

440. Molnár, M., Sütö, T., Tóth, T., & Hertelendy, F. (1994). Prolonged blockade of nitric oxide synthesis in gravid rats produces sustained hypertension, proteinuria, thrombocytopenia, and intrauterine growth retardation. *American Journal of Obstetrics & Gynecology*, *170*(5), 1458-1466. https://doi.org/10.1016/S0002-9378(94)70179-2

441. Winship, A. L., Koga, K., Menkhorst, E., Van Sinderen, M., Rainczuk, K., Nagai, M., Cuman, C., Yap, J., Zhang, J.-G., Simmons, D., Young, M. J., & Dimitriadis, E. (2015). Interleukin-11 alters placentation and causes preeclampsia features in mice. *Proceedings of the National Academy of Sciences*, *112*(52), 15928-15933. https://doi.org/10.1073/pnas.1515076112

442. Hunkapiller, N. M., Gasperowicz, M., Kapidzic, M., Plaks, V., Maltepe, E., Kitajewski, J., Cross, J. C., & Fisher, S. J. (2011). A role for Notch signaling in trophoblast endovascular invasion and in the pathogenesis of pre-eclampsia. *Development*, *138*(14), 2987-2998. https://doi.org/10.1242/dev.066589

443. Doridot, L., Passet, B., Méhats, C., Rigourd, V., Barbaux, S., Ducat, A., Mondon, F., Vilotte, M., Castille, J., Breuiller-Fouché, M., Daniel, N., le Provost, F., Bauchet, A.-L., Baudrie, V., Hertig, A., Buffat, C., Simeoni, U., Germain, G., Vilotte, J.-L., & Vaiman, D. (2013). Preeclampsia-Like Symptoms Induced in Mice by Fetoplacental Expression of STOX1 Are Reversed by Aspirin Treatment. *Hypertension*, *61*(3), 662-668. https://doi.org/10.1161/HYPERTENSIONAHA.111.202994

444. Bolon, B. W., J. M. (2015). 3 - Essential terminology for mouse developmental pathology studies. In B. Bolon (Ed.), *Pathology of the Developing Mouse* (pp. 27-38). CRC Press. https://doi-org.proxy3.library.mcgill.ca/10.1201/b18160

445. Favaro, R., Abrahamsohn, P. A., & Zorn, M. T. (2014). 11 - Decidualization and Endometrial Extracellular Matrix Remodeling. In B. A. Croy, A. T. Yamada, F. J. DeMayo, & S. L. Adamson (Eds.), *The Guide to Investigation of Mouse Pregnancy* (pp. 125-142). Academic Press. https://doi.org/10.1016/B978-0-12-394445-0.00011-4

446. Lawson, K. A., & Wilson, V. (2016). 3 - A Revised Staging of Mouse Development Before Organogenesis. In R. Baldock, J. Bard, D. R. Davidson, & G. Morriss-Kay (Eds.), *Kaufman's Atlas of Mouse Development Supplement* (pp. 51-64). Academic Press. https://doi.org/10.1016/B978-0-12-800043-4.00003-8

447. Downs, K. M. (1998). 1 - The Murine Allantois. In R. A. Pedersen & G. P. Schatten (Eds.), *Current Topics in Developmental Biology* (Vol. 39, pp. 1-33). Academic Press. https://doi.org/10.1016/S0070-2153(08)60451-2

448. Carretero, A., Ruberte, J., Navarro, M., Lope, S., & Pujol, A. (2017). 10 - Anatomy of development. In J. Ruberte, A. Carretero, & M. Navarro (Eds.), *Morphological Mouse Phenotyping* (pp. 253-268). Academic Press. https://doi.org/10.1016/B978-0-12-812972-2.50010-6

449. Pereira, P. N. G., Dobreva, M. P., Graham, L., Huylebroeck, D., Lawson, K. A., & Zwijsen, A. N. (2011). Amnion formation in the mouse embryo: the single amniochorionic fold model. *BMC Developmental Biology*, *11*(1), 48. https://doi.org/10.1186/1471-213X-11-48

450. Palis, J., McGrath, K. E., & Kingsley, P. D. (1995). Initiation of Hematopoiesis and Vasculogenesis in Murine Yolk Sac Explants. *Blood*, *86*(1), 156-163. https://doi.org/10.1182/blood.V86.1.156.bloodjournal861156

451. Kingsley, P. D., Malik, J., Fantauzzo, K. A., & Palis, J. (2004). Yolk sac–derived primitive erythroblasts enucleate during mammalian embryogenesis. *Blood*, *104*(1), 19-25. https://doi.org/10.1182/blood-2003-12-4162

452. Medvinsky, A., & Dzierzak, E. (1996). Definitive Hematopoiesis Is Autonomously Initiated by the AGM Region. *Cell*, *86*(6), 897-906. https://doi.org/10.1016/S0092-8674(00)80165-8

453. Swartley, O. M., Foley, J. F., Livingston, D. P., Cullen, J. M., & Elmore, S. A. (2016). Histology Atlas of the Developing Mouse Hepatobiliary Hemolymphatic Vascular System with Emphasis on Embryonic Days 11.5–18.5 and Early Postnatal Development. *Toxicologic Pathology*, *44*(5), 705-725. https://doi.org/10.1177/0192623316630836

454. Watson, E. D., & Cross, J. C. (2005). Development of Structures and Transport Functions in the Mouse Placenta. *Physiology*, *20*(3), 180-193. https://doi.org/10.1152/physiol.00001.2005

455. Cross, J. C. (2000). Genetic insights into trophoblast differentiation and placental morphogenesis. *Seminars in Cell & Developmental Biology*, *11*(2), 105-113. https://doi.org/10.1006/scdb.2000.0156

456. Gekas, C., Dieterlen-Lièvre, F., Orkin, S. H., & Mikkola, H. K. A. (2005). The Placenta Is a Niche for Hematopoietic Stem Cells. *Developmental Cell*, *8*(3), 365-375. https://doi.org/10.1016/j.devcel.2004.12.016

457. Downs, K. M., & Gardner, R. L. (1995). An investigation into early placental ontogeny: allantoic attachment to the chorion is selective and developmentally regulated. *Development*, *121*(2), 407-416. https://doi.org/10.1242/dev.121.2.407

458. Inman, K. E., & Downs, K. M. (2007). The murine allantois: emerging paradigms in development of the mammalian umbilical cord and its relation to the fetus. *genesis*, *45*(5), 237-258. https://doi.org/10.1002/dvg.20281

459. Gurtner, G. C., Davis V Fau - Li, H., Li H Fau - McCoy, M. J., McCoy Mj Fau - Sharpe, A., Sharpe A Fau - Cybulsky, M. I., & Cybulsky, M. I. (1995). Targeted disruption of the murine VCAM1 gene: essential role of VCAM-1 in chorioallantoic fusion and placentation. *Genes & development*, *9*(1), 1-14. https://doi.org/10.1101/gad.9.1.1

460. Downs, K. M., & Bertler, C. (2000). Growth in the pre-fusion murine allantois. *Anatomy and Embryology*, *202*(4), 323-331. https://doi.org/10.1007/s004290000118

461. Coan, P. M., Ferguson-Smith, A. C., & Burton, G. J. (2004). Developmental Dynamics of the Definitive Mouse Placenta Assessed by Stereology1. *Biology of Reproduction*, *70*(6), 1806-1813. https://doi.org/10.1095/biolreprod.103.024166

462. Adamson, S. L., Lu, Y., Whiteley, K. J., Holmyard, D., Hemberger, M., Pfarrer, C., & Cross, J. C. (2002). Interactions between Trophoblast Cells and the Maternal and Fetal Circulation in the Mouse Placenta. *Developmental Biology*, *250*(2), 358-373. https://doi.org/10.1006/dbio.2002.0773

463. Simmons, D. G. (2014). 12 - Postimplantation Development of the Chorioallantoic Placenta. In B. A. Croy, A. T. Yamada, F. J. DeMayo, & S. L. Adamson (Eds.), *The Guide to Investigation of Mouse Pregnancy* (pp. 143-161). Academic Press. https://doi.org/10.1016/B978-0-12-394445-0.00012-6

464. Baron, M. H., Vacaru, A., & Nieves, J. (2013). Erythroid development in the mammalian embryo. *Blood Cells, Molecules, and Diseases*, *51*(4), 213-219. https://doi.org/10.1016/j.bcmd.2013.07.006

465. Rossant, J., & Cross, J. C. (2001). Placental development: Lessons from mouse mutants. *Nature Reviews Genetics*, *2*(7), 538-548. https://doi.org/10.1038/35080570

466. Edwards, A. K., Janzen-Pang, J., Peng, A., Tayade, C., Carniato, A., Yamada, A. T., Lima, P. D. A., & Tse, D. (2014). 3 - Microscopic Anatomy of the Pregnant Mouse Uterus Throughout Gestation. In B. A. Croy, A. T. Yamada, F. J. DeMayo, & S. L. Adamson (Eds.), *The Guide to Investigation of Mouse Pregnancy* (pp. 43-67). Academic Press. https://doi.org/10.1016/B978-0-12-394445-0.00003-5

467. Blois, S. M., Barrientos, G., Garcia, M. G., Orsal, A. S., Tometten, M., Cordo-Russo, R. I., Klapp, B. F., Santoni, A., Fernández, N., Terness, P., & Arck, P. C. (2008). Interaction between dendritic cells and natural killer cells during pregnancy in mice. *Journal of Molecular Medicine*, *86*(7), 837-852. https://doi.org/10.1007/s00109-008-0342-2

468. Scherjon, S., Lashley, L., van der Hoorn, M. L., & Claas, F. (2011). Fetus specific T cell modulation during fertilization, implantation and pregnancy. *Placenta*, *32*, S291-S297. https://doi.org/10.1016/j.placenta.2011.03.014

469. Bouillot, S., Rampon, C., Tillet, E., & Huber, P. (2006). Tracing the Glycogen Cells with Protocadherin 12 During Mouse Placenta Development. *Placenta*, *27*(8), 882-888. https://doi.org/10.1016/j.placenta.2005.09.009

470. Georgiades, P., Watkins, M., Burton, G. J., & Ferguson-Smith, A. C. (2001). Roles for genomic imprinting and the zygotic genome in placental development. *Proceedings of the National Academy of Sciences*, *98*(8), 4522-4527. https://doi.org/10.1073/pnas.081540898

471. Coan, P. M., Conroy, N., Burton, G. J., & Ferguson-Smith, A. C. (2006). Origin and characteristics of glycogen cells in the developing murine placenta. *Developmental Dynamics*, *235*(12), 3280-3294. https://doi.org/10.1002/dvdy.20981

472. Fowden, A. L., & Moore, T. (2012). Maternal-fetal resource allocation: Co-operation and conflict. *Placenta*, *33*, e11-e15. https://doi.org/10.1016/j.placenta.2012.05.002

473. He, H., Venema, V. J., Gu, X., Venema, R. C., Marrero, M. B., & Caldwell, R. B. (1999). Vascular Endothelial Growth Factor Signals Endothelial Cell Production of Nitric Oxide and Prostacyclin through Flk-1/KDR Activation of c-Src*. *Journal of Biological Chemistry*, *274*(35), 25130-25135. https://doi.org/10.1074/jbc.274.35.25130

474. Perez-Garcia, V., Fineberg, E., Wilson, R., Murray, A., Mazzeo, C. I., Tudor, C., Sienerth, A., White, J. K., Tuck, E., Ryder, E. J., Gleeson, D., Siragher, E., Wardle-Jones, H., Staudt, N., Wali, N., Collins, J., Geyer, S., Busch-Nentwich, E. M., Galli, A., . . . Hemberger, M. (2018). Placentation defects are highly prevalent in embryonic lethal mouse mutants. *Nature*, *555*(7697), 463-468. https://doi.org/10.1038/nature26002

475. Anson-Cartwright, L., Dawson, K., Holmyard, D., Fisher, S. J., Lazzarini, R. A., & Cross, J. C. (2000). The glial cells missing-1 protein is essential for branching morphogenesis in the chorioallantoic placenta. *Nature Genetics*, *25*(3), 311-314. https://doi.org/10.1038/77076

476. Ma, G. T., Soloveva, V., Tzeng, S.-J., Lowe, L. A., Pfendler, K. C., Iannaccone, P. M., Kuehn, M. R., & Linzer, D. I. H. (2001). Nodal Regulates Trophoblast Differentiation and Placental Development. *Developmental Biology*, *236*(1), 124-135. https://doi.org/10.1006/dbio.2001.0334

477. Lotz, K., Pyrowolakis, G., & Jentsch, S. (2004). BRUCE, a Giant E2/E3 Ubiquitin Ligase and Inhibitor of Apoptosis Protein of the trans-Golgi Network, Is Required for Normal Placenta Development and Mouse Survival. *Molecular and Cellular Biology*, *24*(21), 9339-9350. https://doi.org/10.1128/MCB.24.21.9339-9350.2004

478. Kanayama, N., Takahashi, K., Matsuura, T., Sugimura, M., Kobayashi, T., Moniwa, N., Tomita, M., & Nakayama, K. (2002). Deficiency in p57Kip2 expression induces preeclampsia-like symptoms in mice. *Molecular Human Reproduction*, *8*(12), 1129-1135. https://doi.org/10.1093/molehr/8.12.1129

479. Gnarra, J. R., Ward, J. M., Porter, F. D., Wagner, J. R., Devor, D. E., Grinberg, A., Emmert-Buck, M. R., Westphal, H., Klausner, R. D., & Linehan, W. M. (1997). Defective placental vasculogenesis causes embryonic lethality in VHL-deficient mice. *Proceedings of the National Academy of Sciences*, *94*(17), 9102-9107. https://doi.org/10.1073/pnas.94.17.9102

480. Ma, J., Wu, J., Han, L., Jiang, X., Yan, L., Hao, J., & Wang, H. (2019). Comparative analysis of mesenchymal stem cells derived from amniotic membrane, umbilical cord, and chorionic plate under serum-free condition. *Stem Cell Research & Therapy*, *10*(1), 19. https://doi.org/10.1186/s13287-018-1104-x

481. Giroux, S., Tremblay, M., Bernard, D., Cardin-Girard, J. F., Aubry, S., Larouche, L., Rousseau, S., Huot, J., Landry, J., Jeannotte, L., & Charron, J. (1999). Embryonic death of Mek1-deficient mice reveals a role for this kinase in angiogenesis in the labyrinthine region of the placenta. *Current Biology*, *9*(7), 369-376. https://doi.org/10.1016/S0960-9822(99)80164-X

482. Hoffman Julien, I. E. (2013). The global burden of congenital heart disease : review article. *Cardiovascular Journal of Africa*, *24*(4), 141-145. https://doi.org/10.10520/EJC137177

483. Jorgensen, M., McPherson, E., Zaleski, C., Shivaram, P., & Cold, C. (2014). Stillbirth: The heart of the matter. *American Journal of Medical Genetics Part A*, *164*(3), 691-699. https://doi.org/10.1002/ajmg.a.36366

484. A. Richards, A., & Garg, V. (2010). Genetics of Congenital Heart Disease. *Current Cardiology Reviews*, *6*(2), 91-97. https://doi.org/10.2174/157340310791162703

485. Pierpont, M. E., Brueckner, M., Chung, W. K., Garg, V., Lacro, R. V., McGuire, A. L., Mital, S., Priest, J. R., Pu, W. T., Roberts, A., Ware, S. M., Gelb, B. D., Russell, M. W., & null, n. (2018). Genetic Basis for Congenital Heart Disease: Revisited: A Scientific Statement From the American Heart Association. *Circulation*, *138*(21), e653-e711. https://doi.org/10.1161/CIR.0000000000000606

486. Courtney, J. A., Cnota, J. F., & Jones, H. N. (2018). The Role of Abnormal Placentation in Congenital Heart Disease; Cause, Correlate, or Consequence? *Frontiers in Physiology*, *9*, 1045. https://doi.org/10.3389/fphys.2018.01045

487. Langford, M. B., Outhwaite, J. E., Hughes, M., Natale, D. R. C., & Simmons, D. G. (2018). Deletion of the Syncytin A receptor Ly6e impairs syncytiotrophoblast fusion and placental morphogenesis causing embryonic lethality in mice. *Scientific Reports*, *8*(1), 3961. https://doi.org/10.1038/s41598-018-22040-2

488. Zammit, D. J., Berzins, S. P., Gill, J. W., Randle-Barrett, E. S., Barnett, L., Koentgen, F., Lambert, G. W., Harvey, R. P., Boyd, R. L., & Classon, B. J. (2002). Essential Role for the Lymphostromal Plasma Membrane Ly-6 Superfamily Molecule Thymic Shared Antigen 1 in Development of the Embryonic Adrenal Gland. *Molecular and Cellular Biology*, *22*(3), 946-952. https://doi.org/10.1128/MCB.22.3.946-952.2002

489. Ochiai, Y., Suzuki, C., Segawa, K., Uchiyama, Y., & Nagata, S. (2022). Inefficient development of syncytiotrophoblasts in the Atp11a-deficient mouse placenta. *Proceedings of the National Academy of Sciences*, *119*(18), e2200582119. https://doi.org/10.1073/pnas.2200582119

490. Radford, B. N., Zhao, X., Glazer, T., Eaton, M., Blackwell, D., Mohammad, S., Lo Vercio, L. D., Devine, J., Shalom-Barak, T., Hallgrimsson, B., Cross, J. C., Sucov, H. M., Barak, Y., Dean, W., & Hemberger, M. (2023). Defects in placental syncytiotrophoblast cells are a common cause of developmental heart disease. *Nature Communications*, *14*(1), 1174. https://doi.org/10.1038/s41467-023-36740-5

## Chapter 4: General Discussion and Conclusion


1. He, Y., Northey, J. J., Pelletier, A., Kos, Z., Meunier, L., Haibe-Kains, B., Mes-Masson, A. M., Côté, J. F., Siegel, P. M., & Lamarche-Vane, N. (2017). The Cdc42/Rac1 regulator CdGAP is a novel E-cadherin transcriptional co-repressor with Zeb2 in breast cancer. *Oncogene*, *36*(24), 3490-3503. https://doi.org/10.1038/onc.2016.492
2. Migeotte, I., Grego-Bessa, J., & Anderson, K. V. (2011). Rac1 mediates morphogenetic responses to intercellular signals in the gastrulating mouse embryo. *Development*, *138*(14), 3011-3020. https://doi.org/10.1242/dev.059766
3. Migeotte, I., Omelchenko, T., Hall, A., & Anderson, K. V. (2010). Rac1-Dependent Collective Cell Migration Is Required for Specification of the Anterior-Posterior Body Axis of the Mouse. *PLOS Biology*, *8*(8), e1000442. https://doi.org/10.1371/journal.pbio.1000442
4. Wu, X., Li, S., Chrostek-Grashoff, A., Czuchra, A., Meyer, H., Yurchenco, P. D., & Brakebusch, C. (2007). Cdc42 is crucial for the establishment of epithelial polarity during early mammalian development. *Developmental Dynamics*, *236*(10), 2767-2778. https://doi.org/10.1002/dvdy.21309
5. Southgate, L., Machado, Rajiv D., Snape, Katie M., Primeau, M., Dafou, D., Ruddy, Deborah M., Branney, Peter A., Fisher, M., Lee, Grace J., Simpson, Michael A., He, Y., Bradshaw, Teisha Y., Blaumeiser, B., Winship, William S., Reardon, W., Maher, Eamonn R., FitzPatrick, David R., Wuyts, W., Zenker, M., . . . Trembath, Richard C. (2011). Gain-of-Function Mutations of ARHGAP31, a Cdc42/Rac1 GTPase Regulator, Cause Syndromic Cutis Aplasia and Limb Anomalies. *The American Journal of Human Genetics*, *88*(5), 574-585. https://doi.org/10.1016/j.ajhg.2011.04.013
6. Caron, C., DeGeer, J., Fournier, P., Duquette, P. M., Luangrath, V., Ishii, H., Karimzadeh, F., Lamarche-Vane, N., & Royal, I. (2016). CdGAP/ARHGAP31, a Cdc42/Rac1 GTPase regulator, is critical for vascular development and VEGF-mediated angiogenesis. *Scientific Reports*, *6*(1), 27485. https://doi.org/10.1038/srep27485
7. Southgate, L., & Trembath, R. C. (2016). 1203ARHGAP31, DOCK6, RBPJ, EOGT, and Adams-Oliver Syndrome. In *Epstein's Inborn Errors of Development: The Molecular*

*Basis of Clinical Disorders of Morphogenesis* (pp. 0). Oxford University Press. https://doi.org/10.1093/med/9780199934522.003.0183

8. Snape, K. M. G., Ruddy, D., Zenker, M., Wuyts, W., Whiteford, M., Johnson, D., Lam, W., & Trembath, R. C. (2009). The spectra of clinical phenotypes in aplasia cutis congenita and terminal transverse limb defects. *American Journal of Medical Genetics Part A*, *149A*(8), 1860-1881. https://doi.org/10.1002/ajmg.a.32708
9. Jaeggi, E., Kind, C., & Morger, R. (1990). Congenital scalp and skull defects with terminal transverse limb anomalies (Adams-Oliver syndrome): Report of three additional cases. *European Journal of Pediatrics*, *149*(8), 565-566. https://doi.org/10.1007/BF01957693
10. Swartz, E. N., Sanatani, S., Sandor, G. G. S., & Schreiber, R. A. (1999). Vascular abnormalities in Adams-Oliver syndrome: Cause or effect? *American Journal of Medical Genetics*, *82*(1), 49-52. https://doi.org/10.1002/(SICI)1096-8628(19990101)82:1<49::AID-AJMG10>3.0.CO;2-M
11. Sevilla-Montoya, R., Ríos-Flores, B., Moreno-Verduzco, E., Domínguez-Castro, M., Rivera-Pedroza, C. I., & Aguinaga-Ríos, D. M. (2014). Severe phenotype in two half-sibs with Adams Oliver syndrome. *Archivos argentinos de pediatria*, *112*(3), e108–e112. https://doi.org/10.5546/aap.2014.eng.e108
12. Schröder, K. C., Duman, D., Tekin, M., Schanze, D., Sukalo, M., Meester, J., Wuyts, W., & Zenker, M. (2019). Adams–Oliver syndrome caused by mutations of the EOGT gene. *American Journal of Medical Genetics Part A*, *179*(11), 2246-2251. https://doi.org/10.1002/ajmg.a.61313
13. Belkahla, S., Nahvi, I., Biswas, S., Nahvi, I., & Ben Amor, N. (2022). Advances and development of prostate cancer, treatment, and strategies: A systemic review. *Frontiers in Cell and Developmental Biology*, *10*, 991330. https://doi.org/10.3389/fcell.2022.991330
14. Society, A. C. *Cancer Facts & Figures 2023*. American Cancer Society. Retrieved June 30, 2023 from http://cancerstatisticscenter.cancer.org
15. Dai, C., Heemers, H., & Sharifi, N. Androgen Signaling in Prostate Cancer. *Cold Spring Harbor perspectives in medicine*, *7*(9), a030452. https://doi.org/10.1101/cshperspect.a030452

16. Yap, T. A., Smith, A. D., Ferraldeschi, R., Al-Lazikani, B., Workman, P., & de Bono, J. S. (2016). Drug discovery in advanced prostate cancer: translating biology into therapy. *Nature Reviews Drug Discovery*, *15*(10), 699-718. https://doi.org/10.1038/nrd.2016.120
17. Wadosky, K. M., & Koochekpour, S. (2016). Molecular mechanisms underlying resistance to androgen deprivation therapy in prostate cancer. *Oncotarget*, *7*, 64447-64470. https://doi.org/10.18632/oncotarget.10901
18. Sumanasuriya, S., & De Bono, J. (2018). Treatment of Advanced Prostate Cancer-A Review of Current Therapies and Future Promise. *Cold Spring Harbor perspectives in medicine*, *8*(6), a030635. https://doi.org/10.1101/cshperspect.a030635
19. Chang, M. T., Asthana, S., Gao, S. P., Lee, B. H., Chapman, J. S., Kandoth, C., Gao, J., Socci, N. D., Solit, D. B., Olshen, A. B., Schultz, N., & Taylor, B. S. (2016). Identifying recurrent mutations in cancer reveals widespread lineage diversity and mutational specificity. *Nature Biotechnology*, *34*(2), 155-163. https://doi.org/10.1038/nbt.3391
20. Li, Z., Liu, Q., Piao, J., Hua, F., Wang, J., Jin, G., Lin, Z., & Zhang, Y. (2016). Clinicopathological implications of Tiam1 overexpression in invasive ductal carcinoma of the breast. *BMC Cancer*, *16*(1), 681. https://doi.org/10.1186/s12885-016-2724-0
21. He, Y., Northey, J. J., Primeau, M., Machado, R. D., Trembath, R., Siegel, P. M., & Lamarche-Vane, N. (2011). CdGAP is required for transforming growth factor β- and Neu/ErbB-2-induced breast cancer cell motility and invasion. *Oncogene*, *30*(9), 1032-1045. https://doi.org/10.1038/onc.2010.477
22. Wormer, D., Deakin, N. O., & Turner, C. E. (2012). CdGAP regulates cell migration and adhesion dynamics in two-and three-dimensional matrix environments. *Cytoskeleton*, *69*(9), 644-658. https://doi.org/10.1002/cm.21057
23. Wormer, D. B., Davis, K. A., Henderson, J. H., & Turner, C. E. (2014). The Focal Adhesion-Localized CdGAP Regulates Matrix Rigidity Sensing and Durotaxis. *PLoS One*, *9*(3), e91815. https://doi.org/10.1371/journal.pone.0091815
24. Alizadeh, M., & Alizadeh, S. (2014). Survey of clinical and pathological characteristics and outcomes of patients with prostate cancer. *Global journal of health science*, *6*(7), 49-57. https://doi.org/10.5539/gjhs.v6n7p49
25. Brawer, M. K. Prostatic intraepithelial neoplasia: an overview. *Reviews in urology*, *7*(Suppl 3), S11–S18.

26. Kim, H. L., & Yang, X. J. (2002). Prevalence of high-grade prostatic intraepithelial neoplasia and its relationship to serum prostate specific antigen. *International braz j urol : official journal of the Brazilian Society of Urology*, *28*(5), 413-417.
27. Tai, S., Sun, Y., Squires, J. M., Zhang, H., Oh, W. K., Liang, C.-Z., & Huang, J. (2011). PC3 is a cell line characteristic of prostatic small cell carcinoma. *The Prostate*, *71*(15), 1668-1679. https://doi.org/10.1002/pros.21383
28. Cunningham, D., & You, Z. (2015). In vitro and in vivo model systems used in prostate cancer research. *Journal of biological methods*, *2*(1), e17. https://doi.org/10.14440/jbm.2015.63
29. De Maeseneer, D. J., Van Praet, C., Lumen, N., & Rottey, S. (2015). Battling resistance mechanisms in antihormonal prostate cancer treatment: Novel agents and combinations. *Urologic Oncology: Seminars and Original Investigations*, *33*(7), 310-321. https://doi.org/10.1016/j.urolonc.2015.01.008
30. Girling, J. S., Whitaker, H. C., Mills, I. G., & Neal, D. E. (2007). Pathogenesis of prostate cancer and hormone refractory prostate cancer. *Indian Journal of Urology*, *23*(1), 35-42. https://doi.org/10.4103/0970-1591.30265
31. Li, Y., Chan, S. C., Brand, L. J., Hwang, T. H., Silverstein, K. A. T., & Dehm, S. M. (2013). Androgen Receptor Splice Variants Mediate Enzalutamide Resistance in Castration-Resistant Prostate Cancer Cell Lines. *Cancer Research*, *73*(2), 483-489. https://doi.org/10.1158/0008-5472.CAN-12-3630
32. Rajan, P., Elliott, D. J., Robson, C. N., & Leung, H. Y. (2009). Alternative splicing and biological heterogeneity in prostate cancer. *Nature Reviews Urology*, *6*(8), 454-460. https://doi.org/10.1038/nrurol.2009.125
33. Veldscholte, J., Berrevoets, C. A., Ris-Stalpers, C., Kuiper, G. G. J. M., Jenster, G., Trapman, J., Brinkmann, A. O., & Mulder, E. (1992). The androgen receptor in LNCaP cells contains a mutation in the ligand binding domain which affects steroid binding characteristics and response to antiandrogens. *The Journal of Steroid Biochemistry and Molecular Biology*, *41*(3), 665-669. https://doi.org/10.1016/0960-0760(92)90401-4
34. Hanahan, D. (2022). Hallmarks of Cancer: New Dimensions. *Cancer Discovery*, *12*(1), 31-46. https://doi.org/10.1158/2159-8290.CD-21-1059

35. Chaffer, C. L., & Weinberg, R. A. (2011). A Perspective on Cancer Cell Metastasis. *Science*, *331*(6024), 1559-1564. https://doi.org/10.1126/science.1203543

36. Woods-Burnham, L., Basu, A., Cajigas-Du Ross, C. K., Love, A., Yates, C., De Leon, M., Roy, S., & Casiano, C. A. (2017). The 22Rv1 prostate cancer cell line carries mixed genetic ancestry: Implications for prostate cancer health disparities research using pre-clinical models. *The Prostate*, *77*, 1601-1608. https://doi.org/https://doi.org/10.1002/pros.23437

37. Hooker, S. E., Jr., Woods-Burnham, L., Bathina, M., Lloyd, S., Gorjala, P., Mitra, R., Nonn, L., Kimbro, K. S., & Kittles, R. A. (2019). Genetic Ancestry Analysis Reveals Misclassification of Commonly Used Cancer Cell Lines. *Cancer Epidemiology, Biomarkers & Prevention*, *28*(6), 1003-1009. https://doi.org/10.1158/1055-9965.EPI-18-1132

38. Faye-Petersen, O. M., Heller, D. S., & Joshi, V. V. (2005). *Handbook of Placental Pathology* (2nd ed.). CRC Press. https://doi.org/10.3109/9780203489567

39. Narasimha, A., & Vasudeva, D. (2011). Spectrum of changes in placenta in toxemia of pregnancy. *Indian Journal of Pathology and Microbiology*, *54*(1), 15-20. https://doi.org/10.4103/0377-4929.77317

40. Wilson, M. E., & Ford, S. P. (2001). Comparative aspects of placental efficiency. *Reproduction (Cambridge, England). Supplement*, *58*, 223-232.

41. Fowden, A. L., Sferruzzi-Perri, A. N., Coan, P. M., Constancia, M., & Burton, G. J. (2009). Placental efficiency and adaptation: endocrine regulation. *The Journal of Physiology*, *587*(14), 3459-3472. https://doi.org/10.1113/jphysiol.2009.173013

42. Sankhyan, N., Kaushal, R. K., & Jaswal, R. S. (2006). Adams–Oliver syndrome: A case with complete expression. *The Journal of Dermatology*, *33*(6), 435-436. https://doi.org/10.1111/j.1346-8138.2006.00104.x

43. Bonafede, R. P., & Beighton, P. (1979). Autosomal dominant inheritance of scalp defects with ectrodactyly. *American Journal of Medical Genetics*, *3*(1), 35-41. https://doi.org/10.1002/ajmg.1320030109

44. Woods, L., Perez-Garcia, V., & Hemberger, M. (2018). Regulation of Placental Development and Its Impact on Fetal Growth—New Insights From Mouse Models. *Frontiers in Endocrinology*, *9*, 570. https://doi.org/10.3389/fendo.2018.00570

45. Watson, E. D., & Cross, J. C. (2005). Development of Structures and Transport Functions in the Mouse Placenta. *Physiology*, *20*(3), 180-193. https://doi.org/10.1152/physiol.00001.2005

46. Simmons, D. G. (2014). 12 - Postimplantation Development of the Chorioallantoic Placenta. In B. A. Croy, A. T. Yamada, F. J. DeMayo, & S. L. Adamson (Eds.), *The Guide to Investigation of Mouse Pregnancy* (pp. 143-161). Academic Press. https://doi.org/10.1016/B978-0-12-394445-0.00012-6

47. Sarkar, A. A., Nuwayhid, S. J., Maynard, T., Ghandchi, F., Hill, J. T., Lamantia, A. S., & Zohn, I. E. (2014). Hectd1 is required for development of the junctional zone of the placenta. *Developmental Biology*, *392*(2), 368-380. https://doi.org/10.1016/j.ydbio.2014.05.007

48. Elmore, S. A., Cochran, R. Z., Bolon, B., Lubeck, B., Mahler, B., Sabio, D., & Ward, J. M. (2021). Histology Atlas of the Developing Mouse Placenta. *Toxicologic Pathology*, *50*(1), 60-117. https://doi.org/10.1177/01926233211042270

49. Lu, X., Wang, R., Zhu, C., Wang, H., Lin, H.-Y., Gu, Y., Cross, J. C., & Wang, H. (2017). Fine-Tuned and Cell-Cycle-Restricted Expression of Fusogenic Protein Syncytin-2 Maintains Functional Placental Syncytia. *Cell Reports*, *21*(5), 1150-1159. https://doi.org/10.1016/j.celrep.2017.10.019

50. Wang, Y.-N., Ye, Y., Zhou, D., Guo, Z.-W., Xiong, Z., Gong, X.-X., Jiang, S.-W., & Chen, H. (2022). The Role of Syncytin in Placental Angiogenesis and Fetal Growth. *Frontiers in Cell and Developmental Biology*, *10*, 852561. https://doi.org/10.3389/fcell.2022.852561

51. Meakin, A. S., Cuffe, J. S. M., Darby, J. R. T., Morrison, J. L., & Clifton, V. L. (2021). Let's Talk about Placental Sex, Baby: Understanding Mechanisms That Drive Female- and Male-Specific Fetal Growth and Developmental Outcomes. *International Journal of Molecular Sciences*, *22*(12), 6386. https://doi.org/10.3390/ijms22126386

52. Stark, M. J., Clifton, V. L., & Wright, I. M. R. (2009). Neonates Born to Mothers With Preeclampsia Exhibit Sex-Specific Alterations in Microvascular Function. *Pediatric Research*, *65*(3), 291-295. https://doi.org/10.1203/PDR.0b013e318193edf1

53. Trudell, A. S., Cahill, A. G., Tuuli, M. G., Macones, G. A., & Odibo, A. O. (2015). Stillbirth and the small fetus: use of a sex-specific versus a non-sex-specific growth standard. *Journal of Perinatology*, *35*(8), 566-569. https://doi.org/10.1038/jp.2015.17

54. Broere-Brown, Z. A., Adank, M. C., Benschop, L., Tielemans, M., Muka, T., Gonçalves, R., Bramer, W. M., Schoufour, J. D., Voortman, T., Steegers, E. A. P., Franco, O. H., & Schalekamp-Timmermans, S. (2020). Fetal sex and maternal pregnancy outcomes: a systematic review and meta-analysis. *Biology of Sex Differences*, *11*(1), 26. https://doi.org/10.1186/s13293-020-00299-3

55. Roberts, G. A. G., & Tunster, S. J. (2020). Characterising the dynamics of placental glycogen stores in the mouse. *Placenta*, *99*, 131-140. https://doi.org/10.1016/j.placenta.2020.07.010

56. Meester, J. A. N., Sukalo, M., Schröder, K. C., Schanze, D., Baynam, G., Borck, G., Bramswig, N. C., Duman, D., Gilbert-Dussardier, B., Holder-Espinasse, M., Itin, P., Johnson, D. S., Joss, S., Koillinen, H., McKenzie, F., Morton, J., Nelle, H., Reardon, W., Roll, C., . . . Wuyts, W. (2018). Elucidating the genetic architecture of Adams–Oliver syndrome in a large European cohort. *Human Mutation*, *39*(9), 1246-1261. https://doi.org/10.1002/humu.23567

57. Gauster, M., Moser, G., Wernitznig, S., Kupper, N., & Huppertz, B. (2022). Early human trophoblast development: from morphology to function. *Cellular and Molecular Life Sciences*, *79*(6), 345. https://doi.org/10.1007/s00018-022-04377-0

58. Spencer, T. E., & Bazer, F. W. (2004). Conceptus signals for establishment and maintenance of pregnancy. *Reproductive Biology and Endocrinology*, *2*(1), 49. https://doi.org/10.1186/1477-7827-2-49

59. Staun-Ram, E., & Shalev, E. (2005). Human trophoblast function during the implantation process. *Reproductive Biology and Endocrinology*, *3*(1), 56. https://doi.org/10.1186/1477-7827-3-56

60. Beck, S., Wojdyla D Fau - Say, L., Say L Fau - Betran, A. P., Betran Ap Fau - Merialdi, M., Merialdi M Fau - Requejo, J. H., Requejo Jh Fau - Rubens, C., Rubens C Fau - Menon, R., Menon R Fau - Van Look, P. F. A., & Van Look, P. F. (2010). The worldwide incidence of preterm birth: a systematic review of maternal mortality and morbidity.

*Bulletin of the World Health Organization*, *88*(1), 31-38. https://doi.org/10.2471/BLT.08.062554

61. Mercuro, G., Bassareo, P. P., Flore, G., Fanos, V., Dentamaro, I., Scicchitano, P., Laforgia, N., & Ciccone, M. M. (2013). Prematurity and low weight at birth as new conditions predisposing to an increased cardiovascular risk. *European Journal of Preventive Cardiology*, *20*(2), 357-367. https://doi.org/10.1177/2047487312437058
62. Moster, D., Lie, R. T., & Markestad, T. (2008). Long-Term Medical and Social Consequences of Preterm Birth. *New England Journal of Medicine*, *359*(3), 262-273. https://doi.org/10.1056/NEJMoa0706475
63. Courtney, J. A., Cnota, J. F., & Jones, H. N. (2018). The Role of Abnormal Placentation in Congenital Heart Disease; Cause, Correlate, or Consequence? *Frontiers in Physiology*, *9*, 1045. https://doi.org/10.3389/fphys.2018.01045
64. A. Richards, A., & Garg, V. (2010). Genetics of Congenital Heart Disease. *Current Cardiology Reviews*, *6*(2), 91-97. https://doi.org/10.2174/157340310791162703
65. Pierpont, M. E., Brueckner, M., Chung, W. K., Garg, V., Lacro, R. V., McGuire, A. L., Mital, S., Priest, J. R., Pu, W. T., Roberts, A., Ware, S. M., Gelb, B. D., Russell, M. W., & null, n. (2018). Genetic Basis for Congenital Heart Disease: Revisited: A Scientific Statement From the American Heart Association. *Circulation*, *138*(21), e653-e711. https://doi.org/10.1161/CIR.0000000000000606
66. Radford, B. N., Zhao, X., Glazer, T., Eaton, M., Blackwell, D., Mohammad, S., Lo Vercio, L. D., Devine, J., Shalom-Barak, T., Hallgrimsson, B., Cross, J. C., Sucov, H. M., Barak, Y., Dean, W., & Hemberger, M. (2023). Defects in placental syncytiotrophoblast cells are a common cause of developmental heart disease. *Nature Communications*, *14*(1), 1174. https://doi.org/10.1038/s41467-023-36740-5
67. Perez-Garcia, V., Fineberg, E., Wilson, R., Murray, A., Mazzeo, C. I., Tudor, C., Sienerth, A., White, J. K., Tuck, E., Ryder, E. J., Gleeson, D., Siragher, E., Wardle-Jones, H., Staudt, N., Wali, N., Collins, J., Geyer, S., Busch-Nentwich, E. M., Galli, A., . . . Hemberger, M. (2018). Placentation defects are highly prevalent in embryonic lethal mouse mutants. *Nature*, *555*(7697), 463-468. https://doi.org/10.1038/nature26002

68. Thornburg, K. L., O'Tierney, P. F., & Louey, S. (2010). Review: The Placenta is a Programming Agent for Cardiovascular Disease. *Placenta*, *31*, S54-S59. https://doi.org/10.1016/j.placenta.2010.01.002

69. Tenney, B., & Parker, F. (1940). The placenta in toxemia of pregnancy. *American Journal of Obstetrics and Gynecology*, *39*(6), 1000-1005. https://doi.org/10.1016/S0002-9378(40)90458-6

70. Soma, H., Yoshida, K., Mukaida, T., & Tabuchi, Y. (1982). Morphologic Changes in the Hypertensive Placenta1. In *Morphological and Functional Aspects of Placental Dysfunction* (Vol. 9, pp. 0). S.Karger AG. https://doi.org/10.1159/000406845

71. Hypertension in Pregnancy: Executive Summary. (2013). *Obstetrics & Gynecology*, *122*(5), 1122-1131. https://doi.org/10.1097/01.AOG.0000437382.03963.88

72. Albrecht, E. D., & Pepe, G. J. (2020). Regulation of Uterine Spiral Artery Remodeling: a Review. *Reproductive Sciences*, *27*(10), 1932-1942. https://doi.org/10.1007/s43032-020-00212-8

73. Brennan, L. J., Morton, J. S., & Davidge, S. T. (2014). Vascular Dysfunction in Preeclampsia. *Microcirculation*, *21*(1), 4-14. https://doi.org/10.1111/micc.12079

74. Zun, Z., Zaharchuk, G., Andescavage, N. N., Donofrio, M. T., & Limperopoulos, C. (2017). Non-Invasive Placental Perfusion Imaging in Pregnancies Complicated by Fetal Heart Disease Using Velocity-Selective Arterial Spin Labeled MRI. *Scientific Reports*, *7*(1), 16126. https://doi.org/10.1038/s41598-017-16461-8

75. Ochiai, Y., Suzuki, C., Segawa, K., Uchiyama, Y., & Nagata, S. (2022). Inefficient development of syncytiotrophoblasts in the Atp11a-deficient mouse placenta. *Proceedings of the National Academy of Sciences*, *119*(18), e2200582119. https://doi.org/10.1073/pnas.2200582119

76. Langford, M. B., Outhwaite, J. E., Hughes, M., Natale, D. R. C., & Simmons, D. G. (2018). Deletion of the Syncytin A receptor Ly6e impairs syncytiotrophoblast fusion and placental morphogenesis causing embryonic lethality in mice. *Scientific Reports*, *8*(1), 3961. https://doi.org/10.1038/s41598-018-22040-2

77. Hassed, Susan J., Wiley, Graham B., Wang, S., Lee, J.-Y., Li, S., Xu, W., Zhao, Zhizhuang J., Mulvihill, John J., Robertson, J., Warner, J., & Gaffney, Patrick M. (2012). RBPJ Mutations Identified in Two Families Affected by Adams-Oliver

Syndrome. *The American Journal of Human Genetics*, *91*(2), 391-395. https://doi.org/10.1016/j.ajhg.2012.07.005

78. Isrie, M., Wuyts, W., Van Esch, H., & Devriendt, K. (2014). Isolated terminal limb reduction defects: Extending the clinical spectrum of Adams–Oliver syndrome and ARHGAP31 mutations. *American Journal of Medical Genetics Part A*, *164*(6), 1576-1579. https://doi.org/10.1002/ajmg.a.36486
79. Lyons, G. E., Schiaffino, S., Sassoon, D., Barton, P., & Buckingham, M. (1990). Developmental regulation of myosin gene expression in mouse cardiac muscle. *Journal of Cell Biology*, *111*(6), 2427-2436. https://doi.org/10.1083/jcb.111.6.2427
80. Simmons, D. G., Natale, D. R. C., Begay, V., Hughes, M., Leutz, A., & Cross, J. C. (2008). Early patterning of the chorion leads to the trilaminar trophoblast cell structure in the placental labyrinth. *Development*, *135*(12), 2083-2091. https://doi.org/10.1242/dev.020099
81. Coan, P. M., Ferguson-Smith, A. C., & Burton, G. J. (2004). Developmental Dynamics of the Definitive Mouse Placenta Assessed by Stereology1. *Biology of Reproduction*, *70*(6), 1806-1813. https://doi.org/10.1095/biolreprod.103.024166
82. Adamson, S. L., Lu, Y., Whiteley, K. J., Holmyard, D., Hemberger, M., Pfarrer, C., & Cross, J. C. (2002). Interactions between Trophoblast Cells and the Maternal and Fetal Circulation in the Mouse Placenta. *Developmental Biology*, *250*(2), 358-373. https://doi.org/10.1006/dbio.2002.0773
83. Gurtner, G. C., Davis V Fau - Li, H., Li H Fau - McCoy, M. J., McCoy Mj Fau - Sharpe, A., Sharpe A Fau - Cybulsky, M. I., & Cybulsky, M. I. (1995). Targeted disruption of the murine VCAM1 gene: essential role of VCAM-1 in chorioallantoic fusion and placentation. *Genes & development*, *9*(1), 1-14. https://doi.org/10.1101/gad.9.1.1
84. Oechslin, E., & Jenni, R. (2011). Left ventricular non-compaction revisited: a distinct phenotype with genetic heterogeneity? *European Heart Journal*, *32*(12), 1446-1456. https://doi.org/10.1093/eurheartj/ehq508

# Appendix

August 29th 2023

**Agreement on the use of a manuscript in a manuscript-based thesis at McGill**

I hereby confirm that I will not use the manuscript listed below for a manuscript-based thesis at McGill. In this manuscript, Ji-Hyun Chung and I are listed as co-first authors. I agree to my co-first author Ji-Hyun Chung using it in his manuscript-based thesis.

Chahat Mehra*, Ji-Hyun Chung*, Yi He, Monica Lara-Márquez, Marie-Anne Goyette, Nadia Boufaied, Véronique Barrès, Véronique Ouellet, Karl-Phillippe Guérard, Carine Delliaux, Fred Saad, Jacques Lapointe, Jean-François Côté, David P. Labbé, and Nathalie Lamarche-Vane. (2021). ***Communications biology***. 4 (1042).

* co-first authors

Chahat Mehra

Chahat Mehra